C-H Activation Reactions Mediated by Pd Based Heterogeneous Catalysts

Regioselective Formation of C-O and C-X Bonds

Majeed, Maitham

2018

C–H Activation Reactions Mediated by Pd Based Heterogeneous Catalysts

Regioselective Formation of C–O and C–X Bonds

Maitham H. Majeed

LUND
UNIVERSITY

DOCTORAL DISSERTATION
To be publicly defended for the degree of PhD at the Faculty of Science,
Lund University, Sweden on Friday 2nd of February 2018 at 10:00 am, in
lecture hall F at Kemicentrum

Faculty opponent
Prof. Belén Martín-Matute, Stockholms universitet, Sweden

Organization	Document name
LUND UNIVERSITY	DOCTORAL DISSERTATION
	Date of issue
	2018-02-02
Author(s)	Sponsoring organization
Maitham H. Majeed	

Title and subtitle
C–H Activation Reactions Mediated by Pd Based Heterogeneous Catalysts - Regioselective Formation of C–O and C–X Bonds

Abstract
New classes of N-heterocyclic carbene-palladium(II) complexes containing either a vinyl group in different positions or an anthracene tag in the backbone of the N-heterocycle were synthesized and fully characterized. The vinyl based complexes were copolymerized with divinylbenzene to fabricate robust polymer-supported NHC-Pd(II) systems, while the anthracene based complexes were π-stacked onto the surface of reduced graphene oxide (rGO) producing immobilized catalysts with interesting features. Advanced solid-state characterization techniques focused on the structure and oxidation state of the Pd(II) center of the all the supported complexes and showed the presence of Pd(II) species in the native catalysts without any trace of Pd(0) nanoparticles, confirming the success of the preparation pathways. The supported catalysts were applied as heterogeneous catalysts in C–H activation of arenes using different methodologies. In the undirected C–H acetoxylation of simple, methylated, and poly arenes, the supported catalysts showed a similar or superior performance compared to their homogeneous analogues. In addition to that, the polymer based catalysts demonstrated a high catalytic activity and an excellent regioselectivity, up to 100% in many cases, in directed C–H halogenation of arylpyridines. Further advantages of these heterogeneous systems are their high stability and activity, their easy separation and recovery, meaning that they are recyclable for several runs with no leaching of palladium and no loss of activity. Furthermore, the best polymeric catalyst disclosed an exceptional activity and 100% selectivity towards the mono-halogenated product under continuous flow conditions for up to 6 days, during which the original oxidation state of Pd(II) was maintained.

Key words: C–H Activation, N-heterocyclic carbenes, palladium, polymer supported Pd(II), undirected acetoxylation, directed halogenation, continuous flow, reduced graphene oxide supported Pd(II)

Classification system and/or index terms (if any)

Supplementary bibliographical information	Language
	English

ISSN and key title	ISBN 978-91-7422-559-4 (Print)
	ISBN 978-91-7422-560-0 (pdf)

Recipient's notes	Number of pages 210	Price
	Security classification	

I, the undersigned, being the copyright owner of the abstract of the above-mentioned dissertation, hereby grant to all reference sources permission to publish and disseminate the abstract of the above-mentioned dissertation.

Signature _Maitham Majeed_ Date __2017-12-12__

C–H Activation Reactions Mediated by Pd Based Heterogeneous Catalysts

Regioselective Formation of C–O and C–X Bonds

Maitham H. Majeed

LUND
UNIVERSITY

Dedicated to
Who made everything possible…
My wife, Ikram
My lovely daughters & son: Sama, Reem and Hassan

Content

List of Publications

This doctoral thesis is based on the following publications, which are referred to in the text by their Roman numerals I-VI. The contribution of the author to each publication is clarified.

I. **Synthesis and crystal structure of *trans*-dichlorido-[3-methyl-1-(4-vinylbenzyl)-1*H*-imidazol-3-ium-2-yl-$\varkappa C^2$](4-phenylpyridine-$\varkappa N$)palladium(II)**

Maitham H. Majeed, Ola F. Wendt. *Acta Cryst*., **2016**, *E72*, 534-537.

II. **Polymer-supported palladium(II) carbene complexes: catalytic activity, recyclability, and selectivity in C–H acetoxylation of arenes**

Maitham H. Majeed, Payam Shayesteh, L. Reine Wallenberg, Axel R. Persson, Niclas Johansson, Lei Ye, Joachim Schnadt, Ola F. Wendt. *Chem. Eur. J.* **2017**, *23*, 8457-8465

III. **Directed C–H halogenation reactions catalysed by Pd(II) supported on polymers under batch and continuous flow conditions**

Maitham H. Majeed, Payam Shayesteh, Per Tunå, Axel R. Persson, Roman Gritcenko, L. Reine Wallenberg, Lei Ye, Christian Hulteberg, Joachim Schnadt, Ola F. Wendt. *Submitted for publication*.

IV. **A Pd(II) carbene complex with anthracene side arms for π-stacking on reduced graphene oxide (rGO): activity towards undirected C–H oxygenation of arenes**

Maitham H. Majeed†, Payam Shayesteh†, Axel R. Persson, L. Reine Wallenberg, Joachim Schnadt, Ola F. Wendt. *manuscript*.

V. **Reduced graphene oxide supported Pd(II) carbene complex: activity and selectivity in directed C–H halogenation of arenes**

Maitham H. Majeed, Dino Redzic, Payam Shayesteh, Axel R. Persson, L. Reine Wallenberg, Joachim Schnadt, Ola F. Wendt. *manuscript*.

VI. **Operando X-ray absorption spectroscopy investigation of active species of Pd(II)@rGO catalyse C–H oxygenation reaction**

Ning Yuan†, Maitham H. Majeed†, Éva Bajnóczi, Niclas Heidenreich, Norbert Stock, Ingmar Persson, Ola F. Wendt, Xiaodong Zou. *manuscript*.

Publications not included in the current thesis:

- **Synthesis and characterization of chiral phosphirane derivatives of [(μ-H)$_4$Ru$_4$(CO)$_{12}$] and their application in the hydrogenation of an α,β-unsaturated carboxylic acid**

Ahmed F. Abdel-Magied, Maitham H. Majeed, Manuel F. Abelairas-Edesa, Arne Ficks, Radwa M. Ashour, Ahibur Rahaman, William Clegg, Matti Haukka, Lee J. Higham, Ebbe Nordlander. *J. Organomet. Chem.* 849-850 (**2017**) 71-79.

† Equal contribution

My contributions to the publications

I.   I have performed all the synthesis work, except for the X-ray characterization. I wrote most of the article.

II. I have participated in planning of the project, performed all the experiments including the design and the synthesis of the catalyst, I did the single crystal and powder X-ray diffractions, I have participated in the TEM, SEM, SSNMR and XPS measurements and the data analysis. I wrote most of the article.

III. I have conceptualised the project. I performed all the experiments and I have participated in the TEM, SSNMR and XPS measurements and the data analysis. and I have participated in planning and performing the continuous flow experiments. I wrote most of the manuscript.

IV. I have conceptualised the project. I performed all the experiments and I have participated in the TEM and XPS measurements and the data analysis. I wrote the full manuscript.

V.   I have conceptualised the project. I have designed and supervised all the experiments. I have participated in the TEM and XPS measurements and the data analysis. I did the X-ray characterisation. I wrote the full manuscript.

VI. I have participated in planning of the project and performed most of the experiments. I participated in the XAS measurements and collaborated on the interpretation of the data. I wrote part of the manuscript.

Populärvetenskaplig sammanfattning

Katalys är ryggraden i många processer i vardagen. Även människokroppen styrs huvudsakligen av katalysatorer. Detta viktiga koncept tillåter oss att på ett miljövänligt sätt konvertera råmaterial som råolja och naturgas till värdefulla och oersättliga produkter, till exempel motorbränslen, läkemedel och agrokemikalier. En katalysprocess drivs av en katalysator, vilket således är en substans som, utan att förbrukas under processen, gör reaktionen snabbare och mer selektiv genom att förändra reaktionsvägen.

Kolvätebindningar (C–H-bindningar) är bland de mest stabila och oreaktiva kemiska bindningarna och dessa återfinns i hög utsträckning i de flesta kolkällor i naturen, inte minst råolja. Att hitta en miljövänlig väg för att konvertera eller klyva C–H-bindningar är en process som brukar kallas C–H aktivering, och denna metod för att producera användbara material har blivit en central frågeställning för organiska kemister under de senaste decennierna. Utveckling av katalysatorer är en av nycklarna för att lösa detta.

I denna avhandling framställdes palladium baserade molekyler som deponerats på bärare för att få heterogena katalysatorer för C–H-aktiveringsreaktioner, som till exempel oxidation och halogenering av arener, vilket är väldigt viktiga transformationer inom läkemedels- och agrokemikalieindustrin. Heterogena katalysatorer kännetecknas av de är lätta att separera från reaktanter och produkter. För att simulera storskaliga applikationer testades dessa katalysatorer också i kontinuerlig flödesproduktion, där de visade sig ha hög aktivitet och stabilitet över tiden.

Avhandlingen uppfyllde framgångsrikt de uppställda målen att syntetisera, tillämpa och förstå dessa katalysatorer.

Abbreviations

Ag–NHC	Silver(I) N-heterocyclic carbene
AIBN	Azobisisobutyronitrile
BDEs	Bond dissociation energies
BF	Bright field
C–H	Carbon–hydrogen
CMD	Concerted metallation deprotonation
CP	Cross polarization
DVB	Divinylbenzene
ESCA	Electron spectroscopy for chemical analysis
EXAFS	Extended x-ray absorption fine structure
FFT	Fast fourier transform
GC	Gas chromatography
GC-MS	Gas chromatography-mass spectrometry
GO	Graphene oxide
HAADF	High-angle annular dark-field
HOMO	Highest energy occupied molecular orbital
HRMASS	High-resolution mass spectrometry
HRTEM	High-resolution transmission electron microscopy
ICDD	International center for diffraction data
ICP-OES	Inductively coupled plasma-optical emission spectroscopy
IR	Infrared
MAS	Magic angle spinning
MeCN	Acetonitrile
MesI(OAc)$_2$	Diacetoxy(mesityl)-λ3-iodane
MMO	Methane monooxygenase
MOF	Metal organic framework
MS	Mass spectrometry
NAD(P)	Nicotinamide adenine dinucleotide phosphate
NHC	N-heterocyclic carbene
NMP	N-methyl-2-pyrollidone
NMR	Nuclear magnetic resonance
NPs	Nano particles

OAc	Acetoxy
OTf	Triflate
PAHs	Polycyclic aromatic hydrocarbons
PEPPSI	Pyridine-enhanced precatalyst preparation stabilization and initiation
$Pd(TFA)_2$	Palladium(II) trifluoroacetate
PIDA	Diacetoxyiodo benzene
PXRD	Powder x-ray diffraction
rGO	Reduced graphene oxide
r.t.	Room temperature
SEM	Scanning electron microscopy
SS-NMR	Solid-state nuclear magnetic resonance
STEM	Scanning transmission electron microscopy
SWNTs	Single-walled carbon nanotubes
TEM	Transmission electron microscopy
TGA	Thermogravimetric analysis
TMs	Transition metals
TOF	Turnover frequency
TON	Turnover number
UV-vis	Ultraviolet-visible
XANES	X-ray absorption near edge spectroscopy
XAS	X-ray absorption spectroscopy
XEDS	X-ray energy dispersive spectroscopy
XPS	X-ray photoelectron spectroscopy
XRD	X-ray diffraction

Acknowledgement

To all my family members, specially to my best friend my brother Muthana, you make my world special just by being in it, thanks for helping me whenever I needed, *Hala Madrid…*

Many people walk in, or walk out of my life but only the one that left footprints in my heart, is my wife Ikram, the words cannot explain how grateful I am to have you in my life, your love, understanding, and support enabled me to withstand in life and because of you I could finish my PhD, I wish you all the success in your career.

But most of all… to the driving force in my life, my daughters and son Sama, Reem and Hassan. Your smiles and jokes giving me the strength and energy to start every day, *love you* ♡*…*

1. General Introduction

1.1. C–H Activation

Everything in the universe seeks to be stable, and this stability can be reached when it is at the lowest level of energy. In chemistry, all chemical elements tend to reach the lowest energy state (highest entropy) by achieving noble gas configurations. However, this is done according to the laws of Nature either by losing, acquiring, or sharing an electron or more from the outer shells to obtain what is known to us in this era as the *chemical bond*.

Carbon–hydrogen (C–H) bonds are among the most stable and unreactive chemical bonds in Nature. In organic chemistry, we usually draw the benzene moiety for instance without indication to C–H bond. This invisibility of C–H bonds reflects their lack of reactivity and their prevalent nature in our world. However, this characteristic inactive nature is due to the significant high bond dissociation energies (BDEs) required to cleave C–H bonds as shown in Figure 1.1. From the kinetics' point of view, the C–H bonds are free of appropriate lone pairs of electrons to make them reactive and facilitate the cleaving transformations.[1,2]
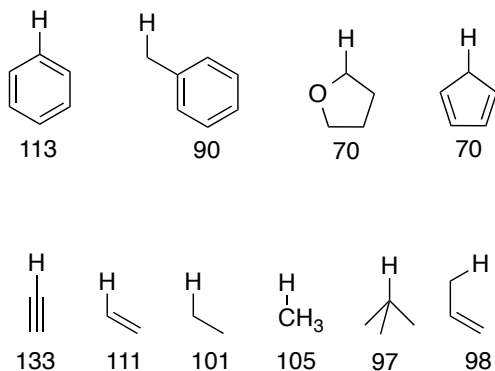
Figure 1.1. Experimental bond dissociation energies (BDEs) of common carbon–hydrogen bonds.

The majority of organic products for example engine fuels, pharmaceuticals, and agrochemicals are obtained from feedstocks such as crude oil and natural gas. However, these organic molecules contain diverse functional groups in their chemical structure (Figure 1.2), therefore finding environmentally friendly pathways to convert crude carbon sources to useful materials has become a central concern of organic chemists in the past decades.
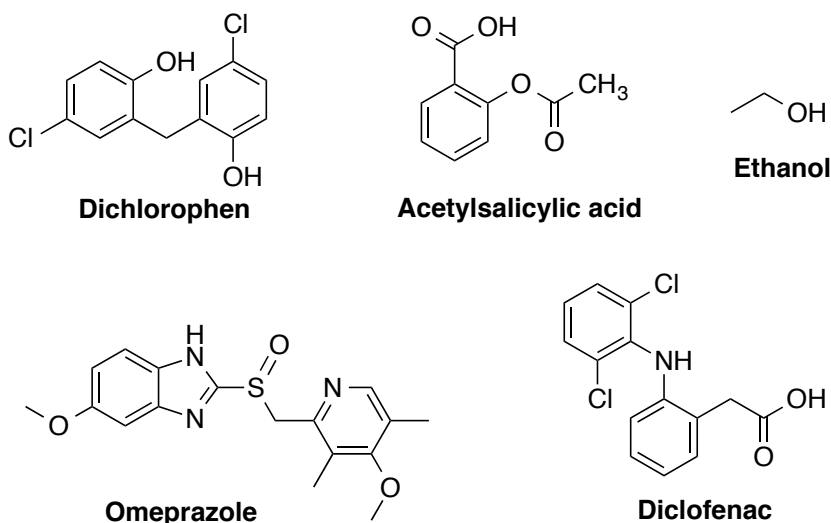
Figure 1.2. Common examples of desired commodity chemicals and pharmaceutical products.

Illustrated by Table 1.1, traditional chemical industry processes using stoichiometric reagents offer high E-factor, meaning greater negative environmental impact according to Sheldon.[3] The central challenge confronting us today is, how do we produce the prevalent chemical products cheaply, greenly and by an efficient way?

Table 1.1. Waste generation in different types of industry. Adapted from ref. 3.

Industry process	Product tonnage[a]	E-factor (Kg waste/ Kg product)
Oil refining	10^6-10^8	<0.1
Bulk chemicals	10^4-10^6	<1-5
Fine chemicals	10^2-10^4	5->50
Pharmaceuticals	10-10^3	25->100

[a]Annual production volume of a product at one site.

17

However, mother nature has engineered over billions of years ago to carry out the chemical transformations in water and at ambient temperature, in high efficiency, with shorter synthesis steps, low toxicity of chemical products, and low E-factor. A very good example in this regard, methanol production by Methane monooxygenase (MMO) multiprotein complexes found in methanotrophic bacteria, which shows a high capability to activate the C–H bond in methane under aerobic conditions. The mechanistic manifold involves, when two equivalents of NAD(P)H (reducing agent) split the O–O bond of oxygen, one oxygen atom is reduced to water and the second atom is incorporated into the substrate, yielding methanol as shown in Figure 1.3. [4, 5]
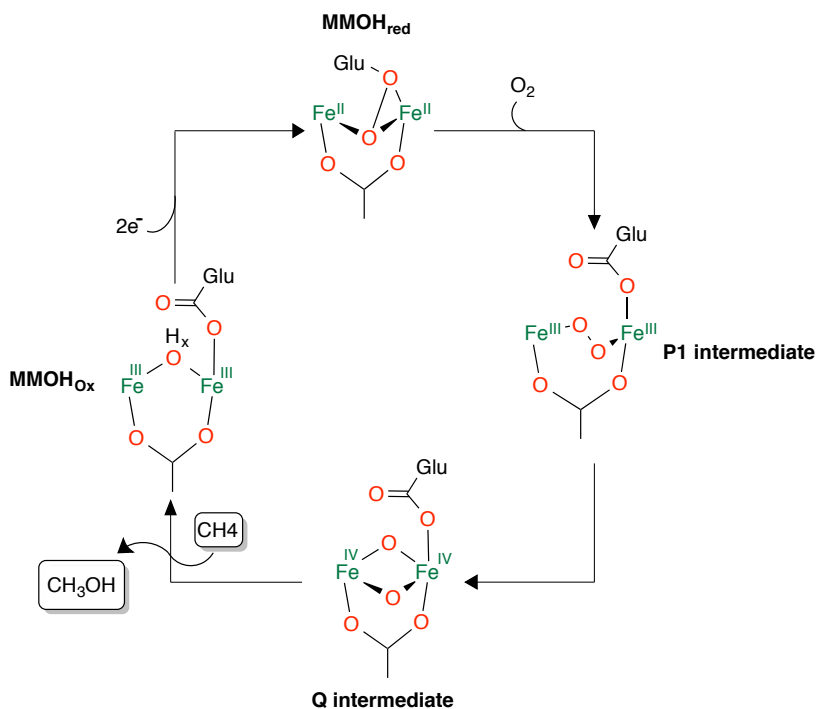
Figure 1.3. Pathway of aerobic methane oxidation by Methane monooxygenase (MMO) multiprotein.

Obviously in this example, the methane oxidation reaction carried out over an iron-iron core, which enables the reaction to proceed by stabilizing the intermediates, without being consumed, and minimizing the waste during the process. From this point, an important concept is proposed, which is considered as the key to green chemistry and an important tool in organic reactions called *Catalysis*.

1.2. Background to catalysis

The concept of *Catalysis* was introduced for the first time in 1820 by J. J. Berzelius in his annual review articles to the Royal Swedish Academy of Sciences. Later, M. Faraday assumed (without explanation) that the hydrogen and oxygen have to adsorb at platinum surface in order for the electrolysis of water take place.[6] In 1835, Berzelius described and defined the observed phenomenon as a *Catalysis*. This term remained incomprehensible for the chemical society and the scientists until 1900, where W. Ostwald (Nobel laureate in chemistry 1909) accomplished the definition of the catalyst as "A substance which affects the rate of a chemical reaction without being part of its end products".[7] According to this definition, the catalysis is considered as a kinetic phenomenon.
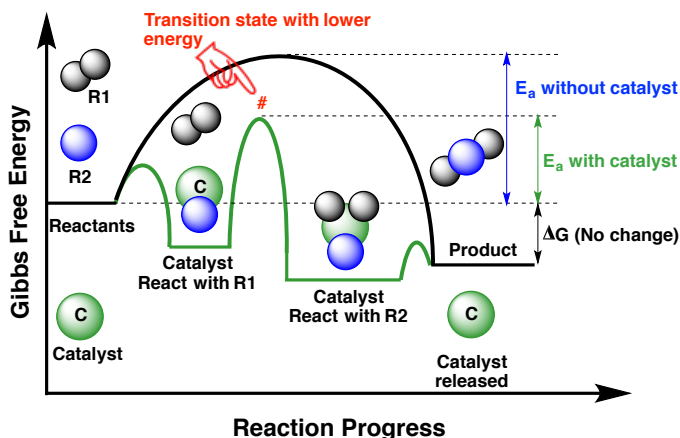
Figure 1.4. Catalysts reduce the required activation energy, thereby increasing the rate of reaction.

In the present day, *Catalyst* is accurately defined as a substance that makes the reaction go faster and more selective by changing the path of the reaction or by stabilizing the reaction transition states, without being consumed during the process. Figure 1.4 shows the difference in activation energy between an uncatalyzed reaction (of R1 and R2 reagents) and a catalyzed reaction in the presence of a catalyst (C). However, the uncatalyzed reaction displays a high energy barrier, which leads to a slow reaction in the end. In contrast, the reaction of R1, R2 and C is energetically more favored (lower energy barrier), therefore it accelerates the reaction via combining and stabilizing R1 and R2 reagents with help of C (in a transition state #) in the way that makes them more capable to react and form the

final product. The regenerated catalyst (C) is unconsumed and able to be used in another cycle.

1.3. Catalysis: A step towards a sustainable world

From a fundamental perspective, adding an excess of R1 or R2 reagent or heating the reaction in Figure 1.4, waste formation, production of stoichiometric amounts of byproducts, and waste of energy are inevitable. However, catalysis is considered as a clean and efficient alternative way to produce the desired commodity chemicals and pharmaceutical products in high atom economy. A good example of this is the transformation of secondary alcohol to a ketone. The uncatalyzed oxidation of methylbenzyl alcohol using stoichiometric quantities of Jones reagent (chromium trioxide in sulfuric acid) offers acetophenone in 44% atom economy as shown in Scheme 1.1a.[8] The formation of chromium sulfate as a byproduct and using carcinogenic chromium(VI) reagent are the main drawbacks of this reaction.
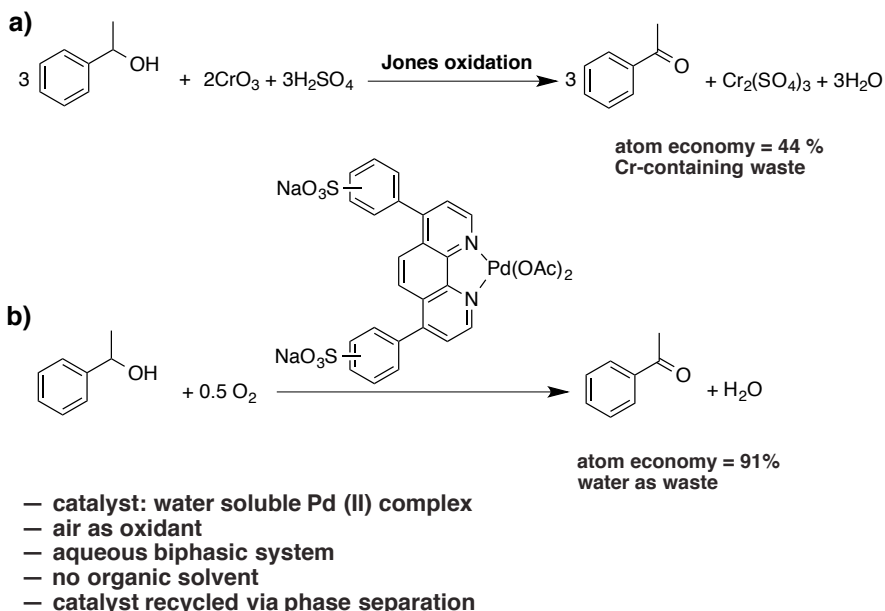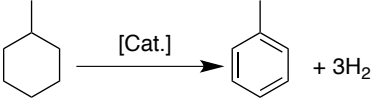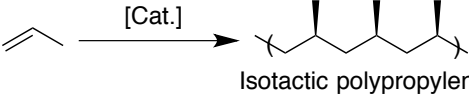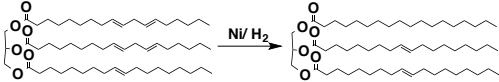
Scheme 1.1. Oxidation of methylbenzyl alcohol to acetophenone via **a)** uncatalyzed, and **b)** catalyzed pathway. Modified from ref. 8, 9.

In contrast, water soluble Pd(II) catalyzed solvent free aerobic oxidation of methylbenzyl alcohol affording the corresponding ketone in high yield and 91% atom economy, with no loss of activity (Scheme 1.1b).[9]

1.4. Heterogeneous, homogeneous, and heterogenized catalyst

In line with the context of this thesis, it is very important to highlight and understand the term *heterogeneous* in catalysis world, because it will be used many times in the following chapters. Thus, *heterogeneous catalysis* is the catalytic process in which the catalyst and the reactants are in different phases. In this case and based on the modern definition of catalysis, a *heterogeneous catalyst* is "a functional material that continually creates active sites with its reactants under reaction conditions, these sites change the rates of chemical reactions of the reactants localized on them without changing the thermodynamic equilibrium between the materials"[10]. Approximately 90% of the industrial catalytic processes are heterogeneously catalyzed,[11] some examples are shown in Table 1.2.

Table 1.2. Examples of industrial processes using heterogeneous catalysis.

process	Reaction	Cat.	Product
Fischer-Tropsch process	$(2n+1)\ H_2 + n\ CO \xrightarrow{[Cat.]} C_nH_{(2n+2)} + n\ H_2O$	Fe, Co	C5-C11 hydroc-arbons
Methanol production	$CO + 2H_2 \xrightarrow{[Cat.]} CH_3OH$	Cu/ZnO/ Al$_2$O$_3$	Methanol
Haber-Bosch process	$N_2 + 2H_2 \xrightarrow{[Cat.]} 2NH_3$	Fe	NH$_3$
Dehydrogenation process	$\xrightarrow{[Cat.]}$ + 3H$_2$	Pt/ Al$_2$O$_3$	Alkenes
Polymerization	$\xrightarrow{[Cat.]}$ Isotactic polypropylene	Ziegler–Natta catalyst Ti	Polymers
Margarine manufacture/ Hydrogenation	$\xrightarrow{Ni/\ H_2}$	Ni or Pd	saturated organic compou-nds

Due to its competitive advantages, like economical, high stability and reactivity, easy to separate and recover, recyclable, and their use in continuous flow processes,

heterogeneous catalysts have a considerable standing in the industry and green chemistry disciplines.

Nevertheless, low selectivity, difficulties to tune and modify, and the requirements of the specialized set of advanced techniques to define the structure and reaction mechanisms (e.g. X-ray methods, operando spectroscopies…etc.) remain unsolved issues in heterogeneous catalysts.[12] In homogeneous catalysis, reactants, product(s), and the catalyst are in the same phase, therefore, this process faces major challenges, like product separation, economic cost, metal contamination, short catalyst life time and recovery. Thus, the presence of homogeneous catalytic processes in the chemical industry is significantly more modest compared to the heterogeneous catalytic reactions. However, although the instability factor related to most homogeneous catalysts, homogeneous catalysts are employed in many important industrial processes as shown in Table 1.3.

Table 1.3. Examples of industrial processes using homogeneous catalysis.

process	Reaction	Cat.	Product
Shell higher olefins process (SHOP)[13]	$x\,H_2C{=}CH_2$ $\xrightarrow[69\text{-}138\ bar]{80\text{-}120\ ^oC}$ $H_2C{=}CH(CH_2CH_2)_{x\text{-}1}H$	Ni^{II}	Medium-long chain olefins
Hoechst-Wacker oxidation process[14]	$H_2C{=}CH_2 + 1/2O$ $\xrightarrow{[PdCl_4]^{-2}/CuCl_2/HCl}$ CH_3CHO	$Pd^{II}/$ Cu^{II}	Acetald-ehyde
Hydroformylation (Oxo process), aldehydes from alkenes.		Co^0 or Rh^0	Aldehyde
Monsanto process/ Cativa process	$CH_3OH + HI$ $\xrightarrow{[Ir(CO)_2I_2]^-\ or\ [Rh(CO)_2I_2]^-}$ CH_3COOH	Ir^{II} or Rh^{II}	Acetic acid

On the other hand, homogeneous catalysis uses reaction conditions milder than for heterogeneous catalysis, and the high activity and selectivity can be possibly tuned either by using different ligands/ additives or by modifying the ligand/ catalyst system. Additionally, investigation of the reaction mechanism directly in solution is possible, by using common spectroscopic methods such as IR, NMR, UV-Vis, MS... etc..

Today, tethering these two fields by attaching covalently (but not always[15] as we will see in papers IV and V) well defined and discrete catalyst molecules to an insoluble support, is still an ongoing goal in catalysis (example of that shown in Figure 1.5). The modification of homogeneous catalysts, which is so called-

22
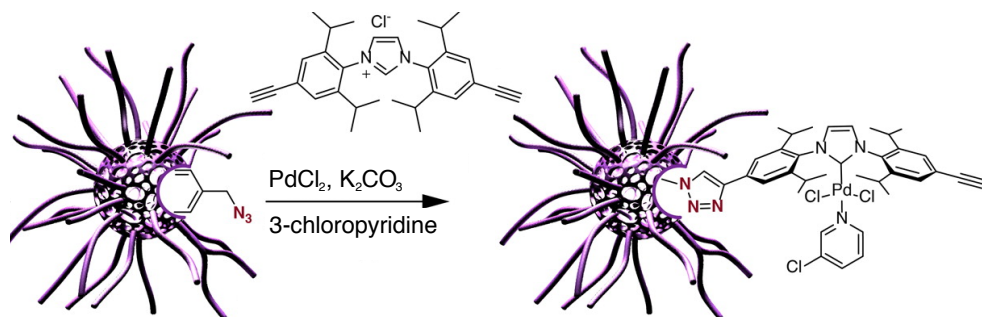
Figure 1.5. Immobilization of palladium N-heterocyclic carbene cross-coupling reactions catalyst in the core of a star polymer, makes it easily recoverable and recyclable catalyst. Modified from ref. 17.

-heterogenization, will adjust the homogeneous nature of the original catalyst, by making it:[16]

1) Easily recoverable and reusable (easy product separation, less waste, and less expensive).
2) More efficient (taking advantages from the support to increase selectivity, affinity…etc.).
3) Discrete catalyst sites (no dimerization or agglomeration increasing the life time of the catalyst).
4) Possible to use in continuous flow process (facilitate the continuous implementation of synthetic reactions, as described in paper III).

Although, massive efforts have been made in immobilization of homogeneous catalysts, none of these immobilized catalysts have been used by industry so far.[18] The main reasons for that is due to:

1) Instability of the homogeneous catalysts, thus heterogenizing them is pointless.
2) Use of an expensive support.
3) Metal leaching and low turnover numbers, making these catalysts not suitable for industrial use.
4) The heterogenized system could be too complicated to characterize and develop.

However, to get a heterogenized catalyst fitting to the industrial applications (Generally, for industrial applications, the TOF and TON have to be in the ranges 10^{-2}-10^2 s^{-1} and 10^6-10^7 respectively),[19] the shortcomings mentioned need to be addressed, and this is the main theme of this thesis.

1.5. N-heterocyclic carbene: Synthetic toolkit

Since the first crystalline free carbene was isolated by A. J. Arduengo in 1991, *N*-heterocyclic carbene (NHC) ligands have garnered considerable attention in both academia and industry.[20, 21] However, NHC has emerged as a powerful metal supporting ligand in many important chemical transformations such as hydrogenation,[22] olefin metathesis,[23] water splitting,[24] hydrosilylation,[25] solar energy and photocatalysis,[26, 27] etc., due to the tuning capability of electronic and steric properties of the metal complexes (Figure 1.6a). The electronic structure of M–NHC bond shows a domination of σ-donation from the HOMO of the NHC ligand, located on the carbene C atom to empty d orbitals of the metal. However, the most recent model suggests the π-acid feature of the NHC ligands by accepting back-donation from filled d orbitals of metals (Figure 1.6a). [28-31]
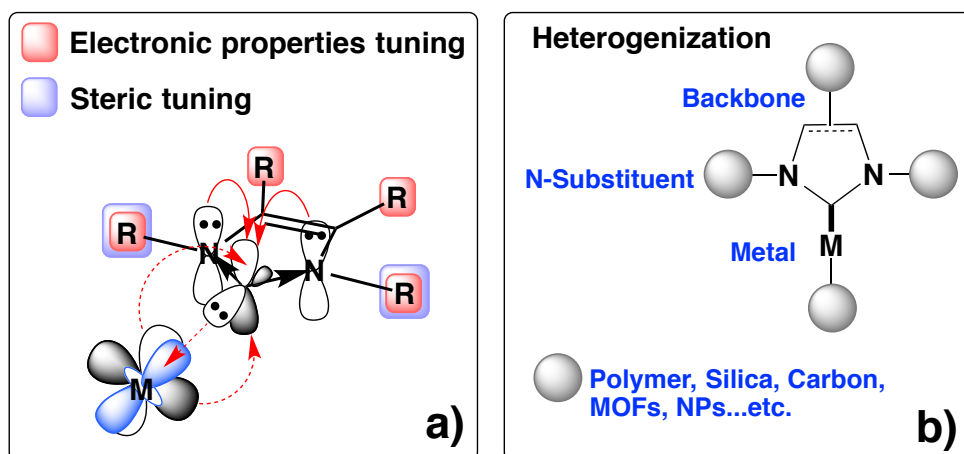
Figure 1.6. The electronic features of M–NHC. **b)** positions can be used to heterogenize M–NHC complexes.

Tuning the electronic properties of NHC ligand has a significant influence over the ligand donicity, therefore it is a critical issue when optimizing the catalytic activity of transition metal based complex. However, structural modification is required to tune the donation ability, which predominantly includes:

1) The substituents on the NHC backbone.[32]
2) The N-substituents.[33]

The positions which are available to use to immobilize M–NHC complexes are summarized in Figure 1.6b.

1.6. C–H activation in continuous flow reactors

The operation of a chemical reaction in a continuous manner under controlled conditions and using mini or micro flow reactors, is known as a *Continuous Flow Synthesis*. Compared to the batch reaction mode, continuous flow processes made a significant mutation from the early stage lab research to industrial sector in the past decades. However, it offers attractive advantages in terms of the safety (no accumulation of highly unstable intermediates), reaction efficiency (saving in time and materials), and atom economy (by reducing in the use of environmentally harmful chemicals, and minimizing side reactions).[34] In recent years, supported palladium *N*-heterocyclic carbene complexes catalyzing C–H activation and C–C bond formation in continuous flow regimes have gained a great interest in the catalysis communities.[35-40] However, the advantages that a continuous flow process brings is more efficient, high catalytic activity even at room-temperature, and high selectivity (will be discussed later in paper III) for C–C and C–H functionalization reactions, which meets the standards for production of biologically active molecules and pharmaceutical industry.[41]

1.7. Objective of this thesis

This thesis aims at:

i. *Developing* heterogeneous transition metal based catalyst materials for selective C–H activation of hydrocarbons based on self-supporting and π–π stacking methodologies. The proposed methodologies are able to combine the high chemical reactivity of the synthesized metal complexes with the unique properties of the solid supports.

ii. *Understanding* the nature and character of these novel systems, based on spectroscopy techniques, microscopy, operando spectroscopy and theoretical calculations. The center of attention is to improve the catalyst design in such a way that increases the activity, reusability, and sustainability of these systems.

iii. *Applying* the catalysts for continuous flow conditions to allow scale up of the process and to fully utilize the potential of heterogeneous catalysis in C–H activation.

2. Functionalized Pd(II)–NHC complexes: Synthesis and characterization (Papers I-V)

2.1. Introduction

Since the discovery of the synthesis routes of N-heterocyclic carbene (NHC) ligands and complexes particularly with the transition metals (TMs), TMs–NHC have become universal complexes in organometallic, inorganic coordination chemistry, and homogeneous catalysis. Free carbenes show a considerable stability under inert conditions, however these reaction intermediates are unstable in the presence of oxygen and moisture, thus hindering their commercial availability in large quantity. Therefore, the unusual stability of imidazolium precursor over free carbenes made them significant and easy alternative substrates to synthesize TMs–NHC complexes. The historical success story begins in 1968, when Öfele and Wanzlick reported the first TM–NHC complexes derived from the reaction of imidazolium salts with a transition metal hydride, and transition metal acetate respectively as shown in Scheme 2.1. [42-46]
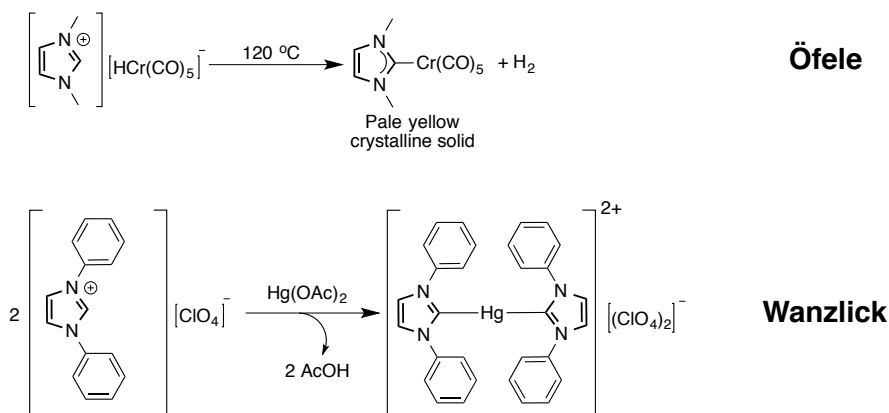
Scheme 2.1. Synthesis pathways of the first TM–NHC complexes. Modified from ref. 46.

2.2. Synthesis of functionalized imidazolium salts and silver(I)–carbene complexes

In general, there are three synthetic routes to obtain imidazolium salts bearing different functionalities, which is required to immobilize or support homogeneous catalyst into insoluble materials:

1) Nucleophilic substitution on the imidazole heterocycle ring.[45]
2) Modification of functional groups already present in the backbone of imidazolium salts or imidazole heterocycle ring to appropriate substituents.
3) Building up the imidazole heterocycle ring with the desired functional group already in place.[45]

The first method, *Direct Quaternization*, is the most straightforward to generate functionalized imidazolium salts in one synthesis step. Mostly, by reacting functionalized or unfunctionalized alkyl halides with N-substituted imidazoles the products are afforded as precipitated salts (easy to purify and separate by washing with solvents and simple filtration respectively) in good to excellent yields as shown in Scheme 2.2.[21, 47]
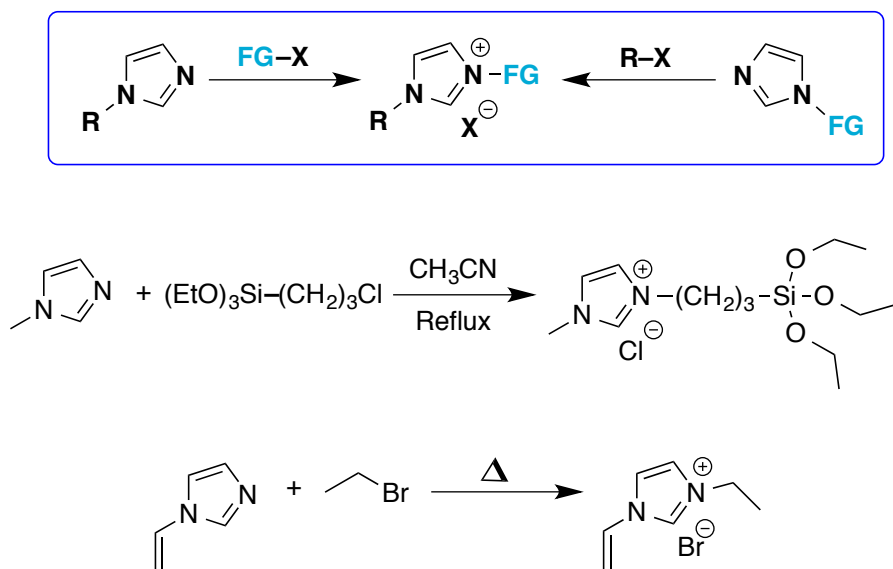
Scheme 2.2. Selected examples of *direct quaternization method* to form functionalized imidazolium salts. Modified from ref. 21.

In our study, we started to synthesize different functionalized imidazolium salts based on the desired heterogenization method, adapting the *Direct Quaternization* method. As shown in Scheme 2.3, the procedure to install either one or two polymerizable arms on the N-heterocycle ring is a well-known nucleophilic substitution reaction that usually proceeds under mild reaction conditions affording moderate to good yields.[48-51] Adapting a similar reaction fashion, imidazolium salts tagged either with one or two anthracene moieties were produced successfully in comparable yields. [50, 52]
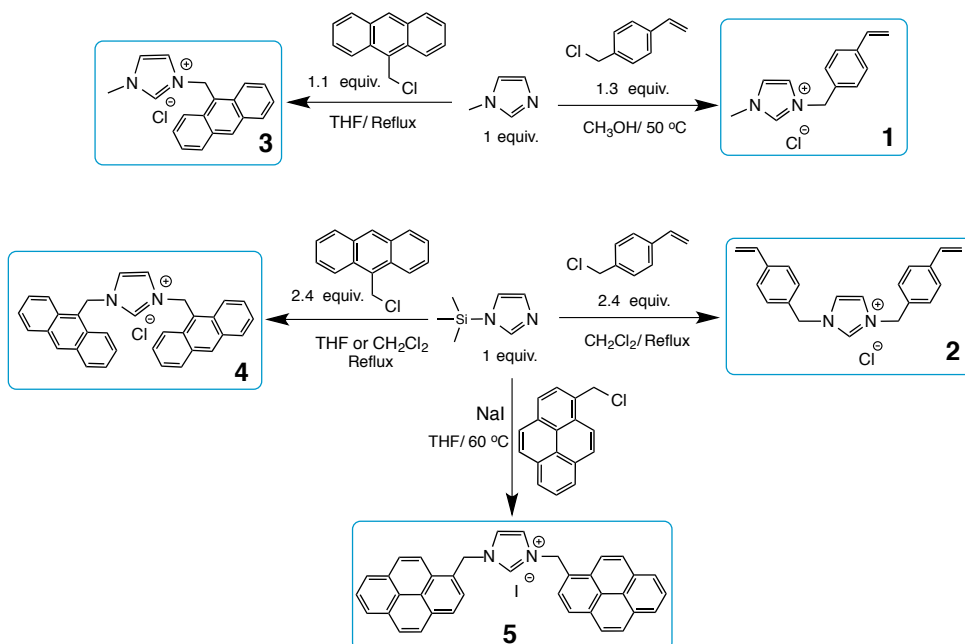
Scheme 2.3. Synthesis of **1-5**

Furthermore, we were interested in expanding the scope of double tagged species, and our choice was centered on pyrene, due to the extraordinary π-stacking character of such ligand.[53] Attempts to synthesize an imidazolium chloride salt from 1-(chloromethyl)pyrene and 1-(trimethylsilyl)-1*H*-imidazole were unsuccessful, due to the lack of reactivity of the ligand. However, substituting chlorine with iodine in-situ by adding sodium iodide to the reaction offered imidazolium iodide salt **5** in good yield.
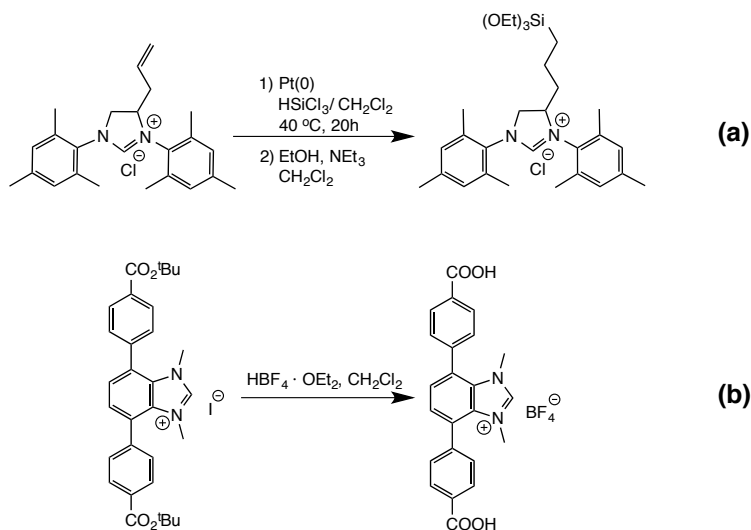
Scheme 2.4. Examples of modification of functional groups already present in the backbone of imidazolium salts. Modified from ref. 54, 55.

In contrast, to get the required substituents for the heterogenization purposes, the functionalization step might occur on a functional group that is already attached to the imidazolium salts or imidazole heterocycle ring at an earlier synthesis stages. In the Grubbs lab, they reported Pt(0) catalyzed hydrosilylation of functionalized NHC chloride salt using $HSiCl_3$ and subsequent treatment with ethanol/NEt_3 produced the triethoxysilyl backbone functionalized NHC salt (Scheme 2.4a).[55] In another example, Yaghi and co-workers reported the deprotection of the synthesized diester with $HBF_4 \cdot OEt_2$ affording the desired dicarboxyl functionalized NHC precursor for Metal-Organic Framework (MOF) synthesis (Scheme 2.4b).[54, 55]

In line with this, and for the modification purposes, the vinyl group on the backbone of 4-vinylimidazole was installed by decarboxylation of urocanic acid as illustrated in Scheme 2.5.[56] The preparation of 1-vinylimidazolium salt **6**, which has been similarly described in the same literature, does not present the synthetic challenges inherent in the sensitivity of the 1-trimethylsilyl-4-vinylimidazole analogues to air and moisture.
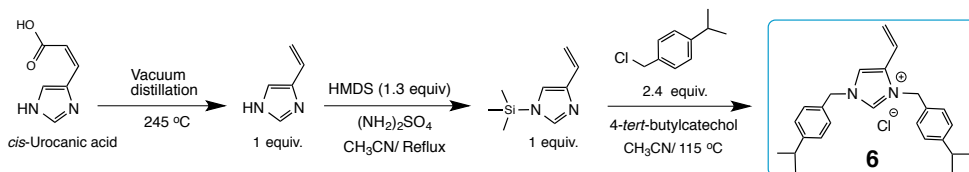
Scheme 2.5. Synthesis of **6** via functional group modification strategy.

All the precipitated salts (**1**-**6**) were simply isolated by filtration or recrystallization method, purified by washing with organic solvents, characterized by ^{1}H NMR, ^{13}C NMR spectroscopy and elemental analysis, and they are easy to handle and store under ambient conditions.

Other synthetic routes

Many examples have been reported in the literature outlining the cyclization synthetic steps, to prepare functionalized imidazolium salts. Generally, there are many procedures depending on the final ring closing step, in which the use of a cyclization reagent, usually ortho-formate, is inevitable (Scheme 2.6).[21, 55]
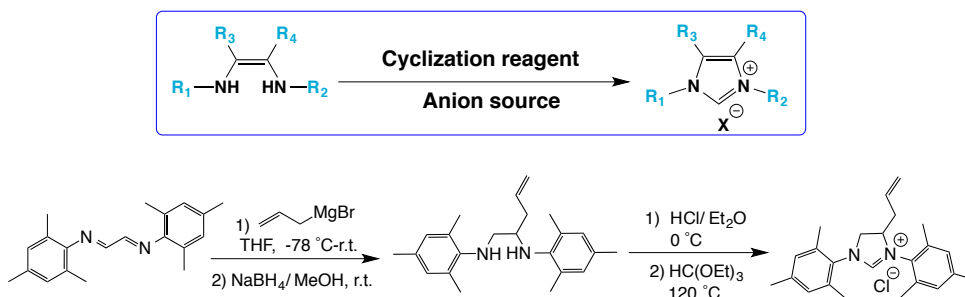
Scheme 2.6. Introduction of C2 carbon to form the functionalized NHC salts at the final step via cyclization synthetic route.

Silver(I)–carbene complexes (Ag(I)–NHC)

Ag(I)–NHC complexes are easy to synthesize and less air sensitive than free carbenes, therefore they gained a considerable role as carbene transferring agents. The lability of Ag–C$_{carbene}$ bond allow them to be easily used in further transformations such as transmetallation to diverse transition metals.[46, 57, 58] Hence, and in addition to the mentioned advantages of the silver intermediates, we noticed in our study that the use of silver intermediates precluded any radical polymerization of the vinyl moiety at an earlier stage. Other protocols use harsh reaction conditions under which such unwanted side reactions could occur.[59] A series of Ag(I)–NHC chloride complexes were prepared by the reaction of functionalized imidazolium salts with Ag$_2$O or Ag$_2$CO$_3$ at ambient temperature as shown in Scheme 2.7. **3a** and **4a** were obtained in good yields using methanol as a reaction solvent instead of dichloromethane.
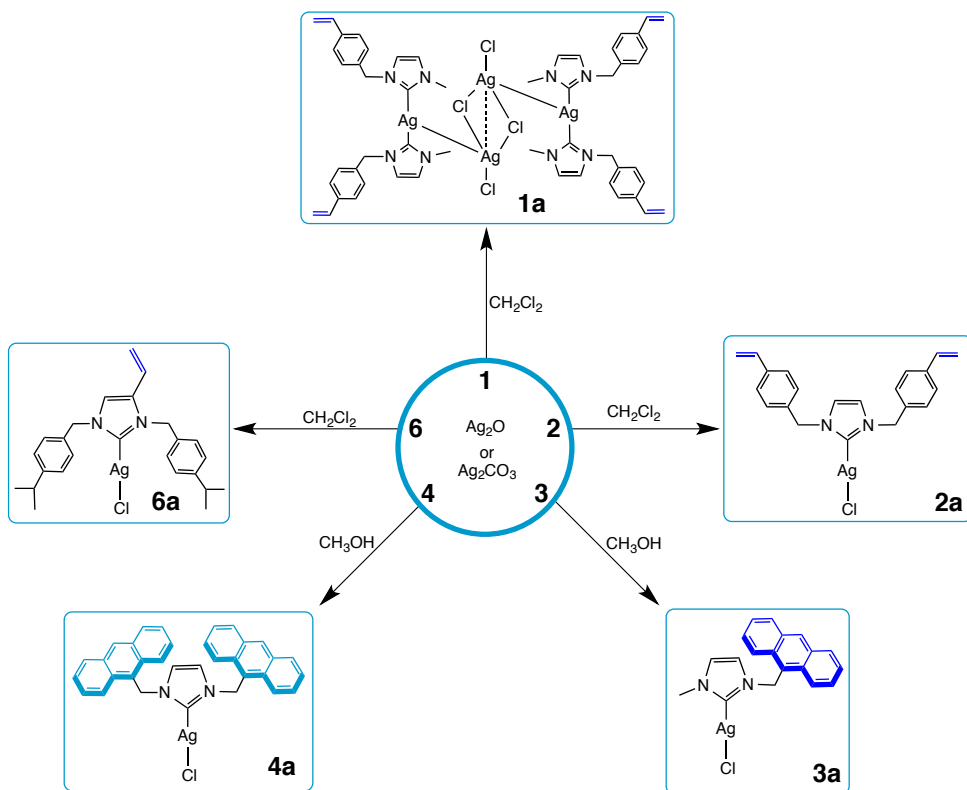
Scheme 2.7. Synthesis pathways of Ag(I)–NHCs intermediates (**1a-4a** and **6a**). In all reactions, Ag$_2$O was added to the soluble mixture except for **6a**, where Ag$_2$CO$_3$ was used in order to increase the yield.

^{13}C NMR spectra of these silver intermediates showed the characteristic carbene signals around 169-180 ppm.[60-62] All reactions were carried out with exclusion of light, and the products slowly decomposed within a week to a month under air and light.

2.3. Functionalized Pd(II)–NHC complexes

(For example, but not limited to), N-heterocyclic carbene transition metal complexes are synthesized by:[63]

1) The *in situ* reaction of a transition metal complex with a free carbene.
2) The reaction of a transition metal complex with an imidazolium salt possessing a basic anion.
3) The use of carbene transfer agent.

4)   The reaction a transition metal salt with an imidazolium salt in the presence of a weak base.

In our study, we employed the carbene transfer agent methodology, due to the above-mentioned reasons, to synthesize functionalized N-heterocyclic carbene Pd(II) (Pd(II)–NHC) complexes as summarized in Scheme 2.8.
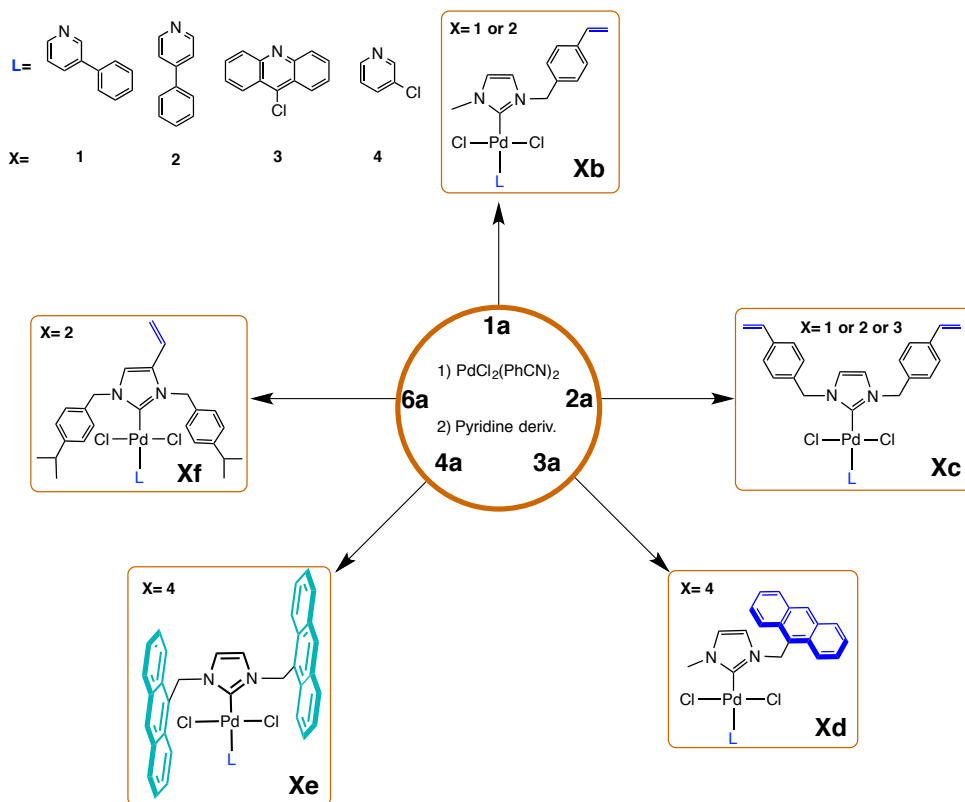
Scheme 2.8. A summary of the synthesis pathways (via carbene transfer agent) of functionalized Pd(II)–NHC complexes. In all reactions, PdCl$_2$(PhCN)$_2$ was added to the soluble mixture of Ag(I)–NHCs in CH$_2$Cl$_2$ or CH$_3$CN. The final products are formed by addition of pyridine derivatives to Pd(II)–NHC dimers.
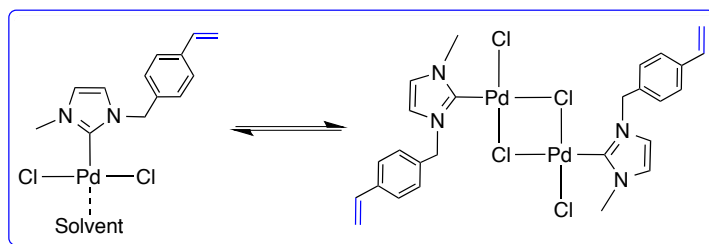
Scheme 2.9. Putative dynamic equilibrium.

Noteworthy, transmetallation of Ag(I)–NHCs with $PdCl_2(PhCN)_2$ afforded functionalized Pd(II)–NHC dimers, which showed broad signals in ^{1}HNMR spectra due to the dynamic equilibrium between monomeric and dimeric species as shown in Scheme 2.9. Adding pyridine derivatives gave the functionalized Pd(II)–NHC monomers (bearing polymerizable vinyl moieties) in excellent yields (Scheme 2.8). The complexes were characterized by ^{1}H, ^{13}C NMR spectroscopy, and the molecular structures were confirmed by X-ray diffraction (XRD) analysis (Figure 2.1).
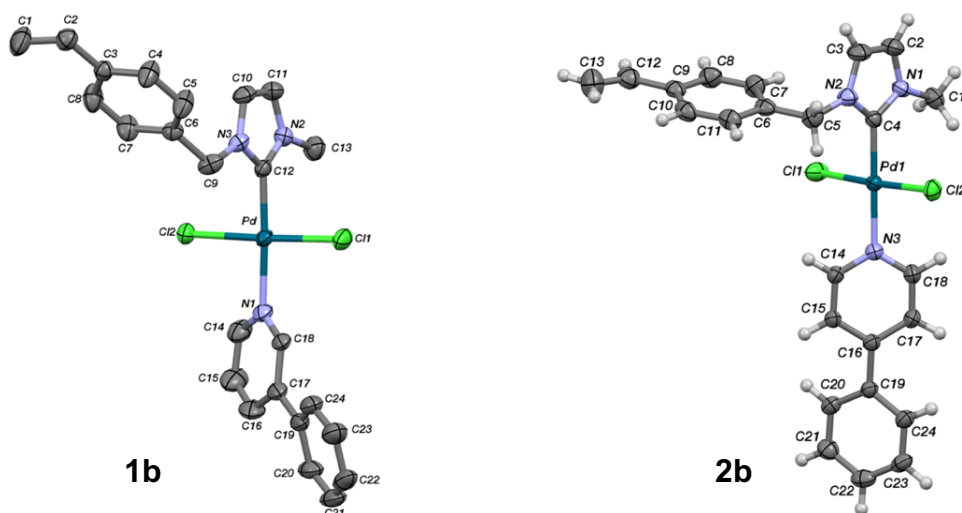
Figure 2.1. Molecular structures of **1b**, **2b**, **1c**, and **3c** with thermal ellipsoids displayed at 50% probability. Disorder was observed in the crystal of **1b**. Selected bond lengths (Å) and bond angles (°) with estimated standard deviations of **2b** crystal: Pd1–C4 1.9532 (16), Pd1–N3 2.0938 (14), C4–Pd1–N3 179.52(6), Cl1–Pd1–Cl2 176.789 (17). Modified from papers I and II.
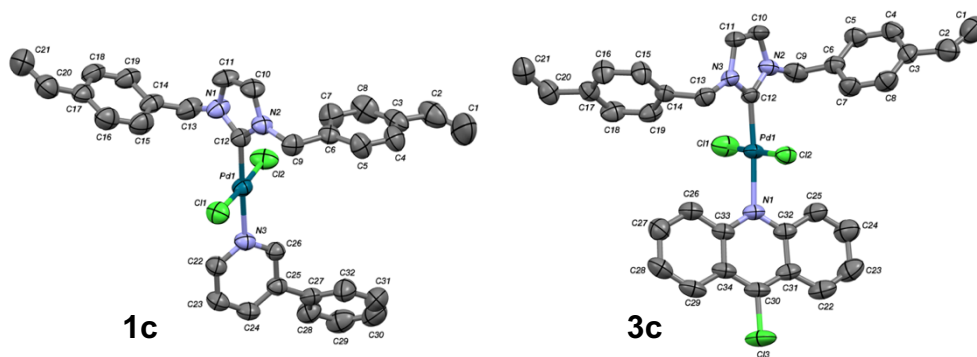
Figure 2.1. Continued.

Single and double anthracene tagged Pd(II)–NHC complexes (**4d** and **4e** respectively) were synthesized in a similar fashion to the functionalized Pd(II)–NHC monomer analogues. However, the solubility of complex **4a** was very challenging through the synthesis steps, therefore it was difficult to run the reaction at ambient temperature. However, refluxing intermediate **4a** in CH_3CN afforded **4e** in good yield. The formation of complex **4d** was remarkably more facile than preparation of analogue **4e**, and the reaction could be performed at ambient temperature. The product was characterized by NMR spectroscopy and XRD as illustrated in Figure 2.2. Initial attempts to prepare a double tagged pyrene Pd(II)–NHC complex **4g** from **5** proved difficult, due to the lack of solubility of the imidazolium salt in many solvents. The *in situ* reaction of $PdCl_2(PhCN)_2$ precursor with the corresponding free carbene to form **4g** was revealed to be an ineffective approach and afforded very low yield (Scheme 2.9). The resulting compound was studied by NMR spectroscopy and X-ray methods as shown in Figure 2.2.
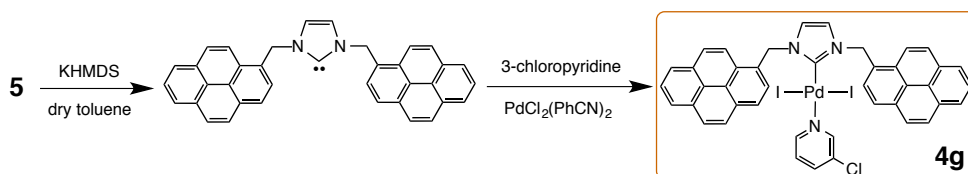
Scheme 2.9. Synthesis of **4g** via free carbene route.
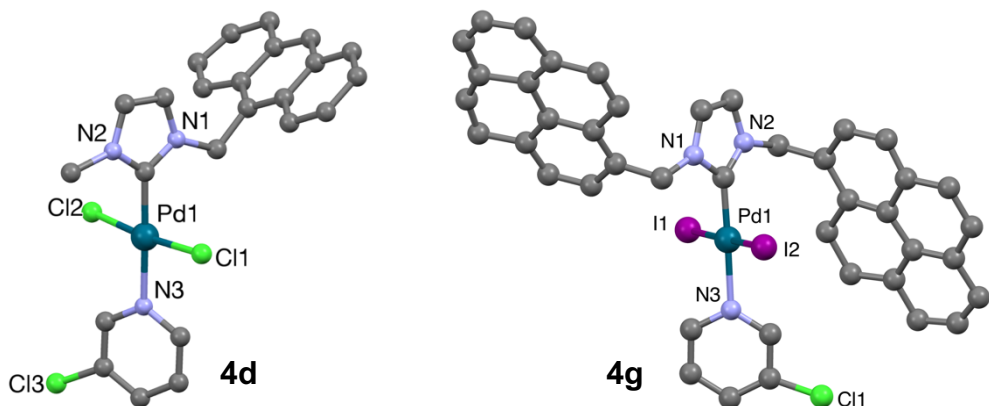
Figure 2.2. Molecular structures of **4d** and **4g** with thermal ellipsoids displayed at 50% probability. Hydrogen atoms have been omitted for clarity. Selected bond lengths (Å) and bond angles (°) with estimated standard deviations of **4d** crystal: Pd1–C 1.909 (2), Pd1–N3 2.16(2), I1–Pd1–I2 177.04 (13). Modified from paper V.

2.4. Conclusions

In conclusion, we have described the design of novel functionalized N-heterocyclic carbene Pd(II) complexes bearing diverse functionalities on the N-heterocycle ring. Direct quaternization and/or the use of a carbene transferring agent are indeed compatible synthesis approaches with most functional groups in the present work. The synthesis of an imidazolium chloride containing two pyrene moieties was more difficult than expected. The functionalized Pd(II)–NHC complexes were synthesized and insightfully characterized by means of a combination of ^{1}H NMR, ^{13}C NMR spectroscopy, X-ray methods, and elemental analysis. Preparation of the Pd(II)–NHC precursors is straightforward and they exhibit high stability at ambient conditions.

3. Supported Pd(II)–NHC complexes: Heterogenization strategies and characterization (Papers II-VI)

3.1. Introduction

Considering the immobilization (heterogenization) conditions, immobilization position, and the nature of supporting materials, the immobilization strategies of N-heterocyclic carbene-transition metal (TM–NHC) complexes can be classified into:

i)   Covalent immobilization.
ii)   Noncovalent interactions.

Chapter 3 highlights the more predominant methods under these two main categories and the major techniques implemented to characterize the heterogenized systems. In the covalent immobilization of TM–NHC complexes, heterogeneous metalation, homogeneous metalation, and self-supporting method are the most common strategies among the various immobilization methods. On the other hand, electro-static interaction, π–π stacking, and physical interaction are the main methods in noncovalent pathways.

3.2. Immobilization via covalent bonding

Heterogeneous metalation route

In this route, the functionalized NHC salts/ precursors are immobilized into the solid support, which are subsequently reacted with metal salts/ precursors in the metalation step under heterogeneous conditions (Scheme 3.1, route I).[21] Two important issues must be taken into consideration during the construction of the immobilized TM–NHC complexes via the heterogeneous metalation route. First, mass transport into the porous supporting materials, and second, the supports and the metal complex should maintain its structure and original oxidation state of the metal respectively after immobilization step. However, reduction of the metal center during metalation steps, aggregation of metal nanoparticles, and inhomogeneous metalation leading to differentiation of the metal centers remain unsolved problems in many cases. Examples where the heterogeneous metalation pathway results reduction of Pd(II) species to Pd(0) (Scheme 3.2a), and fabricating supported materials bearing undefined and multi-transition metal centers (Scheme 3.2b), were reported previously.[64, 65]

Route I (Heterogeneous metalation)

NHC precursor → (Solid support / Heterogenization) → supported NHC precursor → (TM / Metalation) → supported TM–NHC complex
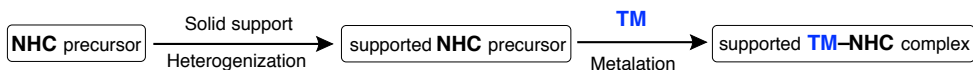
Route II (Homogeneous metalation)

NHC precursor → (TM / Metalation) → TM–NHC complex → (Solid support / Heterogenization) → supported TM–NHC complex

Route III (Self-supporting)

Functionalized TM–NHC complex → (Support synthesis / Single step) → supported TM–NHC complex
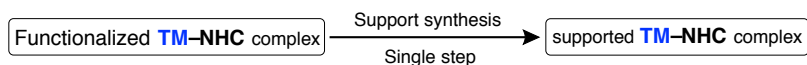
Scheme 3.1. Common strategies to immobilize TM–NHC complexes. Modified from ref. 21.

Homogeneous metalation route

Initially, metalation of functionalized NHC salts/ precursors occurs under homogeneous conditions, thereafter the metallated precursors are immobilized in a second step under heterogeneous conditions as illustrated in Scheme 3.1, route II. Importantly, in this route, the metalation reaction conditions have to be accordant with the functional groups of the NHC salts/ precursors. In addition to that, the functionalized TM–NHC complexes have to be able to maintain their catalytic activity after the immobilization step.[66]
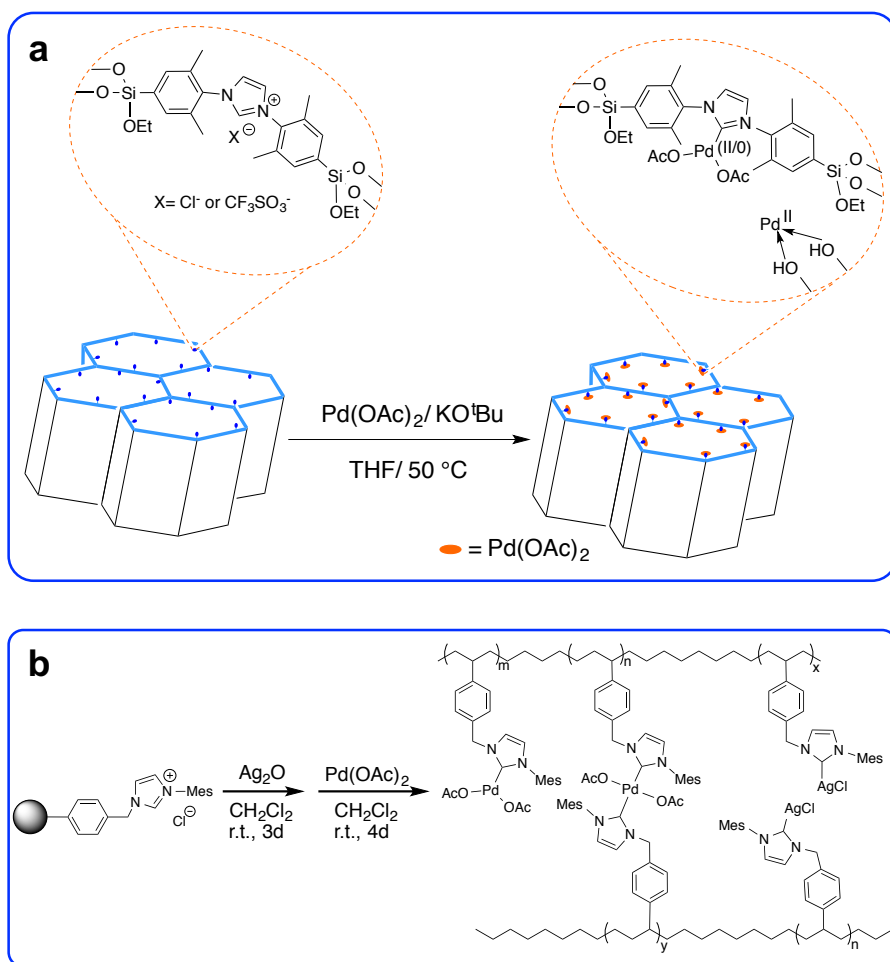
Scheme 3.2. (**a**) and (**b**) show selected examples of heterogeneous metalation route. (**c**) shows example of homogeneous metalation route. Modified from ref.64-66.
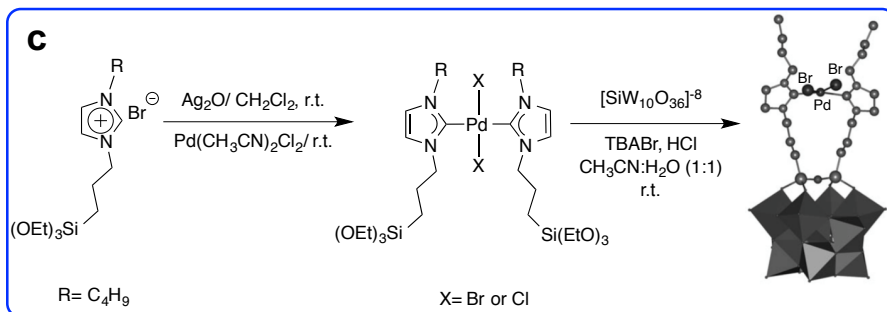
Scheme 3.2. Continued.

Self-supporting route

In this process, small molecules or monomers containing a metal center are converted into solid materials in a single step reaction (Scheme 3.1, route III), for example, the formation of metal-organic assemblies, polymerization, sol-gel...etc. Easy tuning of the metal loading on the supports, well defined and homogeneous dispersion of catalytically active centers, are the main advantages of self-supporting method. An example of that, is the copolymerization of the Ru–NHC complex with a dianhydride in NMP solution affording polyimide supported Ru–NHC complex as shown in Scheme 3.3.[67, II]
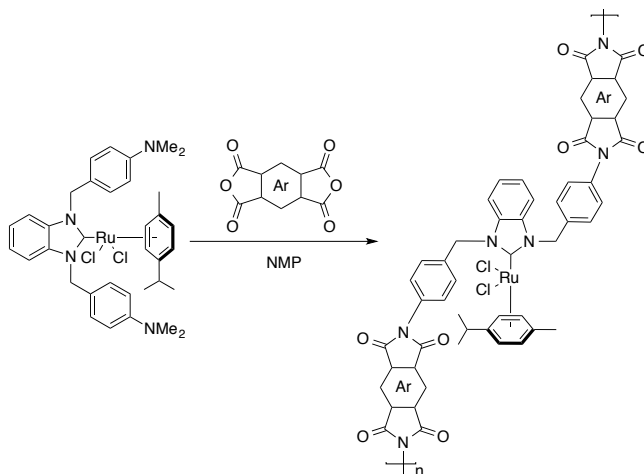
Scheme 3.3. Immobilization of Ru–NHC complex by copolymerization. Modified from ref.67.

Therefore, in our study, the utilization of the self-supporting route as an immobilization method of the functionalized Pd(II)–NHC monomers was set on

achieving supported catalysts in a controllable and well-defined fashion which leads to greater efficiency. In particular, the degree of cross-linking is expected to vary with the number of vinyl groups in the monomer, which could lead to a difference in stability or selectivity of the supported polymer systems. Based on that, we chose the monomers that either have one or two polymerizable arms. Palladium monomers **1b**, **2b**, **1c**, **2c**, **3c**, and **2f** were co-polymerized with divinylbenzene (DVB) using precipitation polymerization (Scheme 3.4).[II, III]
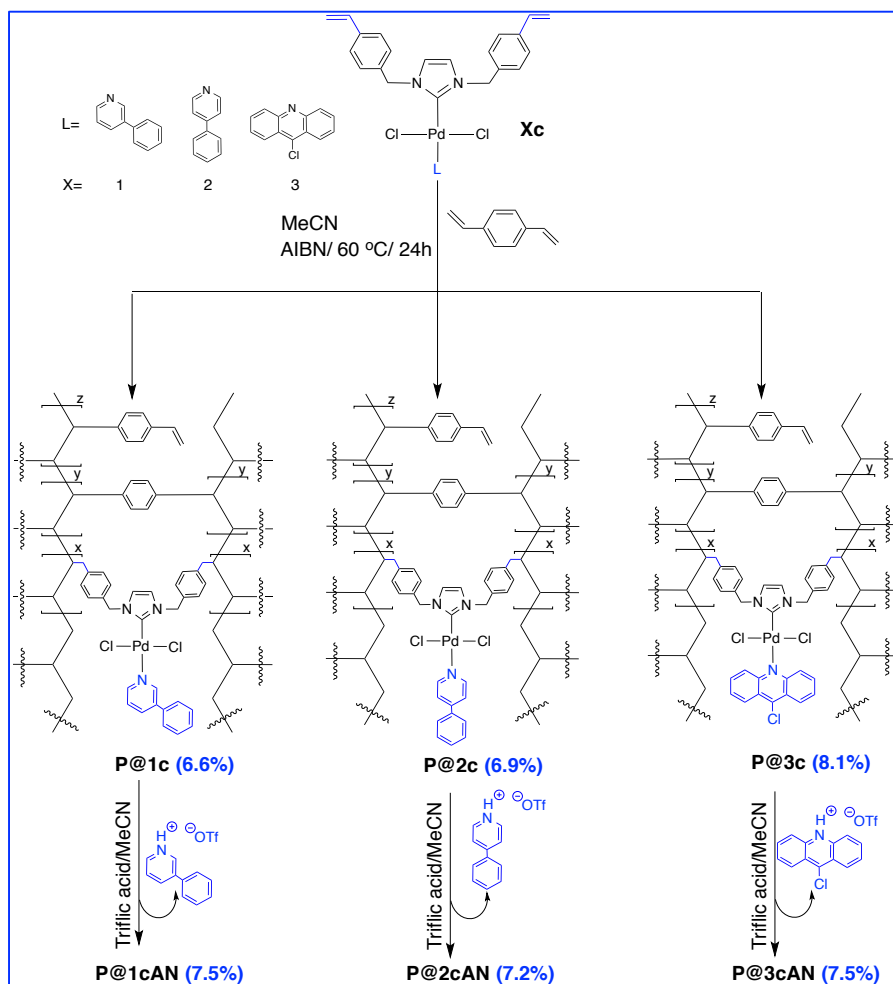
Scheme 3.4. Immobilization of Pd(II)–NHC complexes via copolymerization, and pyridine derivatives removing step from the cross-linked polymers. Pd wt% (reported in parentheses) Modified from papers II and III.
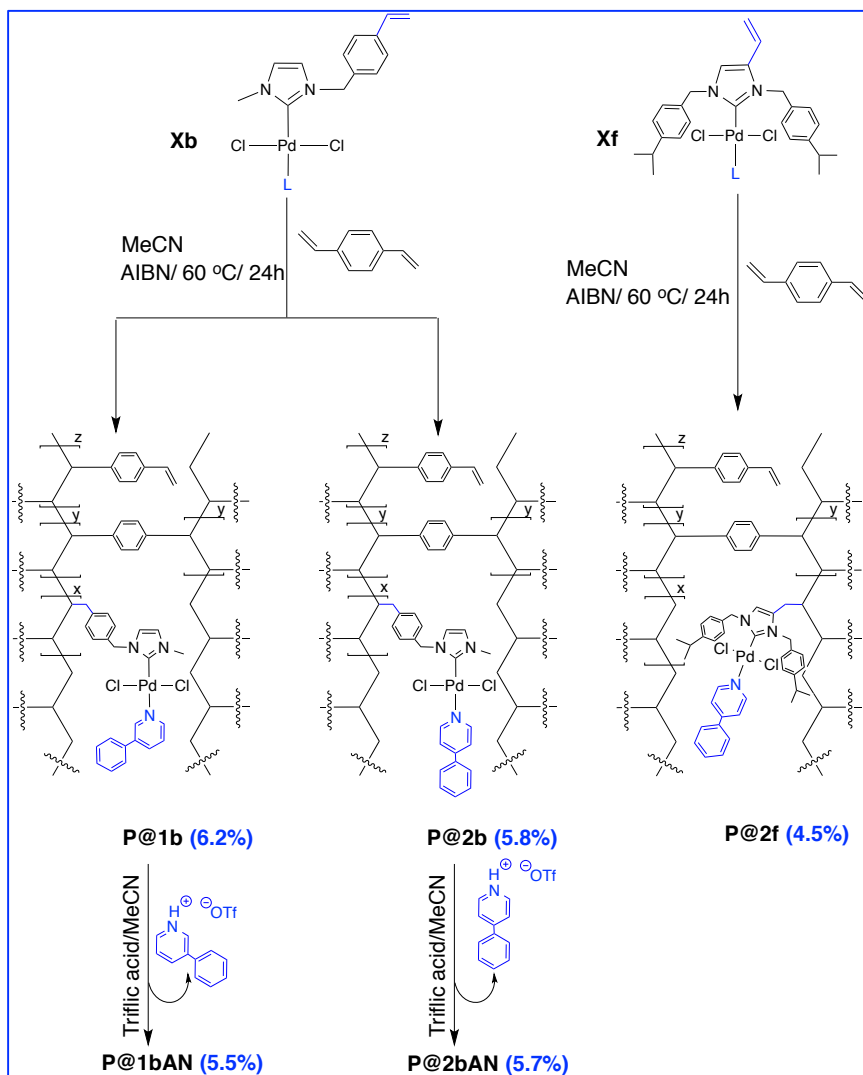
Scheme 3.4. Continued.

The Pd:DVB ratio was 1:4 and the total monomer concentration used in our study was around 2 % (w/v) of the solvent. The polymerization conditions formed a clean surface of microspheres and porous polymer beads, which is very important for catalysis. Importantly, under these conditions, the metal center is not influenced by, for example, the free radical initiator AIBN.[II] The polymerization afforded polymers **P@1b**, **P@2b**, **P@1c**, **P@2c**, **P@3c**, and **P@2f** (Scheme 3.4). The use of the different pyridines could have induced differences in the shape of the polymer cavity. Therefore, to study the impact of the pyridines on the catalytic performance

and regioselectivity, the ligands were removed through protonation with triflic acid/CH$_3$CN solution; giving the acetonitrile adducts **P@1bAN**, **P@2bAN**, **P@1cAN**, **P@2cAN**, and **P@3cAN** as shown in Scheme 3.4.

3.3. Immobilization via non-covalent interactions

Electro-static interaction, physical interaction, and π–π stacking are common heterogenization methods using weaker interaction modes between the NHC species and the support. Even though the immobilization by these methods are less utilized due to the weak interaction effect, and low stability against leaching, they can still be applicable as an immobilization strategy. This can be achieved by a special care in the selection of the catalytic complex, tuning the reaction conditions, and nature of the support. Interestingly, immobilization by these methods usually does not require additional functionalization or modification of the ligand or complex (which probably could change the original reactivity of the catalyst) that aid the anchoring step to the solid surface.[21, 53]

Electro-static interaction

Using this method, charged complexes or ligands are deposited onto the support materials bearing opposite charge by an exchange reaction. Pahlevanneshan et al.[68] reported the immobilization of a sulfonated palladium(II) N-heterocyclic carbene complex by an electrostatic interaction method (Scheme 3.5).
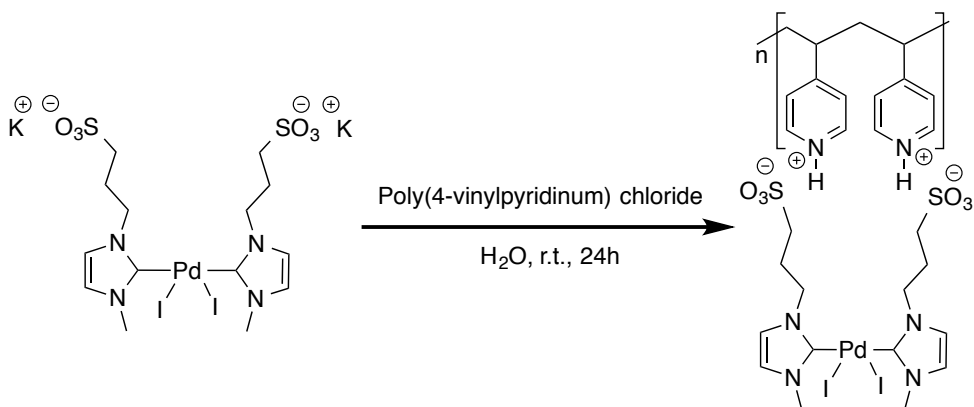
Scheme 3.5. Preparation of PdI$_2$(NHC)$_2$(SO3)$_2$@PVP catalyst. Modified from ref. 68.

The immobilization process was carried out by mixing the protonated poly-vinylpyridine with the corresponding sulfonated Pd–NHC complex in water at room temperature for 24 h.

Physical interaction

An Ru–NHC catalyst was immobilized by a direct absorption method as shown in Figure 3.1. Although the immobilization process was performed under effortless conditions, the supported catalyst suffered from leaching especially in polar solvents.
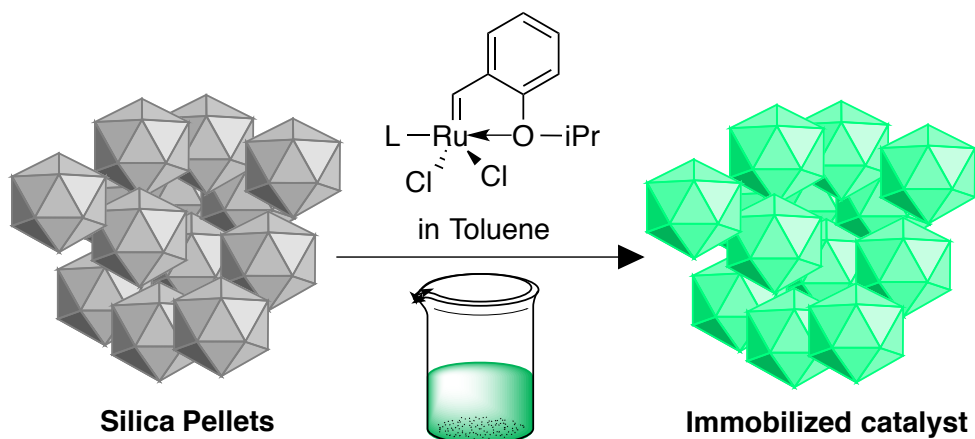
Figure 3.1. immobilization of Ru–NHC catalyst by direct absorption. Modified from ref. 69.

π–π stacking

π–π stacking or π–π interaction is one of the most common non-covalent bonding fashion. The relative dissociation energies of π–π or CH–π non-covalent interaction with graphenic materials are less than 50 kJ mol^{-1}.[70] As we mentioned, the nature of the support plays a very important role, not only as a tool for supporting or π–interacting materials but also tuning the catalytic activity by avoiding aggregation and aiding the interaction between substrates and active catalytic center.[53] Undoubtedly, graphene (two-dimensional carbon sheet), has gained a tremendous interests due to its unique chemical, mechanical, thermal and electronic properties. Figure 3.2 illustrates the general π–π interaction types observed between aromatic molecules and graphenic surface, where CH⋯π, face-to-face and edge-to-face interactions are very likely.[70]
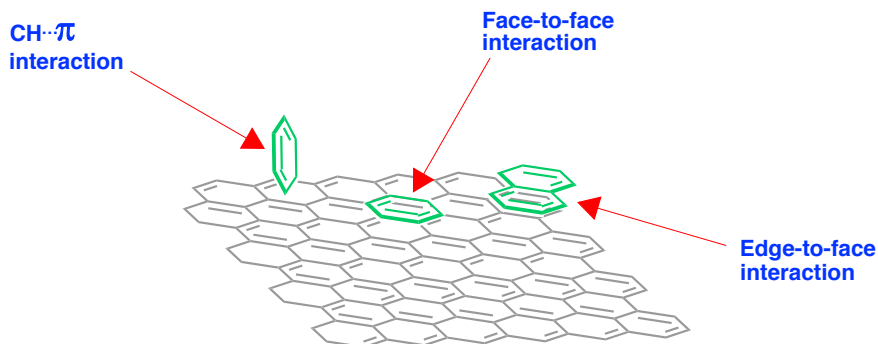
Figure 3.2. π–π and C–H···π interactions types observed from benzene or naphthalene molecules above the basal plane of graphene. Modified from ref. 70.

Graphene oxide (**GO**) and reduced graphene oxide (**rGO**), are typical supports utilized in the immobilization of TM–NHC complexes for catalytic purposes due to the high specific surface area (for graphene ca. 2600 m^2/g), stability, inertness, and large-scale availability.[53] The capability of π–π interaction depend on the number of aromatic rings in contact with the surface.[71] The adsorption of some polycyclic aromatic hydrocarbons PAHs (i.e., naphthalene, anthracene, and pyrene) on **rGO** was studied as a function of pH. Increasing the pH from 2 to 11 did not influence the adsorption of PAHs on rGOs. However, theoretical modeling reveals that the most stable stacked structures of naphthalene, anthracene, and pyrene on the surface of rGO have interplanar distances of 3.389, 3.447, and 3.455 Å respectively, and the binding energy increases with an increasing number of aromatic rings.[72]According to recently reported results,[73] the π–π interactions of pyrene-tagged ruthenium carbene complex on the surface of single-walled carbon nanotubes SWNTs (Scheme 3.6) were found to be greatly affected by the polarity of the solvent.
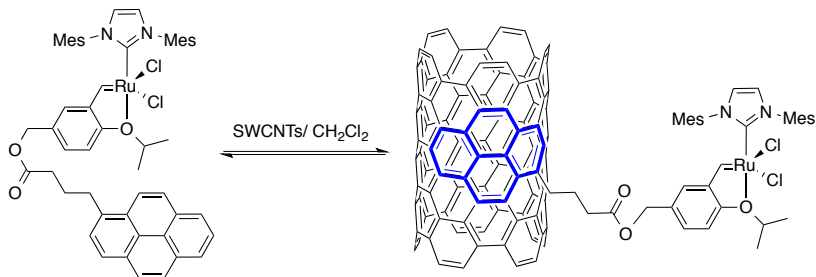
Scheme 3.6. Pyrene-tagged ruthenium carbene complex π–π interacts on the surface of SWNTs (surface area ≥700 m^2/g). Modified from ref. 73.

In our study, **rGO** (Surface area= 400-500 m^2/g) was selected as supporting surface. **GO** was prepared from the graphite powder by Hummers method.[74] Subsequently it was reduced in water with hydrazine hydrate to obtain **rGO** as shown in Figure 3.3.[75] Treating the **GO** with hydrazine hydrate lead to the formation of pyrazoles at the edges of the **rGO** sheets,[76] therefore, elemental analysis indicates that **rGO** contains 0.19% N in the structure. Double and single anthracene-tagged Pd(II) carbene complexes were simply π-stacked onto **rGO** by sonication of the supporting materials in dry CH$_2$Cl$_2$. Subsequently, the metal complex was added to the sonicated **rGO** and the mixture was stirred vigorously for two days at room temperature as shown in Scheme 3.7.
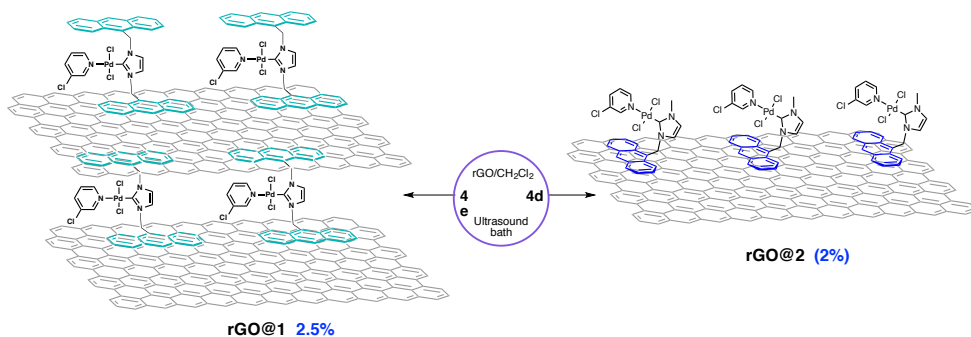
Scheme 3.7. Preparation of **rGO@1** and **rGO@2**. Pd wt% (reported in parentheses). Modified from papers IV and V.
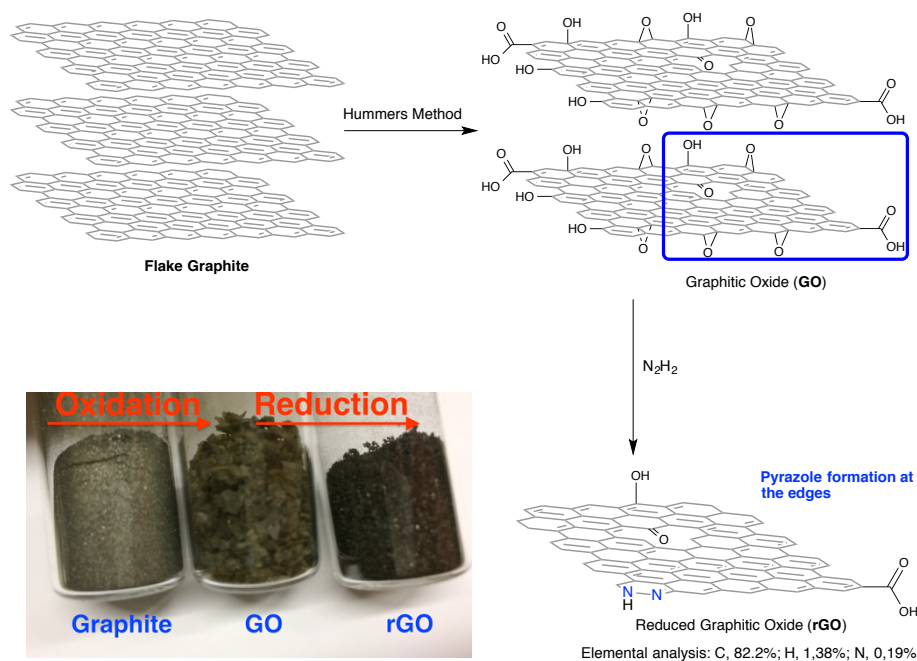
Figure 3.3. preparation of **rGO**. Modified from ref. 76.

3.4. Techniques employed to characterize heterogeneous catalysts

3.4.1. Solid-State nuclear magnetic resonance (SS-NMR)

Cross Polarization-Magic Angle Spinning (CP-MAS)

CP-MAS is one of the most commonly employed method in SS-NMR technique. It can be used, when the nuclei of interest suffer from low sensitivity due to low natural abundance. It combines cross-polarization (CP) and magic angle spinning (MAS), to offer a high-resolution SS-NMR by increasing the sensitivity of nuclei of interest. In our study, basically, the SS-NMR signal was enhanced by spinning the sample at the magic angle (ca. 54.74°) and transferring the polarization from the abundant proton (1H) spins to the low natural abundance spins (^{13}C). Polymers are finely powdered and packed tightly in rotors suitable for high speed rotation, where spin stability is influenced by the packing of the samples. If the spinning rate of the

sample is less than the magnitude of the anisotropic interaction, sidebands will appear in the SS-NMR spectrum; they are spaced by a distance equal to the spinning rate in Hertz. Therefore, in our ^{13}C CP-MAS experiments, the measurements were performed at 296-298 Kelvin, using spinning rates in the range of 7.2-10 kHz, which was somewhat enough to eliminate the sidebands.[77-80]
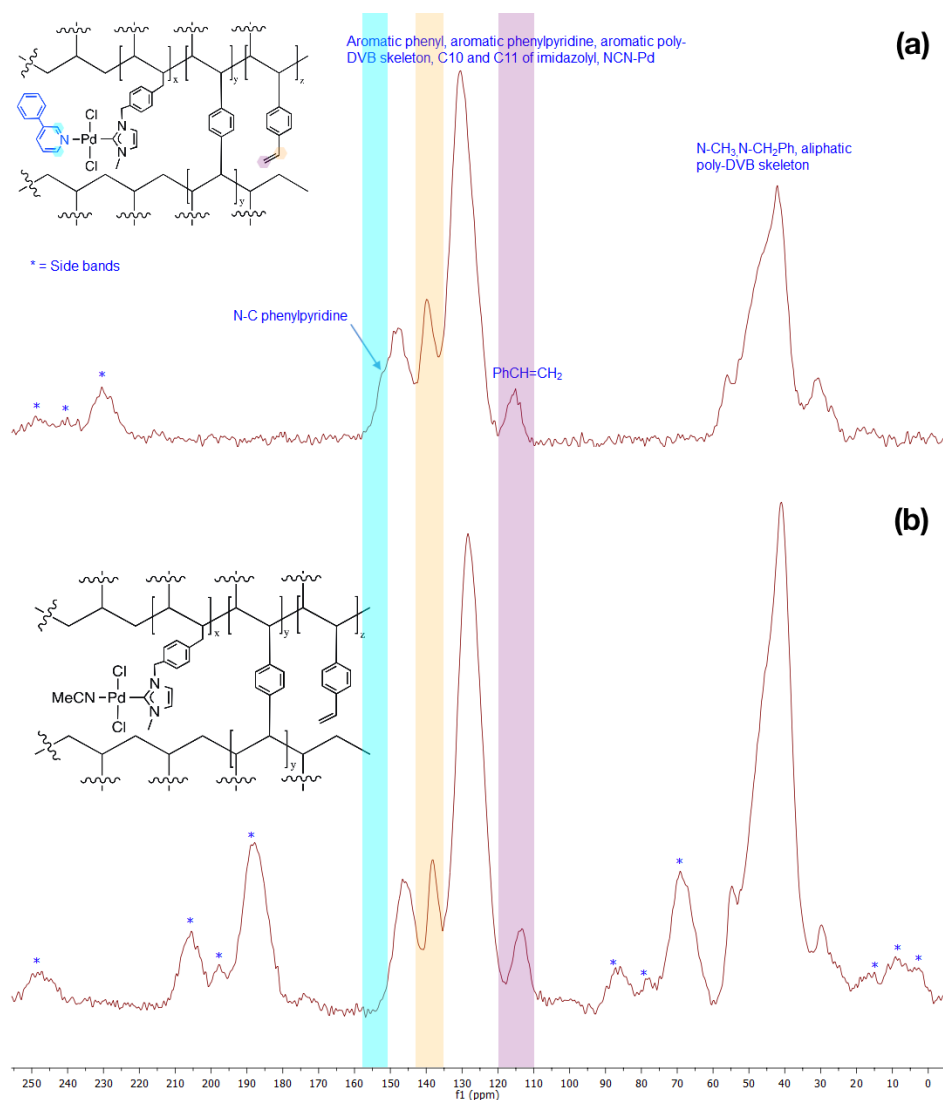
Figure 3.4. (a) SSNMR spectrum of **P@1b**, spinning rate is 10 KHz. **(b)** SSNMR spectrum of **P@1bAN**, spinning rate is 7.5 KHz. Modified from paper II.

All polymers show almost identical ^{13}C CP-MAS spectra. For different polymers containing pyridine, shoulder peaks in the range of 150-151 ppm are present, but these shoulder peaks disappeared if the pyridine ligands were displaced. For example, the pyridine shoulder peak at 150 ppm in the structure of **P@1b** polymer disappeared from SSNMR spectrum of **P@1bAN** polymer (Figure 3.4a and 3.4b); which is a good evidence for the success of the washing process and formation of pyridine free polymer **P@1bAN** in this case. On the other hand, ^{13}C CP-MAS experiments provide valuable information about the polymer structure. Importantly, it reveals the presence of unreacted vinyl linkers in the poly-DVB skeleton, as seen from two peaks around 113 and 138 ppm assigned to the terminal and internal carbons, respectively (Figure 3.4). [II]

3.4.2. Transmission Electron Microscopy (TEM)

In general, TEM is an analytical technique that utilizes the interaction of energetic electrons with the sample to form an image and providing compositional, morphological and crystallographic information of an object. A TEM is used in two modes depending on the beam. Transmission electron microscopy (TEM) mode if the beam is parallel and broad, and scanning transmission electron microscopy (STEM) mode if the beam is focused. In the TEM mode, the incident electrons (waves) interact with the thin sample. Some are transmitted through, without interaction, and others are diffracted by the presence of atoms and their crystals. The transmitted and the diffracted waves have different phases. In the STEM mode, the beam is focused to a very small probe, which is scanned back and forth on the specimen, and when the coming electrons see atoms they can scatter, while between the atoms they don't. Thus, light elements scatter less strongly than heavy elements. Inside a TEM, various signals are generated that can be used for different purposes as shown in Figure 3.5 for the STEM mode. For instance, X-ray energy dispersive spectroscopy (XEDS) can determine elemental composition present in the chemical structure of the sample. Additionally, information of density and its variations over the sample can be provided by collecting high-angle scattered electrons with an annular detector, high-angle annular dark-field (HAADF) images. The bright field (BF) detector collects the non-scattered transmitted beam, therefore samples appear dark against the bright background, while a dark field (DF) detector excludes the transmitted beam, thus the samples appear bright.[81, 82] For selected polymers, high-resolution TEM (HRTEM) images were recorded. Subsequently, a Fast fourier transform (FFT) analysis of HRTEM images is performed in order to detect easily the presence of lattice fringes in the sample. For example, the FFT analysis of HRTEM images for **P@2b** and **P@2f** polymer showed no indication of that metallic palladium was formed during the polymerization reaction (Figure 3.6a and 3.6d).[III]
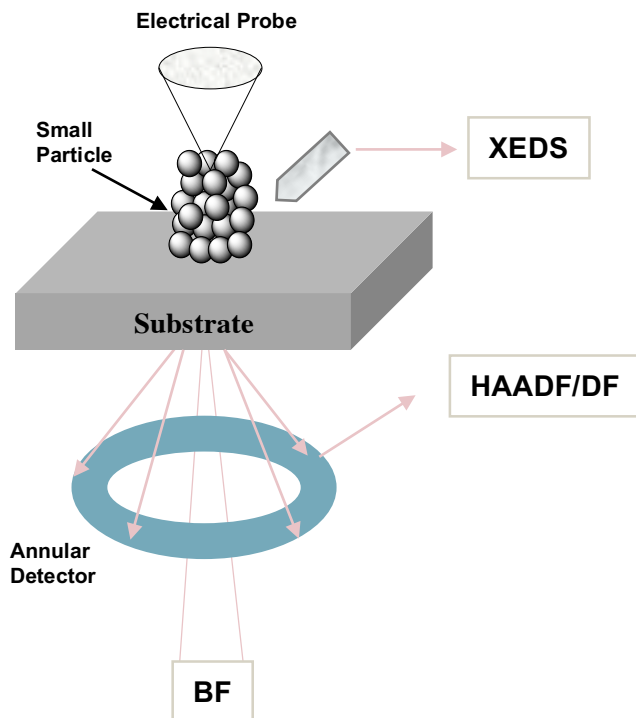
Figure 3.5. Various signals that are used in STEM. X-ray energy dispersive spectroscopy (XEDS); high-angle annular dark-field (HAADF); bright-field (BF) and dark-field (DF). Modified from ref. 81.

XEDS mapping provide information about the homogeneous dispersion of Pd and Cl (as brighter areas) in the **P@2b** and **P@2f** matrixes (Figure 3.6b and 3.6e) and it also showed that the Pd and Cl are present exclusively inside the polymeric particles (Figure 3.6c and 3.6f). High resolution transmission electron microscope (HRTEM) image of the native rGO support shows an intralayer distance around 3.8-4.3Å (Figure 3.7a). Figure 1b shows a HRTEM image of the **rGO@1**. No indication of metallic Pd particles from the process of attaching the Pd-containing molecules could be found. XEDS data confirmed the presence of Pd and Cl exclusively inside **rGO@1** (Figure 3.7c). A homogeneous dispersion of Pd and Cl (as brighter areas) was determined by EDX mapping in **rGO@1** catalyst (Figure 3.7d). In addition to that, other elements were detected, for instance sulfur and potassium in both rGO and **rGO@1** as a result of using sulfuric acid and potassium permanganate in the synthesis of rGO support.
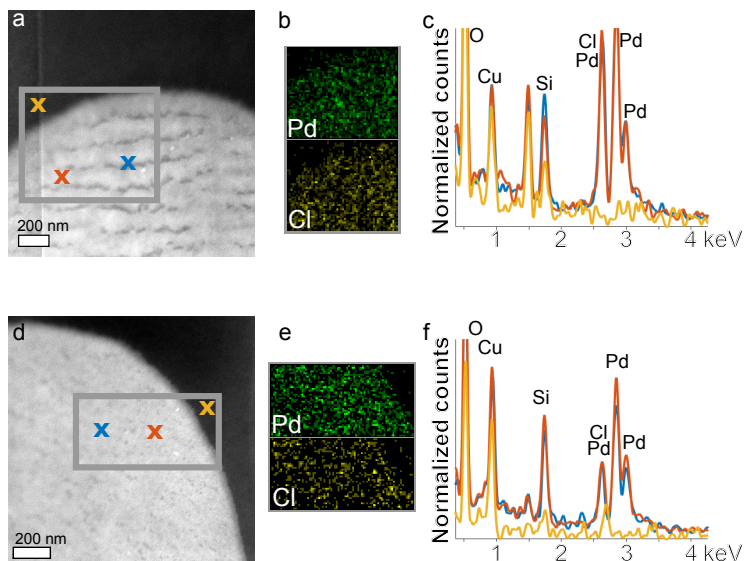
Figure 3.6. **(a)** and **(d)** Dark-field STEM images of **P@2b** and **P@2f** respectively, the gray boxes mark the areas for which the elemental mapping was carried out. **(b)** and **(e)** Pd and Cl elemental mapping on the edge of **P@2b** and **P@2f** particles respectively. **(c)** and **(f)** XEDS spectra for three sites (blue and red from within the polymers, yellow from outside the polymers) on the images of **P@2b** and **P@2f**. Modified from paper III.
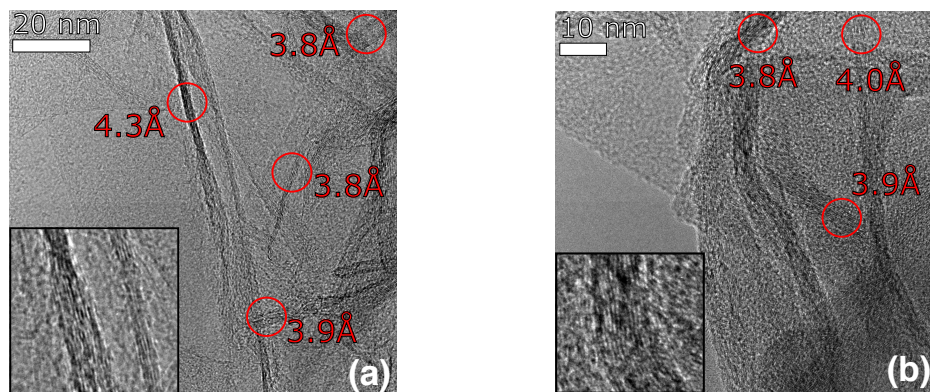
Figure 3.7. **(a)** and **(b)**, HRTEM images of rGO and **rGO@1** respectively, showing resolved individual graphene-like sheets with insets enhancing the lattice from which distances are measured. Some measurements are marked in both images. **(c)** EDX spectra, averaged for three sites of **rGO@1** (red line) and three sites of rGO (blue line). **(d)** High angle annular dark-field (HAADF) STEM image and XEDS-mapping of **rGO@1**. The red box in the STEM image marks the areas for which the elemental mapping was carried out. Note that there is no indication of Pd or Cl on the amorphous carbon film from the TEM support grid (upper part of the image).
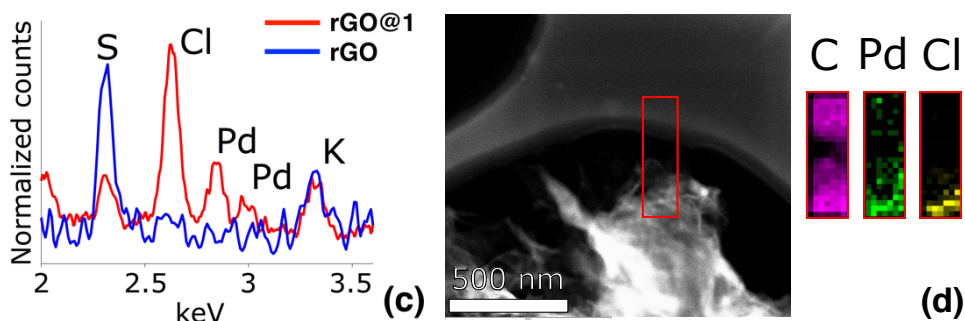
Figure 3.7. Continued.

3.4.3. X-ray techniques

Powder X-ray Diffraction (PXRD)

Is considered as a common analytical technique that has numerous advantages in solid state characterization, like effortless sample preparation, high sensitivity, easy to operate and easy to analyze the outcome data. The technique is based on the interactions of the incident X-rays (the source is either Cu K$_\alpha$ or Mo K$_\alpha$) with the atoms in a sample. These atoms sit on sets of lattice planes spaced by the interplanar distance d_{hkl}, where h, k, l (Miller indices) denotes the orientation of the family of the respective planes. Thus, X-rays are diffracted when the conditions follow Bragg's law (Scheme 3.8):

$$n\lambda = 2d \sin \theta$$

where n is the order of reflection, λ is the wavelength of the incident X-rays, d is the interplanar spacing of the crystal, and θ is reflection angle. The powder sample contains many individual crystalline phases in random orientations. However, the crystallites need to be large enough to give a high amount of constructive interference of diffracted photons. Otherwise diffraction intensity is to small and the sample is amorphous. A diffraction pattern plots intensity against the angle of the detector 2θ. In our study, samples were scanned in a 2θ range of 10-100°. In order to identify the phases, the observed diffraction peaks from the samples were compared with the experimental diffraction pattern of pure references available by International Center for Diffraction Data (ICDD).[83-85]
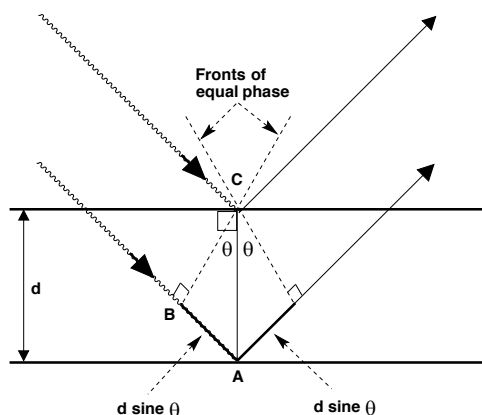
Scheme 3.8. Bragg's law reflection. Modified from ref. 84.

X-ray Photoelectron Spectroscopy (XPS)

X-ray photoelectron spectroscopy (XPS) or Electron spectroscopy for chemical analysis (ESCA) is a powerful technique for surface chemical analysis and for studying physical and chemical phenomena occurring at surfaces of materials. Fundamentally, the XPS technique is based on the emission of electrons when light is shone onto a matter (photoelectric effect), an effect discovered by Heinrich Hertz in 1887. This discovery and the experimental data from the photoelectric effect was explained by Einstein, who was awarded the Nobel Prize in Physics in 1921 for his discovery of the law of the photoelectric effect. Later, in 1981, Kai Siegbahn obtained the Nobel Prize in Physics for improving and developing the ESCA method, which today is an important technique in many scientific fields. In this technique, X-rays, often from a Mg K_α (1253.6 eV), Al K_α (1486.6 eV), or synchrotron source, are used as the exciting photon source. The X-ray photon (photon energy $h\nu$)interacts with a core level electron or valence electron, that has a binding energy (E_b), causing electron emission by the photoelectric effect as shown in Figure 3.5. These emitted photoelectrons have a kinetic energy (E_k), and ϕ_s is the work function of the spectrometer:

$$E_b = h\nu - \phi_s - E_k$$

Thus, another electron from a higher-level will fall to occupy the resulting core hole due to the electron emitting, and energy gained during this relaxation will transfer to another electron (Auger electron) causing emission of that electron.[86-88]
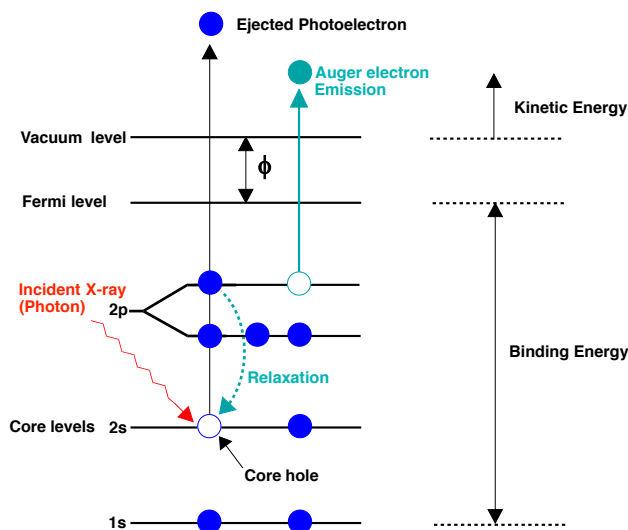
Figure 3.8. Schematic representation of the photoemission process. Modified from ref. 86.

The emitted photoelectrons consist of characteristic peaks in the X-ray photoelectron spectra (XP spectra) related to the binding energy of the photo-ionized element. XPS can provide information about the chemical composition, oxidation state metals, and the changes in chemical environments around metal centers.

X-ray Absorption Spectroscopy (XAS)

X-ray Absorption Spectroscopy (XAS) is a synchrotron based technique to measure the x-ray absorption coefficient (μ) at energies near and above the x-ray absorption edge of an element in a material. Scheme 3.9 shows the basic configuration of a XAS beamline in a transmission mode. XAS spectrum is obtained by tuning the x-ray energy while following the corresponding x-ray absorption coefficients of the sample. Generally, a XAS spectrum can be divided into two spectral regions, X-ray absorption near edge spectroscopy (XANES) and Extended x-ray absorption fine structure (EXAFS) (see figure 10). The information about the oxidation state and symmetry of the absorbing atoms can be obtained by XANES spectrum while bond distances and coordination numbers can be determined by EXAFS spectrum.[89] Figure 10a shows the XAS spectra of Pd foil and **rGO@1**. Their spectra have significant differences indicating a local structure differences in those two materials.
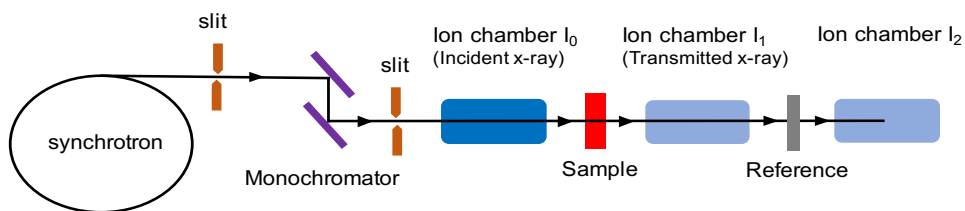
Scheme 3.9. Schematic representation of the incident and transmitted X-ray beam in XAS. Scheme made by Ning Yuan.

In catalysis, XAS is a powerful tool for probing the local structure of active center in a catalyst regardless the sample state. *In situ* XAS provides opportunities to monitor the possible structural changes of a catalyst under reaction conditions which can improve our understanding about pre-catalyst activation, catalytically active species and possibly deactivation mechanism. A custom-made *in situ* reactor (see Figure 10b) was used for *in situ* XAS measurement with the catalytic reactions performed in the vessel. The evolution of the Pd species in the system was successfully followed.
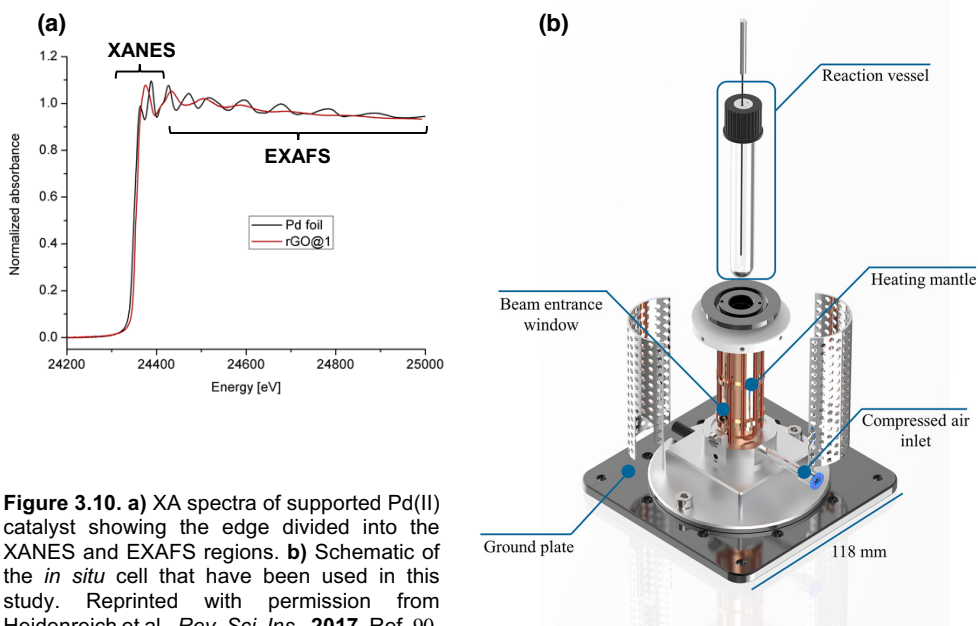
Figure 3.10. a) XA spectra of supported Pd(II) catalyst showing the edge divided into the XANES and EXAFS regions. **b)** Schematic of the *in situ* cell that have been used in this study. Reprinted with permission from Heidenreich et al., *Rev. Sci. Ins.*, **2017**. Ref. 90.

PXRD was used to confirm the results from TEM analysis. **P@1c** polymer was treated with ascorbic acid to reduce any Pd(II) to Pd(0) and form **P@1c (reduced)**. A PXRD pattern was recorded for **P@1c (reduced)**, which was used as a reference phases for the native polymers. The PXRD patterns of the native polymers are featureless, but the PXRD pattern of **P@1c (reduced)** shows peaks at 40.8, 47.8, and 67.8 2θ which can be assigned to the (111), (200), and (220) crystal planes of Pd(0) particles in the polymer matrix (Figure 3.11). By the obtained PXRD results, the native polymers don't contain Pd(0) which are only obtained upon reduction.[II]
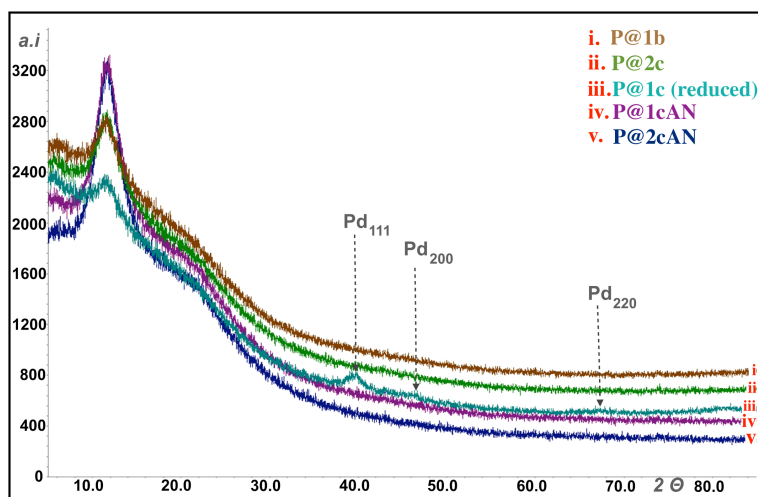
Figure 3.11. XRD patterns of various polymers in comparison with **P@1c (reduced)** polymer. The spectra show the absolute intensities (a.i). Modified from paper II.

In our study, we employed XPS to investigate and characterize the elemental composition, oxidation state, and coordination environment of the Pd species in the synthesized monomers and fresh polymers. Pd 3d core level spectra of the monomer **1c** and fresh polymers before and after removing the phenylpyridine ligand show the Pd $3d_{5/2}$ and Pd $3d_{3/2}$ peaks at approximately 340 and 345.5 eV binding energy in agreement with the energies expected for a Pd(II) species (Figure 3.12a).[II] In the same context, the XP spectra of **2b**, **2f**, **P@2b**, and **P@2f** show Pd $3d_{5/2}$ and Pd $3d_{3/2}$ peaks at approximately 338.3 and 343.8 eV binding energy compatible with the

energies for a Pd(II) species (Figure 3.12a).[III] In general, XP spectra of all polymers show small shifts to lower or higher binding energy, and line broadening in comparison with the monomers. These observations can be probably due to the polymerization and concomitant change in the Pd environment (polydispersity in the Pd 3d spectra), or it is related to the replacement of phenylpyridine ligands by solvents. The N 1s spectrum of **1c** shows a high energy peak (ca. 402.4 eV) related to the imidazole nitrogen atoms, and a lower energy peak (ca. 401.7 eV) associated with the phenylpyridine nitrogen in 2:1 ratio as expected (Figure 3.12c). Peak broadening it can be assigned to the variation of the N chemical environment by polymerization and washing steps.[II]
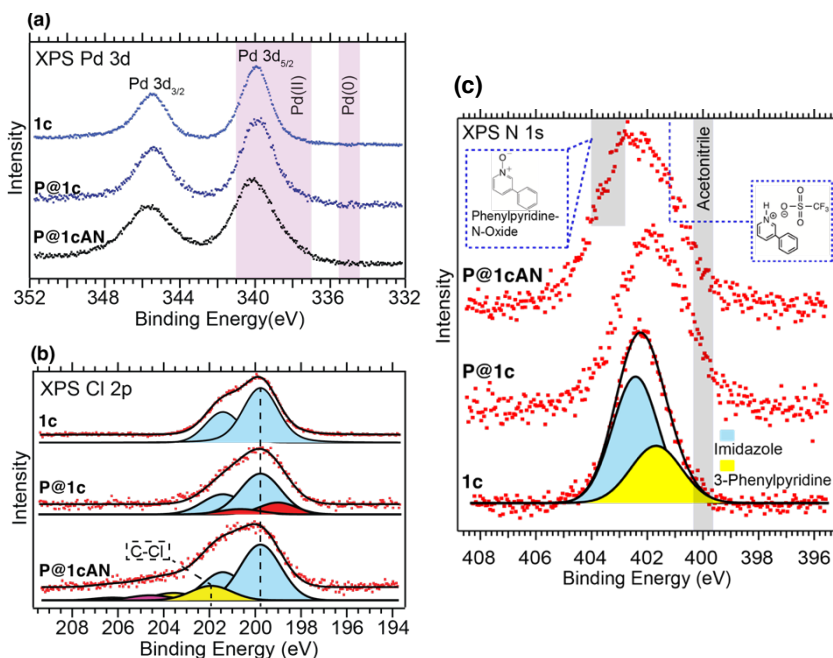
Figure 3.12. (a), **(b)**, and **(c)** Pd 3d, Cl 2p, and N 1s XP spectra of the indicated samples. Modified from paper II.

XPS analysis played a very important role to monitor the changes in the surrounding environment of the Pd center. For example, In the Cl 2p spectrum of polymer **P@1cAN** a high binding energy species at around 201.9 eV is found, which indicates the formation of C–Cl bond due to H–Cl addition to the vinyl groups occurring to some extent during washing with triflic acid (Figure 3.12b). Another example, specifically in N 1s spectrum of **2f**, a peak broadening towards higher binding energies (ca. 401.9 eV) is observed (Figure 3.13b).[III] Apparently, the two

nitrogen atoms of this NHC ligand are sufficiently different to give a broadened peak. Calculations show a noticeable difference of two NHC nitrogen atomic charges for, at least, one of the coexistent conformers of **2f**. This difference can be attributed to the electronic effects of the vinyl group, as well as different geometrical parameters, caused by the orientation of bulky NHC arms (more details about computational calculations are shown in Paper III, the Supporting Information). However, the XP spectrum of the intentionally reduced polymer **P@1c(Reduced)** (**P@1c** was treated with ascorbic acid to reduce Pd(II) to Pd(0)), show Pd $3d_{5/2}$ and Pd $3d_{3/2}$ peaks at approximately 335 and 340.3 eV binding energy corresponding to the binding energy of Pd(0) (Figure 3.13c). At this point we can conclude, that in all polymers there are no peaks that correspond to the binding energies of Pd in the metallic state, and thus no reduction to Pd(0) takes place during polymers synthesis and washing process.
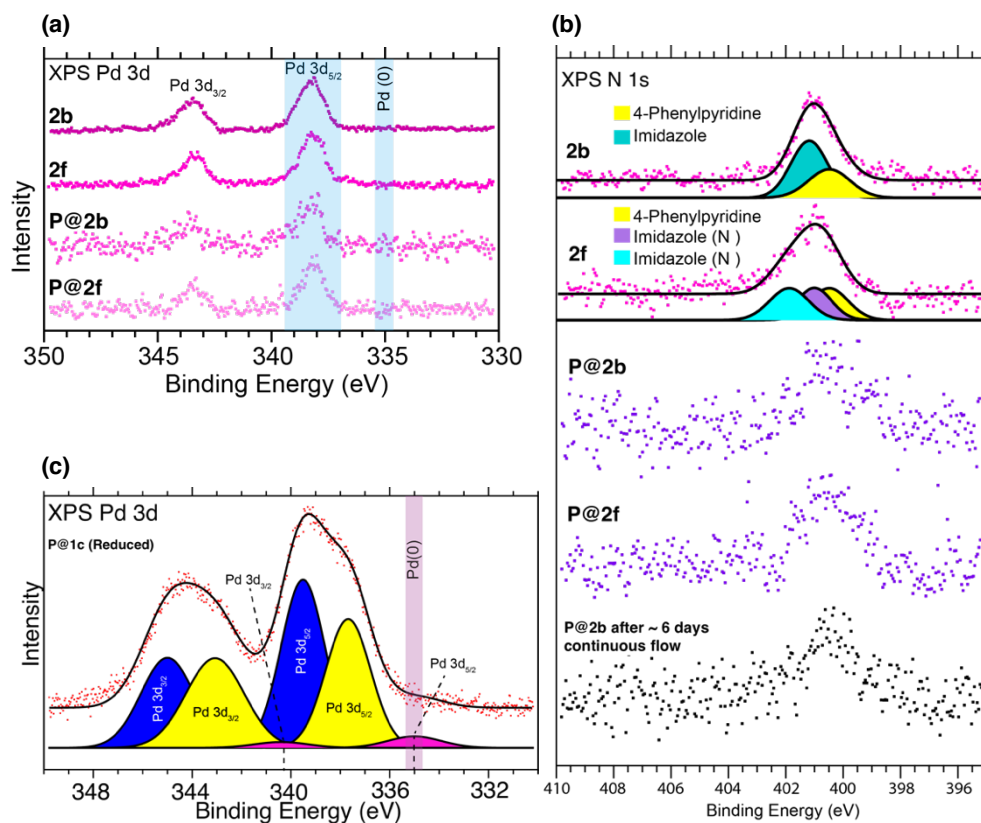
Figure 3.13. (a) and **(c)** Pd 3d XP spectra of the indicated samples. **(b)** N 1s XP spectrum of the indicated samples. Modified from paper II and III.

In the π-stacked systems, Pd 3d spectra of complex **4e** and **rGO@1** show the Pd $3d_{5/2}$ and Pd $3d_{3/2}$ peaks at approximately 337.9 and 343.4 eV binding energy in the range of the expected energies for a Pd(II) species (Figure 3.14a). Remarkably, a new peak at lower binding energy at around 337.6 eV is seen as the result of the supporting of **4e** onto rGO. The occurrence of this new peak in XP spectra of **rGO@1** (which is still within the Pd(II) region), can probably be explained by the replacement of the chloropyridine ligand during the immobilization step. The mentioned observation was in agreement with Cl 2p spectra of **4e** complex and **rGO@1**. Thus, the Cl $2p_{3/2}$ XP spectrum of **4e** shows a lower energy peak and a higher energy peak (ca. 197.9 and 198.7 eV respectively) which are assigned to the palladium chlorine, and chloropyridine chlorine in 2:1 ratio as expected (Figure 3.14b). However, Cl 2p spectrum of **rGO@1** showed significant broadening in the spectral features and shifts by 1.5 eV toward higher binding energies (Figure 3.14b); indicating that the chloropyridine ligands probably dissociate to large extent on rGO surface during the preparation of the catalyst.
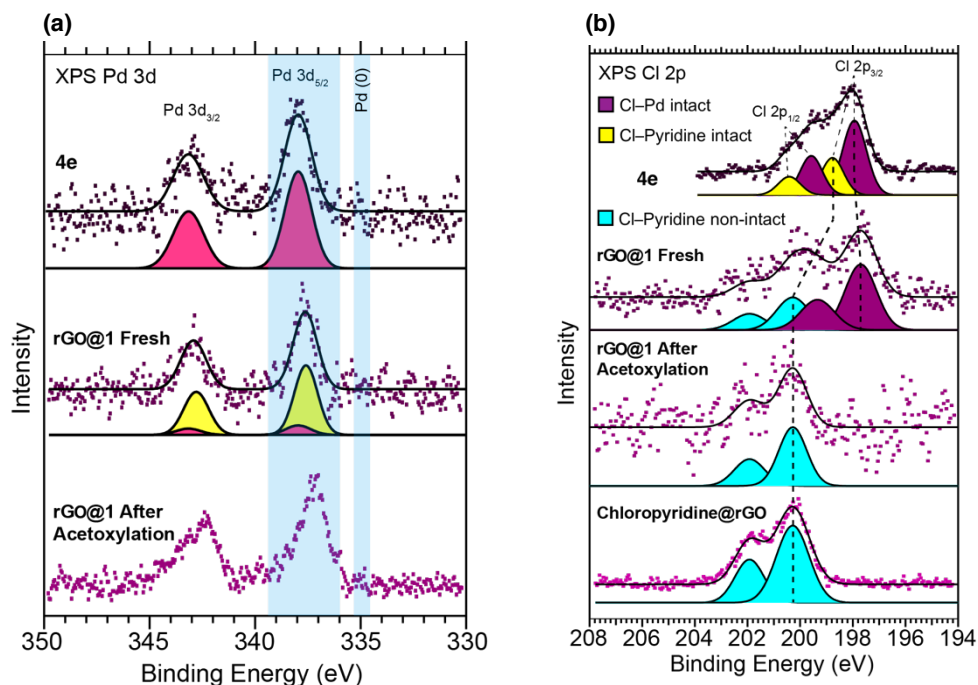
Figure 3.14. (a) and **(b)** Pd 3d and Cl 2p XP spectra of the indicated samples. Modified from paper IV.

In order to thoroughly identify whether the change in Cl 2p binding energy is due to the displacement of chloropyridine on the support surface, we performed XPS analysis for only chloropyridine deposited onto rGO (Chloropyridine@rGO). XP spectrum of Chloropyridine@rGO shows Cl $2p_{3/2}$ peak at higher binding energy around 200.28 eV, in match with binding energy for the dissociated chloropyridine species in **rGO@1** (Figure 3.14b). Worth mentioning, without going into the detailed XPS analysis, is that the earlier noticed displacement of chloropyridine ligand in **rGO@1** catalyst, has been observed in a similar fashion in **rGO@2** catalyst (Figure 3.15a and 3.15b). Even though chloropyridine ligand dissociates on rGO support, the π-stacked materials **rGO@1** and **rGO@2** are free of Pd in metallic state in their structure.
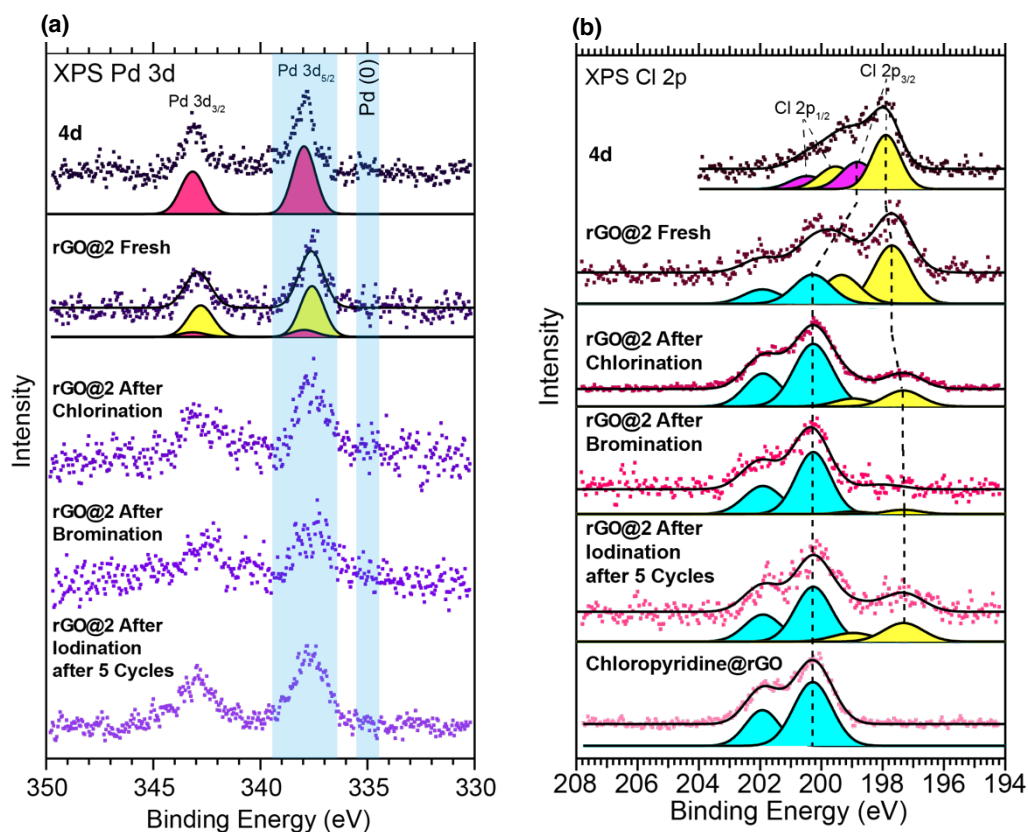
Figure 3.15. (a) and **(b)** Pd 3d and Cl 2p XP spectra of the indicated samples. Modified from paper V.

In addition to the above mentioned techniques that have been used to characterize different heterogeneous systems in this study, other techniques were also employed to gain more information about the nature of these heterogeneous systems. Such techniques are scanning electron microscopy (SEM), inductively coupled plasma-optical emission spectroscopy (ICP-OES), thermogravimetric analysis (TGA), and surface area analysis.

3.5. Conclusions

The synthesis of polymer supported Pd(II)–NHC complexes bearing polymerizable vinyl moiety in different positions in the structure of the N-heterocyclic carbene ligands is described. The immobilization of double and single anthracene-tagged Pd(II) carbene complexes on rGO support is carried out by π-stacking method. Characterization of Pd(II)–NHC polymers showed the presence of Pd(II) species in these polymers without any trace of Pd(0) nanoparticles. Although, the chloropyridine ligands are probably displaced during the immobilization step of π-stacked systems, the palladium oxidation state is the same as the original oxidation state of Pd(II) in the parent molecular complexes.

4. Supported Pd(II)–NHC catalyzed undirected C–H activation/ oxygenation reaction (Papers II, IV and VI)

4.1. Introduction

In general, the development of methods for the direct replacement of unactivated carbon–hydrogen bonds with functional groups (such as O, N, C, Halogen) remains a critical challenge in organic chemistry. The inert nature of most carbon–hydrogen bonds is the hardest challenge. A multitude of efforts have been made to overcome these challenges by developing new functionalization strategies, but limitations are always presence. One of the most important strategies which received considerable attention was by demonstrating that transition metals such as Ru, Rh, Pt, and Pd can react under mild conditions with C–H bonds to produce C–M bonds (which are far more reactive than their C–H counterparts) in a process known as C–H activation.[91, 92] So far, the success of this strategy is constrained by the necessity of using specific types of reactants (ligand-directed C–H functionalization approach), in which a heteroatom controls the regioselectivity; and specific conditions (such as rather low temperatures to avoid the decomposition of the catalyst).[93, 94] Thus, the undirected C–H bond functionalization method (functionalization of a C–H bond without the assistance of chelation) are much less developed than the directed C–H bond functionalizations approach, due to the many challenges faced. For instance, the requirements to control site selectivity in molecules that contain diverse C–H groups is very difficult to fulfil. However, no limitation on use substrate bearing a heteroatom is found in this strategy. Therefore, substantial research efforts have been devoted during several decades to develop transition metal based catalysts for the undirected C–H activation of hydrocarbons.[95-97] Important to mention, there are various mechanisms for C–H bond cleavage by transition metal complexes, and these mechanisms are depending on the relative reactivity of different classes of C–H bonds.[98-101]
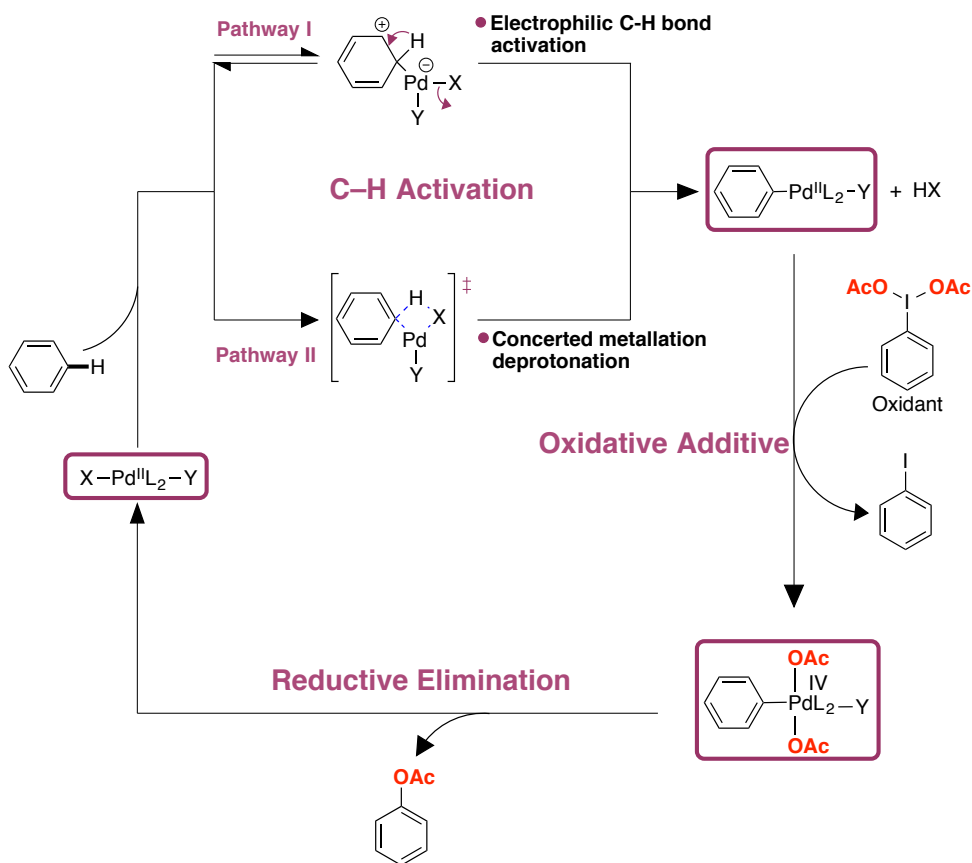
Scheme 4.1. Proposed mechanisms of C–H bond cleavage and C–H bond oxygenation of arene. Modified from ref.99-102.

Under undirected C–H bond activation, the first step in the reaction mechanism is C–H activation (it can be termed as a *palladation* step, if Pd is used). Basically, C–H bond cleaves to form Aryl–M intermediates, which is probably the rate-limiting step according to the experimental data. Scheme 4.1 is showing the possible pathways of C–H bond cleavage (Arene–H bond in our study) by transition metal (for example, Pd).[99, 100, 102, 103]

Electrophilic C–H Bond Activation pathway

Aromatic C–H bonds are activated by an electrophilic C–H activation in a fashion similar to a Freidel-Craft type metallation mechanism, followed by rearomatization to form aryl–M intermediates (Scheme 4.1). It is very common to occur with electrophilic palladium(II) catalysts such as $Pd(OAc)_2$, $PdCl_2$, $Pd(TFA)_2$, and it is selective for electron-rich arenes.

Concerted metallation deprotonation (CMD) pathway

It depends on the acidity of the C–H bond being cleaved rather than arene nucleophilicity. Remarkably, computational studies have confirmed that the carboxylate assists C–H activation by forming short M···C–H and C–H···O interactions that facilitate the heterolytic cleavage of the C–H bonds within a variety of catalytic processes as shown in Figure 4.1.[104-106]
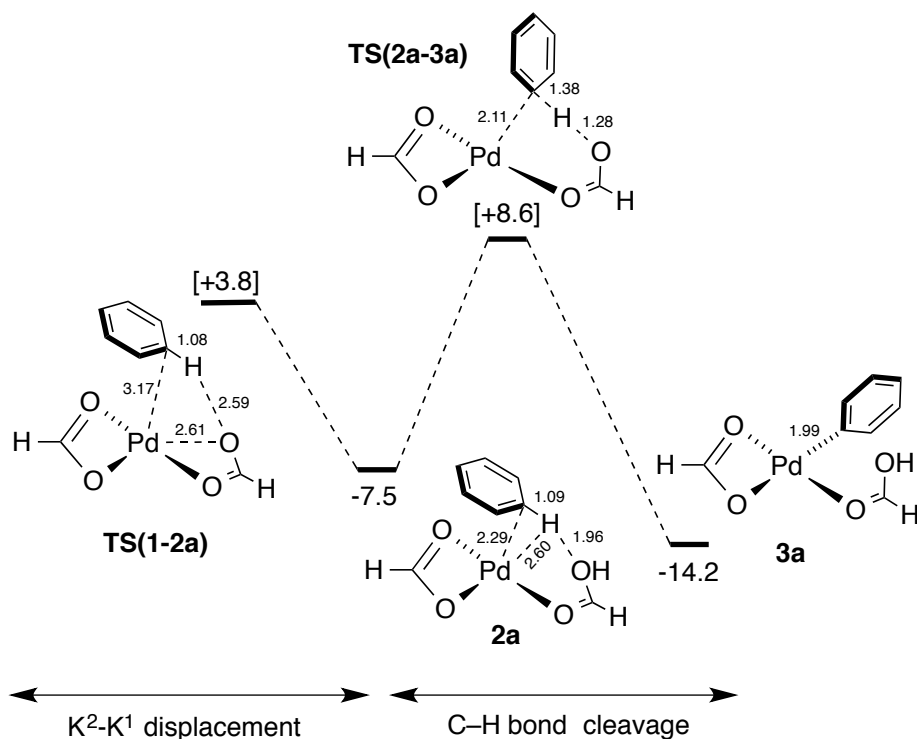
Figure 4.1. Computed reaction profiles for C−H activation of C_6H_6 at $[Pd(\kappa^2\text{-}CO_2H)_2]$. Modified from ref.106.

In oxygenation of arenes, and after the palladation step, the reaction mechanism could involve the oxidation of Pd(II) center by an oxidant (diacetoxyiodo benzene (PIDA) in Scheme 4.1). Subsequently, reductive elimination step affords C–O bond formation and a released Pd(II) catalyst.[107]

4.2. Supported palladium(II) carbene complexes catalyze C–H acetoxylation of arenes

Homogeneous Pd(II)–NHC catalysts are active in both ligand-directed[108] and undirected C–H bond acetoxylation,[107, 109-111] mainly using $PhI(OAc)_2$ or its derivatives as an oxidant. Besides that, Pd(II)–NHC catalysts are capable of catalyzing a wide range of C–C cross-coupling transformations.[112, 113] However, water-soluble PEPPSI type Pd(II)–NHC complex generated Pd nano particles (NPs) with narrow size distributions after the first run of Suzuki-Miyaura cross-coupling reaction: according to TEM analysis, kinetic studies and mercury poison experiments (Figure 4.2).[114]
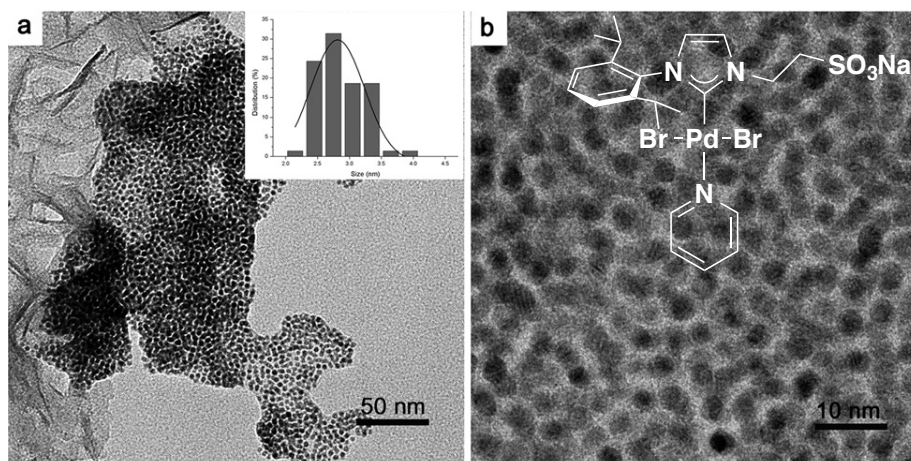
Figure 4.2. **(a)** and **(b)** TEM images of Pd NPs generated after the first run of the coupling reaction with the indicated complex. Modified from ref. 114.

In our study, the activities of palladium(II) carbene complexes supported by different strategies in selective oxidation of C–H bonds have been examined. As a reference for homogeneous catalysts, we used a PEPPSI-iPr (PE-iPr) and **4e** catalysts in comparison with polymer and graphene supported catalysts. Full details

of the optimization of the catalytic reaction conditions for different catalysts are described in papers II and IV. As a benchmark for the activity and selectivity of our supported systems, we chose the undirected C–H acetoxylation of biphenyl. Having the optimized conditions in hand, we proceeded with catalysis under the reaction conditions given in Table 4.1.

Table 4.1. C–H acetoxylation of biphenyl using Pd(II) based catalysts.

E	[Catalyst]	PIDA [M]	Cat. Mol. (%)	Biphenyl (equiv.)	Temp. (°C)	Yield (%)[a]	TON
1	None	0.05	-	5	104	n.f	-
2	PE-iPr	0.05	5	5	104	44	-
3	Pd(OAc)$_2$	0.05	2	5	104	58	29
4	P@2b	0.05	4	5	104	38	-
5	P@2bAN	0.05	4	5	104	56	14
6	P@1c	0.05	4	5	104	52	-
7	P@1cAN	0.05	4	5	104	50	-
8	P@1cAN[b]	0.05	4	5	104	56	-
9	4e	0.6	0.3	2.5	92	59	197
10	rGO@1	0.6	0.3	2.5	92	56	187

[a] Yield and selectivity were determined by GC using a calibration curve based on decane as an internal standard.
[b] [Oxidant]= MesI(OAc)$_2$.

There is no reaction in the absence of catalyst (Table 4.1, Entry 1). In all catalyst systems, the yield of ortho-substituted biphenyl was formed as a minor product in comparison with meta- and para-substituted biphenyls, due to the steric hindrance in the biphenyl substrate. However, X-ray quality crystals were obtained after the catalysis with **P@2bAN**, confirming the molecular structure of the minor formation of ortho-acetoxybiphenyl product (Figure 4.3). In general, the polymer and graphene supported Pd(II)–NHC catalysts show similar or superior efficiency compared to homogeneous analogues in C–H oxygenation of biphenyl (Table 4.1). However, **rGO@1** catalyst recorded the highest turnover number among all the supported systems under optimized reaction conditions (Table 4.1, Entry 10).
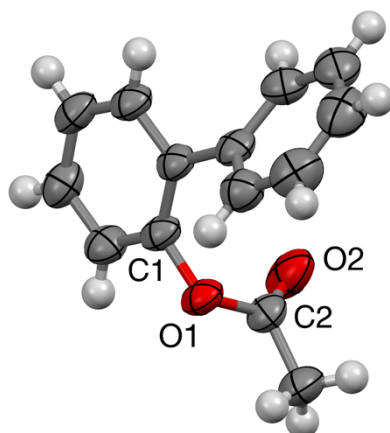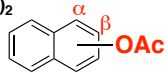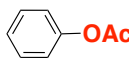
Figure 4.3. Molecular structures of ortho-acetoxybiphenyl with thermal ellipsoids displayed at 50% probability. Selected bond lengths (Å): C1–O1 1.4804, C2–O1 1.4100, C2–O2 1.1666.

All NHC–Pd(II)–MeCN polymers, in general, afforded higher yield of acetoxybiphenyl products compared to the NHC–Pd(II)–pyridine derivative polymers. No notable differences were observed in the regioselectivities among all catalysts.
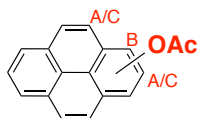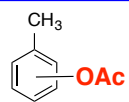
4.3. Oxidation of other arenes

Further, we investigated the scope of C–H acetoxylation for other arenes using the optimized reaction conditions. With naphthalene as a substrate, NHC–Pd(II)–pyridine derivative polymers showed a remarkable increase in selectivity compared to homogeneous ones and NHC–Pd(II)–MeCN polymers in favors of β-substitution (Figure 4.4). No improvement in selectivity was obtained for NHC–Pd(II)–MeCN polymers even when using a bulky oxidant MesI(OAc)$_2$. Thus, the presence of phenylpyridines increase the selectivity substantially and this goes hand in hand with a decreased activity. Dramatically, the selectivity improved to (11:89) upon addition of one equivalent of 4-phenylpyridine (with respect to Pd) to the reaction mixture using **P@2cAN**, while a lower activity was found compared to previously reported systems.[115, 116] However, the polymeric catalysts showed lower activity than the homogeneous ones. In the C–H oxygenation of benzene, **rGO@1** catalyst shows higher activity offering 50% yield, compared to homogeneous and polymeric catalysts (Figure 4.4).

PhI(OAc)$_2$
or
MesI(OAc)$_2$

(1 equiv.)

[Catalyst]
[mol. catalyst/ mol. oxidant]= 4%

———————————————————→ **Arene—OAc**

Arene (excess)
AcOH:Ac$_2$O (9:1)
92 or 104°C, 24h

Oxidant: MesI(OAc)$_2$

α β
OAc (naphthalene)

P@1c	18%[d]	α 17%;	β 83%
P@1cAN	26%[d]	α 54%;	β 46%
P@2c	15%[d]	α 20%;	β 80%
P@2cAN	19%[d]	α 47%;	β53%
P@2cAN[h]	9%[d]	α 11%;	β89%
PEPPSI-iPr[b]	33%[d]	α 33%;	β 67%

OAc (phenyl)

P@2c	32%[d]
P@2c[a]	29%[d]
PEPPSI-iPr[b]	45%[d]
rGO@1[c]	50%[d]
4e[c]	42%[d]

A/C
B OAc (pyrene)
A/C

P@2c	(27%)	A+C 9%[f]; **B** 91%
P@2c[a]	(25%)	A+C 11%[f]; **B** 89%
PEPPSI-iPr[b]	(27%)	A+C 16%[g]; **B** 84%

CH$_3$
OAc (toluene)

P@2c	(33%)
P@2c[a]	(15%)
PEPPSI-iPr[b]	(18%)
rGO@1[c]	(24%)[d]
4e[c]	(26%)[d]

Figure 4.4. C–H acetoxylation of naphthalene mediated by Pd(II) based catalysts, Isolated yields (reported in parentheses). [a] Oxidant= MesI(OAc)$_2$. [b] PEPPSI-iPr= 5 mol%. [c] mol. catalyst/ mol. Oxidant= 0.3%. [d] Yields and selectivity were determined by GC using a calibration curve and based on decane as an internal standard. [f] Only two products B and A or C were obtained. [g] Three products A, B and C were obtained. [h] 1 equiv. of 4-Phenylpyridine/Pd added to the reaction mixture. Modified from paper II and IV.

In contrast, particularly in the acetoxylation of toluene, the polymeric catalyst **P@2c** exhibited higher yields (33%) of acetoxylated products compared to homogeneous and graphenic catalyst. Finally, we examined the polymeric catalyst in C–H acetoxylation of a polycyclic arene substrate, the polymer showed modest yields but a higher selectivity compared with PEPPSI- iPr (Figure 4.4).

4.4. Reusability and heterogeneity

The polymer and graphene supported Pd(II)–NHC catalysts can all be separated and recovered easily from the reaction mixture by a simple centrifugation process. Thus, the recovered **P@1c** catalyst was shaken with 5 ml of 3-phenylpyridine/CH$_2$Cl$_2$ solutions after each cycle and then washed with CH$_3$CN to remove the remaining non-bonded phenylpyridines. The treated catalysts were dried and used directly for the next reaction cycle. **P@1c** was found to be effective in four cycles (probably in more, but this was not tested) of the acetoxylation of biphenyl (Figure 4.5c). The slight increase of activity that is observed could possibly mean that the polymer material opens up during the reaction giving better access to the palladium and therefore a slightly higher activity.
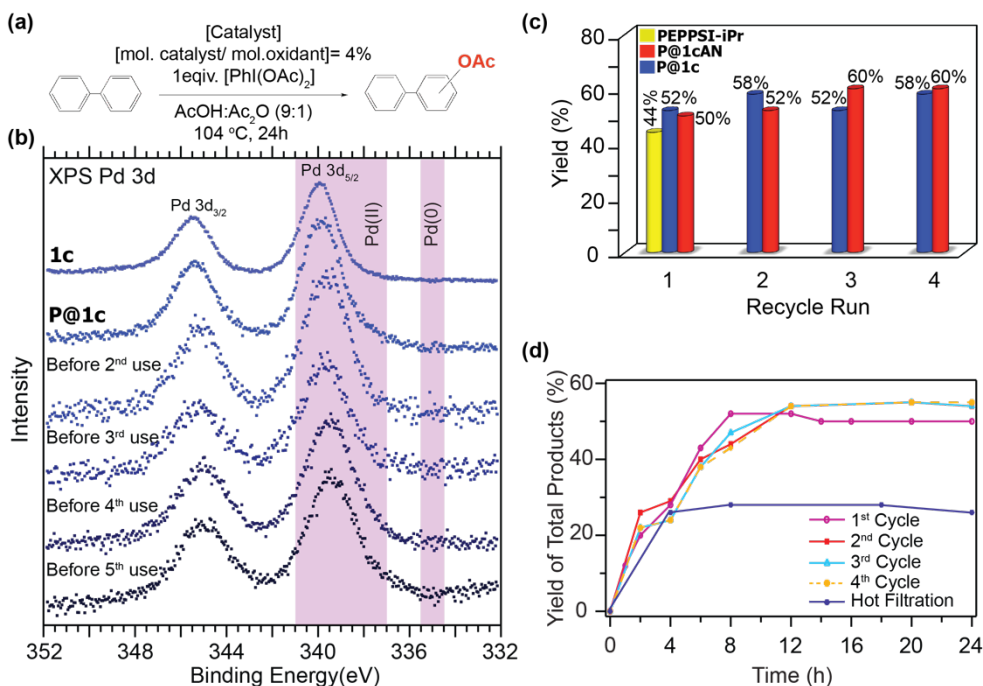
Figure 4.5. (a) C–H acetoxylation reaction of biphenyl over **P@1c**, **P@1cAN** and PEPPSI-iPr catalysts. **(b)** Pd 3d XP spectra of **1c**, **P@1c** fresh and **P@1c** after each reuse. **(c)** Reusability and productivity of **P@1c** and **P@1cAN**; the results are compared to those for a [PEPPSI-iPr] catalyst at 5 mol %. **(d)** Time profile and hot filtration study of **P@1c** catalyzed C–H acetoxylation of biphenyl. Modified from paper II.

Impressively, the kinetic profile for the four runs was more or less identical (Figure 4.5d). However, the catalysis stops almost completely after eight hours and we found by using ^{1}H NMR spectroscopy, no traces of PhI(OAc)$_2$ left in the catalysis mixture. Interestingly, the reaction continues and the yield of acetoxybiphenyl derivatives approximately doubles upon addition of 1 additional equivalent of PhI(OAc)$_2$ into the reaction vessel after eight hours, confirming that the yields are controlled by the access to oxidant not by the stability of the catalyst. A hot filtration test reveals the heterogeneous nature of the catalyst with a complete inhibition of the activity after removal of the solid catalyst (Figure 4.5d). ICP-OES analysis detected only a small leaching of Pd from the polymer after each catalytic cycle (Pd wt % = 6.58, 6.52, 6.41, and 6.30 after the 1st, 2nd, 3rd, and 4th catalytic cycle, respectively).

As we mentioned early, one of the central goals is to investigate the character of these novel systems, not only after the synthesis but even after many catalytic cycles. Therefore, we probed the palladium oxidation state of **P@1c** by XPS, the Pd $3d_{5/2}$ and Pd $3d_{3/2}$ binding energies after each catalytic cycle (ca. 339.3 and 344.6 eV, respectively) showed only a small shift compared to those of the monomer and fresh polymer (Figure 4.5c). This shift is probably related to ligand exchange between chloride and acetate. Importantly, the palladium remains in oxidation state (II) for all cycles. Similar results were obtained for **P@1cAN** after the fourth catalytic cycle. Next, we focused our attention to the Cl 2p core level of **P@1c** after each catalytic cycle, which showed significant broadening in the spectral features and shifts by 2 eV toward higher binding energies compared to the spectra of the monomer and fresh polymer (Figure 4.6). One system gave rise to two Cl atoms, one Cl with a $2p_{3/2}$ at binding energy of 199.8 eV, which fits with the monomer and corresponds to a Pd–Cl species. The second Cl $2p_{3/2}$ peak at 201.9 eV, can be assigned to a C–Cl species in agreement with the literature.[117, 118] Thus, and according to the XPS results, the majority of the chlorine (around 75%) has been transferred to the polymer matrix, while the rest is still coordinated to Pd; around 15 % have been washed out from the catalyst according to the ICP analysis that confirms that the ratio between Pd:Cl is almost 1:2 (85% of Cl is still present in the catalyst).

^{13}C CP-MAS experiments were performed for **P@1c** before and after catalysis at two different spin rates, in order to understand this remarkable change in Cl 2p binding energy and to differentiate between any new peaks that could appear and side bands. A new peak detected after catalysis at 169.8 ppm corresponds to (C=O) of an acetate group (Figure 4.7).[119, 120] In contrast, the peaks related to terminal and internal carbons of vinyl linkers at around 113 and 138ppm, respectively, observed for the fresh catalyst are absent after catalysis. The obtained data suggest that PhI(OAc)$_2$ can functionalize unreacted vinyl groups in the absence

of a catalyst, and in the presence of a catalyst we suggest that all remaining vinyl groups in the polymer are acetoxylated or chlorinated during catalysis.

rGO@1 was analyzed by XPS after C–H acetoxylation of benzene. Broadening toward lower and higher binding energies compared to fresh **rGO@1** were observed after the acetoxylation reaction (Figure 3.12a, Chapter 3). This broadening is probably related to the existence of slight differences in the chemical environments of the Pd atoms after catalysis and to ligand exchange between chloride and acetoxy group. These data were confirmed by XPS analysis of Cl 2p core level of **rGO@1** after catalysis, where the two Cl atoms corresponding to a Pd–Cl species were completely absence as shown in Figure 3.12a, Chapter 3. However, and importantly, the palladium remains in oxidation state (II) after the reaction. These results are in line with the previous observations from the XPS of the polymeric catalyst.
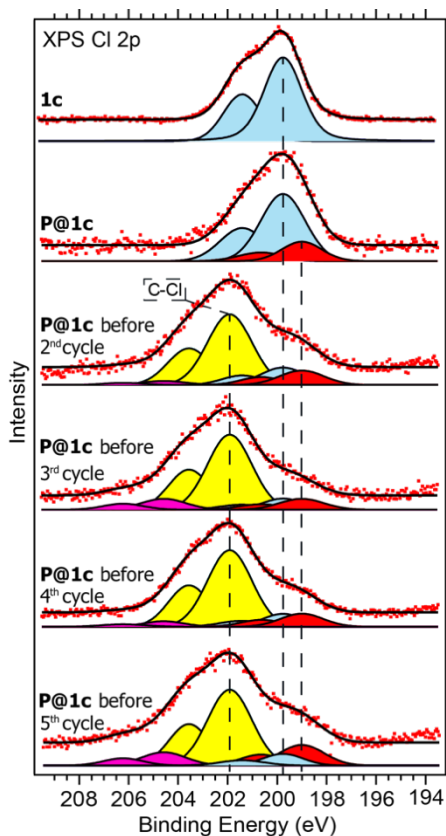
Figure 4.6. Cl 2p XP spectra of **1c**, **P@1c** fresh and **P@1c** after each catalytic cycle. Modified from paper II.
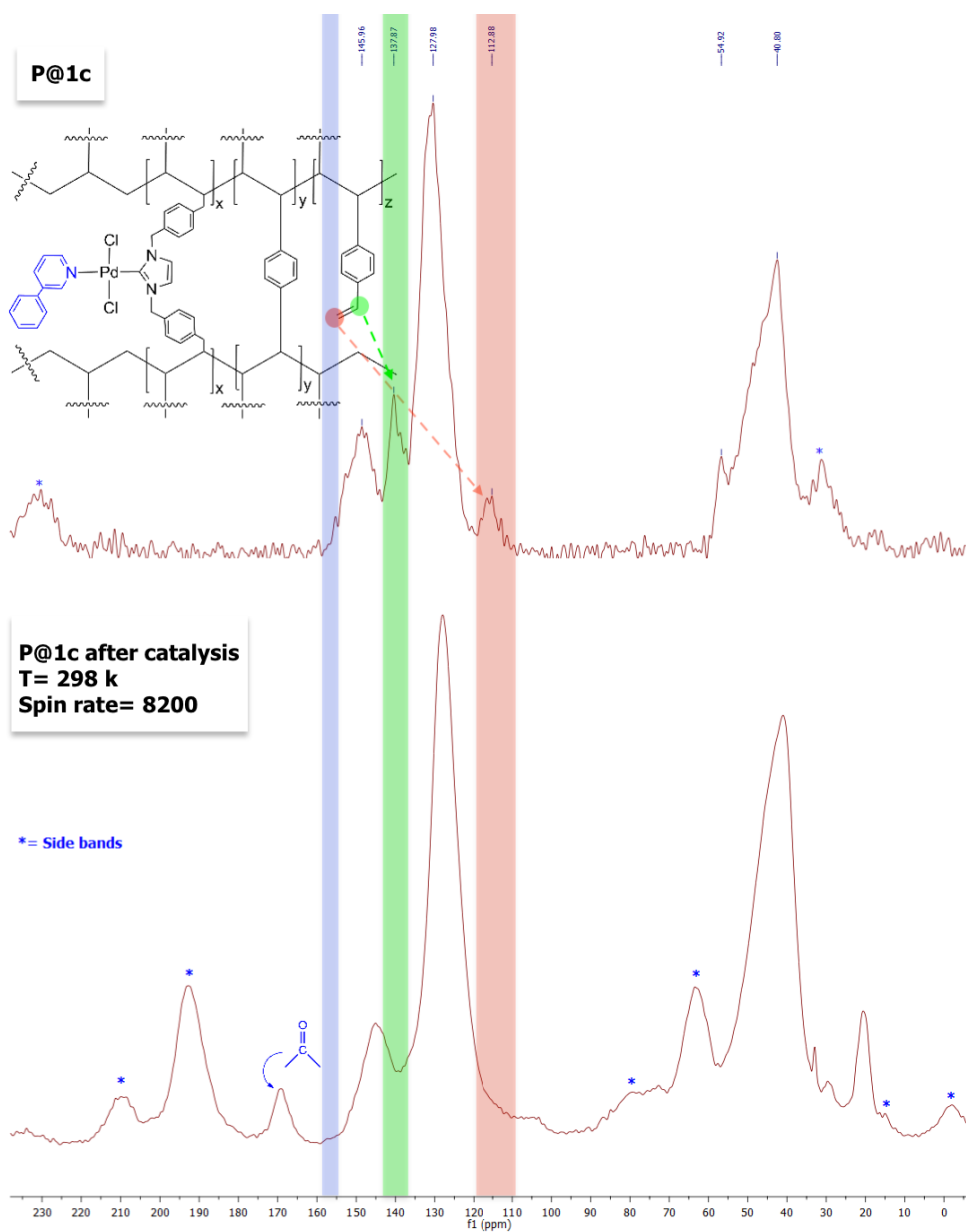
Figure 4.7. ^{13}C CP-MAS NMR spectra of **1c**, **P@1c** before and after catalysis, side bands are marked with asterisks. Modified from paper II.

4.5. Mechanistic investigation of **rGO@1** catalysed C–H acetoxylation reaction

In complement to our study (Paper IV) and in order to rationalize the nature of the active species of **rGO@1** catalysed undirected C–H acetoxylation of benzene, which gives 50% yield of acetoxybenzene (see Figure 4.4), we set out to investigate the mechanism using *in situ* X-ray absorption spectroscopy (XAS). Figure 4.8 shows XANES and Fourier transformed EXAFS spectra of **rGO@1** after the activation step (15 min at room temperature and then the reaction heated to 90 °C for 5 min). Catalyst **rGO@1** changes its coordination environment around the Pd center, without any change in the oxidation state of Pd(II). The structure evolution from fresh **rGO@1** to its active state in the reaction was represented by significant shifts of the main peak leftwards probably due to the partial loss of a Cl atom as shown in Figure 4.8b. The modeling used for the EXAFS refinement proposes the replacement of a Cl atom by an acetoxy group (AcO) at the Pd(II) center. In order to follow the possible changes at different reaction stages, *in situ* XAS measurements were performed. Figure 4.8c shows almost identical XANES spectra of activated catalyst and after 8 and 24 hours reactions, confirming no change of the dominant Pd active species during the catalysis, however the average oxidation states were slightly higher (peak shift of ca. 1 eV) which might be an indication of the partial formation of Pd (III) or (IV) oxidation state. Importantly, the Fourier transformed EXAFS spectra of activated **rGO@1** catalyst after 8 and 24 hours acetoxylation reaction revealed that a small amount of the Pd complexes were reduced into metallic Pd nanoclusters as shown in Figure 4.8d.
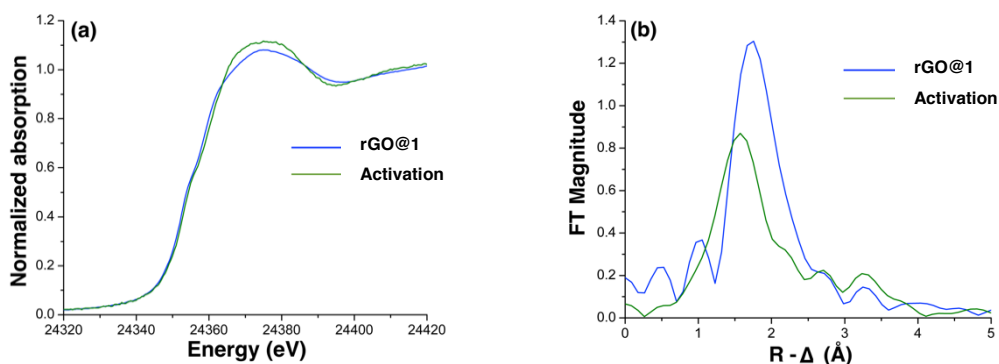
Figure 4.8. (a) XANES spectra and **(b)** Fourier transformed EXAFS spectra without phase correction of **rGO@1** and its active phase during initial step of the reaction. Modified from paper VI.
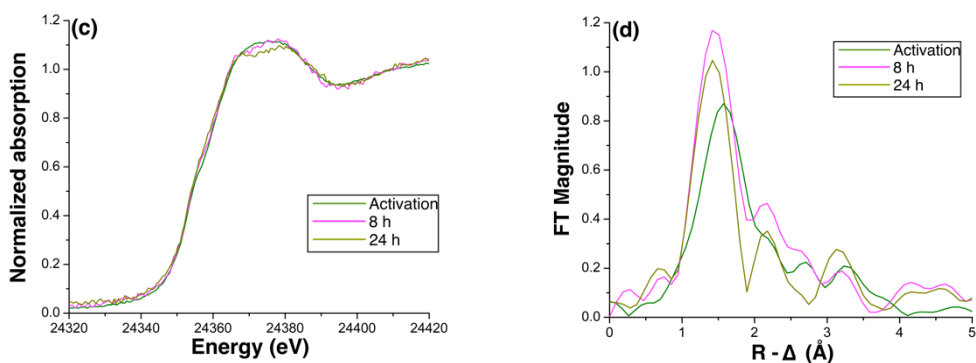
Figure 4.8. Continued.

4.6. Conclusions

The catalytic activity and selectivity in undirected acetoxylation of arenes was evaluated for all graphene and polymer supported Pd(II)–NHC catalysts with and without phenylpyridine as supporting ligands on the palladium. The presence of phenylpyridines increased the selectivity and decreased the activity of the polymers in the acetoxylation of naphthalene. The graphene supported Pd(II)–NHC catalyst exhibited higher activity in C–H acetoxylation of benzene, compared to homogeneous and polymeric catalysts. XAS study confirmed that the oxidation state of Pd center remains +2 during the changes in coordination environment upon the initial activation step. Furthermore, this active species was partly reduced into small Pd nanoclusters over the course of the reaction. Polymer supported Pd(II)–NHC catalysts show no reduction to Pd(0) state after the catalysis. The polymeric catalyst can be recycled four times without any loss of activity, and no significant leaching of Pd from the polymer after each catalysis cycle was detected. The polymeric catalyst was shown to be truly heterogeneous in a hot filtration test. The reactive vinyl moieties in the backbone of the polymer are acetoxylated or chlorinated during catalysis.

5. C–H activation/ halogenation reactions catalysed by Pd based heterogeneous catalysts (Papers III and V)

5.1. Introduction

Utilizing transition metals to activate/halogenate unreactive C–H bonds and form C–Halogen bond has been an attractive area of research for a long time; it could facilitate the production of heterocyclic halides which are representing a very important class of compounds in pharmaceuticals and agrochemicals industry (Figure 5.1).[121-127] This importance encouraged chemists to develop numerous transformations for preparation of organic halides assisted by, for example, Pd based complexes.
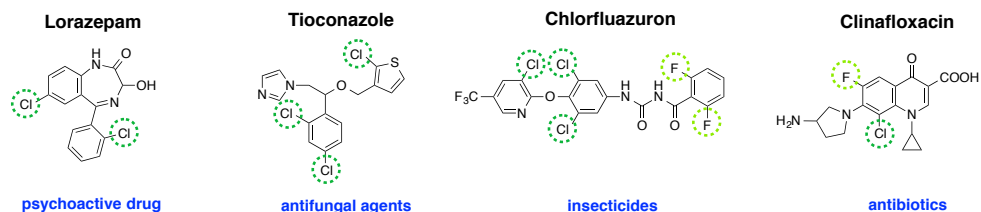
Figure 5.1. Examples of drugs and agrochemical contain halogenated heterocycles.

In traditional halogenation pathways, harsh reaction conditions, low yield, overhalogenations, poor regioselectivity, and low atom efficiency are among many of the drawbacks.[128, 129] Therefore, researchers accomplished several methodologies based on a central assisting concept: metal insertion into C–H bonds. One of the promising methodologies to selectively activate/ halogenate C–H bonds is taking

advantage of the chelating possibility of functional groups in the substrates that direct the metal into C–H bonds allowing selective functionalization. It has been proposed that the directed C–H bond functionalization processes takes place via two main reaction mechanisms, both of which are based on a central step which is C–H activation and formation of cyclometalated intermediate as shown in Figure 5.2. In the first functionalization pathway, the functionalized product is delivered by a reductive step through $Pd^{II}/Pd^{0}/Pd^{II}$ catalytic cycle. In the second functionalization pathway, the cyclometalated intermediate reacts with an electrophilic agent (oxidant). In this case, the reaction between the oxidant and cyclometalated intermediate can undergo several mechanisms[130-132]:
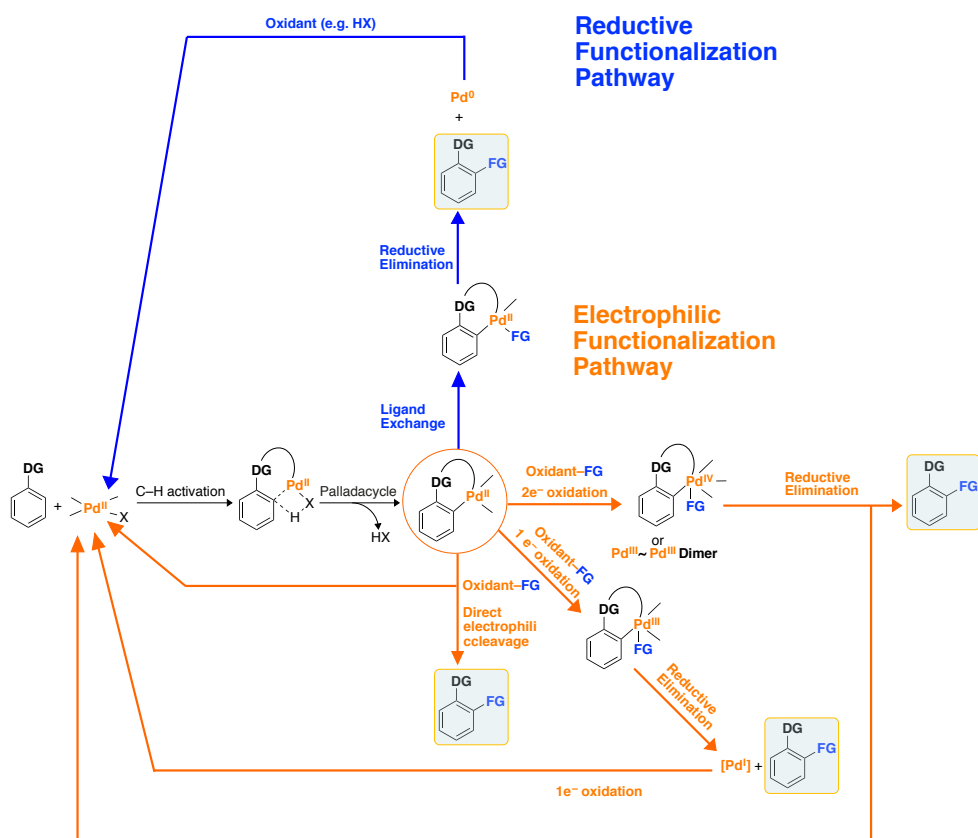
Figure 5.2. Reductive and electrophilic functionalization mechanistic pathways based on Pd(II) as a metal center. Modified from ref. 132.

i.   Direct electrophilic cleavage of M–C bond accompanied by no change in oxidation state of the metal center.

ii. One electron oxidation of cyclometalated intermediate.

iii. Two electron oxidation of cyclometalated intermediate to form either M^{IV} intermediate or M^{III}~M^{III} dimer depending on the chemical environment at the metal center.

5.2. Supported palladium(II) carbene complexes mediated C–H halogenation of arenes

Halogenation of C–H bonds under heterogeneous catalysis conditions has demonstrated great potential to synthesize valuable and structurally complex products from simple starting materials.[133-136] Encouraged by the success of our previous results in undirected oxygenation of C_{sp2}–H bond, we set out to apply our heterogeneous catalysts also in directed C_{sp2}–H halogenation of arenes. After we optimized the reaction conditions, the scope of the C–H chlorination of different aryl pyridines catalysed by **P@2b**, **P@2f** (bearing the polymerizable vinyl arm in the backbone of the NHC ligand), **rGO@2** and **2c** (homogeneous analogue of **rGO@2**) was investigated (Figure 5.3). In the chlorination of the indicated aryl pyridines in Figure 5.3, **P@2b** showed the best activity and regioselectivity (except for substrates **4** and **5**) among all our catalyst systems under this study. In the bromination of benzo[*h*]quinoline **2**, Although, **P@2f** afforded 82% total yield and regioselectivity 67:33 for mono- and di-brominated adducts, **P@2b** provided the mono-brominated product in 68% yield and 100% regioselectivity. Even though the heterogeneous catalysts in this study showed no ability to form C–I bond during the iodination of benzo[*h*]quinoline **2**, these systems exhibited very good activity and excellent regioselectivity in catalytic iodination reaction of aryl pyridines (Figure 5.3). In contrast, the homogeneous analogue afforded 98% total yield of **1-I** and **1-I$_2$**, but the regioselectivity was 82:18 for mono- and di-iodinated adducts.
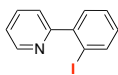
Figure 5.3. Scope of direct C–H halogenation of arylpyridines catalyzed by supported Pd(II) catalysts. [a] Isolated yields were monitored by ^{1}HNMR spectroscopy and HRMS. GC yields and conversions (reported in parentheses) were determined by GC using a calibration curve based on decane as an internal standard. [b] Traces of di-substituted product was detected by GC-MS. [c] Regioselectivity is 67:33 of **1-Br**:**1-Br$_2$**. [d] Traces of mono-chlorinated adduct was detected in GC-MS and analyzed by 1HNMR spectroscopy. Modified from paper III and V.

5.3. Recyclability and the nature of the supported Pd based catalysts

The recyclability of **P@2b**, **P@2f** and **rGO@2** was examined using iodination of 2-phenylpyridine as the model reaction under the conditions described in Figure 5.4.
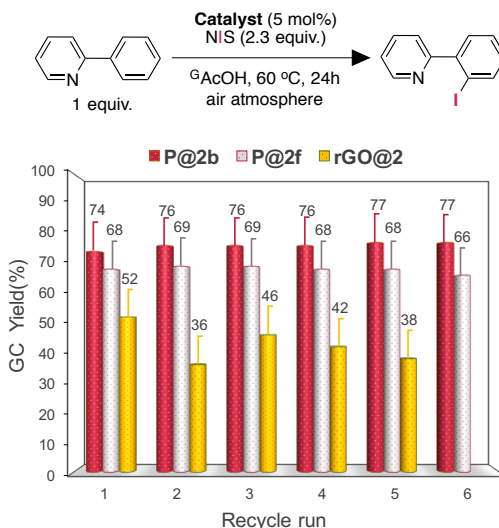
Figure 5.4. Reusability and productivity of **P@2b**, **P@2f** and **rGO@2** catalysed C-H iodination reaction of 2-phenylpyridine. Yields were determined by GC using a calibration curve based on decane as an internal standard. Modified from paper III and V.

The recovered catalysts were separated easily by centrifugation after each run, and then washed with 5 ml of related pyridine ligand/CH_2Cl_2 solutions for 30 min followed by washing with MeCN to remove the remaining non-bonded pyridines. The activity for polymeric catalysts was constant up to six runs (Figure 5.4), while **rGO@2** exhibited a fluctuation in GC yields of the mono-iodinated product during five times reuse. A very small leaching into the supernatant (0.011 and 0.009 ppm) was detected by ICP-OES analysis after the 6th run with **P@2b** and **P@2f** respectively. XP spectra disclosed that the palladium is present in oxidation state (II) up to 6 cycles (and likely more), see paper III for more details. Then, we set out to follow the formation of the product with time. The kinetic profile for **P@2b** and **P@2f** are more or less identical. The catalysis stopped after eight and ten hours in case of **P@2b** and **P@2f** respectively, due to the consumption or degradation of the

oxidant through the catalysis reaction (Figure 5.5a). According to the reaction conditions that is shown in Figure 5.5b, a time profile study of **rGO@1** was performed. No induction period was observed and the catalysis almost stopped after 12 hours. A hot filtration test was performed to confirm the heterogeneous nature of the catalysts. No further reaction was observed for all three catalysts, which is indicating that no catalytically active catalyst remained in the filtrates (Figure 5.5b), corroborating that the catalysts are heterogeneous in nature.
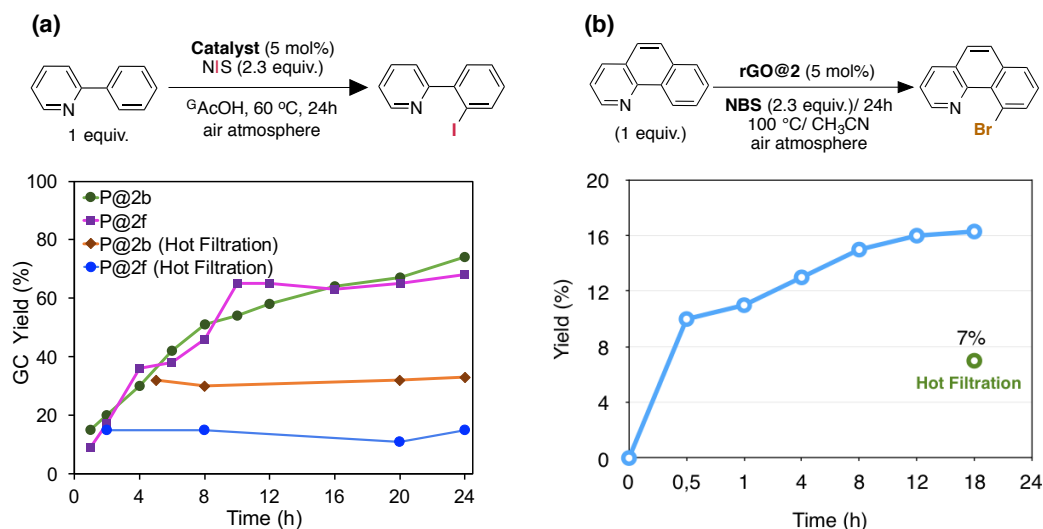
Figure 5.5. a) Time profile and hot filtration study of **P@2b** and **P@2f** catalyzing the indicated reaction. b) Time profile and hot filtration study of **rGO@2** catalyzing the indicated reaction. Yields were determined by GC using a calibration curve based on decane as an internal standard. Modified from paper III and V.

5.4. C–H chlorination and the nature of the catalyst under continuous flow conditions

Continuous-flow processes are strongly preferred in the petro- and bulk chemicals industry. Compared to the batch reaction processes, continuous flow organic synthesis offers attractive advantages in terms of:

i)   The environmental and safety regulations, where no accumulation of highly unstable intermediates occurs, the chemical waste is reduced and side reactions are minimized.

ii)   The reaction efficiency (time and cost effective process).

To our knowledge there are no examples of N-directed C–H functionalizations that make use of heterogeneous catalysts in a packed-bed reactor under continuous flow. Therefore, a packed-bed reactor was employed to investigate the prolonged activity and stability of **P@2b** catalyst under C–H oxidation conditions. As was previously mentioned, the catalysis reaction of benzo[*h*]quinoline **2** in CH₃CN afforded non-directed chlorination in 21% yield; we predicted that the shorter interaction of the product with the catalyst would improve the selectivity in a continuous process. Using the optimal reaction conditions, the continuous flow process was implemented as shown in Figure 5.6.
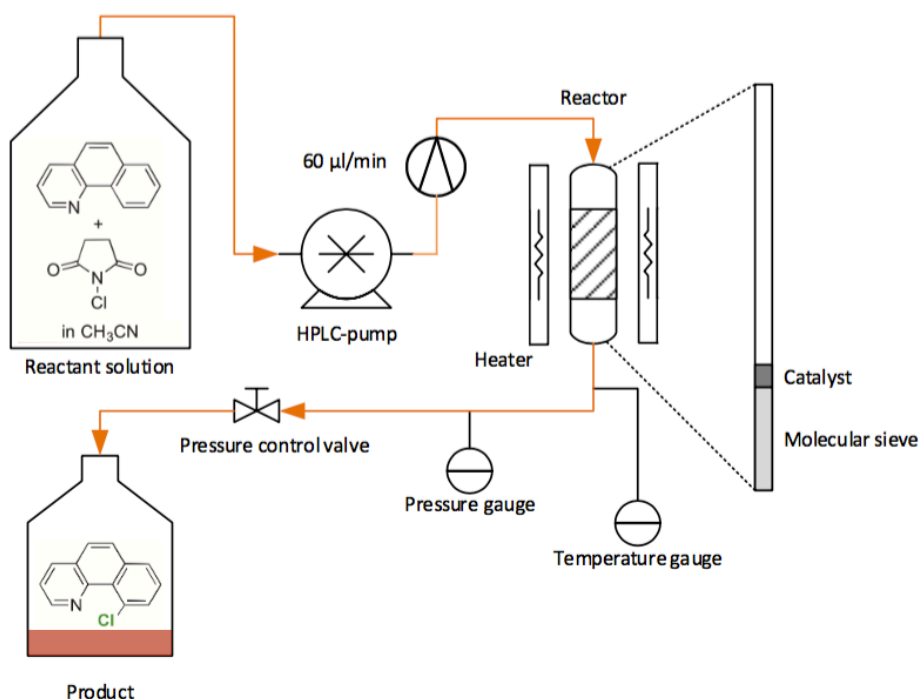
Figure 5.6. Schematic of the continuous flow reactor system. Modified from paper III.

During the whole experiment, we used 0.5 mol% of **P@2b** inside the reactor, one batch of reactants solution, 60 μl/min flow rate, where this can adjust the residence time of the reactants with the catalyst to be short. In the filtration test, we realized that the small particles of the catalyst (<100 nm) easily skipped through the standard filters of the continuous flow system. Therefore, molecular sieves (3Å, powder) were added at the bottom of the reactor to act as an even smaller filter to retain the polymer particles (see the Supporting Information of paper III for details about catalyst packing and experimental procedure under continuous flow). Samples were collected continuously every hour using an auto sampler attached to the reactor outlet. After 5 h reaction time, GC detected only 39% yield of 10-chlorobenzo[*h*]quinoline **2-Cl**. However, the conversion required 10 h to stabilize and attain consistently $\sim$ 90% yield and 100% regioselectivity of the product until the end of the experiment after $\sim$ 6 days (140h) as shown in the conversion plot (Figure 5.7).
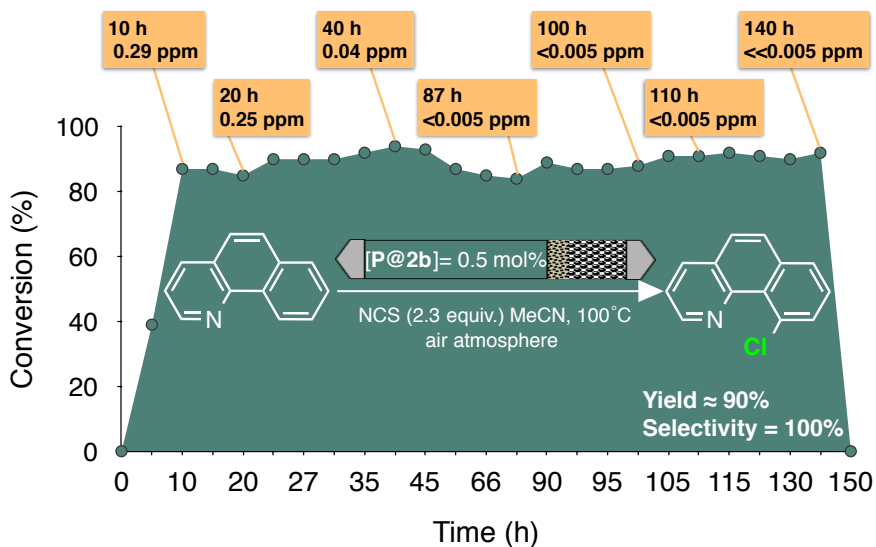
Figure 5.7. Conversion and Pd leaching of **P@2b** catalyzed C-H chlorination under flow conditions. Yield and selectivity were determined by GC using a calibration curve based on decane as an internal standard. Modified from paper III.

The Pd leaching was determined by ICP-OES analysis. Initially, a low level of Pd leaching was detected after 10 h run (0.29 ppm), and it decreased gradually upon increasing the time to record very low levels under the detection limit of ICP technique (0.04, <0.005, <0.005, <0.005, <0.005, and <<0.005 ppm at 40, 87, 100, 110 and 140 h respectively) as shown in Figure 5.7. Importantly, the recovered

catalyst after 6 days continuous reaction shows no significant peak in Pd 3d spectrum, on the level of the spectral noise, associated with Pd(0) Figure 5.8. Additionally, the Pd $3d_{5/2}$ and Pd $3d_{3/2}$ signals at ca 338.5 and 344 eV binding energy match the energies expected for a Pd(II) species. In line with that, the binding energy for the Cl after 6 days continuous reaction (Figure 5.8) is in good agreement with **2b**. The XPS results confirmed the long-term stability of **P@2b** and is probably explained by its robust microsphere polymer structure which maintains the Pd(II) oxidation state during the flow process.
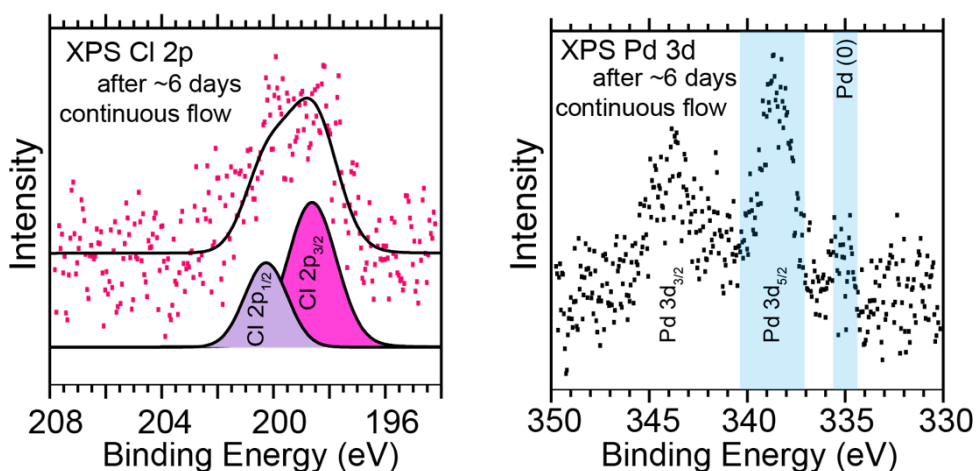
Figure 5.8. XP spectra of the Cl 2p and Pd 3d core level of **P@2b** respectively, obtained after 140 h catalysis under continuous flow conditions. Modified from paper III.

5.5. Conclusions

P@2b, **P@2f** and **rGO@2** can be successfully recovered and reused without loss of reactivity over several cycles in batch mode C–H iodination. The polymeric catalysts active as heterogeneous catalysts with an inconsiderable leaching of Pd. Remarkably, the synthesized heterogeneous catalyst **P@2b** exhibited a tremendous stability and activity under the oxidation conditions, and could be used continuously for at least ~ 6 days without losing its activity; it maintains the original oxidation state of Pd(II) under long-term continuous flow conditions. The heterogeneous character of these catalysts was explored, and the catalysts were heterogeneous according to the hot filtration tests.

6. Perspective and outlooks

This work presented efforts to develop and describe new classes of Pd(II)-NHC based heterogeneous catalysts using several synthetic methods and a variety of characterization techniques. The catalytic activity of these novel catalysts was evaluated in C–H activation reactions involving different arenes and phenylpyridines.

In chapter two, we have described the synthesis and characterization of the Pd(II)–NHC precursors bearing diverse functionalities on the N-heterocycle ring, by using different approaches. It was shown, that some of these methods are not effective for obtaining Pd(II)–NHC complexes containing two pyrene moieties in high yields. Future efforts can be aimed at performing other kinds of synthetic approaches that could lead to increased yield of such Pd(II)–NHC precursors.

In chapter three, we presented our efforts to immobilize Pd(II)–NHC complexes using two different types of supporting systems/ materials and by employing different supporting strategies. We successfully synthesized polymer supported Pd(II)–NHC complexes by co-polymerization method, and attached double and single anthracene-tagged Pd(II) carbene complexes on an rGO support using π-stacking approach. We showed that before performing any catalytic studies, it is important to characterize and understand the prepared catalytic systems. Future efforts can be focused on improving the π-stacking approach in the way that is able to increase the Pd loading in the supported material.

In C–H activation/ oxygenation and halogenation of arenes, the catalytic activity and the selectivity of the supported Pd(II)–NHC catalysts, in comparison to homogeneous analogues, was tested and this is the main themes of chapter four and five. Moreover, we found that the polymer based catalyst has a tremendous stability and activity and it could be used under long-term continuous flow conditions. Therefore, it is worth to apply these new supported catalysts for other catalytic transformations under batch and flow processes.

To further our understanding, we also attempted to investigate the reaction mechanism of a newly developed π-stacked catalyst. The study provided us with important details about the nature of the catalyst during the reaction; this needs to be expanded in the future to reveal more details about the active species during catalysis.

References

1. Blanksby, S. J.; Ellison, G. B., *Acc. Chem. Res.* **2003**, 36, 255-263.
2. Li, J. J., *C-H bond activation in organic synthesis*. Taylor & Francis Group: Boca Raton, **2015**.
3. Sheldon, R. A., *Chem. Commun.* **2008**, 3352-3365.
4. Basch, H.; Mogi, K.; Musaev, D. G.; Morokuma, K., *J. Am. Chem. Soc.* **1999**, 121, 7249-7256.
5. Westerheide, L.; Pascaly, M.; Krebs, B., *Curr. Opin. Chem. Biol.* **2000**, 4, 235-241.
6. Moulijn, J. A.; Leeuwen, P. W. N. M. v.; Santen, R. A. v., *Catalysis : an integrated approach to homogeneous, heterogeneous and industrial catalysis*; New York, **1993**.
7. Ertl, G., *Angew. Chem. Int. Ed.* **2008**, 47 , 3524-3535.
8. Sheldon, R. A., *J R Soc Interface* **2016**, 13.
9. Brink, G. J.; Arends, I. W.; Sheldon, R. A., *Science* **2000**, 287, 1636-1639.
10. Schlogl, R., *Angew. Chem. Int. Ed.* **2015**, 54 , 3465-520.
11. Rothenberg, G., *Catalysis : concepts and green applications*. Wiley-VCH: Weinheim ; Chichester, **2008**.
12. Fadhel, A. Z.; Pollet, P.; Liotta, C. L.; Eckert, C. A., *Molecules* **2010**, 15, 8400-8424.
13. Lutz, E. F., *J. Chem. Ed.* **1986**, 63, 202-203.
14. Falbe, J.; Bahrmann, H., *J. Chem. Ed.* **1984**, 61, 961-967.
15. Lebedeva, M. A.; Chamberlain, T. W.; Schroder, M.; Khlobystov, A. N., *Chem. Mater.* **2014**, 26, 6461-6466.
16. Barbaro, P.; Liguori, F., *Heterogenized homogeneous catalysts for fine chemicals production: materials and processes*. Springer: Dordrecht; New York, **2010**.
17. Bukhryakov, K. V.; Mugemana, C.; Vu, K. B.; Rodionov, V. O., *Org. Lett.* **2015**, 17, 4826-4829.
18. Hubner, S.; de Vries, J. G.; Farina, V., *Adv. Synth. Catal.* **2016**, 358, 3-25.
19. Hagen, J., *Industrial catalysis : a practical approach*. 2nd; Wiley-VCH: Weinheim, **2006**.
20. Arduengo, A. J.; Harlow, R. L.; Kline, M., *J. Am. Chem. Soc.* **1991**, 113, 361-363.

21.   Zhong, R.; Lindhorst, A. C.; Groche, F. J.; Kuhn, F. E., *Chem. Rev.* **2017**, 117, 1970-2058.

22.   Zhao, D. B.; Candish, L.; Paul, D.; Glorius, F., *ACS Catal.* **2016**, 6, 5978-5988.

23.   Hopkinson, M. N.; Richter, C.; Schedler, M.; Glorius, F., *Nature* **2014**, 510, 485-496.

24.   Kaufhold, S.; Petermann, L.; Staehle, R.; Rau, S., *Coordin. Chem. Rev.* **2015**, 304, 73-87.

25.   Bezier, D.; Sortais, J. B.; Darcel, C., *Adv. Synth. Catal.* **2013**, 355, 19-33.

26.   Harlang, T. C. B.; Liu, Y. Z.; Gordivska, O.; Fredin, L. A.; Ponseca, C. S.; Huang, P.; Chabera, P.; Kjaer, K. S.; Mateos, H.; Uhlig, J.; Lomoth, R.; Wallenberg, R.; Styring, S.; Persson, P.; Sundstrom, V.; Warnmark, K., *Nat. Chem.* **2015**, 7, 883-889.

27.   Chabera, P.; Liu, Y. Z.; Prakash, O.; Thyrhaug, E.; El Nahhas, A.; Honarfar, A.; Essen, S.; Fredin, L. A.; Harlang, T. C. B.; Kjaer, K. S.; Handrup, K.; Ericson, F.; Tatsuno, H.; Morgan, K.; Schnadt, J.; Haggstrom, L.; Ericsson, T.; Sobkowiak, A.; Lidin, S.; Huang, P.; Styring, S.; Uhlig, J.; Bendix, J.; Lomoth, R.; Sundstrom, V.; Persson, P.; Warnmark, K., *Nature* **2017**, 543, 695.

28.   Credendino, R.; Falivene, L.; Cavallo, L., *J. Am. Chem. Soc.* **2012**, 134, 8127-8135.

29.   Khramov, D. M.; Lynch, V. M.; Bielawski, C. W., *Organometallics* **2007**, 26, 6042-6049.

30.   Hu, X. L.; Tang, Y. J.; Gantzel, P.; Meyer, K., *Organometallics* **2003**, 22, 612-614.

31.   Garrison, J. C.; Simons, R. S.; Kofron, W. G.; Tessier, C. A.; Youngs, W. J., *Chem. Commun.* **2001**, 18, 1780-1781.

32.   Pompeo, M.; Froese, R. D. J.; Hadei, N.; Organ, M. G., *Angew. Chem. Int. Ed.* **2012**, 51, 11354-11357.

33.   Leuthausser, S.; Schwarz, D.; Plenio, H., *Chem. Eur. J.* **2007**, 13, 7195-7203.

34.   Wiles, C.; Watts, P., *Green Chem.* **2014**, 16, 55-62.

35.   Rueping, M.; Vila, C.; Bootwicha, T., *ACS Catal.* **2013**, 3, 1676-1680.

36.   Gemoets, H. P. L.; Laudadio, G.; Verstraete, K.; Hessel, V.; Noel, T., *Angew. Chem. Int. Ed.* **2017**, 56, 7161-7165.

37.   Price, G. A.; Bogdan, A. R.; Aguirre, A. L.; Iwai, T.; Djuric, S. W.; Organ, M. G., *Catal. Sci. Technol.* **2016**, 6, 4733-4742.

38.   Martinez, A.; Krinsky, J. L.; Penafiel, I.; Castillon, S.; Loponov, K.; Lapkin, A.; Godard, C.; Claver, C., *Catal. Sci. Technol.* **2015**, 5, 310-319.

39.   Price, G. A.; Hassan, A.; Chandrasoma, N.; Bogdan, A. R.; Djuric, S. W.; Organ, M. G., *Angew. Chem. Int. Ed.* **2017**, 56, 13347-13350.

40.   Manabe, Y.; Kitawaki, Y.; Nagasaki, M.; Fukase, K.; Matsubara, H.; Hino, Y.; Fukuyama, T.; Ryu, I., *Chem. Eur. J.* **2014**, 20, 12750-12753.

41. Pascanu, V.; Hansen, P. R.; Gomez, A. B.; Ayats, C.; Platero-Prats, A. E.; Johansson, M. J.; Pericas, M. A.; Martin-Matute, B., *ChemSusChem* **2015**, 8, 123-130.

42. Herrmann, W. A., *Angew. Chem. Int. Ed.* **2002**, 41, 1290-1309.

43. Ofele, K.; Tosh, E.; Taubmann, C.; Herrmann, W. A., *Chem. Rev.* **2009**, 109, 3408-44.

44. Spessard, G. O.; Miessler, G. L., *Organometallic chemistry*. Third edition. ed.; Oxford University Press: New York, **2016**.

45. Weskamp, T.; Bohm, V. P. W.; Herrmann, W. A., *J. Organomet. Chem.* **2000**, 600, 12-22.

46. Lin, I. J. B.; Vasam, C. S., *Comment. Inorg. Chem.* **2004**, 25, 75-129.

47. Wang, L.; Chen, E. Y. X., *ACS Catal.* **2015**, 5, 6907-6917.

48. Kim, J. H.; Kim, J. W.; Shokouhimehr, M.; Lee, Y. S., *J. Org. Chem.* **2005**, 70, 6714-6720.

49. Zhao, D. B.; Fei, Z. F.; Ang, W. H.; Dyson, P. J., *Small* **2006**, 2, 879-883.

50. Fu, C. L.; Meng, L. J.; Lu, Q. H.; Fei, Z. F.; Dyson, P. J., *Adv. Funct. Mater.* **2008**, 18, 857-864.

51. Ghazali-Esfahani, S.; Song, H. B.; Paunescu, E.; Bobbink, F. D.; Liu, H. Z.; Fei, Z. F.; Laurenczy, G.; Bagherzadeh, M.; Yan, N.; Dyson, P. J., *Green Chem.* **2013**, 15, 1584-1589.

52. Blackburn, G. M.; Lockwood, G.; Solan, V., *J. Chem. Soc. Perkin Trans. 2* **1976**, (12), 1452-1456.

53. Mähärrämov, A. M.; Mahmudov, K. T.; Kopylovich, M. N.; Pombeiro, A. J. L., *Non-covalent interactions in the synthesis and design of new compounds*. John Wiley & Sons: Hoboken, New Jersey, **2016**.

54. Oisaki, K.; Li, Q. W.; Furukawa, H.; Czaja, A. U.; Yaghi, O. M., *J. Am. Chem. Soc.* **2010**, 132, 9262-9264.

55. Allen, D. P.; Van Wingerden, M. M.; Grubbs, R. H., *Org. Lett.* **2009**, 11, 1261-1264.

56. Smith, T. W.; Zhao, M.; Yang, F.; Smith, D.; Cebe, P., *Macromolecules* **2013**, 46, 1133-1143.

57. Wang, H. M. J.; Lin, I. J. B., *Organometallics* **1998**, 17, 972-975.

58. Fremont, P.; Scott, N. M.; Stevens, E. D.; Ramnial, T.; Lightbody, O. C.; Macdonald, C. L. B.; Clyburne, J. A. C.; Abernethy, C. D.; Nolan, S. P., *Organometallics* **2005**, 24, 6301-6309.

59. Chartoire, A.; Frogneux, X.; Boreux, A.; Slawin, A. M. Z.; Nolan, S. P., *Organometallics* **2012**, 31, 6947-6951.

60. Lu, X. Y.; Chen, F.; Xu, W. F.; Chen, X. T., *Inorg. Chim. Acta.* **2009**, 362, 5113-5116.

61. Citta, A.; Schuh, E.; Mohr, F.; Folda, A.; Massimino, M. L.; Bindoli, A.; Casini, A.; Rigobello, M. P., *Metallomics* **2013**, 5, 1006-1015.

62.   Hintermair, U.; Englert, U.; Leitner, W., *Organometallics* **2011**, 30, 3726-3731.

63.   Kühl, O., *Functionalised N-heterocyclic carbene complexes*. Wiley: Chichester, U.K., **2010**.

64.   Zeng, X. M.; Zhang, T. X.; Qin, Y. C.; Wei, Z. J.; Luo, M. M., *Dalton Trans.* **2009**, 39, 8341-8348.

65.   Yang, H. Q.; Han, X. J.; Li, G. A.; Ma, Z. C.; Hao, Y. J., *J. Phys. Chem. C* **2010**, 114, 22221-22229.

66.   Berardi, S.; Carraro, M.; Iglesias, M.; Sartorel, A.; Scorrano, G.; Albrecht, M.; Bonchio, M., *Chem. Eur. J.* **2010**, 16, 10662-10666.

67.   Koytepe, S.; Seckin, T.; Yasar, S.; Ozdemir, I., *Des. Monomers Polym.* **2008**, 11, 409-422.

68.   Pahlevanneshan, Z.; Moghadam, M.; Mirkhani, V.; Tangestaninejad, S.; Mohammadpoor-Baltork, I.; Rezaei, S., *App.l Organomet. Chem.* **2015**, 29, 678-682.

69.   Van Berlo, B.; Houthoofd, K.; Sels, B. F.; Jacobs, P. A., *Adv. Synth. Catal.* **2008**, 350, 1949-1953.

70.   Georgakilas, V.; Tiwari, J. N.; Kemp, K. C.; Perman, J. A.; Bourlinos, A. B.; Kim, K. S.; Zboril, R., *Chem. Rev.* **2016**, 116, 5464-5519.

71.   Podeszwa, R.; Szalewicz, K., *Phys. Chem. Chem. Phys.* **2008**, 10, 2735-2746.

72.   Sun, Y. B.; Yang, S. B.; Zhao, G. X.; Wang, Q.; Wang, X. K., *Chem. Asian J.* **2013**, 8 (11), 2755-2761.

73.   Liu, G. Y.; Wu, B.; Zhang, J. Z.; Wang, X. L.; Shao, M. B.; Wang, J. H., *Inorg. Chem.* **2009**, 48 (6), 2383-2390.

74.   Hummers, W. S.; Offeman, R. E., *J. Am. Chem. Soc.* **1958**, 80, 1339-1339.

75.   Stankovich, S.; Dikin, D. A.; Piner, R. D.; Kohlhaas, K. A.; Kleinhammes, A.; Jia, Y.; Wu, Y.; Nguyen, S. T.; Ruoff, R. S., *Carbon* **2007**, 45, 1558-1565.

76.   Park, S.; Hu, Y. C.; Hwang, J. O.; Lee, E. S.; Casabianca, L. B.; Cai, W. W.; Potts, J. R.; Ha, H. W.; Chen, S. S.; Oh, J.; Kim, S. O.; Kim, Y. H.; Ishii, Y.; Ruoff, R. S., *Nat. Commun.* **2012**, 3, 1-8.

77.   Taylor, R. E., *Concept. Magn. Reson. A* **2004**, 22a, 37-49.

78.   Blanc, F.; Coperet, C.; Lesage, A.; Emsley, L., *Chem. Soc. Rev.* **2008**, 37, 518-26.

79.   McDermott, A. E.; Polenova, T., *Solid-state NMR studies of biopolymers*. Wiley: Oxford, **2010**.

80.   Hennel, J. W.; Klinowski, J., *New Techniques in Solid-State NMR,* Springer Berlin Heidelberg: Imprint: Springer, **2005**.

81.   Liu, J. Y., *J. Electron. Microsc.* **2005**, 54, 251-278.

82.   Williams, D. B.; Carter, C. B., *Transmission electron microscopy: A textbook for materials science*. 2nd ed. ed.; Springer: New York ; London, **2009**.

83. Langford, J. I.; Louer, D., *Rep. Prog. Phys.* **1996**, 59, 131-234.

84. Fultz, B.; Howe, J.; SpringerLink, Transmission Electron Microscopy and Diffractometry of Materials. In *Graduate Texts in Physics*, 4th ed.; Springer Berlin Heidelberg : Imprint: Springer, **2013**.

85. Jenkins, R.; Snyder, R. L., *Introduction to X-ray powder diffractometry*. Wiley: New York, **1996**.

86. Sardela, M., *Practical materials characterization*. Springer: New York, NY, **2014**.

87. Schmal, M., *Heterogeneous Catalysis and its Industrial Applications*. Springer International Publishing : Imprint: Springer, **2016**.

88. Kumar, C. S. S. R., *Surface Science Tools for Nanomaterials Characterization*. Springer Berlin Heidelberg: Imprint: Springer, **2015**.

89. Schnohr, C. S. e.; Ridgway, M. C. e., *X-ray absorption spectroscopy of semiconductors*. In Springer Series in Optical Sciences, Springer Berlin Heidelberg : Imprint, **2015**.

90. Heidenreich, N.; Rutt, U.; Koppen, M.; Inge, A. K.; Beier, S.; Dippel, A. C.; Suren, R.; Stock, N., *Rev. Sci. Instru.* **2017**, 88, 104102(1)-104102(12).

91. Seregin, I. V.; Gevorgyan, V., *Chem. Soc. Rev.* **2007**, 36, 1173-1193.

92. Labinger, J. A.; Bercaw, J. E., *Nature* **2002**, 417, 507-514.

93. Neufeldt, S. R.; Sanford, M. S., *Acc. Chem. Res.* **2012**, 45, 936-946.

94. Lyons, T. W.; Sanford, M. S., *Chem. Rev.* **2010**, 110, 1147-1169.

95. Eberson, L.; Gomezgon.L, *J. Chem. Soc. Chem. Comm.* **1971**, 6, 263.

96. Eberson, L.; Jonsson, L., *J. Chem. Soc. Chem. Comm.* **1974**, 21, 885-886.

97. Yoneyama, T.; Crabtree, R. H., *J. Mol. Catal. A* **1996**, 108, 35-40.

98. Goldberg, K. I.; Goldman, A. S.; *Activation and functionalization of C–H bonds*. American Chemical Society : Distributed by Oxford University Press: Washington, DC, **2004**.

99. Hartwig, J. F.; Larsen, M. A., *ACS Central Sci.* **2016**, 2, 281-292.

100. Cook, A. K.; Sanford, M. S., *J. Am. Chem. Soc.* **2015**, 137, 3109-3118.

101. Cernak, T.; Dykstra, K. D.; Tyagarajan, S.; Vachal, P.; Krska, S. W., *Chem. Soc. Rev.* **2016**, 45, 546-576.

102. Yu, J.-Q.; Shi, Z.; *Topics in Current Chemistry*, Springer Berlin Heidelberg : Imprint, **2010**.

103. Li, J. J., *C-H bond activation in organic synthesis*. Taylor & Francis Group: Boca Raton, **2015**.

104. Davies, D. L.; Macgregor, S. A.; McMullin, C. L., *Chem. Rev.* **2017**, 117, 8649-8709.

105. Garcia-Cuadrado, D.; de Mendoza, P.; Braga, A. A.; Maseras, F.; Echavarren, A. M., *J. Am. Chem. Soc.* **2007**, 129, 6880-6886.

106. Biswas, B.; Sugimoto, M.; Sakaki, S., *Organometallics* **2000**, 19, 3895-3908.

107. Tato, F.; Garcia-Dominguez, A.; Cardenas, D. J., *Organometallics* **2013**, 32, 7487-7494.
108. Bolbat, E.; Wendt, O. F., *Eur. J. Org. Chem.* **2016**, 20, 3395-3400.
109. Meyer, D.; Taige, M. A.; Zeller, A.; Hohlfeld, K.; Ahrens, S.; Strassner, T., *Organometallics* **2009**, 28, 2142-2149.
110. Desai, S. P.; Mondal, M.; Choudhury, J., *Organometallics* **2015**, 34, 2731-2736.
111. Mondal, M.; Choudhury, J., *J. Mol. Catal. A* **2017**, 426, 451-457.
112. Glorius, F.; SpringerLink, N-Heterocyclic Carbenes in Transition Metal Catalysis. In *Topics in Organometallic Chemistry*, Springer Berlin Heidelberg : Imprint, **2007**.
113. Marion, N.; Nolan, S. P., *Acc. Chem. Res.* **2008,** 41, 1440-1449.
114. Zhong, R.; Pothig, A.; Feng, Y. K.; Riener, K.; Herrmann, W. A.; Kuhn, F. E., *Green Chem.* **2014**, 16, 4955-4962.
115. Cook, A. K.; Emmert, M. H.; Sanford, M. S., *Org. Lett.* **2013**, 15, 5428-5431.
116. Valderas, C.; Naksomboon, K.; Fernandez-Ibanez, M. A., *ChemCatChem* **2016**, 8, 3213-3217.
117. Gao, J.; Teplyakov, A. V., *Catal. Today* **2014**, 238, 111-117.
118. Kang, E. T.; Ti, H. C.; Neoh, K. G.; Tan, T. C., *Polym. J.* **1988**, 20, 399-406.
119. Wang, L. Y.; Fang, P. F.; Ye, C. H.; Feng, J. W., *J. Polym. Sci. Pol. Phys.* **2006**, 44, 2864-2879.
120. De Souza, C. M. G.; Tavares, M. I. B., *J. Appl. Polym. Sci.* **2002**, 86, 116-124.
121. Nelson, W. M.; *Agricultural applications in green chemistry*. American Chemical Society : Distributed by Oxford University Press: Washington, DC, **2004**.
122. Wiese, W. H., *Libr. J.* **2003**, 128, 104.
123. Ford, M. C.; Ho, P. S., *J. Med. Chem.* **2016**, 59, 1655-1670.
124. Iskra, J.; Decker, A., Halogenated heterocycles synthesis, application and environment. In *Topics in Heterocyclic Chemistry*, Springer,: Berlin ; New York, **2012**.
125. Taylor, A. P.; Robinson, R. P.; Fobian, Y. M.; Blakemore, D. C.; Jones, L. H.; Fadeyi, O., *Org. Biomol. Chem.* **2016**, 14, 6611-6637.
126. Ho, P. S., *Halogen Bonding I: Impact on Materials Chemistry and Life Sciences*, Springer International Publishing: Imprint: Springer, **2015**.
127. Elsayed, M. S. A.; Su, Y. F.; Wang, P.; Sethi, T.; Agama, K.; Ravji, A.; Redon, C. E.; Kiselev, E.; Horzmann, K. A.; Freeman, J. L.; Pommier, Y.; Cushman, M., *J. Med. Chem.* **2017**, 60, 5364-5376.
128. Zhan, B. B.; Liu, Y. H.; Hu, F.; Shi, B. F., *Chem. Commun.* **2016**, 52, 4934-4937.
129. Do, H. Q.; Daugulis, O., *Org. Lett.* **2009**, 11, 421-3.
130. Racowski, J. M.; Sanford, M. S., *Top Organomet. Chem.* **2011**, 35, 61-84.

131. Kalyani, D.; Sanford, M. S., *Top Organomet. Chem.* **2007**, 24, 85-116.
132. Lyons, T. W.; Sanford, M. S., *Chem. Rev.* **2010**, 110, 1147-69.
133. Korwar, S.; Brinkley, K.; Siamaki, A. R.; Gupton, B. F.; Ellis, K. C., *Org. Lett.* **2015**, 17, 1782-1785.
134. Fei, H.; Cohen, S. M., *J. Am. Chem. Soc.* **2015**, 137, 2191-2194.
135. Pascanu, V.; Carson, F.; Solano, M. V.; Su, J.; Zou, X.; Johansson, M. J.; Martin-Matute, B., *Chem. Eur. J.* **2016**, 22, 3729-3737.
136. Mondal, M.; Joji, J.; Choudhury, J., *Chem. Commun.* **2017**, 53, 3185-3188.

Paper I

Synthesis and crystal structure of *trans*-dichlorido-[3-methyl-1-(4-vinylbenzyl)-1*H*-imidazol-3-ium-2-yl-κC^2](4-phenylpyridine-κN)palladium(II)

Maitham H. Majeed and Ola F. Wendt*

Centre for Analysis and Synthesis, Department of Chemistry, Lund University, Box 124 221 00, Lund, Sweden. *Correspondence e-mail: ola.wendt@chem.lu.se

The title compound, $[PdCl_2(C_{11}H_9N)(C_{13}H_{14}N_2)]$, represents a new class of palladium-based polymerizable monomer which could give a potentially catalytically active polymer. It was synthesized *via* transmetallation from the corresponding silver complex. The Pd^{II} ion coordinates two Cl anions, one C atom from the N-heterocyclic carbene (NHC) ligand and one N atom from the 4-phenylpyridine ligand, displaying a slightly distorted square-planar geometry. The dihedral angle between the imidazole ring and the pyridine ring is 34.53 (8)°. The Pd—C bond length between the NHC ligand and the Pd^{II} ion is 1.9532 (16) Å. In the crystal, weak non-classical C—H···Cl hydrogen bonds link the molecules into a tape structure along [101]. A weak π–π interaction is also observed [centroid–centroid distance = 3.9117 (11) Å].

1. Chemical context

In the last few years, palladium complexes with N-heterocyclic carbene ligands (Pd-NHCs) have received attention, *inter alia* as catalysts for cross-coupling in organic synthesis (Hadei *et al.*, 2005; Nasielski *et al.*, 2010; Valente *et al.*, 2010, 2012). NHC complexes derived from vinyl imidazolium salts are of growing significance in organometallic transformations because of their potential as precursors in heterogeneous catalysis, biocompatibility, anti-microbial activity and fuel cell applications (Dani *et al.*, 2015; Ghazali-Esfahani *et al.*, 2013; Anderson & Long, 2010; Kim *et al.*, 2005; Kuzmicz *et al.*, 2014; Seo & Chung, 2014; Li *et al.*, 2011). The crystal structures of 1-methyl-3-(4-vinylbenzyl) imidazolium hexafluoridophosphate and silver complexes with 1-methyl-3-(4-vinylbenzyl) imidazole as a carbene ligand have been reported previously (Lu *et al.*, 2009, 2010). Here we report on the crystal structure of a new type of Pd-NHC complex belonging to the group of PEPPSI (pyridine-enhanced precatalyst preparation stabilization and initiation) catalysts, which are stable towards air and moisture, and have the advantage of being easy to synthesize and handle (Hadei *et al.*, 2005).

2. Structural commentary

In the title compound, the Pd^{II} ion coordinates the five-membered NHC ligand with a Pd1—C4 bond length of 1.9532 (16) Å and the 4-phenylpyridine ligand with a Pd1—N3
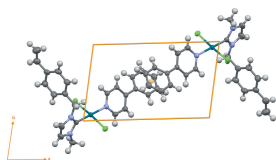
bond length of 2.0938 (14) Å. The two mutually *trans* Cl ions fulfil the coordination sphere (Fig. 1). Bond angles in the so-formed distorted square-plane are all close to 90° with the C4—Pd1—Cl angles slightly less than 90° and the others slightly more. The C4—Pd1—N3 angle shows an expected value 179.52 (6)°, while Cl1—Pd1—Cl2 exhibits a slightly distorted angle of 176.789 (17)°, probably due to the steric influence of the aromatic rings (Sevinçek *et al.*, 2007). The dihedral angle between the N1/C4/N2/C3/C2 and C6–C11 rings in the NHC ligand is 77.90 (5)°.
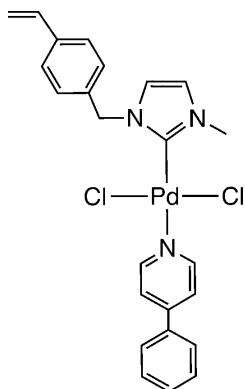
The dihedral angles between the N1/C4/N2/C3/C2 ring on one hand and the N3/C14–C18 and C19–C24 rings on the other are 34.53 (8) and 65.78 (7)°, respectively. The C12—C13 bond length of the vinyl group is 1.299 (3) Å, corroborating the double-bond character. The same goes for the C2—C3 distance which is 1.330 (3) Å. The N2—C4—Pd1—N3, N1—C4—Pd1—Cl2, C18—N3—Pd1—Cl2 and C17—C16—C19—C24 torsion angles are −30 (7), 81.15 (15), −49.40 (15) and 32.42 (3)°, respectively. A Cambridge Structural Database (CSD) search to validate the Pd—Cl and Pd—N bonding was performed over 47 entries. The Cl—Pd—Cl and N—C—N angles range from 170 to 180° and from 104.8 to 106.2°, respectively; the Pd—Cl bond lengths are in the range 2.286–2.318 Å. The bond lengths and angles of the title compound **4** are comparable to the literature values.

3. Supramolecular features

In addition to dispersion interactions, the crystal of title compound **4** shows a π–π interaction between the C19–C24

Table 1
Hydrogen-bond geometry (Å, °).

D—H$\cdots A$	D—H	H$\cdots A$	$D\cdots A$	D—H$\cdots A$
C20—H20$\cdots$Cl1^i	0.95	2.81	3.6021 (18)	142
C23—H23$\cdots$Cl2^{ii}	0.95	2.74	3.6537 (19)	162

Symmetry codes: (i) −x + 1, −y, −z + 2; (ii) −x, −y, −z + 1.
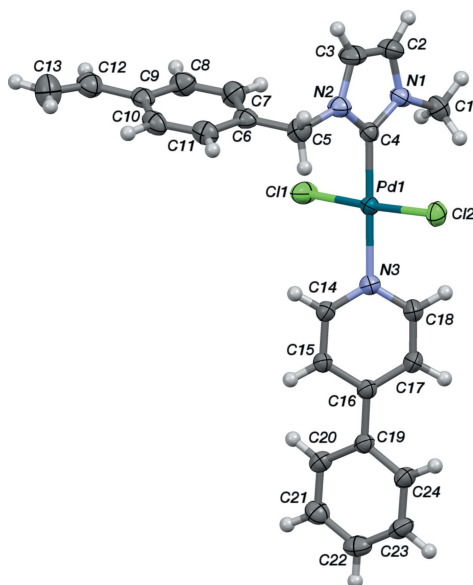
Figure 1
The molecular structure of the title compound (**4**). All non-H atoms are represented as displacement ellipsoids drawn at the 50% probability level and H atoms as small spheres with arbitrary radii.

phenyl rings of neighbouring molecules with a centroid–centroid distance of 3.9117 (11) Å (Fig. 2). Two weak non-classical C—H$\cdots$Cl hydrogen bonds are detected (Table 1). No C—H$\cdots\pi$ contacts are present in the crystal packing diagram of compound **4** (Fig. 3).

4. Synthesis and crystallization

General: Solvents and chemicals were purchased from commercial suppliers and used as received. The imidazolium salts **1** and **2** were prepared according to previously reported
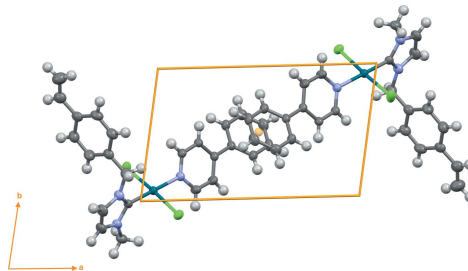
Figure 2
The dimer of the title compound (**4**) linked through the π–π interaction.
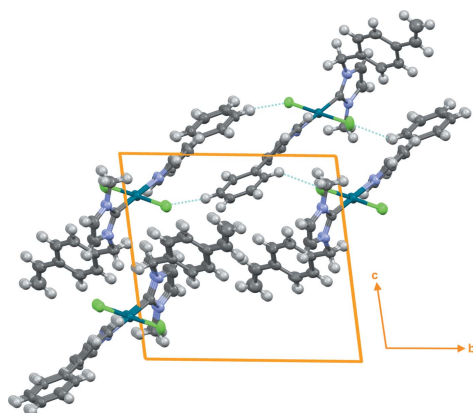
Figure 3
A crystal packing diagram of the title compound (**4**). The non-classical C—H···Cl hydrogen bonds are shown by dotted lines.

Table 2
Experimental details.

Crystal data	
Chemical formula	$[PdCl_2(C_{11}H_9N)(C_{13}H_{14}N_2)]$
M_r	530.75
Crystal system, space group	Triclinic, $P\bar{1}$
Temperature (K)	183
a, b, c (Å)	7.8768 (3), 12.2939 (5), 12.6120 (4)
α, β, γ (°)	95.692 (3), 97.267 (3), 103.574 (3)
V (Å^3)	1167.09 (8)
Z	2
Radiation type	Mo $K\alpha$
μ (mm^{-1})	1.04
Crystal size (mm)	$0.39 \times 0.27 \times 0.1$
Data collection	
Diffractometer	Agilent Xcalibur Ruby
Absorption correction	Analytical (*CrysAlis PRO*; Agilent, 2012)
T_{min}, T_{max}	0.727, 0.916
No. of measured, independent and observed [$I > 2\sigma(I)$] reflections	28730, 7116, 6179
R_{int}	0.037
$(\sin\theta/\lambda)_{max}$ (Å^{-1})	0.714
Refinement	
$R[F^2 > 2\sigma(F^2)]$, $wR(F^2)$, S	0.027, 0.068, 1.04
No. of reflections	7116
No. of parameters	272
H-atom treatment	H-atom parameters constrained
$\Delta\rho_{max}, \Delta\rho_{min}$ (e Å^{-3})	0.45, −0.42

Computer programs: *CrysAlis PRO* (Agilent, 2012), *SUPERFLIP* (Palatinus & Chapuis, 2007), *SHELXL2013* (Sheldrick, 2015) and *OLEX2* (Dolomanov *et al.*, 2009).

procedures (Kim *et al.*, 2005; Lu *et al.*, 2009). The title compound **4** was synthesized according to the carbene silver(I) route, as shown in Fig. 4. Transmetallation of the ligand from the tetrameric silver complex **2** gave the chlorido-bridged palladium dimer **3**. Cleavage of the dimer with phenylpyridine afforded complex **4** in excellent yield. With its vinyl groups it can serve as a precursor in co-polymerization reactions with *e.g.* styrene to form polymeric materials with catalytic properties.

[PdCl₂(bmim)]₂ (3). A 100 ml Schlenk flask was charged with **2** (7.0 g, 20.5 mmol), 50 ml of dry CH$_2$Cl$_2$ and Pd(PhCN)$_2$Cl$_2$ (7.8 g, 20.5 mmol). The mixture was stirred for 48 h at room temperature, during which time the solution changed colour to cloudy light brown. It was filtered through Celite and the filtrate was reduced to *ca* 10 ml. Upon addition of *n*-hexane, a light-brown solid was formed, which was collected on a frit and dried under vacuum to give 5.97 g (yield 78%).

[PdCl₂(bmbim)(4-Phenylpyridine)] (4). 4-Phenylpyridine (0.085 g, 0.55 mmol) was added to a 40 ml solution of **3** (0.25 g, 0.26 mmol) in dry CH$_3$CN and stirred at ambient temperature

for 24 h, during which time the solution changed colour to clear yellow. The mixture was filtered through Celite and all solvents were evaporated. The solids were dissolved in CH$_2$Cl$_2$ and, upon addition of *n*-hexane, a yellow solid was formed, which was collected on a frit and dried under vacuum to give 0.153 g (93%) of **4**.

Single crystals of **4** suitable for X-ray diffraction were obtained by slow diffusion of *n*-hexane into a saturated CH$_2$Cl$_2$ solution of the compound.

5. Refinement details

Crystal data and structure refinement details are summarized in Table 2. H atoms were treated as riding, with C—H = 0.95–0.99 Å, and with $U_{iso}(H) = 1.2U_{eq}(C)$.
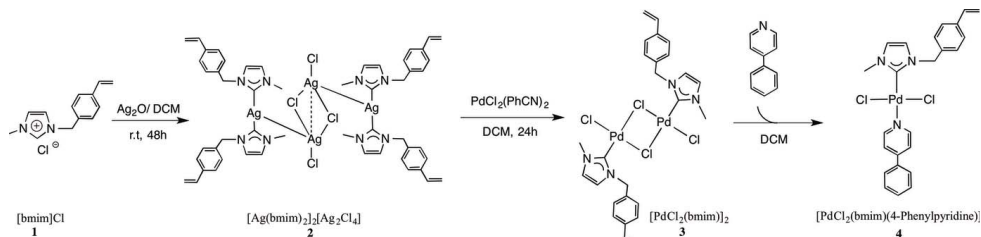
Figure 4
Synthesis pathway of the title compound (**4**).

References

Agilent (2012). *CrysAlis PRO*. Agilent Technologies Ltd, Yarnton, England.

Anderson, E. B. & Long, T. E. (2010). *Polymer*, **51**, 2447–2454.

Dani, A., Groppo, E., Barolo, C., Vitillo, J. G. & Bordiga, S. (2015). *J. Mater. Chem. A*, **3**, 8508–8518.

Dolomanov, O. V., Bourhis, L. J., Gildea, R. J., Howard, J. A. K. & Puschmann, H. (2009). *J. Appl. Cryst.* **42**, 339–341.

Ghazali-Esfahani, S., Song, H. B., Păunescu, E., Bobbink, F. D., Liu, H. Z., Fei, Z. F., Laurenczy, G., Bagherzadeh, M., Yan, N. & Dyson, P. J. (2013). *Green Chem.* **15**, 1584–1589.

Hadei, N., Kantchev, E. A. B., O'Brien, C. J. & Organ, M. G. (2005). *Org. Lett.* **7**, 3805–3807.

Kim, J. H., Kim, J. W., Shokouhimehr, M. & Lee, Y. S. (2005). *J. Org. Chem.* **70**, 6714–6720.

Kuzmicz, D., Coupillaud, P., Men, Y., Vignolle, J., Vendraminetto, G., Ambrogi, M., Taton, D. & Yuan, J. Y. (2014). *Polymer*, **55**, 3423–3430.

Li, W., Fang, J., Lv, M., Chen, C., Chi, X., Yang, Y. & Zhang, Y. (2011). *J. Mater. Chem.* **21**, 11340–11346.

Lu, X. Y., Chen, F., Xu, W. F. & Chen, X. T. (2009). *Inorg. Chim. Acta*, **362**, 5113–5116.

Lu, X.-Y., Sun, J.-F., Zhang, L. & Chen, X.-T. (2010). *Acta Cryst.* E**66**, o378.

Nasielski, J., Hadei, N., Achonduh, G., Kantchev, E. A. B., O'Brien, C. J., Lough, A. & Organ, M. G. (2010). *Chem. Eur. J.* **16**, 10844–10853.

Palatinus, L. & Chapuis, G. (2007). *J. Appl. Cryst.* **40**, 786–790.

Seo, U. R. & Chung, Y. K. (2014). *RSC Adv.* **4**, 32371–32374.

Sevinçek, R., Türkmen, H., Aygün, M., Çetinkaya, B. & García-Granda, S. (2007). *Acta Cryst.* C**63**, m277–m279.

Sheldrick, G. M. (2015). *Acta Cryst.* C**71**, 3–8.

Valente, C., Belowich, M. E., Hadei, N. & Organ, M. G. (2010). *Eur. J. Org. Chem.* pp. 4343–4354.

Valente, C., Çalimsiz, S., Hoi, K. H., Mallik, D., Sayah, M. & Organ, M. G. (2012). *Angew. Chem. Int. Ed.* **51**, 3314–3332.

Paper II

■ **N-Heterocyclic Carbenes** |*Hot Paper*|

Polymer-Supported Palladium(II) Carbene Complexes: Catalytic Activity, Recyclability, and Selectivity in C—H Acetoxylation of Arenes

Maitham H. Majeed,[a] Payam Shayesteh,[b] L. Reine Wallenberg,[a, c] Axel R. Persson,[a, c] Niclas Johansson,[b] Lei Ye,[d] Joachim Schnadt,[b] and Ola F. Wendt*[a]

Abstract: Heterogeneous catalysts for selective oxidation of C—H bonds were synthesized by co-polymerization of new N-heterocyclic carbene-palladium(II) (NHC-Pd^{II}) monomers with divinylbenzene. The polymer-supported NHC-Pd^{II}-catalysed undirected C—H acetoxylation of simple and methylated arenes as well as polyarenes, with similar or superior efficiency compared to their homogeneous analogues. In particular, the regioselectivity has been improved in the acetoxyla-tion of biphenyl and naphthalene compared to the best ho-mogeneous catalysts. The new polymer-supported catalysts maintain the original oxidation state of Pd^{II} after repeated catalytic reactions, and exhibit no significant leaching of pal-ladium. In addition, the new catalysts have been successfully recovered and reused without loss of activity over several cycles of reactions.

Introduction

The selective oxidation of undirected C—H bonds can simplify the functionalization of hydrocarbons and is therefore poten-tially very useful in the synthesis of both fine and bulk chemi-cals.[1] Thus, it can help in reducing waste in large-scale trans-formations, and in the synthesis of more complex molecules it can enable late-stage functionalization. So far, the most suc-cessful approach to the selective oxidation of C—H bonds has been ligand-directed C—H functionalization, in which a heteroa-tom controls the regioselectivity.[2,3] However, although some progress has been made,[4,5] there are still no general, regiose-lective methods for the functionalization of simple alkanes or arenes neither by homogeneous nor heterogeneous catalysts. To address this shortcoming substantial research efforts have been devoted during several decades to developing Pd cata-

lysts for the undirected C—H acetoxylation of arenes using dif-ferent oxidants.[6–8] One successful strategy has been the use of Pd(OAc)$_2$ as a catalyst, PhI(OAc)$_2$ as an oxidant, and pyridine derivatives as supporting ligands,[9] a system that catalyses the acetoxylation of undirected arenes via non-radical pathways.[10] As a ligated alternative to the Pd acetate catalyst in C—H acti-vation NHC-Pd complexes have been reported recently.[11–18] The ligand adds stability to the system due to the strong NHC···M interaction, and it also enables functionalization and ligand control.[15,19,20] Moreover, to further aid catalyst separa-tion and recovery, the NHC-M complex can be heterogen-ized.[21] Indeed, the development of stable heterogeneous cata-lysts would substantially facilitate any industrial application.[22] There are many examples of supported Pd^{II} catalysts,[23–27] and polymer-supported NHC-Pd complexes have been successfully used in many applications and for different chemical transfor-mations, and advances in support strategies have been made recently.[26,28–35] However, metal leaching, reduction of the Pd^{II} species during preparation steps and catalysis and aggregation of Pd^0 nanoparticles inside the polymer matrixes remains an unsolved problem in many cases.[36,37] However, although di-rected C—H activation over supported Pd complexes has been reported, there are no examples of the application of such cat-alysts for undirected C—H activation reactions.[38–41]

Herein we report on the synthesis and characterization of a Pd^{II} containing a polymeric material based on the co-poly-merization of polymerizable arms in the structure of an N-het-erocyclic carbene ligand and divinylbenzene (Scheme 1). Our concept gave a material which is stable towards reduction and recyclable with no or little loss in activity. Its reactivity and re-gioselectivity in the C—H oxidation of arenes is reported to-gether with the effect of various stabilizing pyridine ligands.

[a] M. H. Majeed, Prof. L. R. Wallenberg, A. R. Persson, Prof. O. F. Wendt
Centre for Analysis snd Synthesis, Department of Chemistry
Lund University, Box 124, 221 00, Lund (Sweden)
E-mail: ola.wendt@chem.lu.se

[b] P. Shayesteh, N. Johansson, Prof. J. Schnadt
Division of Synchrotron Radiation Research
Department of Physics, Lund University
Box 118, 221 00, Lund (Sweden)

[c] Prof. L. R. Wallenberg, A. R. Persson
National Center for High Resolution Electron Microscopy
Lund University, Box 124, 221 00, Lund (Sweden)

[d] Prof. L. Ye
Centre for Applied Life Sciences
Department of Chemistry, Lund University
Box 124, 221 00, Lund (Sweden)

Supporting information and the ORCID number(s) for the author(s) of this article can be found under https://doi.org/10.1002/chem.201700777.
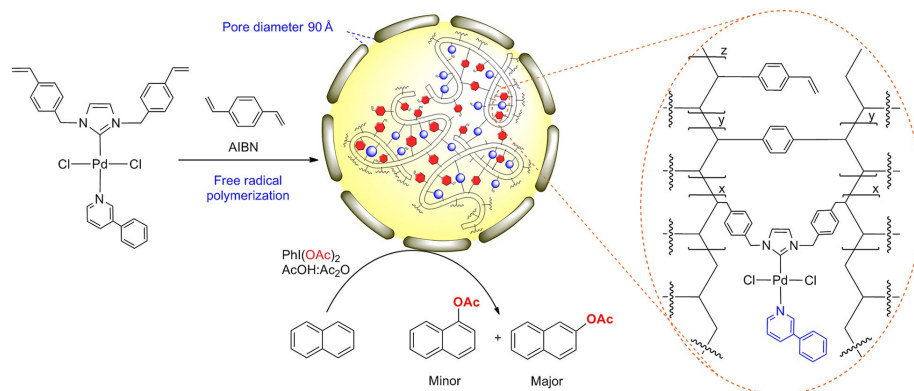
Scheme 1. Polymerized NHC-Pd^{II} monomer can catalyse C–H acetoxylation of undirected arene.

Productivity is equal to the corresponding homogeneous catalysts and selectivity is in many cases substantially better.

Results and Discussion

Monomers: synthesis and characterization

Imidazolium chloride precursors [bmim]Cl **1a** and [bvbim]Cl **1b** were synthesized according to previously reported procedures.[42–45] We chose these precursors based on that they either have one (**1a**) or two (**1b**) polymerizable arms to investigate whether this leads to a difference in stability or selectivity. In particular, the degree of cross-linking is expected to vary with the number of vinyl groups in the monomer. Direct metallation using literature procedures afforded [Ag(bmim)]$_2$ [Ag$_2$Cl$_4$] **2a**[46] and Ag[bvbim]Cl complex **2b** in good yield (Figure 1). ^{13}C NMR spectra showed the characteristic carbene signals at 180.7 and 180.9 ppm for **2a** and **2b**, respectively.[46–50] The use of silver intermediates precluded any radical polymerization of the vinyl moiety at an earlier stage; some other protocols use harsh reaction conditions under which such unwanted side reactions could occur.[51] Transmetallation with PdCl$_2$(PhCN)$_2$ gave NHC-Pd^{II} dimers **3a** and **3b** (Ref. 47 and Figure 1), which showed broad signals in the ^{1}H NMR spectra due to the dynamic equilibrium between monomeric and dimeric species as previously shown.[16] Adding pyridine derivatives cleaved the dimer and afforded NHC-Pd complexes **4a**, **4b**, **5a**, **5b** and **6b** in excellent yield with one (**a**) or twovinyl (**b**) moieties and 3-phenylpyridine (**4**), 4-phenylpyridine (**5**), and 9-chloroacridine (**6**) as stabilizing ligands, respectively (cf. Figure 1 and Scheme 2). They were characterized by ^{1}H and ^{13}C NMR spectroscopy and elemental analysis. All signals were sharp and, again, characteristic carbene signals around 150 ppm were observed in the ^{13}C NMR spectra in CDCl$_3$.[51,52] Slow diffusion of *n*-hexane into a CH$_2$Cl$_2$ solution of the complexes gave X-ray quality crystals and an X-ray diffraction (XRD) analysis confirmed the molecular structures of **4a**, **5a**,[47] **4b**
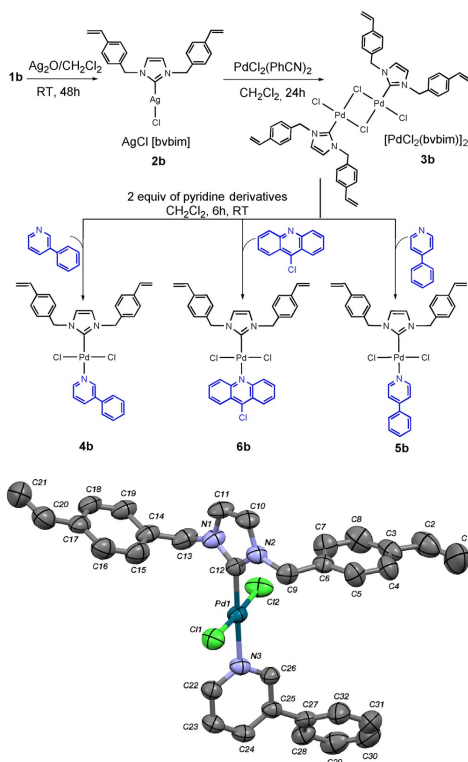
Figure 1. Synthesis of NHC-Pd^{II} monomers and crystal structure of **4b** with thermal ellipsoids displayed at 50% probability. Hydrogen atoms have been omitted for clarity.
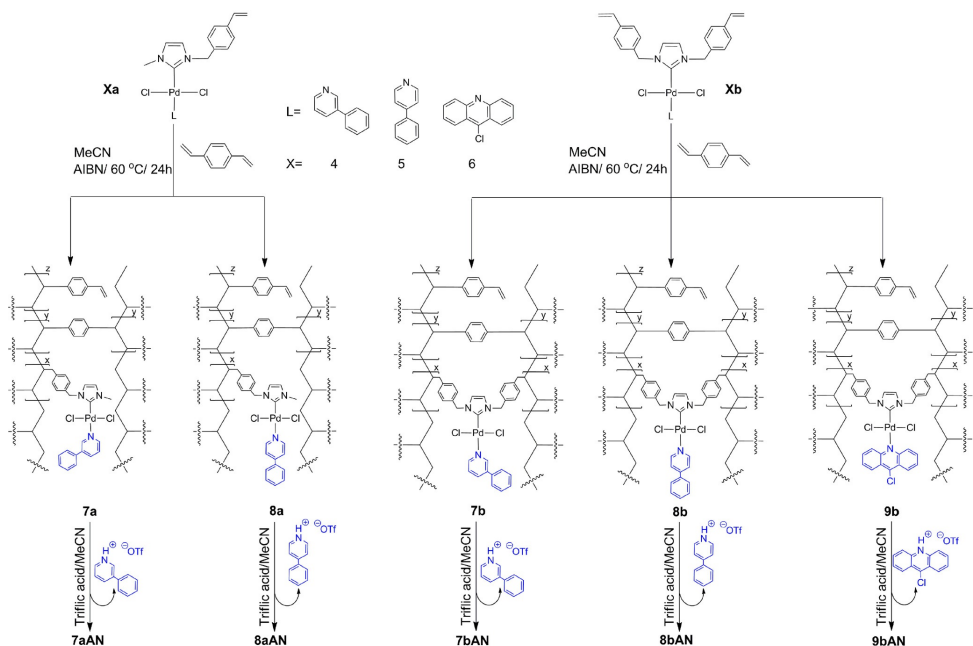
Scheme 2. Precipitation polymerization of NHC-Pd^{II} monomers and pyridine derivatives removing step from the microspheres.

and **6b**. They are given in Figures 1 and S1; all details including selected bond distances and angles are, likewise, found in the Supporting Information.

Polymers: synthesis and characterization

Palladium monomers **4a**, **4b**, **5a**, **5b**, and **6b** were co-polymerized with divinylbenzene (DVB) using precipitation polymerization which has been previously shown to give microspheres.[53–55] The polymerization conditions did not influence similar palladium complexes without polymerizable arms, that is, the metal centre is not influenced by for example, the free radical initiator AIBN (see Supporting Information for details). The polymerization gave polymers **7a**, **7b**, **8a**, **8b** and **9b**, respectively (Scheme 2).

Neat acetonitrile or a mixture of acetonitrile and toluene, which are near θ-solvents for DVB-type polymers, were used. These solvents are known to form a clean surface of microspheres of 2–5 μm and to create porous polymer beads, which is very important for catalysis.[56–59] The Pd:DVB ratio was 1:4 and the total monomer concentration used in this study was around 2% (w/v) of the solvent; all preparation details are given in the Supporting Information, Table S3. In order to study the impact of the pyridine ligands on the catalytic performance they were removed through protonation in one series of catalysts, giving the acetonitrile adducts **7aAN**,

7bAN, **8aAN**, **8bAN**, and **9bAN** (Scheme 2). This procedure in principle renders the metal centres of the **a** and **b** series identical. However, the different catalysts within each series (**a** and **b**) could still display different activities and selectivities, since the use of the different pyridines could have induced differences in the shape of the polymer cavity.

All polymers were characterized by an inductively coupled plasma (ICP) analysis. For selected polymers we also performed Solid state NMR spectroscopy (SS-NMR), High resolution transmission electron microscopy (HRTEM), X-ray energy-dispersive spectroscopy (XEDS), and X-ray photoelectron spectroscopy (XPS). The solid-state ^{13}C-cross polarization magic angle spinning (CP-MAS) spectra are almost identical for the different polymers except a shoulder peak which is present near 150 ppm for the pyridine polymers, but absent in the acetonitrile series. This is shown in Figure S2 for **7a** and **7aAN** and provides good evidence for the success of the washing process. Figure S3 in the Supporting Information show similar details for polymers **8b** and **8bAN**, respectively. Peaks near 30, 41, and 55 ppm are assigned to the aliphatic CH$_3$-, CH$_2$-, and CH- carbons for the NHC-Pd^{II} and poly-DVB skeleton. Unreacted vinyl linkers in the poly-DVB skeleton exhibit two peaks around 113 and 138 ppm assigned to the terminal and internal carbons, respectively.[60] Aromatic phenyl, aromatic phenylpyridine, aromatic poly-DVB skeleton and C10, C11 of the imidazolyl show resonances near 129, 138 and 146 ppm, respectively.

HRTEM images were recorded for polymer **7 bAN**. EDX data show a low, but detectable level of Pd and Cl inside the particles of **7 bAN** (Figure S4a and S4b), whereas the concentrations of those two elements were below the detection limit outside the particles. Furthermore, HRTEM images showed no metallic palladium particles in the polymer (Figure 2 a and 2b). This was
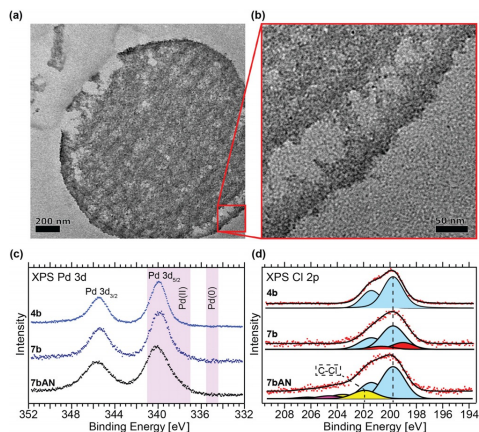
Figure 2. (a) and (b) TEM-images of 7bAN. (c) and (d) Pd 3d and Cl 2p XP spectra of the indicated samples.

confirmed by fast Fourier transform (FFT) analysis of HRTEM images which revealed no spots corresponding to lattice fringes. The palladium found is thus homogeneously dispersed and presumably molecular,; although no information on the oxidation state can be inferred. Using bright-field STEM mode, an EDX mapping of the edge of the particles of **7 bAN** was performed. Again, Pd and C are clearly visible (as brighter areas) in the particles, while the area outside the particles contains very little Pd and C (Supporting Information Figure S6). To confirm the previous results (and address the issue of oxidation state), **7 b** was treated with ascorbic acid to reduce any Pd^{II} to Pd^0. Powder X-ray diffraction (PXRD) patterns were recorded for the native polymers and compared with that of the reduced polymer **7 b(red)**. The PXRD patterns of the native polymers are featureless, but the PXRD curve of **7 b(red)** shows peaks at $40°$, $47°$, and $67°$ which can be assigned to the (111), (200), and (220) crystal planes of Pd^0 particles in the polymer matrix (Supporting Information Figure S5a). These results demonstrate the presence of Pd^{II} in the native polymer which only upon reduction gives Pd^0 particles.[61] To further characterize and investigate the elemental composition, oxidation state, and coordination environment of the Pd species in the monomer and fresh polymer XPS was employed. Pd 3d core-level spectra of the monomer **4 b** and polymers **7 b** and **7 bAN** show the Pd $3d_{5/2}$ and Pd $3d_{3/2}$ peaks at approximately 340 and 345.5 eV binding energy in agreement with the energies expected for a Pd^{II} species (Figure 2 c).[62] A small shift to lower

binding energy between the lines of **4 b** and **7 b** is seen as the result of the polymerization and concomitant change in Pd environment, while the shift to somewhat higher binding energy between **7 b** and **7 bAN** likely is related to the replacement of phenylpyridine by acetonitrile. The occurrence of a small shoulder at around 337.5 eV, which is still within the Pd^{II} region, can probably be explained by a variation of the chemical environment of the Pd ion.[63, 64] More importantly, there are no peaks that correspond to the binding energies of Pd in the metallic state. This confirms that no reduction to Pd^0 takes place during the polymer synthesis and washing steps.[65, 66] For comparison, the XP spectrum of **7 b(red)** shows peaks at around 335 and 340.3 eV binding energy corresponding to the binding energy of Pd^0 (Supporting Information Figure S14). The Cl $2p_{3/2}$ and Cl $2p_{1/2}$ peaks at 199.8 and 201.4 eV are clearly visible for monomer **4 b** (Figure 2 d). In addition, the Cl 2p X-ray photoelectron (XP) spectrum of **7 b** exhibits an additional component to lower energy. The presence of several components can probably be attributed to the larger variation of chemical environments upon polymerization. A corresponding line broadening due to polydispersity is observed in the Pd 3d spectrum of **7 b**. In the Cl 2p spectrum of polymer **7 bAN** a high binding energy species at around 201.9 eV is found. Such high Cl 2p energies are typical for C—Cl bonds and thus are an indication that H—Cl addition to the vinyl groups occurs to some extent during washing with triflic acid.[67–69] The N 1s spectra for **4 b**, **7 b**, and **7 bAN** are shown in Figure S7 (Supporting Information). The high energy peaks (ca. 402.4 eV) are related to the imidazole nitrogen atoms,[62, 70] and the lower energy peaks (ca. 401.7 eV) are associated with the phenylpyridine nitrogen. The ratio between the imidazole and phenylpyridine peaks is 2:1 as expected. Peak broadening towards lower and higher binding energies is observed in the N 1s spectra of **7 b** and **7 bAN**; as above it can be assigned to the variation of the N chemical environment by polymerization and washing steps.[71–73] Polymers **7 b** and **7 bAN** are spherical particles within a size range of several hundred nm to 4 μm according to scanning electron microscopy (SEM) (Supporting Information Figures S5b, S5c, S5d, and S5e). In general, the polymer beads were found to have a more uniform size distribution after removing the phenylpyridine, probably due to loss of the nanospheres (less than 1 μm) during the washing process. Details of the N_2 adsorption experiment and ICP analyses of all polymers are given in the Supporting Information, Figure S16 and Table S3. There were no considerable differences in the palladium loading, which is between 6–8%. Thermogravimetric analysis (TGA) shows that all polymers possess a high thermal stability up to 200 °C (see Figure S8a and S8b for details).

Activity in C—H activation

Homogeneous Pd^{II} catalysts are active in both ligand-directed[3, 75–77] and non-directed C—H bond acetoxylation,[4, 10, 78–80] mainly using $Pd(OAc)_2$ as a catalyst, pyridines as ancillary ligands, and $PhI(OAc)_2$ as an oxidant. As a benchmark for the activity and selectivity of our palladium-containing polymers we chose the non-directed C—H acetoxylation of arenes, and for

the optimization of reaction conditions we used biphenyl as the substrate, so that there would also be a selectivity issue. A PEPPSI-*i*Pr[52] catalyst was employed as a reference homogeneous catalyst. Although monomers **4–6** would have been preferred these are not stable towards polymerization under the reaction conditions. It is expected that the electronic properties of PEPPSI-*i*Pr are not substantially different than those of **4–6**.[81,82] The initial screening of oxidants using polymer **8 bAN** as catalyst revealed that only PhI(OAc)$_2$ and MesI(OAc)$_2$ gave any turnover in the reaction with 45 and 49% yields, respectively (Supporting Information Table S4). We clearly observed that the catalysis reaction proceeded without formation of chlorinated biphenyl products. Traces of phenyl iodide were, however, detected in the gas chromatography (GC) analysis. Subsequently, we tested different temperatures (Table 1, entries 1–6). The results show traces of acetoxybiphenyl derivatives at 70 °C and 18% yield at 92 °C with a ca 61:39 regioselectivity in favour of the *para*-substituted over the *meta*-substituted. The yield of acetoxybiphenyl derivatives increased to 45% (Table 1, entry 3) at 104 °C with a decrease in the regioselectivity to around 45:43 for *para*- and *meta*-substituted positions, while *ortho*-substituted biphenyl was formed as a minor product due to the steric hindrance in the biphenyl substrate. At higher temperatures the yield decreased (entries 4–6); this decrease can be attributed to the decomposition of PhI(OAc)$_2$ in

the reaction mixture in accordance with a previous study.[83] There is no reaction in the absence of catalyst (entry 7).

The homogeneous PEPPSI-*i*Pr (5 mol%) catalyst shows very similar productivity and selectivity as **8 bAN** (entry 8) and the same is true for Pd(OAc)$_2$/pyridine (1:1), a known homogeneous Pd^{II} system with high activity in C–H oxygenation of arenes (entry 18).[79] Comparing the different polymeric catalyst all NHC-Pd^{II}(MeCN) polymers in general afforded higher yield of acetoxybiphenyl products compared to the NHC-Pd^{II} (pyridine derivative) polymers (Supporting Information Table S5, entries 1–9). However, **7 bAN** and **8 bAN** show comparable activity to **7 b** and **8 b,** respectively in the presence of PhI(OAc)$_2$. No prominent differences were observed in the regioselectivities among the polymeric catalysts except for **7 aAN** (Table 1, entry 10), which exhibited a regioselectivity of around 58:29 for *para*- and *meta*-substituted positions as opposed to the 1:1 selectivity for the other types of catalysts including the homogeneous one. MesI(OAc)$_2$ increased the yields compared to PhI(OAc)$_2$ except for **9 bAN** (Table 1, entry 17) when used as an oxidant with the acetonitrile series of polymers. However, with the pyridine containing polymers a decrease of the yields was observed using MesI(OAc)$_2$ as an oxidant (Table S5, entries 1–9). The origin of this observation is likely connected to an increased steric congestion in the pyridine derivatives. The use of various pyridine ligands was introduced to probe if there is any effect on the polymer cavity induced by the different pyridines. An increase in yields was identified when **7 a** and **7 b** were used in the reaction compared to **8 a** and **8 b** (Table S5, Entries 1, 3–7). This is possibly due to the creation of a larger cavity when using the 3-phenylpyridine during polymerization. There was no significant influence of increase of the reaction time on the yield of acetoxybiphenyl derivatives (Table 1, entries 14 and 15).

The fact that the polymer bound catalysts behave similarly as the molecular catalysts in terms of oxidation state and reactivity suggests a similar reaction mechanism as previously proposed for molecular Pd^{II} systems.[16]

Reusability and heterogeneity

All the polymer-based catalysts **7–9** were evaluated for recyclability and they can all be separated easily from the reaction mixture by a simple centrifugation process. We chose to investigate **7 b** further since this gave the best turnover in the catalysis (Table S5). Additionally, we also tested **7 bAN** for recyclability to shed some light on the issue of pyridine vs. acetonitrile ligand. Thus, the recovered **7 b** was shaken with 5 mL of 3-phenylpyridine/CH$_2$Cl$_2$ solutions for 30 min after each cycle and then washed with MeCN to remove the remaining non-bonded phenylpyridines, a procedure which, however, was not entirely effective for all cycles as can be seen from the shifts in the N 1s spectra in Supporting Information Figure S7. **7 bAN** was shaken only with MeCN. The so-treated catalysts were dried and used directly for the next reaction cycle. Both **7 b** and **7 bAN** were found to be effective in four cycles (probably in more, but this was not tested) of the acetoxylation reaction. No significant change in the productivity and selectivity of the

Table 1. NHC-Pd^{II} polymer-catalysed C–H acetoxylation of biphenyl.

| Entry | [Cat.][a] | Temp. [°C] | Yield[b] [%] | Selectivity [%] | | |
				o-	m-	p-
1	8bAN	70	trace	–	–	–
2	8bAN	92	18	–	39	61
3	8bAN	104	45	12	43	45
4	8bAN	115	28	22	32	46
5	8bAN	125	28	22	32	46
6	8bAN	135	30	27	30	43
7	None	104	0	–	–	–
8	PE-iPr[c]	104	44	13	41	46
9	8aAN	104	56[d]	13	41	46
10	7aAN	104	45	13	29	58
11	7aAN[e]	104	53	13	40	47
12	7bAN	104	50	12	42	46
13	7bAN[e]	104	56	14	41	45
14	7bAN[f]	104	51	14	41	45
15	7bAN[g]	104	46	13	41	46
16	9bAN	104	53	13	41	45
17	9bAN[e]	104	47	15	38	47
18	Pd(OAc)$_2$	104	58[h]	10	46	44

[a] Pd loading described in Table S3. [b] Yield and selectivity were determined by GC using a calibration curve based on decane as an internal standard. [c] PE-ipr = PEPPSI-iPr (5 mol%). [d] TON ≈ 14. [e] [Oxidant] = MesI(OAc)$_2$. [f] Reaction time = 48 h. [g] Reaction time = 72 h. [h] 2 mol% of Pd(OAc)$_2$ and 2 mol% of pyridine (1:1 ratio of [Pd] to [pyr]; catalyst loading relative to oxidant) Ref. [79].

Reaction scheme:

[Catalyst]
[mol. catalyst/ mol. oxidant]= 4%
1 equiv. [PhI(OAc)$_2$]
AcOH:Ac$_2$O (9:1)
104 °C, 24h

biphenyl (5 equiv.) → acetoxybiphenyl (OAc)

Figure 3. (a) C–H acetoxylation reaction of biphenyl over **7b** and **7bAN** catalysts using PhI(OAc)₂ as an oxidant. (b) Pd 3d XP spectra of **4b**, **7b** fresh and **7b** after each reuse. (c) Reusability and productivity of **7b** and **7bAN**; the results are compared to those for a [PEPPSI-*i*Pr] catalyst at 5 mol%. (d) Time profile and hot filtration study of **7b**-catalyzed C–H acetoxylation of biphenyl.

recovered catalysts was observed (Figure 3c and Supporting Information Figure S9), and importantly the kinetic profile for the four runs was more or less identical (Figure 3d). The slight increase of activity that is observed could possibly mean that the polymer material opens up during the reaction giving a better access to the palladium and therefore a slightly higher activity. The catalysis stops almost completely after eight hours and ^{1}H NMR spectroscopy showed no traces of PhI(OAc)₂ in the catalysis mixture. However, in terms of mass balance what has not been converted to acetoxylated product is almost exclusively unreacted starting material. Thus, upon addition of 1 additional equivalent of PhI(OAc)₂ into the reaction vessel after eight hours, the reaction continues and the yield of acetoxybiphenyl derivatives approximately doubles (Table S5, entry 10). The yields are thus primarily controlled by the access to oxidant not by the stability of the catalyst. In line with this the recycled catalysts have (within error) the same activity as the fresh one. A hot filtration test (Figure 3d) underlines the heterogeneous nature of the catalyst with a complete inhibition of the activity after removal of the solid catalyst. These results were supported with results from an ICP-OES analysis, in which only a small leaching of Pd from the polymer is detected after each catalytic cycle (Pd wt% = 6.58, 6.52, 6.41, and 6.30 after the 1st, 2nd, 3rd, and 4th catalytic cycle, respectively). To probe the palladium oxidation state after catalysis, **7b** was analysed by XPS. The Pd 3d$_{5/2}$ and Pd 3d$_{3/2}$ binding energies of **7b** after each catalytic cycle (ca. 339.3 and 344.6 eV, respectively) showed only a small shift compared to those of the monomer and fresh polymer (Figure 3b). This shift is probably related to ligand exchange between chloride and acetate. It is clear, however, from the spectra that the palladium remains in oxidation state (II) for all cycles. Similar results were obtained for **7bAN** after the fourth catalytic cycle (Supporting Information Figure S15). Subsequently, we focused our attention to the Cl 2p core level of **7b** after each catalytic cycle, which

showed significant broadening in the spectral features and shifts by 2 eV toward higher binding energies compared to the spectra of the monomer and fresh polymer (Supporting Information Figure S10). The spectrum can be convoluted into two peaks, one corresponding to a Pd–Cl species (with a Pd 2p$_{3/2}$ binding energy of 199.8 eV) and a second Cl 2p$_{3/2}$ peak at 201.9 eV, which can be assigned to a C–Cl species according to literature.[67–69] In order to understand this remarkable change in Cl 2p binding energy, we also characterized **7b** before and after catalysis with SS-NMR spectroscopy. ^{13}C CP-MAS NMR spectra (which were performed at two different spinning rates to differentiate between peaks and side bands) revealed a new peak after catalysis at 169.8 ppm, which corresponds with (C=O) of an acetate group (Supporting Information Figures S11 and S12).[84–87] In contrast, the peaks related to terminal and internal carbons of vinyl linkers at around 113 and 138 ppm, respectively observed for the fresh catalyst are absent after catalysis (Supporting Information Figure S12). For comparison the biphenyl acetoxylation reaction was carried out in the presence of poly(divinylbenzene) under the described reaction conditions. This gave no conversion of biphenyl but, again, ^{13}C CP-MAS NMR spectra showed a sharp peak from an acetate group at 169.5 ppm and the intensities of carbon peaks related to vinyl linkers were reduced (Supporting Information Figure S13). These data suggest that PhI(OAc)₂ can functionalize unreacted vinyl groups (but not aromatic groups) in the absence of a catalyst. In the presence of a catalyst we therefore suggest that all remaining vinyl groups in the polymer are acetoxylated or chlorinated during catalysis. These results were supported by elemental analysis of **7b** after catalysis, which confirmed that the ratio between Pd:Cl is almost 1:2 (85% of Cl is still present in the catalyst). Thus, the majority of the chlorine, around 75% according to the XPS results, have been transferred to the polymer matrix, while the rest is still coordinated to Pd; around 15% have been washed out from the catalyst according to the ICP analysis.

Oxidation of naphthalene and other arenes

We further investigated the scope of C–H acetoxylation for other arenes using the optimized reaction conditions. With naphthalene as a substrate (Table 2) the polymeric catalysts showed a significant increase in selectivity compared to homogeneous ones. Thus, PEPPSI-*i*Pr showed no regioselectivity using PhI(OAc)₂ as an oxidant, while a moderate regioselectivity of around 33:67 in favour of the β-substitution was observed with MesI(OAc)₂ (Table 2, entries 2 and 3). This is in line with other homogeneous catalysts such as Pd(OAc)₂ and sulfinyl-NHC-Pd complexes reported previously.[16,79] On the other hand, the polymeric catalysts are significantly better with a regioselectivity in favour of acetoxylation at the β-position of around 28:72 using **7b**/PhI(OAc)₂ (Table 2, entry 4). This improvement in selectivity was diminished significantly using **7bAN**, in slight favour of acetoxylation at the α-position (α:β = 56:44) (Table 2, entry 5). For the acetonitrile-supported systems no improvement in selectivity was obtained using MesI(OAc)₂, but for **8b** and **7b** the bulky oxidant gave an even better se-

Table 2. Polymer catalysed C—H acetoxylation of naphthalene.

Entry	[Catalyst][a]	Yield[b] [%]	Selectivity [%] (α:β)
1	None	0	–
2	PEPPSI-iPr[c]	36	44:56
3	PEPPSI-iPr[c,d]	33	33:67
4	7b	18	28:72
5	7bAN	25	56:44
6	7b[d]	18	17:83
7	7bAN[d]	26	54:46
8	8b[d]	15	20:80
9	8bAN[d]	19	47:53
10	8bAN[d,e]	9	11:89
11	Pd(OAc)₂/Acridine[79]	88	20:80
12	Pd(OAc)₂/FPCA[80]	69	29:71

[a] Pd loading described in Table S3. [b] Yield and selectivity were determined by GC using a calibration curve and based on decane as an internal standard. [c] [PEPPSI-iPr] = 5 mol %, [d] [Oxidant] = MesI(OAc)₂, [e] 1 equiv. of 4-phenylpyridine/Pd added to the reaction mixture. [80] FPCA = 6-Fluoropicolinic acid.

lectivity of α:β = 20:80 and 17:83, respectively. Thus, the presence of phenylpyridines increase the selectivity substantially and this goes hand in hand with a decreased activity. To confirm the improved selectivity one equivalent of 4-phenylpyridine (with respect to Pd) was added to the reaction mixture using **8 bAN**. As expected this gave a lower activity compared to previously reported Pd(OAc)₂ systems (Table 2, entries 11 and 12), but a dramatically increased selectivity (11:89) (Table 2, entry 10). In general the polymeric catalysts showed lower activity than the homogeneous ones. Finally, we tested catalyst **8 b** under the optimized reaction conditions in C—H acetoxylation of mono- and polycyclic arene substrates. It exhibited modest yields but a higher selectivity (compared with PEPPSI-iPr) when employed to the acetoxylation of pyrene. For simple aromatic substrates the polymeric catalyst offered only a modest improvement in terms of selectivity but surprisingly, some improvement in terms of activity in the acetoxylation of toluene (Supporting Information Table S6).

Conclusion

The development of a catalytically active, reusable and selective NHC-Pd^{II} polymer based on co-polymerization of divinyl benzene with vinyl moieties in the structure of the N-heterocyclic carbene ligand is described. Characterization of the NHC-Pd^{II} polymers showed the presence of Pd^{II} species in the native polymer without any trace of Pd^0 nanoparticles. The catalytic activity and selectivity in direct acetoxylation of unactivated C—H bonds in arenes was evaluated for all polymers with and without phenylpyridine as supporting ligands on the palladium. The presence of phenylpyridines increased the selectivity and decreased the activity of the polymers, reaching a 9:1 se-

lectivity in the acetoxylation of naphtalene. While the catalysis stops almost completely after eight hours due to decomposition of the oxidant it can be restarted through addition of fresh oxidant and there is no indication that the catalyst loses its activity. Thus, it can be recycled four times without any loss of activity, but likely it will be effective for many more cycles. Moreover, the catalyst was shown to be truly heterogeneous in a hot filtration test. No significant leaching of Pd from the polymer after each catalysis cycle was detected. The supported polymer contains reactive vinyl moieties in the backbone of the polymer, and these are acetoxylated or chlorinated during catalysis. The present system is the first heterogeneous catalyst for acetoxylation of non-functionalized arenes. The heterogeneous nature of these catalysts could open up for continuous flow catalysis.

Experimental Section

Procedure for the acetoxylation of biphenyl catalysed by NHC-Pd^{II} heterogeneous catalysts

The catalytic reactions were performed in a glass-threaded vial with a magnetic stir bar, which was loaded with biphenyl (0.2 g, 1.29 mmol, 5 equiv), PhI(OAc)₂ (0.083 g, 0.25 mmol, 1 equiv), catalyst (4 mol % proportion to the amount of the oxidant), glacial acetic acid (4.5 mL), and acetic anhydride (0.5 mL) and sealed tightly by using a screw cap. The mixture was stirred at ambient temperature for 10 min before it was heated to 104 °C using a heating block. At the end of the reaction the vessel was cooled to room temperature, and the catalyst was separated by centrifugation. The mixture was diluted with Et₂O (5 mL), shaken for 2 min, and extracted with saturated aqueous solution of K₂CO₃ (9 M in distilled water, 3×2 mL). The organic layer was then separated and the solvent was removed by evaporation. CH₂Cl₂ (1.2 mL) and decane (20 µl, as an internal standard for quantitative GC analysis) were added to the resulting solids and analysed by GC.

Recyclability, heterogeneity and time study experiments

Recycling experiment: The acetoxylation reaction was carried out under the same reaction conditions as described above. The reaction mixture was centrifuged after it had reached room temperature. The remaining solid was washed with a pyridine derivative/ CH₂Cl₂ solution (1×5 mL) and MeCN (3×10 mL), dried, and reused for the following run. Using these conditions, the recyclability study was performed at designated reaction times (2, 4, 6, 8, 12, 20, and 24 h).

Hot filtration test: The acetoxylation reaction was carried out under identical reaction conditions as described above. After 4 h (yield 28 %) the catalyst was filtered off at the reaction temperature (104 °C) and the catalyst free filtrate was allowed to stir under identical reaction conditions. The GC analysis of the products after 8 h, 18 h, and 24 h revealed no further acetoxylation of biphenyl (GC final yield 26 %).

Acknowledgements

Conflict of interest

The authors declare no conflict of interest.

[1] R. Giri, J. Liang, J. G. Lei, J. J. Li, D. H. Wang, X. Chen, I. C. Naggar, C. Guo, B. M. Foxman, J. Q. Yu, *Angew. Chem. Int. Ed.* **2005**, *44*, 7420; *Angew. Chem.* **2005**, *117*, 7586.
[2] T. W. Lyons, M. S. Sanford, *Chem. Rev.* **2010**, *110*, 1147.
[3] S. R. Neufeldt, M. S. Sanford, *Acc. Chem. Res.* **2012**, *45*, 936.
[4] J. B. Gary, A. K. Cook, M. S. Sanford, *ACS Catal.* **2013**, *3*, 700.
[5] N. Kuhl, M. N. Hopkinson, J. Wencel-Delord, F. Glorius, *Angew. Chem. Int. Ed.* **2012**, *51*, 10236; *Angew. Chem.* **2012**, *124*, 10382.
[6] L. Eberson, L. Gomezgon, *J. Chem. Soc. D* **1971**, 263.
[7] L. Eberson, L. Gomezgon, *Acta Chem. Scand.* **1973**, *27*, 1255.
[8] L. Eberson, L. Jonsson, *J. Chem. Soc. Chem. Commun.* **1974**, 885.
[9] T. Yoneyama, R. H. Crabtree, *J. Mol. Catal. A* **1996**, *108*, 35.
[10] A. K. Cook, M. S. Sanford, *J. Am. Chem. Soc.* **2015**, *137*, 3109.
[11] D. Meyer, M. A. Taige, A. Zeller, K. Hohlfeld, S. Ahrens, T. Strassner, *Organometallics* **2009**, *28*, 2142.
[12] M. Muehlhofer, T. Strassner, W. A. Herrmann, *Angew. Chem. Int. Ed.* **2002**, *41*, 1745; *Angew. Chem.* **2002**, *114*, 1817.
[13] D. Munz, T. Strassner, *Inorg. Chem.* **2015**.
[14] B. M. Prince, T. R. Cundari, *Organometallics* **2012**, *31*, 1042. M. G. Organ, *Chem. Eur. J.* **2010**, *16*, 10844.
[15] P. L. Arnold, M. S. Sanford, S. M. Pearson, *J. Am. Chem. Soc.* **2009**, *131*, 13912.
[16] F. Tato, A. Garcia-Dominguez, D. J. Cardenas, *Organometallics* **2013**, *32*, 7487.
[17] S. P. Desai, M. Mondal, J. Choudhury, *Organometallics* **2015**, *34*, 2731.
[18] E. Bolbat, O. F. Wendt, *Eur. J. Org. Chem.* **2016**, *20*, 3395.
[19] R. Credendino, L. Falivene, L. Cavallo, *J. Am. Chem. Soc.* **2012**, *134*, 8127.
[20] M. N. Hopkinson, C. Richter, M. Schedler, F. Glorius, *Nature* **2014**, *510*, 485.
[21] I. Karamé, M. Boualleg, J. M. Camus, T. K. Maishal, J. Alauzun, J. M. Basset, C. Coperet, R. J. Corriu, E. Jeanneau, A. Mehdi, C. Reye, L. Veyre, C. Thieuleux, *Chem. Eur. J.* **2009**, *15*, 11820.
[22] M. P. Conley, C. Coperet, C. Thieuleux, *ACS Catal.* **2014**, *4*, 1458.
[23] H. Duan, M. Li, G. Zhang, H. Duan, J. R. Gallagher, Z. Huang, Y. Sun, Z. Luo, H. Chen, J. T. Miller, R. Zou, A. Lei, Y. Zhao, *ACS Catal.* **2015**, *5*, 3752.
[24] T. Park, A. J. Hickman, K. Koh, S. Martin, A. G. Wong-Foy, M. S. Sanford, A. J. Matzger, *J. Am. Chem. Soc.* **2011**, *133*, 20138.
[25] S. Santoro, S. I. Kozhushkov, L. Ackermann, L. Vaccaro, *Green Chem.* **2016**, *18*, 3471.
[26] Y. M. A. Yamada, S. M. Sarkar, Y. Uozumi, *J. Am. Chem. Soc.* **2012**, *134*, 3190.
[27] X. Li, R. V. Zeeland, R. V. Maligal-Ganesh, Y. Pei, G. Power, L. Stanley, W. Huang, *ACS Catal.* **2016**, *6*, 6324.
[28] K. V. S. Ranganath, S. Onitsuka, A. K. Kumar, J. Inanaga, *Catal. Sci. Technol.* **2013**, *3*, 2161.
[29] K. V. Bukhryakov, C. Mugemana, K. B. Vu, V. O. Rodionov, *Org. Lett.* **2015**, *17*, 4826.
[30] S. J. Xu, K. P. Song, T. Li, B. Tan, *J. Mater. Chem. A* **2015**, *3*, 1272.
[31] W. J. Sommer, M. Weck, *Coord. Chem. Rev.* **2007**, *251*, 860.
[32] B. Tamami, F. Farjadian, S. Ghasemi, H. Allahyari, *New J. Chem.* **2013**, *37*, 2011.
[33] E. Mohammadi, B. Movassagh, *J. Organomet. Chem.* **2016**, *822*, 62.
[34] C. A. Witham, W. Huang, C. Tsung, J. N. Kuhn, G. A. Somorjai, F. D. Toste, *Nat. Chem.* **2010**, *2*, 36.

[35] W. Huang, J. H. Liu, P. Alayoglu, Y. Li, C. A. Witham, C. Tsung, F. D. Toste, G. A. Somorjai, *J. Am. Chem. Soc.* **2010**, *132*, 16771.
[36] M. Pagliaro, V. Pandarus, R. Ciriminna, F. Beland, P. D. Cara, *ChemCatChem* **2012**, *4*, 27.
[37] M. Arpad, *Chem. Rev.* **2011**, *111*, 2251.
[38] P. C. Perumgani, S. P. Parvathaneni, S. Keesara, M. R. Mandapati, *Appl. Organomet. Chem.* **2016**, 1.
[39] H. Fei, S. M. Cohen, *J. Am. Chem. Soc.* **2015**, *137*, 2191.
[40] V. Pascanu, F. Carson, M. V. Solano, J. Su, X. Zou, M. J. Johansson, B. Martín-Matute, *Chem. Eur. J.* **2016**, *22*, 3729.
[41] L. Lee, J. He, J. Yu, C. W. Jones, *ACS Catal.* **2016**, *6*, 5245.
[42] J. H. Kim, J. W. Kim, M. Shokouhimehr, Y. S. Lee, *J. Org. Chem.* **2005**, *70*, 6714.
[43] D. Zhao, Z. Fei, W. H. Ang, P. J. Dyson, *Small* **2006**, *2*, 879.
[44] C. Fu, L. Meng, Q. Lu, Z. Fei, P. J. Dyson, *Adv. Funct. Mater.* **2008**, *18*, 857.
[45] S. Ghazali-Esfahani, H. Song, E. Paunescu, F. D. Bobbink, H. Liu, Z. Fei, G. Laurenczy, M. Bagherzadeh, N. Yan, P. J. Dyson, *Green Chem.* **2013**, *15*, 1584.
[46] X. Y. Lu, F. Chen, W. F. Xu, X.-T. Chen, *Inorg. Chim. Acta* **2009**, *362*, 5113.
[47] M. H. Majeed, O. F. Wendt, *Acta Crystallogr. Sect. E* **2016**, *72*, 534–537.
[48] I. J. B. Lin, C. S. Vasam, *Coord. Chem. Rev.* **2007**, *251*, 642.
[49] U. Hintermair, U. Englert, W. Leitner, *Organometallics* **2011**, *30*, 3726.
[50] S. Warsink, J. A. Venter, A. Roodt, *J. Organomet. Chem.* **2015**, *775*, 195.
[51] A. Chartoire, X. Frogneux, A. Boreux, A. M. Z. Slawin, S. P. Nolan, *Organometallics* **2012**, *31*, 6947.
[52] J. Nasielski, N. Hadei, G. Achonduh, E. A. Kantchev, C. J. O'Brien, A. Lough, M. G. Organ, *Chem. Eur. J.* **2010**, *16*, 10844.
[53] L. Ye, R. Weiss, K. Mosbach, *Macromolecules* **2000**, *33*, 8239.
[54] C. Cacho, E. Turiel, A. Martin-Esteban, C. Perez-Conde, C. Camara, *J. Chromatogr. B* **2004**, *802*, 347.
[55] B. Y. Zu, G. Q. Pan, X. Z. Guo, Y. Zhang, H. Q. Zhang, *J. Polym. Sci. Part A J. Polym. Sci. Pol. Chem.* **2009**, *47*, 3257.
[56] K. Li, H. D. H. Stover, *J. Polym. Sci. Part A* **1993**, *31*, 3257.
[57] J. S. Downey, R. S. Frank, W. H. Li, H. D. H. Stover, *Macromolecules* **1999**, *32*, 2838.
[58] W. H. Li, K. Li, H. D. H. Stover, *J. Polym. Sci. Part A* **1999**, *37*, 2295.
[59] W. H. Li, H. D. H. Stover, *J. Polym. Sci. Part A* **1999**, *37*, 2899.
[60] M. Gaborieau, L. Nebhani, R. Graf, L. Barner, C. Barner-Kowollik, *Macromolecules* **2010**, *43*, 3868.
[61] N. Z. Shang, S. T. Gao, C. Feng, H. Y. Zhang, C. Wang, Z. Wang, *RSC Adv.* **2013**, *3*, 21863.
[62] S. Men, K. R. J. Lovelock, P. Licence, *RSC Adv.* **2015**, *5*, 35958.
[63] R. Arrigo, M. E. Schuster, Z. Xie, Y. Yi, G. Wowsnick, L. L. Sun, K. E. Hermann, M. Friedrich, P. Kast, M. Hävecker, A. Knop-Gericke, R. Schlögl, *ACS Catal.* **2015**, *5*, 2740.
[64] R. Arrigo, M. E. Schuster, S. Abate, S. Wrabetz, K. Amakawa, D. Teschner, M. Freni, G. Centi, S. Perathoner, M. Hävecker, R. Schlögl, *ChemSusChem* **2014**, *7*, 179.
[65] M. C. Militello, S. J. Smiko, *Surf. Sci. Spectra* **1994**, *3*, 387.
[66] G. Kumar, J. R. Blackburn, R. G. Aldridge, W. E. Moddeman, M. M. Jones, *Inorg. Chem.* **1972**, *11*, 296.
[67] J. Gao, A. V. Teplyakov, *Catal. Today* **2014**, *238*, 111.
[68] E. T. Kang, H. C. Ti, K. G. Neoh, T. C. Tan, *Polym. J.* **1988**, *20*, 399.
[69] D. T. Clark, D. Kilcast, D. B. Adams, W. K. R. Musgrave, *J. Electron Spectrosc. Relat. Phenom.* **1975**, *6*, 117.
[70] J. P. Mathew, M. Srinivasan, *Eur. Polym. J.* **1995**, *31*, 835.
[71] J. R. Pels, F. Kapteijn, J. A. Moulijn, Q. Zhu, K. M. Thomas, *Carbon* **1995**, *33*, 1641.
[72] S. Maldonado, S. Morin, K. J. Stevenson, *Carbon* **2006**, *44*, 1429.
[73] Y. Zhang, J. Zhang, C. Sheng, J. Chen, Y. Liu, L. Zhao, F. Xie, *Energy Fuels* **2011**, *25*, 240.
[74] D. Kalyani, M. S. Sanford, *Org. Lett.* **2005**, *7*, 4149.
[75] L. V. Desai, H. A. Malik, M. S. Sanford, *Org. Lett.* **2006**, *8*, 1141.
[76] L. V. Desai, K. J. Stowers, M. S. Sanford, *J. Am. Chem. Soc.* **2008**, *130*, 13285.
[77] K. J. Stowers, M. S. Sanford, *Org. Lett.* **2009**, *11*, 4584.
[78] M. H. Emmert, A. K. Cook, Y. J. Xie, M. Sanford, *Angew. Chem. Int. Ed.* **2011**, *50*, 9409; *Angew. Chem.* **2011**, *123*, 9581.
[79] A. K. Cook, M. H. Emmert, M. S. Sanford, *Org. Lett.* **2013**, *15*, 5428.
[80] C. Valderas, K. Naksomboon, M. Á. Fernández-Ibáñez, *ChemCatChem* **2016**, *8*, 3213.

[81] F. Glorius, In *Topics in Organometallic Chemistry*; Springer: Berlin, **2007**, vol. 21, pp. 1.

[82] J. L. Farmer, M. Pompeo, M. G. Organ, In *Ligand Design in Metal Chemistry: Reactivity and Catalysis*; Wiley: United Kingdom, **2016**, pp. 134.

[83] J. E. Leffler, L. J. Story, *J. Am. Chem. Soc.* **1967**, *89*, 2333.

[84] L. Y. Wang, P. F. Fang, C. H. Ye, J. W. Feng, *J. Polym. Sci. Part A* **2006**, *44*, 2864.

[85] C. M. G. De Souza, M. I. B. Tavares, *J. Appl. Polym. Sci.* **2002**, *86*, 116.

[86] G. C. Stael, M. I. B. Tavares, *Polym. Test.* **1997**, *16*, 193.

[87] D. L. Trumbo, *Polym. Bull.* **1996**, *37*, 617.

Paper III

Directed C–H halogenation reactions catalysed by Pd(II) supported on polymers under batch and continuous flow conditions

Maitham H. Majeed,[a] Payam Shayesteh,[b] Per Tunå,[c] Axel R. Persson,[a,d] Roman Gritcenko,[a] Reine Wallenberg,[a,d] Lei Ye,[e] Christian Hulteberg,[c] Joachim Schnadt[b] and Ola F. Wendt[a,*]

[a]Centre for Analysis and Synthesis, Department of Chemistry, Lund University, Box 124, SE-221 00 Lund, Sweden

[b]Division of Synchrotron Radiation Research, Department of Physics, Lund University, Box 118, SE-221 00 Lund, Sweden

[c]Department of Chemical Engineering, Lund University, Box 124, 221 00 Lund, (Sweden)

[d]National Center for High Resolution Electron Microscopy, Lund University, Box 124, SE-221 00 Lund, Sweden

[e]Centre for Applied Life Sciences, Department of Chemistry, Lund University, Box 124, SE-221 00 Lund, Sweden

ABSTRACT: Two *N*-heterocyclic carbene palladium(II) complexes containing a vinyl group in different positions in the backbone of the *N*-heterocycle were synthesized and fully characterized. The monomers were copolymerized with divinylbenzene to fabricate robust polymer supported *N*HC-Pd(II) complexes and these polymers were applied as heterogeneous catalysts in directed C–H halogenation of arenes with a pyridine type directing group. Both catalysts demonstrated high catalytic activity with up to 90% conversion and 100% selectivity in chlorination, heterogeneous character and recyclability (up to 6 times) with no significant leaching of palladium in batch mode catalysis. The best catalyst also disclosed an exceptional activity (90% conversion) and 100% selectivity for the mono-halogenated product under continuous flow conditions for up to 6 days, with no leaching of palladium, no loss of activity and an ability to maintain the original oxidation state of Pd(II).

The continued increase in the use of halogenated organic compounds to synthesize natural products, pharmaceuticals and agrochemicals has attracted organic chemists to develop numerous transformations for this demanding purpose.[1-10] Overhalogenations, harsh reaction conditions, poor regiocontrol, low yield and low atom efficiency due to the use of stoichiometric reagents are common disadvantages of traditional halogenation routes.[11-15] Therefore, many methodologies have been employed in order to address these drawbacks and selectively install diverse functional groups into aromatic carbon-hydrogen bonds. One of these methods is the application of transition metals to regioselectively catalyse C–H bond activations/ functionalizations which has addressed many of the problems.[16-25] The pioneering work by Sanford and co-workers using palladium in chelate-directed functionalization of C–H bonds is one promising route to selectively halogenate arenes.[26-33] While these reaction typically are carried out in the homogeneous phase, heterogeneous catalysts undoubtedly are more common in industrial applications, due to their significant advantages in terms of robustness, recyclability and ease of separation, but there are few examples of such catalysts for selective C–H activation. Recently, we reported an example of a polymer-supported N-heterocyclic carbene palladium(II) (NHC-Pd(II)) complex which selectively catalysed C–H oxygenation of unfunctionalized arenes

Scheme 1. Supported NHC-Pd[II] polymer catalyze C–H chlorination of arenes under batch and continuous flow regimes.
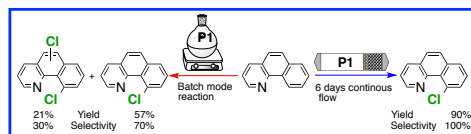
with very good regioselectivity,[34] and there are also examples of N-chelation-directed C(sp²)-H halogenation reactions using supported catalysts.[35-38] The reactions above were run in batch mode and this does not fully utilize the potential of heterogeneous catalysis. On the contrary, continuous flow reactions offer attractive advantages in terms of safety (no accumulation of highly unstable intermediates) and reaction efficiency (time and cost effective process).[39-43] However, to our knowledge there are no examples of N-directed C–H functionalizations that make use of heterogeneous catalysts in a packed-bed reactor under continuous flow. Herein we report on a modification of our previously reported heterogeneous catalyst by installing the polymerizable vinyl moiety in the backbone of the NHC ligand (Figure 1b). Together with our original

system this modified catalyst was applied in directed C–H halogenation of arenes. The reactivity, regioselectivity and recyclability of both systems under batch reaction conditions was evaluated and they show excellent selectivity for the formation of mono-halogenated products in many cases. In addition, the best catalyst was investigated under continuous flow conditions. This is the first example of such a reaction and the catalyst tolerates up to 6 days of continuous flow conditions in a packed-bed reactor giving excellent yields and 100% selectivity of the mono-halogenated product (see Scheme 1) with no loss of activity over time.

Results and Discussion
Monomer synthesis

Polymer **P1** was synthesized according to previously reported methods (Figure 1a).[44-47] The imidazolium chloride precursor **3b** was prepared by means of a slightly modified reaction protocol in moderate yield from the known compound **2b**.[48,49] The intermediate product **4b** was obtained in a good yield via direct metallation, and it was characterised by ^{1}H and ^{13}C NMR spectroscopy showing the characteristic downfield shift of the carbene carbon around 169.93 ppm confirming metallation. Transmetallation of intermediate **4b** with $PdCl_2(PhCN)_2$ followed by phenylpyridine additio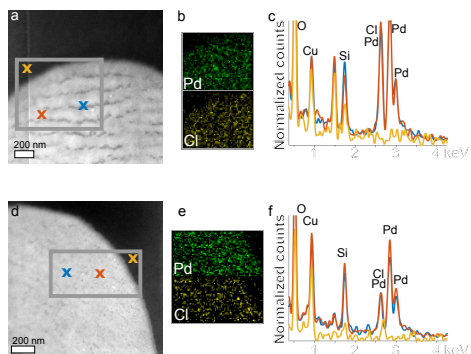n afforded monomer **5b** in good yield (Figure 1b). The $^{13}C\{^1H\}$ NMR spectrum of **5b** exhibited the expected carbenic carbon (Pd-C_{carbene}) signal at 150.99 ppm.[45]
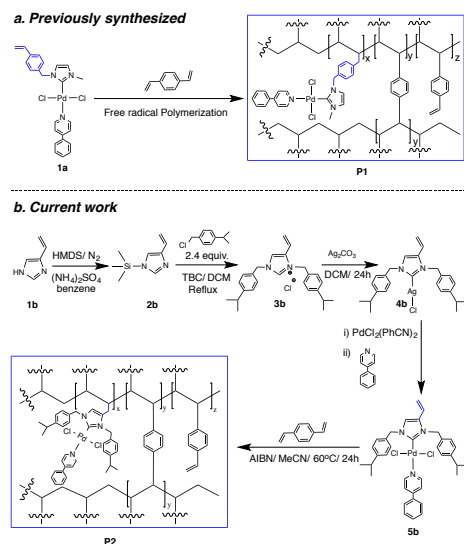
Polymer synthesis and characterization

A typical precipitation polymerization protocol based on a copolymerization reaction of monomer **5b** with divinylbenzene DVB (molar ratio of Pd:DVB= 1:4), was used to offer polymer **P2** (Figure 1 and Supporting Information for more experimental details). As stated in our previous investigation,[34] the polymerization proceeded to form clean surfaces and porous microspheres (2-5 μm) without changing the oxidation state of the metal centre. The palladium loading of polymers **P1** and **P2** was confirmed by an inductively coupled plasma-optical emission spectroscopy (ICP-OES) analysis (Table S1, Supporting Information). All polymers were also characterised by Solid state NMR spectroscopy (SS-NMR), High resolution transmission electron microscopy (HRTEM), X-ray energy-dispersive spectroscopy (XEDS), Powder X-ray diffraction (PXRD) and X-ray photoelectron spectroscopy (XPS). Figure S4 in the Supporting Information compares solid-state ^{13}C-cross polarization magic angle spinning (CP-MAS) spectra of **P1**, **P2** and polydivinylbenzene (PDVB) polymers. In all cases, the aliphatic CH_3-, CH_2-, and CH- carbons, aromatic phenyl and aromatic PDVB skeleton and unreacted vinyl linkers exist and show signals in the following regions: 29, 40, 54 ppm, 128, 145 ppm and 112, 137 ppm, respectively.[50] Moreover, the aromatic phenylpyridine resonance is present and identical in the spectra of **P1** and **P2** at 151 ppm, and no similar peak in the spectrum of PDVB was observed. Fast Fourier transforms (FFT) analysis of high-resolution TEM images of **P1** and **P2** showed no indications of formation of metallic palladium during the polymerization reaction. XEDS mapping was conducted to reveal the homogeneous dispersion of Pd and Cl (as brighter areas) in the **P1** and **P2** matrixes (Figure 2b and 2e) and it also showed that the Pd and Cl are present exclusively inside the particles (Figure 2c and 2f).

Figure 1. Heterogenization strategies and general synthesis of monomer and polymer supported NHC-Pd[II] complexes.

Figure 2. (**a**) and (**d**) Dark-field STEM images of **P1** and **P2** respectively. The gray boxes in the STEM images marks the areas for which the elemental mapping was carried out. (**b**) and (**e**) Pd and Cl elemental mapping on the edge of **P1** and **P2** particles respectively. (**c**) and (**f**) XEDS spectra for three sites (blue and red from within the polymers, yellow from outside the polymers) on the images of **P1** and **P2** respectively.

In the PXRD pattern for the native polymers **P1** and **P2** no characteristic peaks of Pd(0) particles were observed (Supporting Information Figure S1a). For comparison, polymers known to contain Pd(0) show small peaks at θ = 40° and 47° indexed to the Pd(111) and Pd(200) Bragg reflections of Pd(0) particles (see Supporting Information Figure S1b). Thus the native polymers **P1** and **P2** only contain Pd(II).[34, 51, 52] To further support the absence of Pd(0), the oxidation state of Pd of both monomers and polymers was investigated using XPS analysis as shown in Figures 3 and S6a (Supporting Information). The XP spectra of **1a**, **5b**, **P1** and **P2** show Pd 3d$_{5/2}$ and Pd 3d$_{3/2}$ peaks at approximately 338.3 and 343.8 eV binding energy in agreement with the energies expected for a Pd(II) species (Figure 3).[53] Overall, these results confirm that there is no reduction of palladium during the polymerization reaction, and the synthesized polymers contain no Pd in the metallic state.[54] Figure S6 illustrates that, despite the overall similarity in binding energy, a broadening is observed in the Cl 2p spectra measured at different stages. We relate this broadening to the existence of slight differences in the chemical environments of the Cl atoms in the different samples. The effect is also seen for the monomer samples **1a** and **5b**. The N 1s spectra for **1a**, **5b**, **P1**, and **P2** are shown in Figure S6b (Supporting Information). Monomer 1a exhibits a high energy peak (ca. 401.2 eV) which is assigned to the imidazole nitrogen atom, and a lower energy peak (ca. 400.5 eV) assigned to the phenylpyridine nitrogen.[34] The ratio between the imidazole and phenylpyridine peaks is 2:1 as expected. In contrast, a peak broadening towards higher binding energy (ca. 401.9 eV) is observed in **5b**. Apparently, the two nitrogen atoms of this NHC ligand are sufficiently different to give a broadened peak. This is consistent with DFT calculations: there is a noticeable difference in the two NHC nitrogen atomic charges for, at least, one of the coexisting conformers of **5b**. This can be attributed to the electronic effects of the vinyl group, as well as geometrical changes caused by the orientation of the NHC arms. In the case of **1a** model system, both NHC nitrogen atoms are calculated to be very similar. N 1s spectra of **P1** and **P2** show a significant peak broadening, which is probably due to the polydispersity of the N chemical environment upon
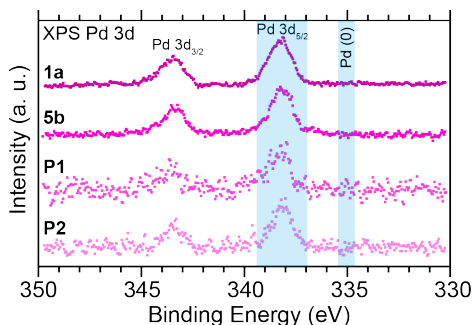
Figure 3. Pd 3d XP spectra of **1a**, **5b** monomers and **P1** and **P2** fresh polymers.

Table 1. Optimization of **P1**-catalyzed C–H chlorination of 2-phenylpyridine in batch mode.[a]

En.	Oxidant	[Ox]/M	Solvent	Isolated yield (%)[b]		
				1-Cl	1-Cl$_2$	D.P.
1	NCS	0.05	^{G}AcOH	50	traces	0
2	NCS	0.05	MeCN	56	traces	0
3	PhICl$_2$	0.05	^{G}AcOH	22	2	0
4	PhICl$_2$	0.05	MeCN	30	23[d]	0
5	PhICl$_2$	0.2	^{G}AcOH:Ac$_2$O[c]	30	1	0
6	PhICl$_2$	0.4	^{G}AcOH:Ac$_2$O[c]	38	<1	0
7	PhICl$_2$	0.6	^{G}AcOH:Ac$_2$O[c]	32	traces	0
8	NCS	0.2	^{G}AcOH:Ac$_2$O[c]	56	0	0
9	NCS	0.4	^{G}AcOH:Ac$_2$O[c]	75	0	0
10	NCS	0.6	^{G}AcOH:Ac$_2$O[c]	55	0	0
11	NCS[e]	0.4	^{G}AcOH:Ac$_2$O[c]	90	traces	0
12	NCS[e,f]	0.4	^{G}AcOH:Ac$_2$O[c]	Products were not formed		
13	NCS[e]	0.4	MeCN	67	multiple products	

[a] Pd loading is 5.8 wt%, reactions temperature is 100 °C. [b] Isolated yields were monitored by ^{1}HNMR and HRMASS. [c] ^{G}AcOH:Ac$_2$O = 9:1. [d] Traces of trichlorophenyl-pyridine detected by HRMASS. [e] Halogenating reagent 2.3 equiv. [f] Without **P1**.

polymerization. Selective scanning electron microscopy (SEM) images of **P1** and **P2** reveal that **P1** microspheres vary in size (within a range of several hundred nm to 4 μm), while highly uniform spherical microspheres are obtained in the case of **P2** (3 μm) (Supporting Information Figure S2). According to the Thermogravimetric analysis (TGA), **P2** possesses a high thermal stability up to 200 °C (see Figure S3 for details), as previously observed for **P1**.[34] Details about the Kr adsorption experiment and BET surface areas of **P1** and **P2** are given in the Supporting Information.

Optimizing reaction conditions in batch mode

C–H halogenation under heterogeneous catalysis conditions has been studied in multiple instances.[35-38, 55-57] As a part of our ongoing work on heterogeneous catalysis, we were interested to compare the activity of **P1** and **P2** as catalysts in C–H halogenation under mild reaction conditions. As a benchmark reaction, we chose the chlorination of 2-phenylpyridine with different chlorinating agents (PhICl$_2$ and N-chlorosuccinimide (NCS)) and solvents using different loadings of **P1**. As shown in Table 1, NCS/glacial acetic acid (^{G}AcOH) and NCS/acetonitrile (MeCN) offered monochlorinated product **1-Cl** in 50% and 56% yield respectively (selectivity almost 100%; only traces of di-chlorinated product 1-Cl$_2$; Table 1, entries 1 and 2). In contrast, PhICl$_2$ worked
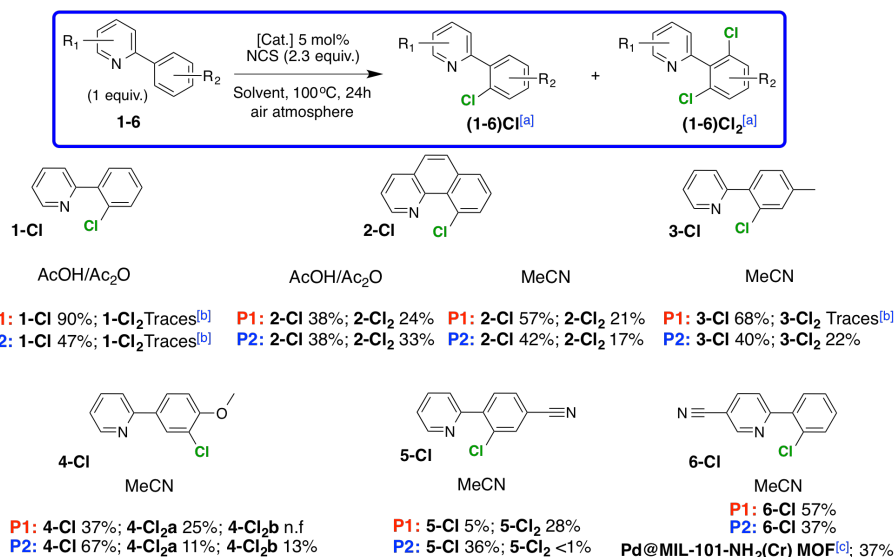
Figure 4. Scope of **P1** and **P2** catalyze direct C–H chlorination of arylpyridines derivatives. Pd loading (see table S1, Supporting Information), [a] Isolated yields were monitored by ^{1}HNMR and HRMASS, [b] Traces of di-chloro substituents detected by GC-MAS. [c] The best isolated yield of **6-Cl** was reported by V. Pascanu (See Reference 37).

poorly irrespective of solvent and in MeCN a tri-chlorinated adduct was detected by GC-MS (Table 1, entry 3-4). These results can be attributed to the expected instability of PhICl$_2$ under the reaction conditions.[26] For NCS, a mixed solvent system (^{G}AcOH/Ac$_2$O) worked better than neat ^{G}AcOH as previously observed,[58, 59] and, interestingly, the yield was sensitive to the concentration of the NCS (Table 1, entries 8-10) in preference of 0.4 M, which gave 75% yield and 100% regioselectivity (Table 1, entry 9). Increasing the excess of halogenating reagent to 2.3 equivalents gave 90% yield and almost 100% regioselectivity of mono-chlorinated product **1-Cl** in ^{G}AcOH/Ac$_2$O solvent (Table 1, entry 11). The highest yield of mono-chlorinated product **1-Cl** reported so far is 55%, which was achieved by using 10 mol% of a heterogeneous catalyst and 1.2 equivalents of the oxidant.[35] Without catalyst there was no product formation (Table 1, entry 12). Importantly, for all optimized chlorination reactions, the dimeric product was not observed.[37, 60] Using **P2** as a catalyst under optimized conditions gave the corresponding product **1-Cl** in a moderate isolated yield (47%) (see Figure 4). ^{13}C CP-MAS NMR spectra of fresh **P1** and **P2** display peaks for terminal and internal vinyl carbons at around 112 and 137 ppm, respectively, but these are absent in the spent catalyst. This suggests that functionalization of unreacted vinyl groups takes place in both polymers during catalysis (see Figures S4a, S4b, and S5a).[34] On the basis of these results, we conclude that a highly

selective formation of mono-chlorinated product **1-Cl** can be achieved by tuning the reaction conditions. Importantly, PXRD patterns of **P1** and **P2** after catalysis under the mentioned reaction conditions showed no peak intensities belonging to the Pd(111), Pd(200), and Pd(220) planes of metallic Pd (Figure S1a, supporting Information).

C–H chlorination of aryl-pyridine derivatives under batch mode conditions

Under the optimized reaction conditions, the scope of the C–H chlorination of different aryl pyridines catalysed by **P1** and **P2** was investigated (Figure 4). With (^{G}AcOH/Ac$_2$O) solvent system, the chlorination of benzo[h]quinoline **2** gave a lower yield and no regioselectivity (almost 50:50 of **2-Cl:2-Cl$_2$** products) using **P1** or **P2** as a catalyst for the model reaction. However, in MeCN **P1** offered 78% yield of the products with a regioselectivity around 73:27 for mono- and di-chlorinated adducts, while **P2** provided the corresponding products in 59% yield and 71:29 regioselectivity. The chlorination of 2-phenylpyrines carrying electron rich functional groups was also examined. Significantly, **P1** catalyses the transformation of 2-(4-tolyl)pyridine **3** into **3-Cl** in 68% yield and almost 100% regioselectivity. In contrast, **P2** exhibited 62% yield and very low regioselectivity 65:35 for mono **3-Cl** and di-chlorinated **3-Cl$_2$** derivatives. 2-(4-Methoxyphenyl)pyridine **4** substrate was more reactive than 2-(4-tolyl)pyridine 3, yielding one mono-chlorinated product **4-Cl**, and two different di-

chlorinated products **4-Cl₂a** and **4-Cl₂b**. Surprisingly, **P1** and **P2** disabled C7 chlorination, and gave C8 chlorination in 37% and 67% yield respectively (Figure 4). As expected electron poor substrates such as 4-(pyridin-2-yl)benzonitrile **5**, gave lower conversions. **P2** exhibited the best catalytic activity reported so far, producing **5-Cl** and **5-Cl₂** in moderate yield, 36%, and very good regioselectivity, 98%, of the mono-chlorinated adduct. Finally, switching the position of the functional group from the phenyl to pyridyl group (4-(pyridin-2-yl)benzonitrile 6) increased the activity and gave the mono-chlorinated product with 100% regioselectivity in 57% and 37% yield for **P1** and **P2**, respectively. To the best of our knowledge these are the best yield of **6-Cl** reported so far.

C–H chlorination under continuous flow conditions

A packed-bed reactor was employed to investigate the activity and stability of the polymeric catalysts in C–H oxidation under continuous conditions. **P1** was chosen as a catalyst, since it displays a higher reactivity in most of the C–H chlorinations of arylpyridines (as shown in Figure 4). Benzo[*h*]quinoline **2** was chosen as a model substrate, so we could also investigate directed vs. non-directed catalysis under flow conditions. As previously mentioned, the catalysis of **2** in MeCN afforded non-directed chlorination in 21% yield; possibly the shorter interaction of the product with the catalyst would improve the selectivity in a continuous process. Using the optimal reaction conditions, the continuous flow process was implemented as shown in Figure 6, with the amount of catalyst set at 0.5 mol% (with respect to the substrate); this afforded approximately 22 min residence time inside the reactor. Using standard filters for continuous flow system was ineffective, giving substantial leakage of the smallest of the catalyst particles (<100 nm). Therefore, molecular sieves (3Å, powder) was added in the end of the reactor to act as an even smaller filter (see the Supporting Information for details about catalyst packing and experimental procedure under continuous flow). The reactor column was packed with **P1** (5.8 wt% Pd) and the flow rate was set to 60 μl/min during the whole experiment. The molecular sieves and the packed catalyst were washed with acetonitrile to make sure the particulate bed was settled. When the pressure was stable substrate solution was introduced and samples were collected continuously every hour by an auto sampler attached to the reactor outlet. The collected samples were analysed by GC to measure the conversion, and the Pd leaching was determined by ICP-OES analysis. After 5 h, 39% conversion was achieved (with 100% selectivity to **2-Cl**). However, the conversion required 10 h to stabilize and at that point it stayed constant at ~ 90% and 100% regioselectivity until the end of the experiment after ~ 6 days (140 h) as shown in the conversion plot (Figure 5a). A low level of Pd leaching was detected by ICP analysis after 10 h run (0.29 ppm), and the leaching gradually decreased as the reaction continued to reach levels below the detection limit of the ICP technique (0.04, <0.005, <0.005, <0.005, <0.005, and <<0.005 ppm at 40, 87, 100, 110 and 140 h respectively) as shown in Figure 5a. The recovered catalyst was washed with acetonitrile and then characterized to shed some light on the leaching is-
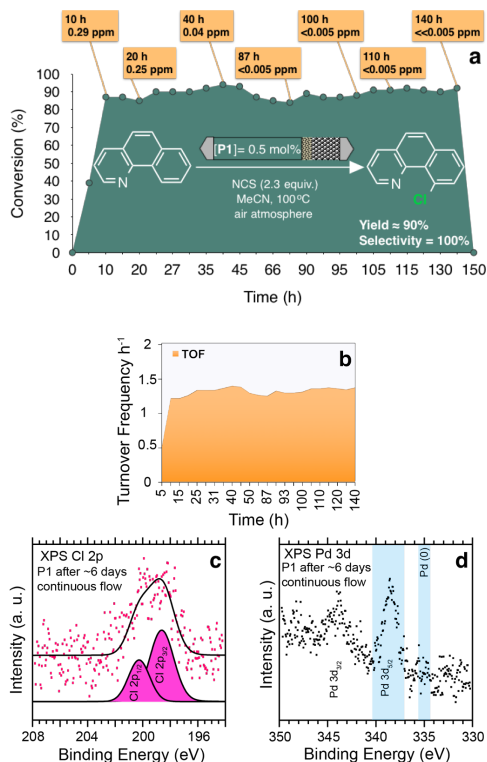
Figure 5. **(a)** Conversion and Pd leaching of **P1** catalyzed C-H chlorination under flow conditions. Yield and selectivity were determined by GC using a calibration curve based on decane as an internal standard. **(b)** Turnover Frequencies of **P1** over ~6 days continuous flow. **(c)** and **(d)** XP spectra of the Cl 2p and Pd 3d core level of **P1** respectively, obtained after 140 h catalysis under continuous flow conditions.

-sue. PXRD pattern of the recovered catalyst after 6 days reaction was featureless and no Bragg reflections related to metallic Pd were detected (Figure S1a, Supporting Information). Figures 5c and 5d show the core level XP spectra of the Cl 2p and Pd 3d core level of **P1**, obtained after 140 h catalysis under continuous flow conditions. Importantly, no significant peak, on the level of the spectral noise, associated with Pd(0) was observed in Pd 3d spectrum (for a description of the peak treatment, cf. Figure S13 and accompanying text in the Supporting Information). Moreover, the Pd 3d₅/₂ and Pd 3d₃/₂ signals at ca 338.5 and 344 eV binding energy match the energies expected for a Pd(II) species. The binding energy for the Cl 2p₃/₂ and Cl 2p₁/₂ appeared at 198.6 and 200.2 eV in good agreement with **1a**. The XPS results demonstrated the long-term stability of **P1** and is probably explained by its robust microsphere polymer structure which maintains the Pd(II) oxidation state during the flow process. The CP-MAS spectrum confirmed again the activation of unreacted vinyl moie-
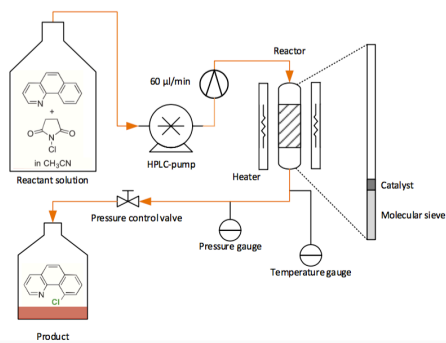
Figure 6. Schematic of the continuous flow reactor system.

-ties as shown in Figure S5b, Supporting Information. It can be concluded that the initial level of leaching observed is not due to the decomposition of the catalyst, but most probably due to the fact that the smallest particles escaped through the molecular sieves in the beginning of the continuous process. Overall, the heterogeneous **P1** catalyst exhibits a tremendous stability and activity under flow conditions. The maximum turnover frequency during catalysis was 1.38 h^{-1} and the overall turnover number was 178 (Figure 5b), based on the palladium remaining after the first hours of leaching.[35,61]

Selective mono-bromination and mono-iodination under batch reaction conditions

Catalysts **P1** and **P2** were also tested for iodination and bromination of different arylpyridines. There are no universal reaction conditions for all substrates and reagents,[15, 27] and, thus, the reaction conditions were optimized for each reaction. Table S2 in the Supporting Information outlines the optimization for the bromination and iodination of benzo[*h*]quinoline **2**. We found that **P1** catalyses the bromination reaction of **2**, with 68% conversion. However, a significant improvement was obtained using **P2** under the same conditions, giving a conversion of 82% as shown in Figure 7. The regioselectivity was the same for **P1** and **P2**: 67:33 for **2-Br**:**2-Br₂** (see Figure 7 and Table S2 entry 9). In contrast, the iodination of **2** was not successful neither with **P1** nor with **P2** (Figure 7), which may be a result of the highly planar benzo[*h*]quinoline **2** and the size of the iodine atom.[27] Using **P1** as the catalyst and phenylpyridine **1** as the substrate [G]AcOH was the best solvent to give mono-brominated **1-Br** or iodinated **1-I** products in 40% and 76% yield respectively with 100% regioselectivity (Table S3, entries 3 and 6). Increasing the temperature gave lower regioselectivity due to over-halogenation of the substrates and formation of **1-Br₂** and **1-I₂** products (Table S3, entries 5 and 9). **P2** was inferior to **P1** for both halogenations (Figure 7). Moreover, for halogenation of **6**, **P1** was also the better catalyst (Figure 7). Noteworthy, di-brominated and di-iodinated
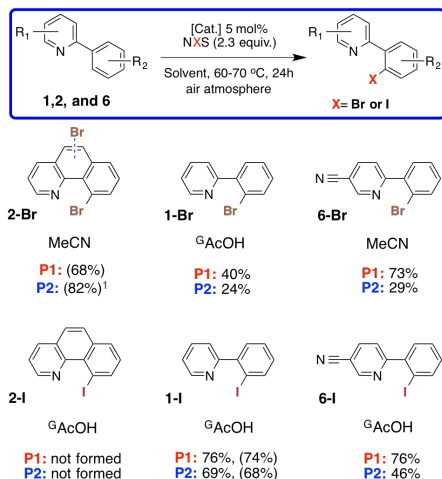

Figure 7. **P1**- and **P2**-catalyzed bromination and iodination of arylpyridines. Isolated yields were monitored by ^{1}HNMR and HRMASS. GC yields and conversions (reported in parentheses) were determined by GC using a calibration curve based on decane as an internal standard.[1]Regioselectivity is 67:33 of **1-Br**:**1-Br₂**.

products were not observed during **P1** and **P2** catalysed halogenation of 4-(pyridin-2-yl)benzonitrile **6**, but these di-substituted adducts were formed as over functionalization products under catalysis with Pd@MOF nanocomposites.[37]

Recyclability and the heterogeneous nature of catalysis

The effortless catalyst separation and recycling after catalysis, are the main potential advantages of heterogeneous catalysts. In line with that, the recyclability of **P1** and **P2** was examined using iodination of 2-phenylpyridine as the model reaction. The recovered catalysts were separated easily by centrifugation after each run, and then washed with 5 mL of 4-phenylpyridine/CH₂Cl₂ solutions for 30 min followed by washing with MeCN to remove the remaining non-bonded phenylpyridines (see the Supporting Information for details). For the catalysis, a fresh reactant solution was mixed with the catalyst, and the reaction was run under the conditions described in Figure 8a. The activity for **P1** and **P2** was constant for six runs (Figure 8b), thus showing the stability and recyclability of these catalysts. The kinetic profile for **P1** and **P2** are more or less identical (Figure 8c). Although GC analysis showed unreacted 2-phenylpyridine **1** in the catalysis mixtures, catalysis stopped after eight and ten hours in case of **P1** and **P2**, respectively. This could possibly suggest that the oxidant is either consumed or degraded through the catalysis reaction as previously reported.[34] Thus, when more NIS (2.3 additional equivalents) was added to the reaction mixtures
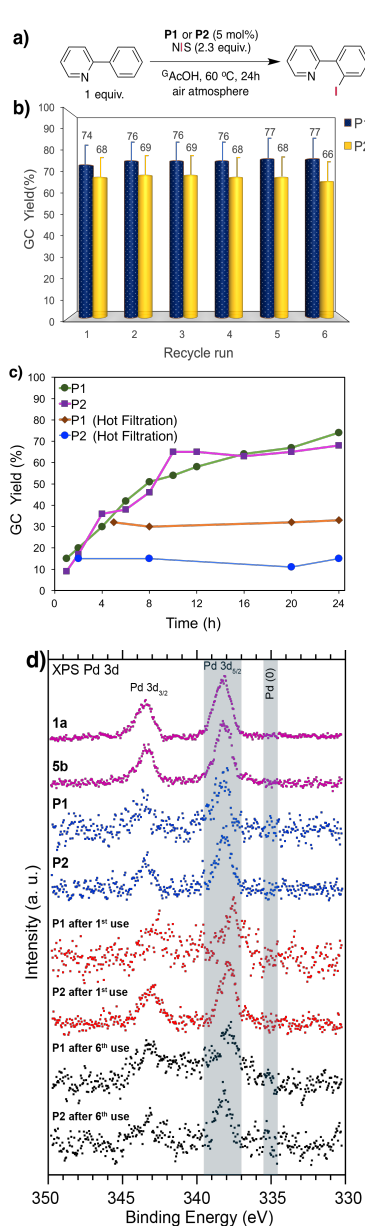
after eight and ten hours for **P1** and **P2**, respectively, and the reactions allowed to continue, mono-iodinated product **2-I** was ultimately obtained in 97% and 92% yield, respectively (Table S3, entries 10 and 11, Supporting Information). A hot filtration test was performed to confirm the heterogeneous nature of the catalysts. No further reaction was observed in the filtrate over time (Figure 8c), corroborating that the catalyst is heterogeneous in nature. These results were supported with results from ICP-OES and XPS analysis. Hence, only a very small leaching into the supernatant (0.011 and 0.009 ppm) was detected after the 6th run with **P1** and **P2** respectively. In addition to that, XP spectra disclosed that the palladium is present in oxidation state (II) up to 6 cycles (and likely more), Figure 8d. Therefore, it can be concluded, that **P1** and **P2** can be successfully recovered and reused without loss of reactivity over several cycles in batch wise C–H iodination. The synthesized polymers operate as heterogeneous catalysts with an inconsiderable leaching of Pd.

Conclusions

New classes of polymer supported molecular NHC-Pd(II) complexes were synthesized via the copolymerization method, and fully characterized with, SS-NMR, SEM, HRTEM, XEDS, PXRD as well as ICP-OES analysis. These solids work as robust and highly efficient heterogeneous molecular catalysts in the directed C–H halogenation of arenes. Both catalysts demonstrated a high catalytic activity and an excellent regioselectivity in batch mode catalysis. Importantly, the catalysts could be reused up to 6 runs without loss of activity and with no significant leaching of palladium. The heterogeneous character of both catalysts was explored, and the catalysts were heterogeneous according to the hot filtration tests. In packed-bed reactor, the best catalyst disclosed an exceptional activity and 100% selectivity of the mono-halogenated product for up to 6 days under continuous flow conditions. No loss of activity, no leaching of palladium, and ability to maintain the original oxidation state of Pd(II) were remarkable observations under long-term continuous flow conditions.

ASSOCIATED CONTENT

Supporting Information

Experimental details and additional data such ^{1}H and ^{13}C NMR spectra, ^{13}C CP-MAS NMR spectra, Elemental analyses, ICP analyses, HRTEM, XPS, PXRD, STEM-HADDF, XEDS, SEM, TGA, N[2] adsorption-desorption.

AUTHOR INFORMATION

Corresponding Author

*Correspondence e-mail: ola.wendt@chem.lu.se

Acknowledgements

Figure 8. a) Reaction conditions of C–H iodination reaction of 2-phenylpyridine. **b)** Reusability and productivity of **P1** and **P2**. **c)** Time profile and hot filtration study of **P1** and **P2** catalysed C–H iodination reaction of 2-phenylpyridine. **d)** Pd 3d XP spectra of **P1** and **P2** fresh and after 1st and 6th reuse.

REFERENCES

(1) Mohamed, Y. S.; Wang, P.; Sethi, T.; Agama, K.; Ravji, A; Redon, C. E.; Kiselev, E; Horzmann, K. A.; Freeman, J. L.; Pommier, Y.; Cushman, M. *J. Med. Chem.* **2017**, 60**,** 5364.

(2) Wang, J.; Sanchez-Rosello, M.; Acena, J. L.; Pozo, C. D.; Sorochinsky, A. E.; Fustero, S.; Soloshonok, V. A.; Liu, H. *Chem. Rev.* **2014**, 114, 2432.

(3) Wilcken, R.; Zimmermann, M. O.; Lange, A.; Joerger, A. C.; Boeckler, F. M. *J. Med. Chem.* **2013**, 56, 1363.

(4) Dai, H. X.; Stepan, A. F.; Plummer, M. S.; Zhang, Y. H.; Yu, J. Q. *J. Am. Chem. Soc.* **2011**, 133.

(5) Jeschke, P. *Pest. Manag. Sci.* **2010**, 66, 10.

(6) Hernandes, M. Z.; Cavalcanti, S. M. T.; Moreira, D. R. M.; De Azevedo, W. F.; Leite, A. C. L. *Curr. Drug Targets* **2010**, 11, 303.

(7) Gribble, G. W. *Chem. Soc. Rev.* **1999**, 28, 335.

(8) Gribble, G. W. *Accounts Chem. Res.* **1998**, 31, 141.

(9) Sharma, M. K.; Murumkar, P. R.; Kanhed, A. M.; Giridhar, R.; Yadav, M. R. *Eur. J. Med. Chem.* **2014**, 79, 298.

(10) Debenham, J. S.; Madsen-Duggan, C. B.; Wang, J. Y.; Tong, X. C., Lao, J. L.; Fong, T. M.; Schaeffer, M. T.; Xiao, J. C.; Huang, C. C. R. R.; Shen, C. P.; Stribling, D. S.; Shearman, L. P.; Strack, A. M.; MacIntyre, D. E.; Hale, J. J.; Walsh, T. F. *Bioorg. Med. Chem. Lett.* **2009**, 19, 2591.

(11) Zhan, B. B.; Liu, Y. H.; Hu, F.; Shi, B. F. *Chem. Commun.* **2016**, 52, 4934.

(12) Do, H. Q.; Daugulis, O. *Org. Lett.* **2009**, 11, 421.

(13) Schreiner, P. R.; Lauenstein, O.; Butova, E. D.; Gunchenko, P. A.; Kolomitsin, I. V.; Wittkopp, A.; Feder, G.; Fokin, A. A. *Chem.-Eur. J.* **2001**, 7, 4996.

(14) Sen, A. *Accounts Chem. Res.* **1998**, 31, 550.

(15) Petrone, D. A.; Ye, J. T.; Lautens, M. *Chem. Rev.* **2016**, 116, 8003.

(16) Vigalok, A.; Kaspi, A. W. *C–X Bond Formation*, **2010**, 31, 19.

(17) Liu, W.; Groves, J. T. *J. Am. Chem. Soc.* **2010**, 132, 12847.

(18) Bloom, S.; Pitts, C. R.; Woltornist, R.; Griswold, A.; Holl, M. G.; Lectka, T. *Org. Lett.* **2013**, 15, 1722.

(19) Du, Z. J.; Gao, L. X.; Lin, Y. J.; Han, F. S. *Chemcatchem* **2014**, 6, 123.

(20) Lied, F.; Lerchen, A.; Knecht, T.; Muck-Lichtenfeld, C.; Glorius, F. *Acs Catal.* **2016**, 6, 7839.

(21) Yu, Q. Z.; Hu, L. A.; Wang, Y.; Zheng, S. S.; Huang, J. H. *Angew. Chem. Int. Edit.* **2015**, 54, 15284.

(22) Van der Werf, A.; Selander, N. *Org. Lett.* **2015**, 17, 6210.

(23) Teskey, C. J.; Lui, A. Y. W.; Greaney, M. F. *Angew. Chem. Int. Edit.* **2015**, 54, 11677.

(24) Schroder, N.; Lied, F.; Glorius, F. *J. Am. Chem. Soc.* **2015**, 137, 1448.

(25) Liu, W.; Groves, J. T. *Accounts Chem. Res.* **2015**, 48, 1727.

(26) Kalyani, D.; Dick, A. R.; Anani, W. Q.; Sanford, M. S. *Org. Lett.* **2006**, 8, 2523.

(27) Kalyani, D.; Dick, A. R.; Anani, W. Q.; Sanford, M. S. *Tetrahedron* **2006**, 62, 11483.

(28) Kalyani, D.; Deprez, N. R.; Desai, L. V.; Sanford, M. S. *J. Am. Chem. Soc.* **2005**, 127, 7330.

(29) Kalyani, D.; Sanford, M. S. *Directed Metallation* **2007**, 24, 85.

(30) Whitfield, S. R.; Sanford, M. S. *J. Am. Chem. Soc.* **2007**, 129, 15142.

(31) Racowski, J. M.; Sanford, M. S. *Higher Oxidation State Organopalladium and Platinum Chemistry* **2011**, 35, 61.

(32) McMurtrey, K. B.; Racowski, J. M.; Sanford, M. S. *Org. Lett.* **2012**, 14, 4094.

(33) Bolbat, E.; Wendt, O. F. *Eur. J. Org. Chem.* **2016**, 20, 3395.

(34) Majeed, M. H.; Shayesteh, P.; Wallenberg, L. R.; Persson, A. R.; Johansson, N.; Ye, L.; Schnadt, J.; Wendt, O. F. *Chem.-Eur. J.* **2017**, 23, 8457.

(35) Korwar, S.; Brinkley, K.; Siamaki, A. R.; Gupton, B. F.; Ellis, K. C. *Org. Lett.* **2015**, 17, 1782.

(36) Fei, H.; Cohen, S. M. *J. Am. Chem. Soc.* **2015**, 137, 2191.

(37) Pascanu, V.; Carson, F.; Solano, M. V.; Su, J.; Zou, X. D.; Johansson, M. J.; Martin-Matute, B. *Chem.-Eur. J.* **2016**, 22, 3729.

(38) Mondal, M.; Joji, J.; Choudhury, J. *Chem. Commun.* **2017**, 53, 3185.

(39) Painter, T. O.; Thornton, P. D.; Orestano, M.; Santini, C.; Organ, M. G.; Aube, J. *Chem.-Eur. J.* **2011**, 17, 9595.

(40) Noel, T.; Maimone, T. J.; Buchwald, S. L. *Angew. Chem. Int. Edit.* **2011**, 50, 8900.

(41) Ullah, F.; Samarakoon, T.; Rolfe, A.; Kurtz, R. D.; Hanson, P. R.; Organ, M. G. *Chem.-Eur. J.* **2010**, 16, 10959.

(42) Wiles, C.; Watts, P. *Green Chem.* **2014**, 16, 55.

(43) Price, G. A.; Bogdan, A. R.; Aguirre, A. L.; Iwai, T.; Djuric, S. W.; Organ, M. G. *Catal. Sci. Technol.* **2016**, 6, 4733.

(44) Mohammadi, E.; Movassagh, B. *J. Mol. Catal. a-Chem.* **2016**, 418, 158.

(45) Majeed, M. H.; Wendt, O. F. *Acta Crystal. Sec. E-Crystal. Comm.* **2016**, 72, 534.

(46) Smith, T. W.; Zhao, M.; Yang, F.; Smith, D.; Cebe, P. *Macromolecules* **2013**, 46, 1133.

(47) Overberger, C. G.; Kawakami, Y. *J. Polym. Sci. Pol. Chem.* **1978**, 16, 1237.

(48) Zhao, D. B.; Fei, Z. F.; Ang, W. H.; Dyson, P. J. *Small* **2006**, 2, 879.

(49) Kim, J. H.; Kim, J. W.; Shokouhimehr, M.; Lee, Y. S. *J. Org. Chem.* **2005**, 70, 6714.

(50) Gaborieau, M.; Nebhani, L.; Graf, R.; Barner, L.; Barner-Kowollik, C. *Macromolecules* **2010**, 43, 3868.

(51) Shil, A. K.; Kumar, S.; Reddy, C. B.; Dadhwal, S.; Thakur, V.; Das, P. *Org. Lett.* **2015**, 17, 5352.

(52) Shang, N. Z.; Gao, S. T.; Feng, C.; Zhang, H. Y.; Wang, C.; Wang, Z. *Rsc. Adv.* **2013**, 3, 21863.

(53) Xu, S. J.; Song, K. P.; Li, T.; Tan, B. *J. Mater. Chem. A* **2015**, 3, 1272.

(54) Maria, S. J. S.; Militello, C. *Surface Science Spectra* **1994**, 3, 387.

(55) Warratz, S.; Burns, D. J.; Zhu, C. J.; Korvorapun, K.; Rogge, T.; Scholz, J.; Jooss, C.; Gelman, D.; Ackermann, L. *Angew. Chem. Int. Edit.* **2017**, 56, 1557.

(56) Pal, P.; Singh, H.; Panda, A. B.; Ghosh, S. C. *Asian J. Org. Chem.* **2015**, 4, 879.

(57) Leyva-Perez, A.; Combita-Merchan, D.; Cabrero-Antonino, Al-Resayes, J. R. S. I.; Corma, A. *Acs Catal.* **2013**, 3, 250.

(58) Stephens, D. E.; Lakey-Beitia, J.; Atesin, A. C.; Atesin, T. A.; Chavez, G.; Arman, H. D.; Larionov, O. V. *Acs Catal.* **2015**, 5, 167.

(59) Davies, D. L.; Macgregor, S. A.; McMullin, C. L. *Chem. Rev.* **2017**, 117, 8649.

(60) Topczewski, J. J.; Sanford, M. S. *Chem. Sci.* **2015**, 6, 70.

(61) Emmert, M. H.; Cook, A. K.; Xie, Y. J.; Sanford, M. S. *Angew. Chem. Int. Edit.* **2011**, 50, 9409.

Supplementary data for:

Directed C–H halogenation reactions catalyzed by Pd(II) supported on polymers under batch and continuous flow conditions

Maitham H. Majeed,[a] P. Shayesteh,[b] P. Tunå,[c] Axel R. Persson,[a,d] R. Gritcenko[a],

L. Reine Wallenberg, [a,d] C. Hulteberg,[c] Lei Ye,[e] J. Schnadt,[b] and Ola F. Wendt[a,*]

[a]Centre for Analysis and Synthesis, Department of Chemistry, Lund University
Box 124, SE-221 00 Lund (Sweden)

[b]Division of Synchrotron Radiation Research, Department of Physics, Lund University
Box 118, SE-221 00 Lund (Sweden).

[c]Department of Chemical Engineering, Lund University, Box 124, 221 00 Lund, (Sweden)

[d]National Centre for High Resolution Electron Microscopy, Lund University
Box 124, SE-221 00 Lund (Sweden)

[e]Centre for Applied Life Sciences Department of Chemistry, Lund University Box 124, 221 00 Lund (Sweden)

* Corresponding author. Tel.: +46 2228153; fax: +46 2228209.
E-mail address: ola.wendt@chem.lu.se (Ola F. Wendt).

Table of contents

List of figures and tables

Experimental part

1. General considerations

All manipulations were conducted under ambient conditions, unless noted. Solvents and chemicals were purchased from commercial suppliers and used as received. Divinylbenzene-80 (DVB-80) was passed through an aluminum oxide column to remove the inhibitor *p*-tert-butylcatechol before the use. AIBN was purified by recrystallization in warm methanol solution. **1a** was synthesized by the decarboxylation of urocanic acid.[1] **P1** polymer and **2b** were synthesized according to previously reported procedures.[2-4] In order to identify the retention time of the product in the gas chromatogram, 10-chloroobenzo[*h*]quinolone, 10-bromobenzo[*h*]quinolone, and 2-(2-iodophenyl)pyridine have been synthesized as in previously reported procedure. [5-7] NMR spectra were acquired on a Bruker Avance 400 FT-NMR spectrometer ([1]H: 400.1 MHz) or a Varian Unity INOVA 500 spectrometer ([1]H: 499.76 MHz). ^{1}H and ^{13}C NMR chemical shifts are reported in parts per million and referenced to the signals of deuterated solvents. Multiplicities are abbreviated as follows: (s) singlet, (d) doublet, (t) triplet, (q) quartet, (m) multiplet and (br) broad. Elemental analyses were performed by H. Kolbe Microanalytisches Laboratorium, Mülheim an der Ruhr, Germany.

2. Synthesis of *N*HC-Pd(II) monomer and its characterization

1,3-bis(4-isopropylbenzyl)-4-vinyl-1H-imidazol-3-ium **3b**
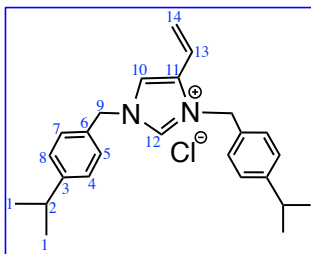
In a Straus flask, freshly distilled 1-(trimethylsilyl)-5-vinyl-1*H*-imidazole **2b** (1.20 g, 7.2 mmol) was transferred inside a nitrogen atmosphere glovebox to 4-isopropylbenzyl chloride (2.92 g, 17.3 mmol) and 4-*tert*-butylcatechol (TBC) (0.053 g, 0.31 mmol) in 25 ml of dry MeCN. The reaction mixture was stirred at 115 °C, during the stirring the solution changed color to orange. After 48h, the reaction

stopped and when the solution cooled down, complex **3b** is formed directly. The formed white solids were filtered, washed with diethyl ether and pentane (2 x 25 ml) and dried under vacuum to afford **3b** as a white powder (1.3 g, 46%). ^{1}H NMR (400 MHz, CDCl$_3$): δ 11.27 (s, 1H, H12), 7.38 (d, J = 8.2 Hz, 2H, H$_{Aromatic}$), 7.29-7.20 (m, overlapping, 6H, H$_{Aromatic}$), 7.12 (s, 1H, H10), 6.38 (dd, J = 17.5, 11.3 Hz, 1H, H13), 5.70 (d, J = 17.5 Hz, 1H, H14$_A$), 5.53 (d, J = 11.4 Hz, 1H, H14$_B$), 5.50 (d, J = 2.2 Hz, 4H, H9), 2.90 (dq, J = 20.3, 6.9 Hz, 2H, H2), 1.22 (dd, J = 9.6, 6.9 Hz, 12H, H1). ^{13}C NMR (400 MHz, CDCl$_3$): δ 150.7 (C3), 150.2 (C3'), 138.6 (C12), 138.5 (C13), 130.3 (C6'), 130.0 (C6), 129.2 (C5' and C7'), 127.9 (C5 and C7), 127.7 (C4' and C8'), 127.6 (C4 and C8), 123.1 (C10), 119.8 (C11), 117.1 (C14), 53.6 and 51.1 (C9 and C9'), 34.0 and 33.9 (C2 and C2'), 23.9 (C1). Anal. Calcd for C$_{26}$H$_{34}$ClN$_2$: C, 76.02; H, 7.91; N, 7.09. Found: C, 75.16; H, 7.97; N, 7.41.

1,3-bis(4-isopropylbenzyl)-4-vinyl-3λ-imidazol-2-yl) silver(I) chloride **4b**
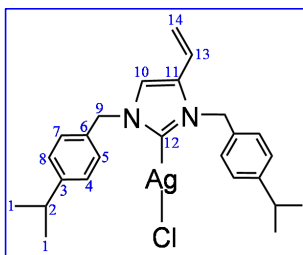
In a nitrogen purged and aluminum foil covered 50 mL Schlenk flask, 1,3-bis(4-isopropylbenzyl)-4-vinyl-1H-imidazol-3-ium salt **3b** (0.305 g, 0.77 mmol) and freshly prepared silver carbonate (0.106 g, 0.38 mmol) were transferred under nitrogen in 30 ml of dry dichloromethane. The reaction mixture was stirred at room temperature. After 24h, the reaction stopped and the suspension was filtered through plug of Celite, all solvents removed under vacuum, the dried residues afford **4b** as a yellow solid (0.37 g, 95%). ^{1}H NMR (400 MHz, CDCl$_3$) δ 7.26 - 7.17 (m, 6H, H$_{Aromatic}$), 7.08 - 7.00 (m, 3H, H$_{Aromatic}$), 6.31 (dd, J = 17.7, 11.5 Hz, 1H, H13), 5.51 (d, J = 17.3 Hz, 1H, H14$_A$), 5.32 (s, 2H, H9), 5.28 (d, J = 11.8 Hz, 1H, H14$_B$), 5.23 (s, 2H, H9'), 2.90 (tt, J = 13.8, 6.9 Hz, 2H, H2), 1.24 (dd, J = 8.6, 6.9 Hz, 12H, H1). ^{13}C NMR (400 MHz, CDCl$_3$) δ 168.93 (C12), 149.80 (C3), 149.26 (C3'), 134.11 (C14), 132.84 (C4), 132.60 (C6, C6'), 128.05 (C5', C7'), 127.41 (C5, C7), 127.27 (C4, C8), 126.72 (C4',

C8´), 121.93 (C10), 119.29 (C11), 117.91 (C13), 56.06 (C9´), 53.17 (C9), 33.98 (C2), 33.91 (C2´), 24.02 (C1, C1´).

1,3-bis(4-isopropylbenzyl)-4-vinyl-3λ-imidazol-2-yl) (4-phenylpyridine) palladium(II) chloride **5b**
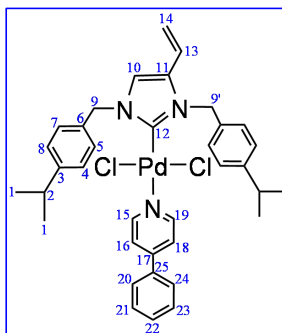
1,3-bis(4-isopropylbenzyl)-4-vinyl-*3λ*-imidazol-2-yl) silver(I) chloride **4b** (0.36 g, 0.71 mmol), 30 mL of dry CH_2Cl_2 and $Pd(PhCN)_2Cl_2$ were charged in a nitrogen purged and aluminum foil covered 50 mL Schlenk flask. The reaction mixture was stirred at room temperature. After 24h, the reaction stopped and the red suspension was filtered through plugs of Celite and silica, then 4-phenylpyridine (0.146 g) was added to the filtrate and stirring of the mixture was continued at room temperature. During the stirring the solution changed colour to clear yellow. After 6h, the reaction stopped and the solution was filtered through Celite and all solvents removed under vacuum, the residue was crystallised in CH_3CN to afford **5b** as yellow crystals (0.41 g, 83%). ^{1}H NMR (400 MHz, CDCl$_3$) δ 8.99 (dd, *J* = 5.2, 1.5 Hz, 2H), 7.60 (dd, *J* = 7.7, 1.8 Hz, 2H), 7.50-7.44 (m, 11H, H$_{Aromatic}$), 7.31-7.21 (m, 2H, H$_{Aromatic}$), 6.85 (s, 1H, H10), 6.19 (dd, *J* = 17.5, 11.3 Hz, 1H, H13), 5.95 (s, 2H, H9), 5.88 (s, 1H, H9´), 5.34 (d, *J* = 17.5 Hz, 1H, H14$_A$), 5.08 (d, *J* = 11.4 Hz, 1H, H14$_B$), 2.91 (tt, *J* = 13.7, 6.9 Hz, 2H, H2), 1.25 (dd, *J* = 10.0, 6.9 Hz, 12H, H1). ^{13}C NMR (400 MHz, CDCl$_3$) δ 151.50 (C15, C19), 150.99 (C12), 150.50 (C17), 149.38 (C3), 148.66 (C3´), 136.98 (C25), 134.82 (C14), 133.32 (C6), 132.81 (C6´), 129.97 (C22), 129.42 (C21, C23), 129.13 (C20, C24), 127.59 (C4, C4´), 127.27 (C5, C5´), 127.19 (C7, C7´), 127.02 (C8, C8´), 122.31 (C16, C18), 122.23 (C10), 118.37 (C11), 117.84 (C13), 54.91 (C9´), 52.70 (C9), 34.02 (C2´), 33.93 (C2), 24.09 (C1, C1´). Anal. Calcd for $C_{36}H_{39}Cl_2N_3Pd.H_2O$: C, 60.98; H, 5.83; N, 5.93. Found: C, 61.15; H, 5.32; N, 5.51.

3. Polymerization procedure

*N*HC-Pd(II) monomer **5b** (0.25 g, 0.361 mmol), the crosslinker DVB-80 (0.188 g, 1.44 mmol), and the initiator AIBN (0.04 g) were dissolved in 22 ml CH_3CN in borosilicate glass-threaded vial. The total monomers concentration was 2 % (w/v) of the solvent. The mixture was purged with a gentle flow of nitrogen for 5 min and then sealed by using Teflon cap. The polymerization reaction mixture in borosilicate glass vial was fixed in a horizontal position in the hybridization oven and heated at 60 °C under rotation speed of 45 rpm for 48 h. After the polymerization, the resulting polymers were separated by centrifugation and washed successively three times with acetonitrile and acetone, then dried under vacuum to afford **P2** as an off-white powder (0.25 g).

4. Inductively coupled plasma-optical emission spectroscopy (ICP-OES) analysis

Pd loadings were measured by a PerkinElmer Optima 8300. Samples (2 mg) were treated with a muffle stove at 1000 °C for 4 h. After cooling to room temperature, 3 mL of aqua regia was added and stirred for 1 h at 100 °C. The resulting solution was filtrated and the filtrate was diluted to 25 mL with distilled water.

Table S1. Pd loadings were analysed by ICP-OES

Entry	Polymer	Pd (wt%)
1	**P1**	5.8
2	**P2**	4.5

5. Powder x-ray diffraction (PXRD) analysis

Diffraction patterns were recorded using a STOE & CIE GmbH diffractometer using Cu Kα radiation and Bragg–Brentano geometry with a curved Ge-monochromator. Samples were scanned in a 2θ range of 10-100°. All measurements were done at room temperature and ambient pressure.

*Reducing procedure of polymer **P1** and **P2***

The experimental steps were according to a method reported in the literature.[16] (0.05 g) of **P1** or **P2** and (0.1 g) of ascorbic acid were dissolved in 50 mL of water and the mixture sonicated continuously (up) till a homogeneous brown solution was formed. The dispersed solution was stirred at 95 °C for 24 h, followed by centrifugation and washing with water. The remains were dried under vacuum overnight to obtain **P1**-reduced or **P2**-reduced.
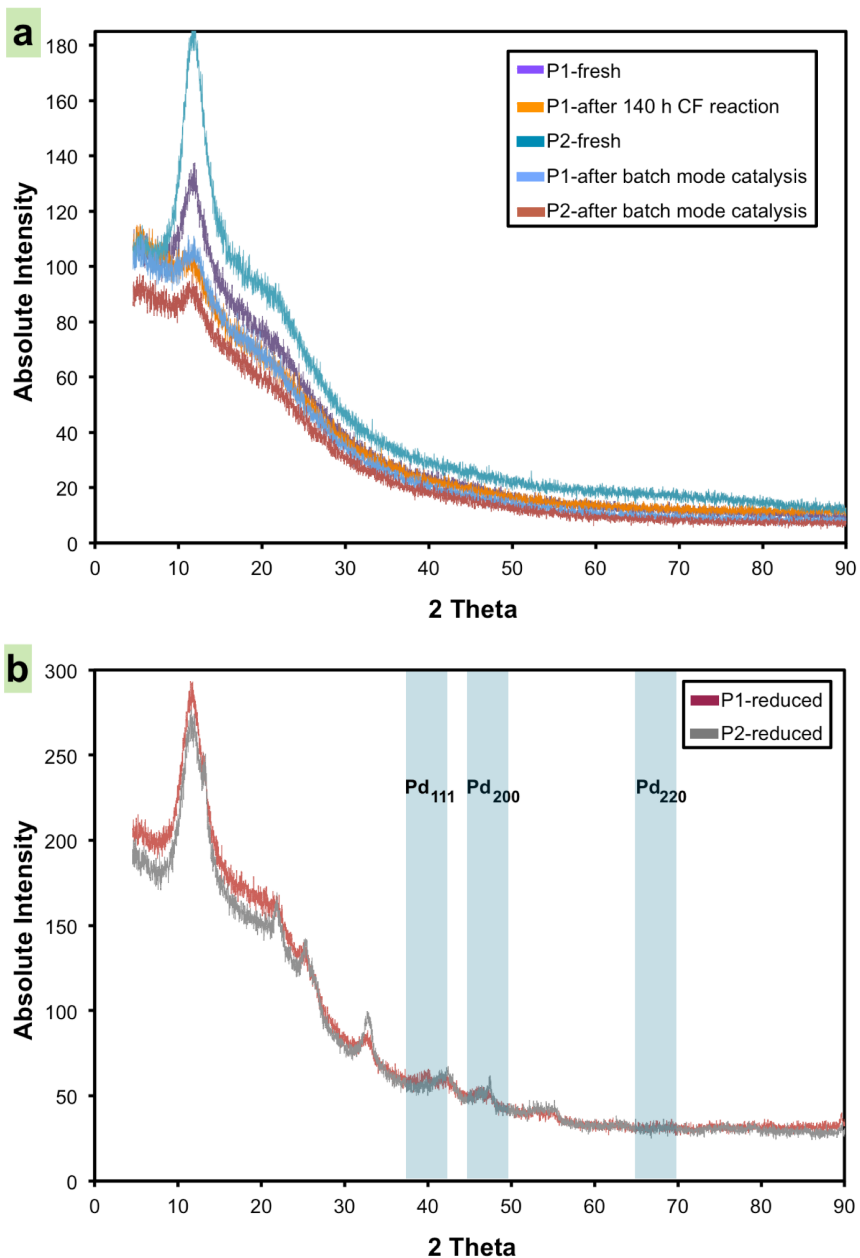
Figure S1. **(a)** XRD patterns of polymers before and after catalysis reactions (in batch and continuous flow mode), **(b)** XRD patterns of polymers **P1** and **P2** after treatment with ascorbic acid, the spectra show the absolute intensities (a.i.).

6. Scanning electron microscopy (SEM)

The characterization was carried out using an SEM LEO 1560 (Zeiss, Oberkochen, Germany) operated at 10 kV. To avoid charging the samples were coated with a 10 nm Pt coating prior to SEM imaging.
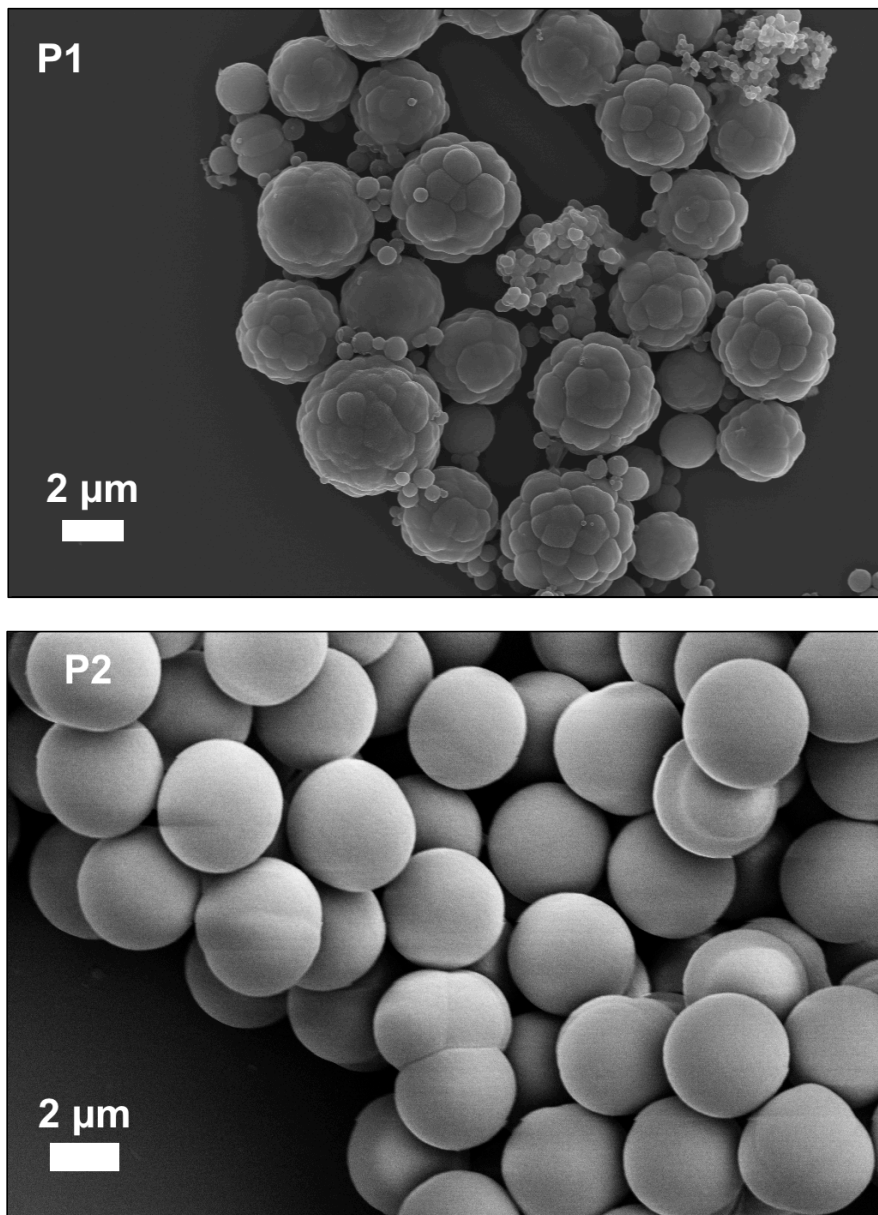
Figure S2. (P1) and **(P2)** SEM images of polymers **P1** and **P2,** respectively.

7. Thermogravimetric analysis (TGA) measurements

The thermal stability of the polymers was investigated by using a Q500 analyser (TA Instruments). Before collecting the data, the polymers were dried under vacuum to remove the washing solvents residues. The first heating scan was from 25-500 °C under N_2 and the second heating scan was from 500-600 °C under air, the heating rates were 10 °C/min.
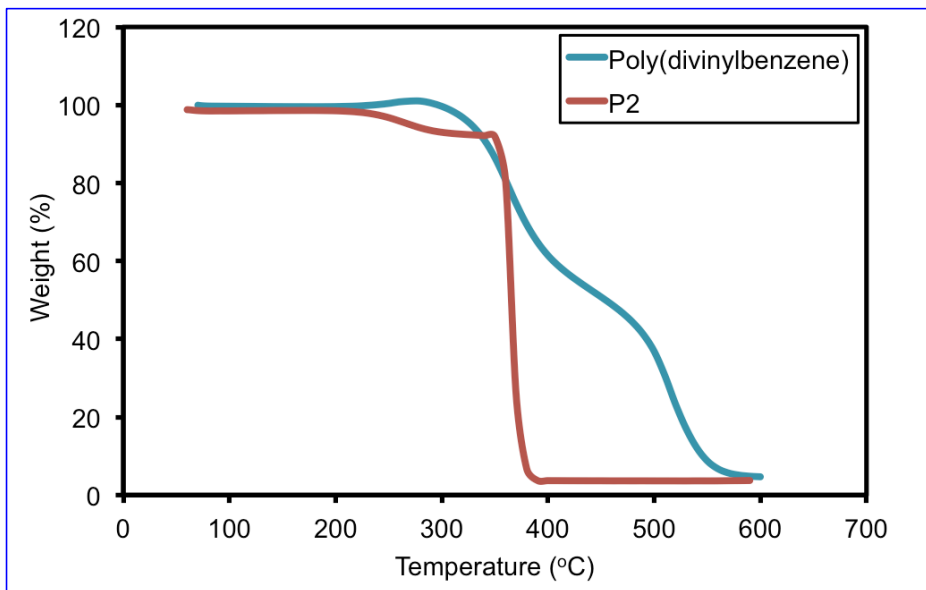
Figure S3. TGA curves of polymer **P2** and poly(divinylbenzene).

8. Solid state nuclear magnetic resonance (SS-NMR) measurements

Magic angle spinning (MAS) experiments were carried out using a Bruker Avance II 500 instrument at 296 K and different mass spinning frequencies.
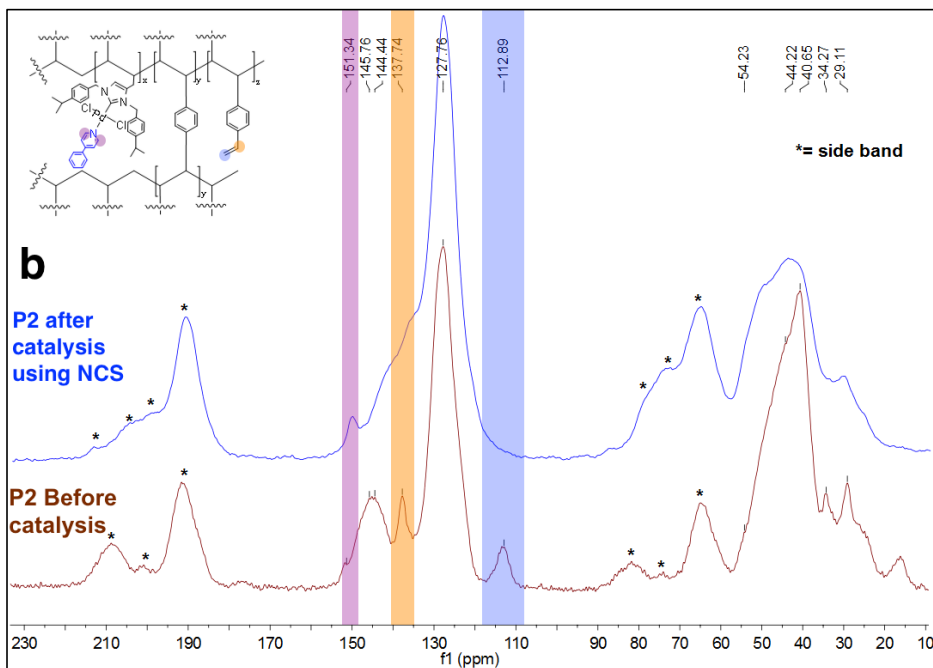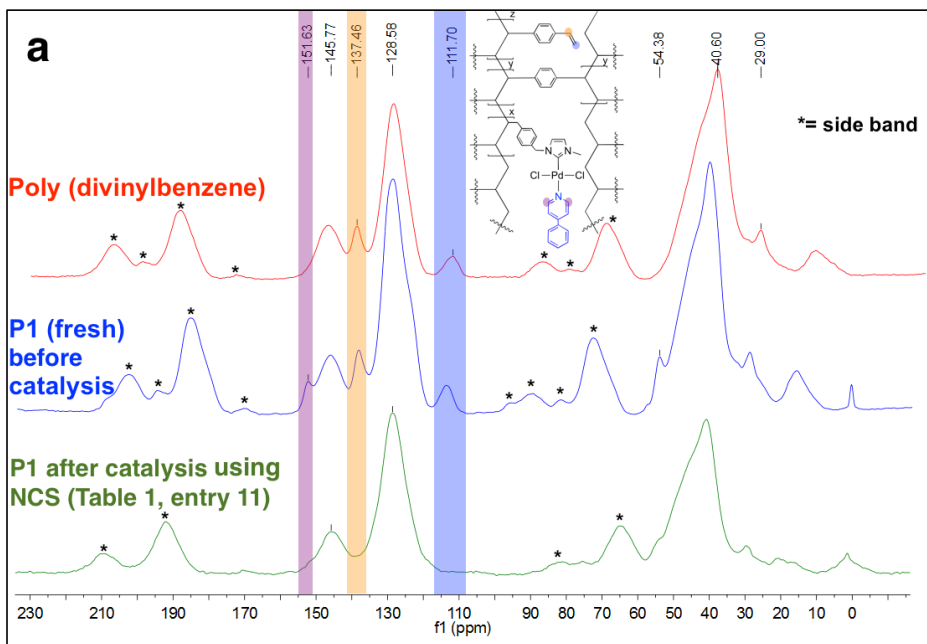
Figure S4. ^{13}C CP-MAS NMR spectra of (a) poly(divinylbenzene) and **P1** before and after catalysis, (b) polymer **P2** before and after catalysis. Side bands are marked with asterisks.
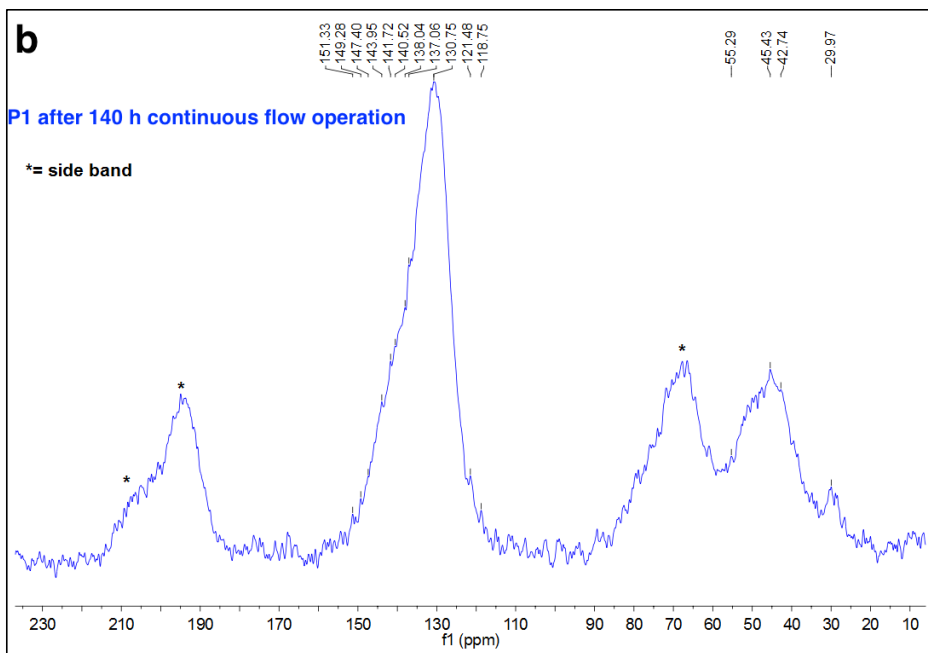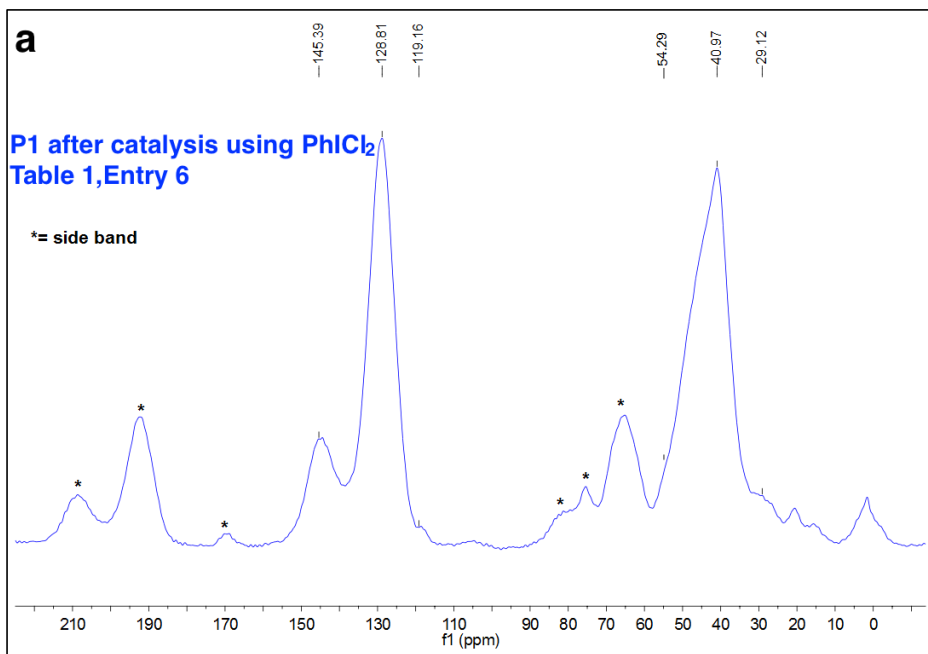
Figure S5. ^{13}C CP-MAS NMR spectra of **P1** after **(a)** catalysis with PhICl$_2$, **(b)** 140 h continuous flow reaction. Side bands are marked with asterisks.

9. High-resolution transmission electron microscopy (HRTEM) analysis

Polymers **P1** and **P2** were sectioned to thin slices by using Agar 100 as an embedding resin. Agar 100 (20 ml), hardener DDSA (16 ml), hardener MNA (8 ml), and accelerator BDMA (2 ml) were mixed all together at room temperature. The polymer was transferred to a dry conical mold followed by transferring the embedding medium, all components were warmed in an oven at 60 °C for 24 h. After the blocks had returned to room temperature, the blocks were trimmed using a diamond knife. The slices of the polymers were imaged using a JEOL 3000F transmission electron microscope (field emission gun, operated at 300 kV) with a point resolution of 0.17 nm. The instrument contained also an Energy-dispersive x-ray spectroscopy (EDX) system from Oxford Instrument with a silicon drift detector (SDD). On areas of interest as well as the whole images, fast fourier transform analysis was performed to detect peaks in the reciprocal plane corresponding to the lattice distances in the images, in order to search for any existence of metallic Pd in the sample.

10. X-ray photoelectron spectroscopy (XPS)

The measurements were carried out at the XPS end station of the HIPPIE beamline of the MAX IV Laboratory in Lund, Sweden. The analysis chamber is equipped with a SCIENTA SES-200 hemispherical electron energy analyser and a separate preparation chamber, which is equipped with surface analysis and preparation tools. The presented data were collected using a SCIENTA SAX100 Al Kα X-ray anode combined with a VG SCIENTA XM780 monochromator (photon energy 1486.7). The anode was operated at 10 kV electron acceleration voltage and 25 mA emission current. The experiment was performed at a pressure lower than 10^{-9} mbar. Single crystal samples were dissolved and polymer samples were dispersed in dichloromethane and then the samples were dropped onto the highly oriented pyrolytic graphite HOPG surface. All spectra were energy calibrated with respect to the C 1s core level of graphite of HOPG at 284.42 eV.[8] No signs of sample charging were detected: all lines could be reproduced reliably at the same energy. In particular, the C 1s line was always found at the same binding energy. Background removal was done by using a Shirley or low-degree polynomial background in the case of the Pd 3d spectra and a Shirley background in the case of the Cl 2p spectra.

For N 1s spectra a polynomial background removal was applied. Curve fitting of the Cl 2p and N 1s spectra was carried out using the Igor Pro software package of Wavemetrics, Inc. using symmetric Voigt lineshapes. The spin-orbit split components in the Cl 2p spectra were restrained to have a 1:2 area ratio between the Cl $2p_{1/2}$ and Cl $2p_{3/2}$ peaks.

The molecular sieves that were used to keep the catalyst in place in the reactor contain Al. Al has a KLL Auger peak with a kinetic energy of ~1150 eV, which appears in the XP spectra at the same binding energy as the Pd 3d core level. This causes the spectrum to have a high and shaped background. In order to be able to remove this background related to the molecular sieves, we measured an Auger spectrum on the clean molecular sieve material (spectrum in red colour in Figure S13). A fourth degree polynomial was fitted to the curve and then re-normalized to match the background of the spectrum measured on the **P1** sample after catalysis (black line). Subtraction of the so-obtained background led to the spectrum displayed in Figure 5d. We refrained from subtracting the Auger background spectrum itself from the Pd 3d spectrum since the noise of the resulting spectrum would have been very large. The here chosen method is valid due to the absence of narrow features in the Auger spectrum.
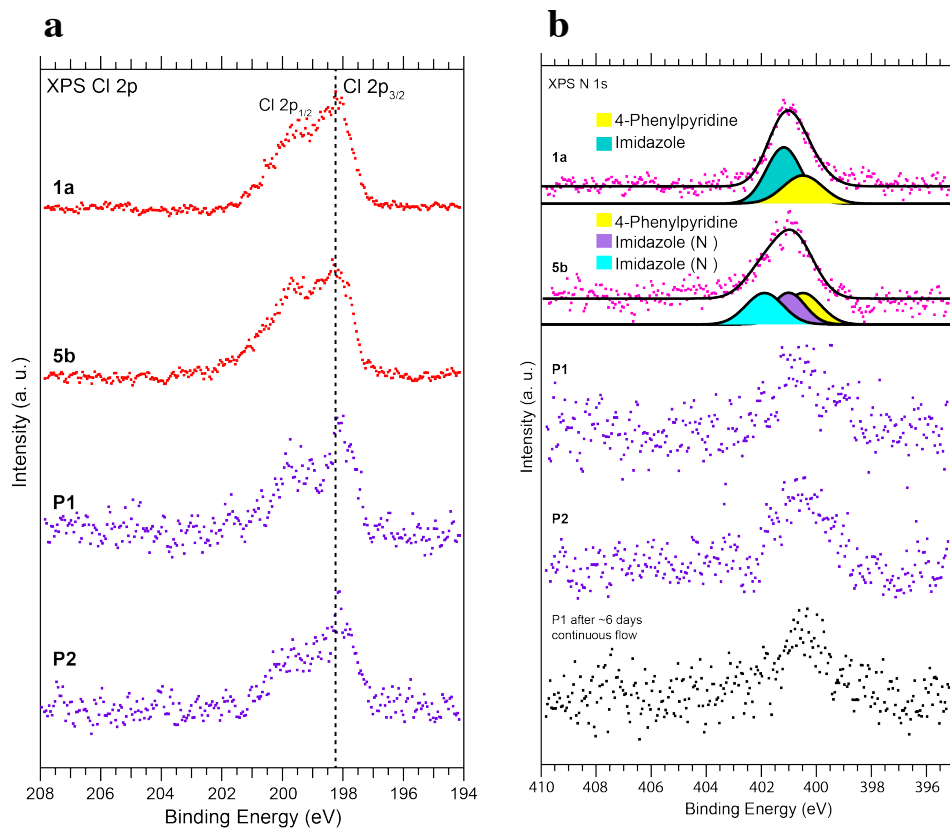
Figure S6. **a)** Cl 2p XP spectra of monomers **1a** and **5b** and fresh polymers **P1** and **P2**. **b)** N 1s XP spectra of monomers **1a** and **5b**, fresh polymers **P1** and **P2** and of polymer **P1** after ~ 6 days continuous flow.

11. Surface area analysis

Krypton sorption isotherms were obtained by using a Micromeritics 3Flex surface characterization analyser. All samples were degassed at 368 K for 12 h prior to the analysis. BET surface area of **P1** and **P2** were 1.8 and 3.0 m^2/g respectively.

12. Chromatography and mass analysis

Gas chromatography (GC)

The analyses were done using a Hewlett-Packard 5890 II instrument with a flame ionization detector (FID) and a capillary column (CP-Sil 19CB 14% cyanopropyl-

phenyl/86% dimethylpolysiloxane, 0.2 μm, 0.2 mm, 25 m) with decane as an internal standard. The retention times of different compounds in the gas chromatogram were identified using commercially available and synthesized pure compounds.

High resolution mass spectroscopy (HRMS)

The measurements were done by direct infusion of samples dissolved in methanol. A Waters XEVO-G2 QTOF equipped with electrospray ionization, run in positive mode, was used.

13. Procedure for catalyst packing and experiments under continuous flow

The reactor consisted of steel tubing (150 mm length) with an inner diameter of approximately 7 mm (3/8" outer diameter); attached to an HPLC-pump that feeds the premixed and continuously stirred reactants solution into the reactor. At each end of the reactor, filters are mounted to keep the catalyst in the tube. Molecular sieves were added at the bottom of the reactor as it is depicted in Figure 6. Pressure in the reactor was controlled using a needle valve after the reactor. The catalyst bed, including the molecular sieves, has enough restriction to increase the pressure at the reactor inlet to 4-5 bar(g), (which is presumably the same pressure over the catalyst bed), with 0 bar(g) at the outlet during normal operation. The reactor is externally heated by means of an electrically heated mantle. The temperature was controlled to maintain the desired outlet temperature out of the reactor.

Catalyst Packing

Prior to running experiments, 0.25 g of the molecular sieves (3 Å, powder) is added to the reactor followed by pumping acetonitrile for a few hours to allow the molecular sieves time to settle in the reactor. After washing with solvents, P1 catalyst (0.306 g, 10 mol%) was added to the reactor on top of the molecular sieves followed by additional washing

Experimental procedure

N-chlorosuccinimide (9.555 g, 71.5 mmol), benzo[h]quinolone (5.5758 g, 31.11 mmol) and decane (3.85 ml) as internal standard in 539 ml of acetonitrile were stirred during the whole 140 h run. Samples were continuously collected every hour by an auto sampler attached to the reactor outlet. Flow rate was almost consistent at 60 μl/min or 3.6 ml/hour and pressure remained constant at 4-5 bar(g) during the 140 hour run. Temperature was controlled to keep 100 °C at the reactor outlet during the experiment.
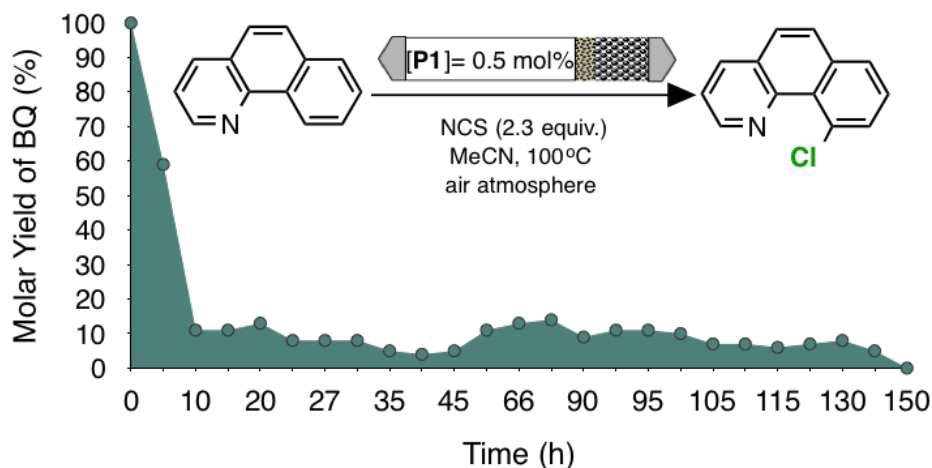
Figure S7. Molar Yield of benzo[*h*]quinoline **2** (BQ) vs. time under flow conditions, Pd loading is 5.8 wt%, yield and selectivity were determined by GC using a calibration curve based on decane as an internal standard.

14. General method for catalysis under batch conditions

In a sealed GC vial, a solution of pyridine derivative (1 equiv.), halogenated or oxidant reagent (2.3 equiv.) and **P1** or **P2** (5 mol% proportion to the amount of the halogenated reagent or oxidant) in AcOH:Ac$_2$O (9:1) or MeCN was stirred at 100 °C using a heating block for 24h. At the end of the reaction the vessel was cooled to room temperature, and the catalyst was separated by centrifugation. The solvent was removed by rotovap, the crude product was dissolved in CH$_2$Cl$_2$, filtered through a pad of silica and washed with a 50/50 mixture of n-hexane/ethyl acetate 25 ml. The

filtrate was concentrated and the residue subjected to thin layer chromatography on silica gel with the eluents.

15. Bromination of benzo[h]quinoline 2

Optimization the reaction conditions of bromination of benzo[h]quinoline **2** was performed using **P1** as a catalyst. As shown in Table S2, initial experiments were run using *N*-iodosuccinimide 2.3 equiv. (0.25 M] as an oxidant and MeCN as a solvent at different temperatures. Multiple products were formed in 99% conversion, when the reaction temperature raised up to 80-100 °C (Table S2, entries 1 and 2). Decreasing the temperature to 50 °C gave no conversion, while switching to more acidic solvent yielding traces of brominated products (Table S2, entries 3 and 4). Attempt to decrease the equivalents of the oxidant (to avoid over bromination) and increasing the temperature slightly up to 60 °C, resulted in 8% conversion to **2-Br** and **2-Br$_2$** in 66:34 regioselectivity respectively (Table S2, entry 5). Interestingly, increasing the concentration of the oxidant up to 0.4 M offered 36% conversion, however the conversion raised slightly upon running the experiment at 72 h (Table S2, entries 6 and 7). Finally, a good improvement on the conversion at mild reaction conditions was rfound, especially when the amount of the oxidant duplicated up to 2.3 equiv. and the concentration kept at 0.4 M (Table S2, entry 8). Repeating the same experiment under the same reaction conditions but without catalyst showed only trace conversion according to GC analysis (Table S2, entry 9).

Table S2. Optimization of C-H bromination and iodination of benzo[*h*]quinoline using **P1** as the catalyst
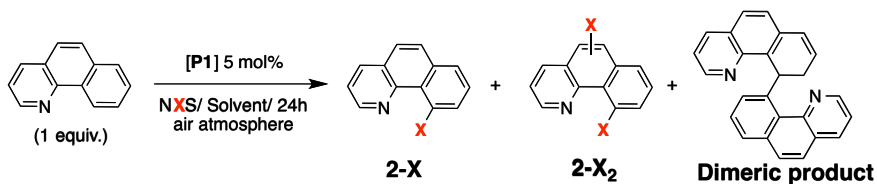
Entry	NXS conc. [M]	X	Temp. (°C)	Solvent	Conversion[b] (%)	Selectivity (%)		
						2-X	2-X₂	D.P.
1	0.25[c]	Br	100	MeCN	99	Multiple Products		
2	0.25[c]	Br	80	MeCN	99	Multiple Products		
3	0.25[c]	Br	50	MeCN	No conversion	-	-	-
4	0.25[c]	Br	50	ᴳAcOH	Traces	-	-	-
5	0.25[d]	Br	60	MeCN	8	66	34	0
6	0.4[d]	Br	60	MeCN	36	67	33	0
7	0.4[d,e]	Br	60	MeCN	39	66	34	0
8	0.4[c]	Br	60	MeCN	68	67	33	0
9[a]	0.4[c]	Br	60	MeCN	Traces	Multiple Products		
10	0.25[c]	I	50	MeCN	No conversion	-	-	-
11	0.25[c]	I	100	MeCN	No conversion	-	-	-
12	0.16[c]	I	100	ᴳAcOH	No conversion	-	-	-
13	0.4[c]	I	70	ᴳAcOH	No conversion	-	-	-

[a]Without catalyst. [b]Conversion and selectivity were determined by GC using a calibration curve based on decane as an internal standard. [c][equiv.] = 2.3, [d][equiv.] = 1.1, [e]Reaction time= 72 h .

Table S3. Optimization of C-H bromination and iodination of 2-phenylpyridine using **P1** as the catalyst.
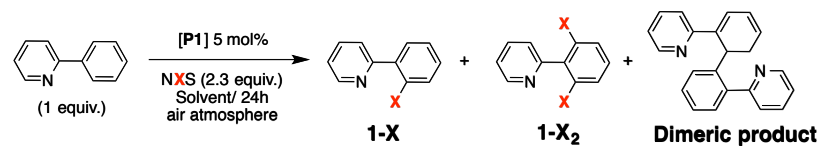
Entry	X[c]	Temp. (°C)	Solvent	Yield (%)[b]	Selectivity (%)		
					1-X	1-X$_2$	D.P.
1[a]	Br	60	[G]AcOH	Traces	-	-	-
2[a]	I	60	[G]AcOH	No conversion	-	-	-
3	Br	60	[G]AcOH	40	100	0	0
4	Br	60	[G]AcOH:Ac$_2$O[d]	25	100	0	0
5	Br	75	[G]AcOH	52	71	29	0
6	I	60	[G]AcOH	76	100	0	0
7	I	60	[G]AcOH:Ac$_2$O[d]	36	100	0	0
8	I	60	MeCN	No conversion	-	-	-
9	I	70	[G]AcOH	49	76	24	0
10	I[e]	60	[G]AcOH	97	100	0	0
11	I[f,g]	60	[G]AcOH	92	100	0	0

[a]Without catalyst. [b]Isolated Yield, [c][NXS] = 0.4 M, [d]Solvent ratio= 9:1. [e]2.3 additional equiv. of NIS was added to reaction mixture after eight hours. [f]2.3 additional equiv. of NIS was added to reaction mixture after ten hours. [g]Catalysis performed with **P2** catalyst.

16. Catalyst Recycling

Iodination reaction was chosen as a model reaction to carry out the recyclability test for **P1** and **P2** under the same reaction conditions as described in Table 6a. The reaction mixture was centrifuged after it had reached room temperature. The solids were washed with a 4-phenylpyridine/CH$_2$Cl$_2$ solution (1 x 5mL) and MeCN (3 x 10 mL), dried, and reused immediately for the following run. Using these conditions, the time profile study was performed at designated reaction times (0.5, 1, 4, 6, 8, 10, 12, 16, 20, and 24) h.

17. Hot filtration experiment

The iodination reaction was carried out under identical reaction conditions as described in Table 6a. After 5h (32% yield), and 2h (15% yield), **P1** and **P2** were filtered off respectively at the reaction temperature (60 °C) and the catalyst free filtrates were allowed to stir under identical reaction conditions. No further iodination of 2-phenylpyridine, according to the GC analysis of the products after 8 h, 20 h, and 24 h.

18. Computational details

General information

Calculations were performed in ORCA 4.0[9] interfaced to NBO6[10,11]. No solvation effects were taken into account. Split-RI-J approximation was applied to GGA DFT functionals in order to speed up calculations.[12] In case hybrid DFT functionals RIJCOSX[13] approximation was used. In both cases default auxiliary basis set Def2/J was used[14], in the cases it wasn't available, AutoAux feature of ORCA was employed.[15] DIIS/KDIIS in conjugation with SOSCF technique were employed in order to speed up SCF convergence.[16–18]

Geometry optimization

Geometry optimization was performed in redundant internal coordinates, using Almoef's initial Hessian and BFGS update method. Default criteria for optimization were tightened: Energy Change tolerance 1.0000e-06 Eh, Max. Gradient tolerance 1.0000e-04 Eh/bohr, RMS Gradient tolerance 3.0000e-05 Eh/bohr, Max. Displacement tolerance 1.0000e-03 bohr, RMS Displacement tolerance 6.0000e-04 bohr. SCF convergence criteria were tightened as well: Energy change tolerance 1.0000e-08, MAX-Density change tolerance 1.0000e-07, RMS-Density change tolerance 5.0000e-09, Orbital Gradient tolerance 1.0000e-05, Orbital Rotation Tolerance 1.0000e-05. Integration grid was tightened to GRID5 and no final grid was used.

The following basis sets (BS1) were used for geometry optimization: for Pd Def2–TZVP and corresponding core potential Def2–SD,[19] for atoms directly bonded to Pd (C^{NHC}, 2Cl, N^{Pyr}) Def2–TZVP basis set, and for the rest of atoms Def2–SVP.[20]

A few DFT functionals were tested for geometry optimization: B97–D3BJ, revPBE, and B3LYP. All of them were used in conjugation with Grimme's empirical dispersion correction D3 and BJ damping, in the case of revPBE and B3LYP three body term (ABC) was also taken into account.[21,22] All employed methods gave the same geometry of the test structure, thus B97–D3BJ functional was chosen as the most cost effective and in the meantime accurate method, which is in line with the benchmark data, obtained by Grimme et all., where this functional was found to be the most accurate among all pure GGA DFT functionals.[23]

The nature of located stationary points was verified by frequencies calculations, no imaginary frequencies were obtained. Quasi-RRHO approach was used for computing entropic contributions.[24]

Wave function analyses

In order to obtain accurate wave function for further population analyses, scalar relativistic all-electron calculations in the framework of Douglas-Kroll-Hess method of the second order (DKH2) were performed on a top of obtained geometries, and Picture-Change Effect was taken into account. Accurate integration grid was used (GRID7) with no final grid, also radial grid on Pd atom was tightened (SpecialGridIntAcc 10). Very accurate SCF convergence criteria (EXTREMESCF) were used as well. In the case of PBE0, more accurate COSX grid was employed (GRIDX7 NOFINALGRIDX). Following basis sets (BS2) were used: old-DKH-TZVP for Pd, DKH-def2-TZVP for non-hydrogen atoms, and DKH-def2-SVP for hydrogens. Auxiliary basis sets were generated by employing AutoAux feature. Calculations were performed by using two different DFT functionals: revPBE (pure GGA) and PBE0 (hybrid GGA).

Description of the results

For the model of complex **5b**, two conformers were obtained, which were compared to the model molecule of **1a**, as well as an analog of conformer 2, in order to clarify the role of the vinylic moiety (Figure S8).
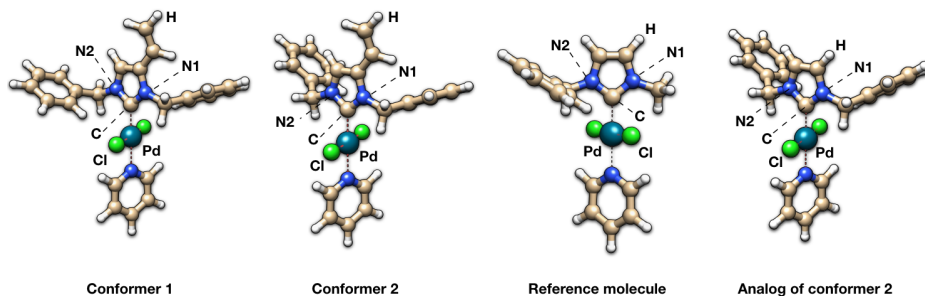

Figure S8. Structures, used in calculations.

Differences in Gibbs Free energies of both conformers (computed in vacuum at 298.15 K) are very small. Also, they are similar for two different methods. For B97–D3BJ/BS1 conformer 2 is less stable than conformer 1 with 0.42 kcal/mol. For

DKH2–PBE0–D3BJ(ABC)/BS2//B97–D3BJ/BS1 conformer 2 is less stable than conformer 1 with 0.45 kcal/mol. Corresponding Boltzmann populations confirm coexistence of both conformers (Figure S9).

Obtained results suggest, that both conformers should be taken into account for further analyses.
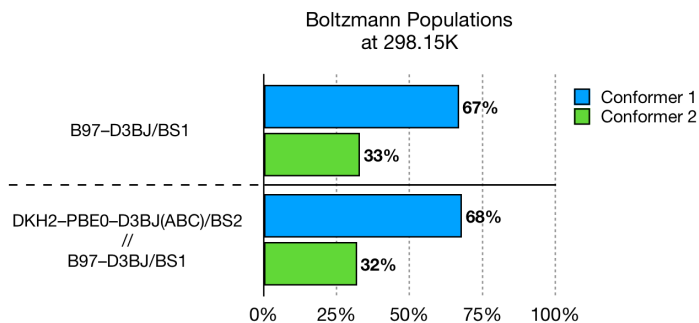
Figure S9. Boltzmann Populations of two conformers of 5b model system.

Many schemes for obtaining charges are available and this circumstance brings some ambiguities into calculations and eventually into interpretation of the obtained results. In order to get consistent results we compared a few different charge definitions: charges based on Natural Population Analysis (NPA)[25], Charges from Electrostatic Potentials using a Grid-based method (CHELPG)[26], Atomic Dipole Corrected Hirshfeld atomic charges (ADCH)[27], original Becke atomic charges[28] with applied atomic dipole correction (ADCB; correction is very similar to the one in ADCH). Calculations were performed with two different methods DKH2–revPBE/BS2 and DKH2–PBE0/BS2.

Noticeable differences in charges of the two nitrogen atoms of the NHC moiety clearly depict differences in chemical environment of at least one of two conformers of **5b** model system. These differences are greater, than differences in the case of model of **1a** (Figure S10). Results of NPA and CHELPG are somewhat independent with respect to the choice of DFT method. In contrast to that, ADCH and ADCB are much more sensitive, sometimes even changing the sign of $\Delta q(N1–N2)$, but, still showing the difference between the two nitrogen atoms. Also, by comparison of conformer 2 and its analog, which has a hydrogen atom instead of a vinylic moiety, we can conclude that such a conformation already creates a difference in the chemical environment, and the vinylic group increases it further.
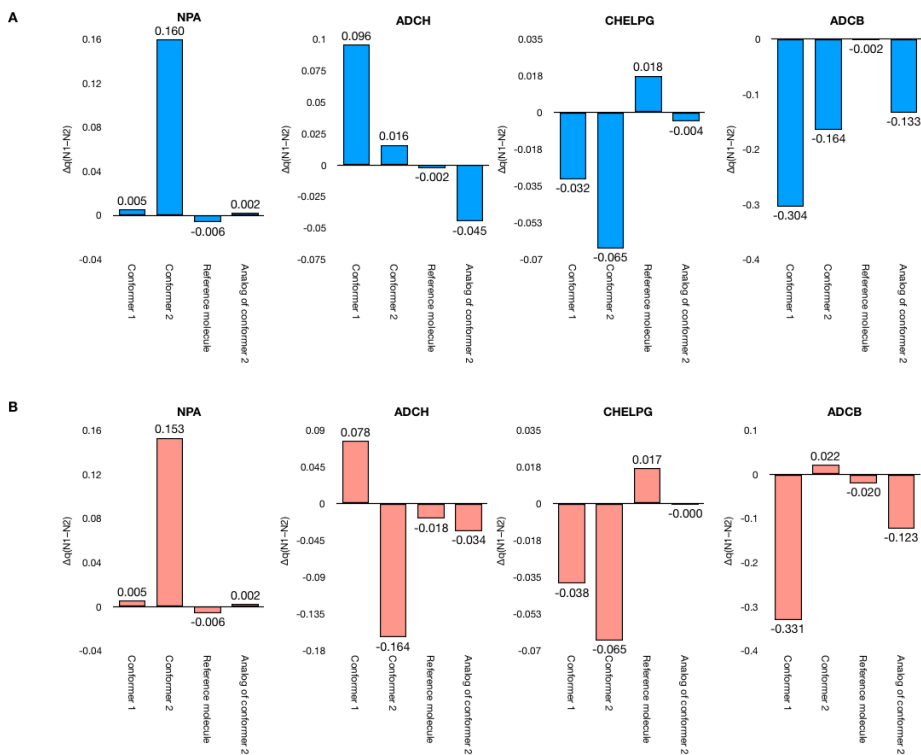
Figure S10. A). Differences in charges between N1 and N2 calculated at DKH2–revPBE/BS2. B). Differences in charges between N1 and N2 calculated at DKH2–PBE0/BS2.

Original charge values are summarized on Figure S11 and Figure S12.

Computed charges
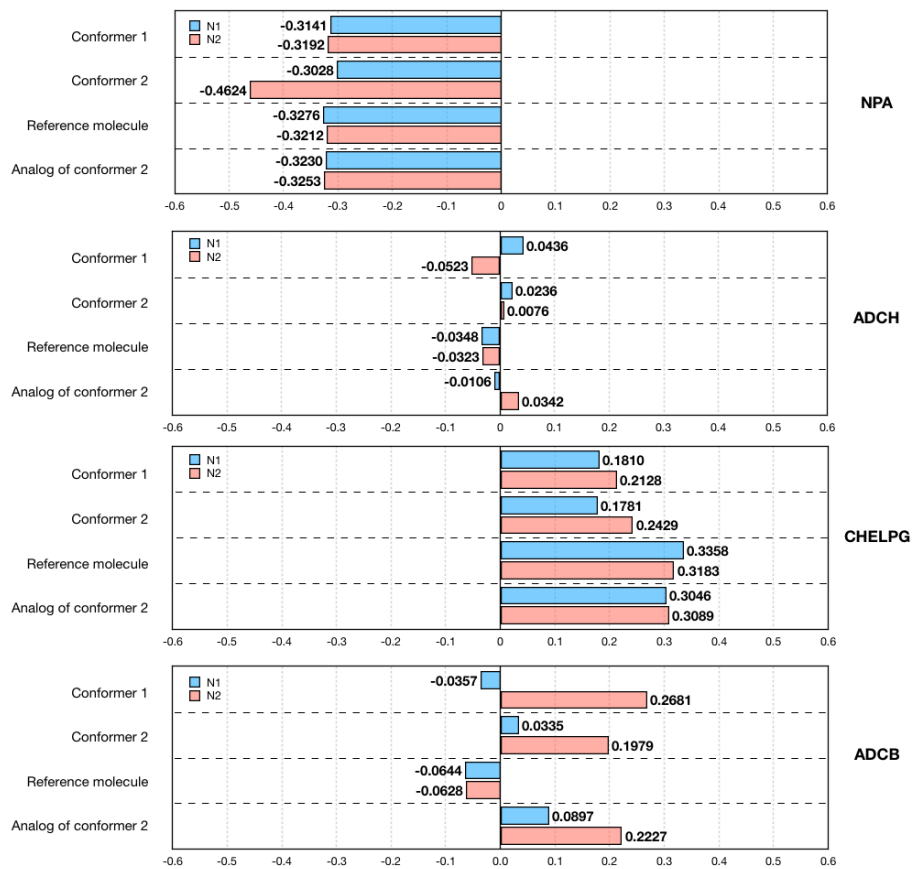
Figure S11. Charges computed using DKH2–revPBE/BS2 level of theory

Figure S12. Charges computed DKH2–PBE0/BS2 level of theory.
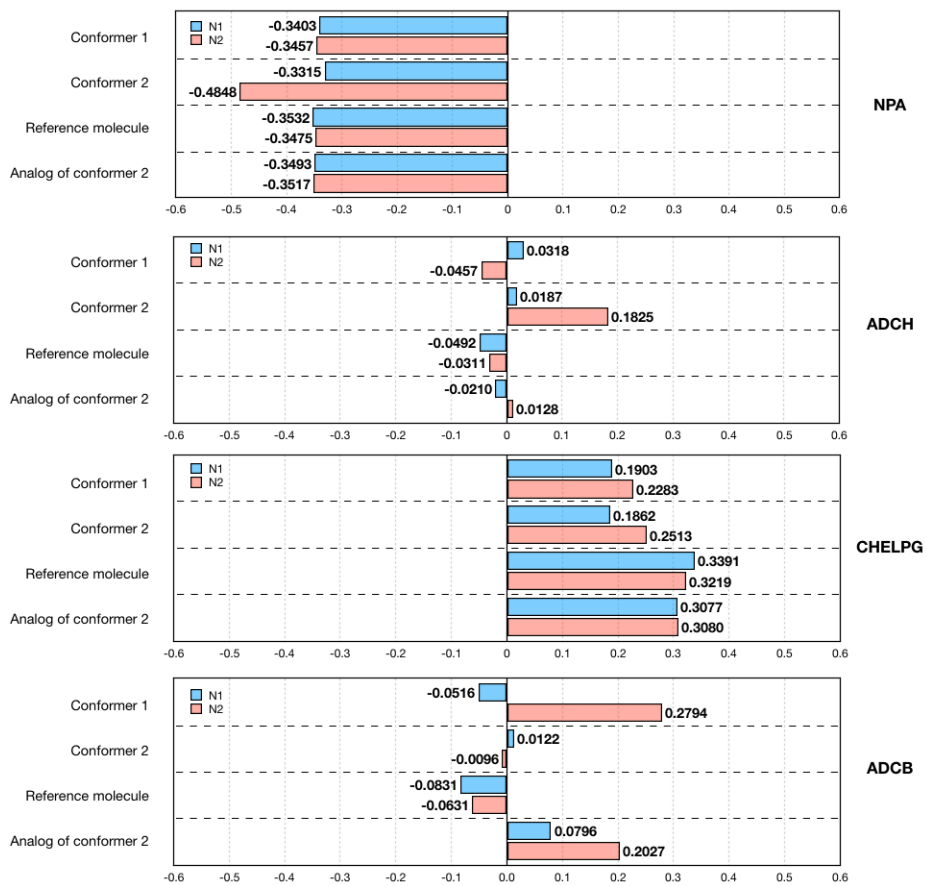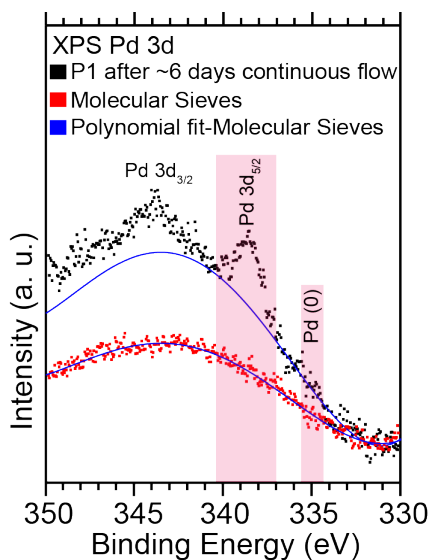
Figure S13. Fitting procedure on XP spectrum of Pd 3d core level after ~6 days continuous flow.

19. Experimental details and spectroscopic characterizations of synthesized products

2-(2-Chlorophenyl)pyridine **1-Cl**
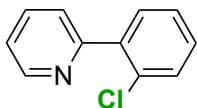
1-Cl was obtained according to the general procedure for catalysis, the crude product was subjected to thin layer chromatography on silica gel with 25% EtOAc/ 75% n-hexane. The product was isolated as a clear oil (36.2 mg, 90%). ^{1}H NMR (400 MHz, CDCl$_3$): δ 8.72 (d, J = 3.9 Hz, 1H), 7.76 (td, J = 7.7, 1.8 Hz, 1H), 7.65 (d, J = 7.9 Hz, 1H), 7.60 (dd, J = 7.0, 2.4 Hz, 1H), 7.48 (dd, J = 7.6, 1.6 Hz, 1H), 7.41-7.31 (m, 2H), 7.29 (ddd, J = 7.5, 4.9, 1.2 Hz, 1H). ^{13}C NMR (400 MHz, CDCl$_3$): δ 157.04, 149.71, 139.35, 135.97, 132.28, 131.68, 130.24, 129.71, 127.14, 125.00, 122.53. HRMS (ESI): calcd. For C$_{11}$H$_8$ClN [M+H]$^+$ 190.0424; found 190.0424.

10-Chlorobenzo[h]quinoline **2-Cl**
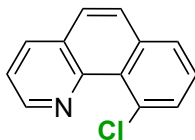
2-Cl was obtained according to the general procedure for catalysis, the crude product was subjected to thin layer chromatography on silica gel with 40% DCM/ 60% n-hexane. The product was isolated as a yellow solid (0.035 g, 78%). ^{1}H NMR (400 MHz, CDCl$_3$) δ 9.12 (dd, J = 4.3, 1.9 Hz, 1H), 8.18 (dd, J = 8.0, 1.9 Hz, 1H), 7.87-7.82 (m, 2H), 7.79 (d, J = 8.8 Hz, 1H), 7.70 (dd, J = 34.8, 8.8 Hz, 1H), 7.56 (ddd, J = 7.8, 5.9, 1.6 Hz, 2H). ^{13}C NMR (400 MHz, CDCl$_3$): δ 147.8, 146.6, 136.4, 135.8, 132.5, 131.7, 128.34, 128.30, 127.8, 127.76, 127.71, 126.7, 121.8. HRMS (ESI): calcd. For C$_{13}$H$_8$ClN [M+H]$^+$ 214.0424; found 214.0430.

5,10-Dichlorobenzo[h]quinoline **2-Cl$_2$**

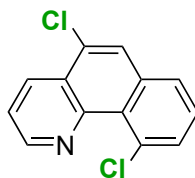**2-Cl$_2$** was obtained according to the general procedure for catalysis, the crude product was subjected to thin layer chromatography on silica gel with 40% DCM/ 60% n-hexane. The product was isolated as a yellow solid (0.0255 g, 57%). ^{1}H NMR (400 MHz, CDCl$_3$) δ 9.16 (dd, J = 4.3, 1.8 Hz, 1H), 8.69 (dd, J = 8.3, 1.8 Hz, 1H), 7.92 (s, 1H), 7.83 (dd, J = 7.7, 1.3 Hz, 1H), 7.77 (dd, J = 7.9, 1.0 Hz, 1H), 7.68 (dd, J = 8.3, 4.3 Hz, 1H), 7.57 (t, J = 7.8 Hz, 1H). ^{13}C NMR (400 MHz, CDCl$_3$): δ 148.0, 146.2, 135.8, 133.7, 132.7, 132.1, 129.9, 128.7, 127.8, 127.2, 126.2, 125.9, 122.4. HRMS (ESI): calcd. For C$_{13}$H$_7$Cl$_2$N [M+H]$^+$ 248.0034; found 248.0032.

2-(2-chloro-4-methylphenyl)pyridine **3-Cl**

3-Cl was obtained according to the general procedure for catalysis, the crude product was subjected to thin layer chromatography on silica gel with 60% petroleum ether/ 30% diethyl ether. The product was isolated as a yellow oil (0.0304 g, 68%). ^{1}H NMR (400 MHz, CDCl$_3$) δ 8.71 (d, J = 4.2 Hz, 1H), 7.74 (td, J = 7.7 Hz, 1H), 7.64 (dd, J = 7.9, 0.7 Hz, 1H), 7.49 (d, J = 7.8 Hz, 1H), 7.30 (s, 1H), 7.29-7.22 (m, 1H), 7.17 (d, J = 7.8 Hz, 1H), 2.38 (s, 3H). ^{13}C NMR (400 MHz, CDCl$_3$): δ 157.0, 149.6, 140.0, 136.4, 135.9, 131.8, 131.4, 130.65, 127.9, 125.0, 122.3, 21.0. HRMS (ESI): calcd. For C$_{12}$H$_{10}$NCl [M+H]$^+$ 204.0580; found 204.0579.

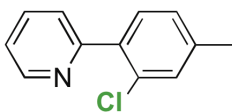*2-(3-chloro-4-methoxyphenyl)pyridine* **4-Cl**

4-Cl was obtained according to the general procedure for catalysis, the crude product was subjected to thin layer chromatography on silica gel with 60% petroleum ether/ 30% diethyl ether. The product was isolated as a white solid (0.0316 g, 67%). 1H NMR (400 MHz, CDCl$_3$) δ 8.66 (dd, J = 4.9, 0.8 Hz, 1H), 8.04 (d, J = 2.3 Hz, 1H), 7.92 (dd, J = 8.6, 2.3 Hz, 1H), 7.76 (td, J = 7.7, 1.8 Hz, 1H), 7.67 (dd, J = 8.0, 0.8 Hz, 1H), 7.23 (ddd, J = 7.4, 4.9, 1.0 Hz, 1H), 7.01 (d, J = 8.6 Hz, 1H), 3.94 (s, 3H). ^{13}C NMR (400 MHz, CDCl$_3$): δ 156.04, 155.47, 149.07, 137.66, 132.02, 128.92, 126.59, 123.11, 122.19, 120.27, 112.20, 56.37. HRMS (ESI): calcd. For C$_{12}$H$_{10}$NOCl [M+H]$^+$ 220.0529; found 220.0531.
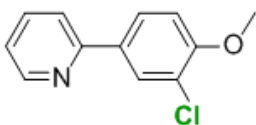
2-(2,5-dichloro-4-methoxyphenyl)pyridine **4-Cl₂b**

4-Cl₂b was obtained according to the general procedure for catalysis, the crude product was subjected to thin layer chromatography on silica gel with 60% petroleum ether/ 30% diethyl ether. The product was isolated as a white solid (0.0069 g, 13%). 1H NMR (400 MHz, CDCl3) δ 8.75 (d, J = 6.7 Hz, 1H), 7.87 (t, J = 7.8 Hz, 1H), 7.72 (d, J = 8.0 Hz, 2H), 7.71 (s, 1H), 7.39 (ddd, J = 7.5, 5.1, 1.0 Hz, 1H), 2.99 (s, 3H). ^{13}C NMR (400 MHz, CDCl₃): δ 156.01, 154.48, 148.28, 137.74, 132.79, 132.75, 131.29, 125.65, 123.06, 121.95, 113.83, 56.73. HRMS (ESI): calcd. For $C_{12}H_9NOCl_2$ [M+H]$^+$ 254.0139; found 254.0140.

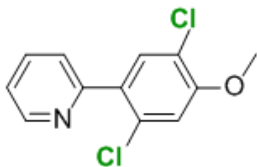*2-(3,5-dichloro-4-methoxyphenyl)pyridine* **4-Cl₂a**

4-Cl₂a was obtained according to the general procedure for catalysis, the crude product was subjected to thin layer chromatography on silica gel with 60% petroleum ether/ 30% diethyl ether. The product was isolated as a white solid (0.0051 g , 11%). ^{1}H NMR (400 MHz, CDCl₃) δ 8.89 (d, J = 4.6 Hz, 1H), 8.09 (t, J = 7.8 Hz, 1H), 8.06 (s, 2H), 7.84 (d, J = 8.0 Hz, 1H), 7.64 – 7.52 (m, 1H), 3.97 (s, 3H). ^{13}C NMR (400 MHz, CDCl₃): δ 158.79, 152.55, 152.17, 146.90, 146.79, 141.45, 141.40, 130.66, 128.33, 124.13, 122.61, 77.48, 77.16, 76.84, 61.14. HRMS (ESI): calcd. For $C_{12}H_9NOCl_2$ [M+H]$^+$ 254.0139; found 254.0136.

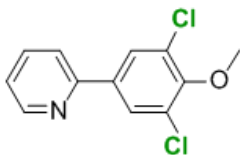*3-chloro-4-(pyridin-2-yl)benzonitrile* **5-Cl**

5-Cl was obtained according to the general procedure for catalysis, the crude product was subjected to thin layer chromatography on silica gel with 74% hexane/ 25% ethyl acetate/ 1% petroleum ether. The product was isolated as a white solid (0.0165 g, 36%). ^{1}H NMR (400 MHz, CDCl$_3$) δ 8.75 (d, J = 4.8 Hz, 1H), 7.88 – 7.78 (m, 2H), 7.75 (d, J = 8.0 Hz, 1H), 7.67 (ddd, J = 11.1, 8.0, 1.2 Hz, 2H), 7.36 (dd, J = 8.6, 4.9 Hz, 1H). ^{13}C NMR (400 MHz, CDCl$_3$): δ 155.08, 150.09, 143.68, 136.32, 133.71, 133.33, 132.57, 130.61, 124.92, 123.48, 117.50, 113.60. HRMS (ESI): calcd. For C$_{12}$H$_7$N$_2$Cl [M+H]$^+$ 215.0376; found 215.0379.

3,5-dichloro-4-(pyridin-2-yl)benzonitrile **5-Cl$_2$**
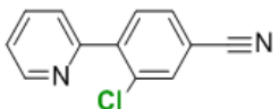

5-Cl$_2$ was obtained according to the general procedure for catalysis, the crude product was subjected to thin layer chromatography on silica gel with 74% hexane/ 25% ethyl acetate/ 1% petroleum ether. The product was isolated as a white solid (g, %). ^{1}H NMR (400 MHz, CDCl$_3$) δ 8.77 (d, J = 4.9 Hz, 1H), 7.86 (td, J = 7.7, 1.7 Hz, 1H), 7.71 (s, 2H), 7.40 (ddd, J = 7.8, 4.8, 1.2 Hz, 1H), 7.33 (d, J = 7.8 Hz, 1H). ^{13}C NMR (400 MHz, CDCl$_3$) δ 153.96, 150.10, 140.09, 136.94, 136.16, 131.51, 124.76, 123.85, 116.31, 114.30.

6-(2-chlorophenyl)nicotinonitrile **6-Cl**

6-Cl was obtained according to the general procedure for catalysis, the crude product was subjected to thin layer chromatography on silica gel with 74% hexane/ 25% ethyl acetate/ 1% petroleum ether. The product was isolated as a white solid (0.0263 g, 57%). ^{1}H NMR (400 MHz, CDCl$_3$) δ 9.00 (d, J = 1.4 Hz, 1H), 8.05 (dd, J = 8.2, 2.2 Hz, 1H), 7.87 (d, J = 7.8 Hz, 1H), 7.66 – 7.62 (m, 1H), 7.53 – 7.50 (m, 1H), 7.44 – 7.40 (m, 2H). ^{13}C NMR (400 MHz, CDCl$_3$): δ 160.13, 152.22, 139.34, 137.27, 132.24, 131.78, 131.06, 130.65, 127.51, 125.16, 116.72, 108.76. HRMS (ESI): calcd. For C$_{12}$H$_7$N$_2$Cl [M+H]$^+$ 215.0376; found 215.0374.

10-Bromobenzo[h]quinoline **1-Br**

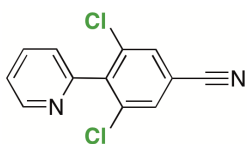
1-Br was obtained according to the general procedure for catalysis, the crude product was subjected to thin layer chromatography on silica gel with 60% hexane/ 40% dichloromethane. The product was isolated as white crystals (g, %). ^{1}H NMR (400 MHz, CDCl$_3$) δ 9.12 (dd, *J* = 4.3, 1.8 Hz, 1H), 8.18 (dt, *J* = 16.9, 8.5 Hz, 1H), 8.11 (dd, *J* = 7.6, 1.2 Hz, 1H), 7.90 (dd, *J* = 7.9, 1.0 Hz, 1H), 7.79 (d, *J* = 8.8 Hz, 1H), 7.72 (d, *J* = 8.8 Hz, 1H), 7.58 (dd, *J* = 8.0, 4.3 Hz, 1H), 7.47 (t, *J* = 7.8 Hz, 1H). ^{13}C NMR (400 MHz, CDCl$_3$): δ 147.18, 135.80, 135.66, 128.53, 128.31, 128.09, 126.70, 122.03. HRMS (ESI): calcd. For C$_{13}$H$_8$BrN [M+H]$^+$ 257.9918; found 257.9918.
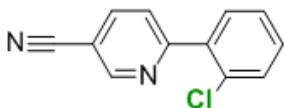
2-(2-Iodophenyl)pyridine **2-I**

1-I was obtained according to the general procedure for catalysis, the crude product was subjected to thin layer chromatography on silica gel with 90% hexane/ 10% ethyl acetate. The product was isolated as a yellow oil (0.04 g, 67%). ^{1}H NMR (400 MHz, CD$_3$CN) δ 8.63 (ddd, *J* = 4.9, 1.7, 0.9 Hz, 1H), 7.97 (dd, *J* = 8.0, 1.1 Hz, 1H), 7.80 (td, *J* = 7.7, 1.8 Hz, 1H), 7.49 – 7.43 (m, 2H), 7.40 (dd, *J* = 7.6, 1.9 Hz, 1H), 7.34 (ddd, *J* = 7.6, 4.9, 1.1 Hz, 1H), 7.12 (ddd, *J* = 7.9, 7.3, 1.9 Hz, 1H). ^{13}C NMR (101 MHz, CD$_3$CN) δ 161.75, 150.03, 146.29, 140.62, 137.21, 131.21, 130.78, 129.34, 125.18, 123.70, 97.16. HRMS (ESI): calcd. For C$_{11}$H$_8$IN [M+H]$^+$ 281.9783; found 281.9780.
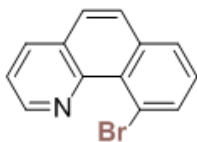
2-(2,6-diiodophenyl)pyridine **2-I$_2$**

1-I$_2$ was obtained according to the general procedure for catalysis, the crude product was subjected to thin layer chromatography on silica gel with 90% hexane/ 10% ethyl acetate. The product was isolated as a yellow oil (7.2 mg, 25%). ^{1}H NMR (400 MHz, CD$_3$CN) δ 8.66 (d, *J* = 4.9 Hz, 1H), 7.97 (d, *J* = 7.9 Hz, 2H), 7.85 (td, *J* = 7.7, 1.8 Hz, 1H), 7.39 (ddd, *J* = 7.6, 4.9, 1.2 Hz, 1H), 7.24 (dt, *J* = 7.8, 1.1 Hz, 1H), 6.81 (t, *J* = 7.9 Hz, 1H). ^{13}C NMR (400 MHz, CD$_3$CN) δ 165.36, 150.09, 149.48, 140.10, 137.72, 132.35, 124.98, 124.43, 97.54. HRMS (ESI): calcd. For C$_{11}$H$_7$I$_2$N [M+H]$^+$ 407.8747; found 407.8746.
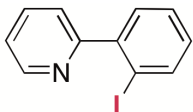
2-(2-bromophenyl)pyridine **2-Br**

1-Br was obtained according to the general procedure for catalysis, the crude product was subjected to thin layer chromatography on silica gel with 90% hexane/ 10% ethyl acetate. The product was isolated as a yellow solid (0.0184 g, 37%). ^{1}H NMR (400 MHz, CDCl$_3$) δ 8.73 (dd, J = 4.9, 0.9 Hz, 1H), 7.79 (td, J = 7.7, 1.8 Hz, 1H), 7.68 (dd, J = 8.0, 1.1 Hz, 1H), 7.62 (d, J = 7.9 Hz, 1H), 7.55 (dd, J = 7.7, 1.7 Hz, 1H), 7.41 (td, J = 7.5, 1.1 Hz, 1H), 7.32 (ddd, J = 7.5, 4.9, 1.1 Hz, 1H), 7.29 – 7.23 (m, 1H). ^{13}C NMR (400 MHz, CDCl$_3$) δ 158.10, 149.11, 140.78, 136.43, 133.44, 131.59, 130.04, 127.71, 125.10, 122.70, 121.87. HRMS (ESI): calcd. For C$_{11}$H$_8$BrN [M+H]$^+$ 233.9917; found 233.9916.
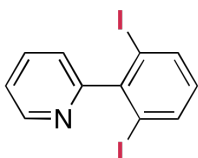
2-(2,6-dibromophenyl)pyridine **2-Br$_2$**

1-Br$_2$ was obtained according to the general procedure for catalysis, the crude product was subjected to thin layer chromatography on silica gel with 90% hexane/ 10% ethyl acetate. The product was isolated as a yellow solid (7.5 mg, 15%). ^{1}H NMR (400 MHz, CDCl$_3$) δ 8.75 (d, J = 4.9 Hz, 1H), 7.82 (td, J = 7.7, 1.8 Hz, 1H), 7.64 (d, J = 8.1 Hz, 2H), 7.35 (ddd, J = 7.6, 4.9, 1.2 Hz, 1H), 7.31 (dt, J = 7.8, 1.1 Hz, 1H), 7.13 (t, J = 8.0 Hz, 1H). ^{13}C NMR (400 MHz, CDCl$_3$) δ 152.82, 149.44, 142.48, 136.54, 131.88, 131.88, 130.62, 124.66, 123.76, 123.06. HRMS (ESI): calcd. For C$_{11}$H$_7$Br$_2$N [M+H]$^+$ 311.9026; found 311.9024.
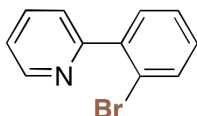
6-(2-Iodophenyl)nicotinonitrile **6-I**
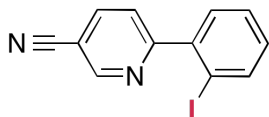
6-I was obtained according to the general procedure for catalysis, the crude product was subjected to thin layer chromatography on silica gel with 74% hexane/ 25% ethyl acetate/ 1% petroleum ether. The product was isolated as a white solid (0.050 g, 76%). ^{1}H NMR (400 MHz, CD$_3$CN) δ 8.95 (dd, J = 2.1, 0.9 Hz, 1H), 8.15 (dd, J = 8.2, 2.2 Hz, 1H), 8.00 (dd, J = 7.9, 1.2 Hz, 1H), 7.67 (dd, J = 8.2, 0.9 Hz, 1H), 7.49 (td, J = 7.5, 1.1 Hz, 1H), 7.42 (dd, J = 7.6, 1.8 Hz, 1H), 7.17 (ddd, J = 8.0, 7.3, 1.9 Hz, 1H). ^{13}C NMR (400 MHz, CD$_3$CN) δ 164.74, 152.97, 144.67, 140.92, 140.87, 131.63, 131.27, 129.54, 125.44, 117.75, 109.51, 96.32. HRMS (ESI): calcd. For C$_{12}$H$_7$IN$_2$ [M+H]$^+$ 306.9732; found 306.9738.
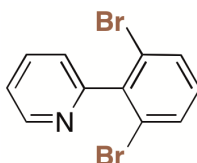
6-(2-bromophenyl)nicotinonitrile **6-Br**
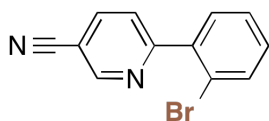
6-Br was obtained according to the general procedure for catalysis, the crude product was subjected to thin layer chromatography on silica gel with 74% hexane/ 25% ethyl acetate/ 1% petroleum ether. The product was isolated as a white solid (0.0404 g, 73%). ^{1}H NMR (400 MHz, CDCl$_3$) δ 8.98 (dd, J = 2.2, 0.9 Hz, 1H), 8.03 (dd, J = 8.2, 2.2 Hz, 1H), 7.79 (dd, J = 8.2, 0.9 Hz, 1H), 7.70 (dd, J = 8.0, 1.2 Hz, 1H), 7.55 (dd, J = 7.7, 1.8 Hz, 1H), 7.45 (td, J = 7.5, 1.2 Hz, 1H), 7.32 (ddd, J = 8.1, 7.4, 1.8 Hz, 1H). ^{13}C NMR (400 MHz, CDCl$_3$) δ 161.66, 152.28, 139.58, 139.09, 133.77, 131.55, 130.96, 127.95, 124.94, 121.50, 116.78, 108.68. HRMS (ESI): calcd. For C$_{12}$H$_7$Br$_2$N$_2$ [M+H]$^+$ 258.9871; found 258.9873.

References:

[1]   Overberger, C. G.; Akami, Y. K. *J. Polym. Sci. Polym. Chem. Ed.* **1978**, 16, 1237.

[2]   Majeed, M. H.; Wendt, O. F. *Acta. Cryst.* **2016**, E72, 534.

[3]   Majeed, M. H.; Shayesteh, P.; Wallenberg, L. R.; Persson, A. R.; Johansson, N.; Ye, L.; Schnadt, J.; Wendt, O. F. *Chem.: Eur. J.* **2017**, 23, 8457.

[4]   Smith, T. W.; Zhao, M.; Yang, F.; Smith, D.; Cebe, P. *Macromolecules* **2013**, 46, 1133.

[5]   Weimar, M.; Costa, R. C.; Lee, F.; Fuchter, M. J. *Org. Lett.,* **2013**, 15, 1706.

[6]   Kalyani, D.; Dick, A. R.; Anani, W. Q.; Sanford, M. S. *Org. Lett.* **2006**, 8, 2523.

[7]   Kalyani, D.; Dick, A. R.; Anani, W. Q.; Sanford, M. S. *Tetrahedron* **2006**, 62, 11483.

[8]   Balasubramanian, T.; Andersen, J. N.; Wallden, L. *Phys. Rev. B*, **2001**, 64, 205420.

[9]   Neese, F. *Wiley Interdiscip. Rev. Comput. Mol. Sci.*, **2017**, 1.

[10] Glendening, E. D.; Landis, C. R.; Weinhold, F. *J. Comput. Chem.*, **2013**, 34, 1429.

[11] Glendening, F. W. E. D.; Badenhoop, J. K.; Reed, A. E.; Carpenter, J. E.; Bohmann, J. A.; Morales, C. M.; Landis, C. R. *Theor. Chem. Institute, Univ. Wisconsin, Madison*.

[12] Neese, F. *J. Comput. Chem.*, **2003**, 24, 1740.

[13] Neese, F.; Wennmohs, F.; Hansen, A.; Becker, U. *Chem. Phys.*, **2009**, 356, 98.

[14] Weigend, F. *Phys. Chem. Chem. Phys.*, **2006**, 8, 1057.

[15] Stoychev, G. L.; Auer, A. A.; Neese, F. *J. Chem. Theory Comput.*, **2017**, 13, 554.

[16] Fischer, T. H.; Almlof, J. *J. Phys. Chem.*, **1992**, 96, 9768.

[17] Neese, F. *Chem. Phys. Lett.*, **2000**, 325, 93.

[18] Kollmar, C. *J. Chem. Phys.*, **1996**, 105, 8204.

[19] Andrae, D.; Häußermann, U.; Dolg, M.; Stoll, H.; Preuß, H. *Theor. Chim. Acta*, **1990**, 77, 123.

[20] Weigend, F.; Ahlrichs R.; Gmbh, F. K. *Phys. Chem. Chem. Phys.*, **2005**, 7, 3297.

[21] Grimme, S.; Ehrlich S.; Goerigk, L. *J. Comput. Chem.*, **2011**, 32, 1456.

[22] Grimme, S.; Antony, J.; Ehrlich S.; Krieg, H. *J. Chem. Phys.*, **2010**, 132, 154104.

[23] Goerigk, L.; Grimme, S. *J. Chem. Theory Comput.*, **2011**, 7, 291.

[24] Grimme, S. *Chem. - A Eur. J.*, **2012**, 18, 9955.

[25] Reed, A. E.; Weinstock, R. B.; Weinhold, F. *J. Chem. Phys.*, **1985**, 83, 735.

[26] Breneman, C. M.; Wiberg, K. B. *J. Comput. Chem.*, **1990**, 11, 361.

[27] LU, T.; CHEN, F. *J. Theor. Comput. Chem.*, **2012**, 11, 163.

[28] Becke, A. D. *J. Chem. Phys.*, **1988**, 88, 2547.

Paper IV

A Pd(II) carbene complex with anthracene side arms for π-stacking on reduced graphene oxide (rGO): activity towards undirected C–H oxygenation of arenes

Maitham H. Majeed,[a]† Payam Shayesteh,[b]† Axel R. Persson,[a,c] L. Reine Wallenberg,[a,c] Joachim Schnadt[b] and Ola F. Wendt*[a]

[a]Centre for Analysis and Synthesis, Department of Chemistry, Lund University, Box 124, SE-221 00 Lund, Sweden

[b]Division of Synchrotron Radiation Physics, Department of Physics, Lund University, Box 118, SE-221 00 Lund, Sweden

[c]National Center for High Resolution Electron Microscopy and NanoLund, Lund University, Box 124, SE-221 00 Lund, Sweden

[†]These authors contributed equally to this work.

Abstract

An N-heterocyclic carbene palladium (II) complex containing two anthracene side arms was immobilized on the surface of reduced graphene oxide (rGO) by π-stacking. The activity of the homogeneous analogue and the supported complex in undirected C–H acetoxylation reaction of arenes was studied. The results show that the catalytic efficiency in acetoxylation of benzene is improved in the immobilized materials compared to the homogeneous analogue. According to an XPS analysis, the immobilized catalyst maintains the original oxidation state of Pd(II) after the catalytic reaction.

Introduction

Considerable efforts have been spent on heterogenizing homogeneous catalysts on an insoluble support as an attempt to not only aid catalyst separation but also to allow recovery and recycling of the catalyst several times; this is a crucial both from an economic and sustainability standpoint.[1] Un-directed metal-catalyzed oxidation of simple arenes is an attractive methodology to obtain valuable chemicals with important applications in many areas.[2] Palladium-catalyzed C–H acetoxylation of organic molecules without directing groups has been described in many reports,[3-6] and the vast majority of these examples employs homogeneous catalysts, particularly Pd(OAc)$_2$. In many cases these systems have problems with

1

Pd black formation and catalyst separation.[6-9] To this end palladium *N*-heterocyclic carbene catalysts have been used to stabilize the higher oxidation state and allow for heterogenization and such materials exhibit a remarkable catalytic activity and selectivity in C–O, C–halogen, and C–C bond formation under both batch and flow conditions.[10-22] However, in many cases the additional functionalization of the ligand that aid the anchoring or immobilization step leads to high costs of preparation and sometimes lead to changes in the original reactivity of the catalyst.[23] Furthermore the supports are often expensive and new, efficient and inexpensive methods to heterogenize and modify homogeneous catalysts are greatly needed by the catalysis community.

In light of this, there has been a recent development of non-covalent support methodologies via π-interactions which minimizes the need for chemical modification of the homogeneous catalyst or the support. The group of Peris recently demonstrated that immobilization of *N*-heterocyclic carbene Pd(II) or Ru(II) complexes onto a graphene surface by noncovalent interactions gave efficient and highly recyclable catalysts for many chemical transformations.[24-26] We have previously used a polymerizable Pd(II) NHC complex for the formation of a heterogeneous C–H activation catalysts.[20] Encouraged by the results of Peris, we set out to modify the π-stacking capability of our Pd(II) system by installing two anthracene moieties in the backbone of the NHC ligand (Scheme 1).
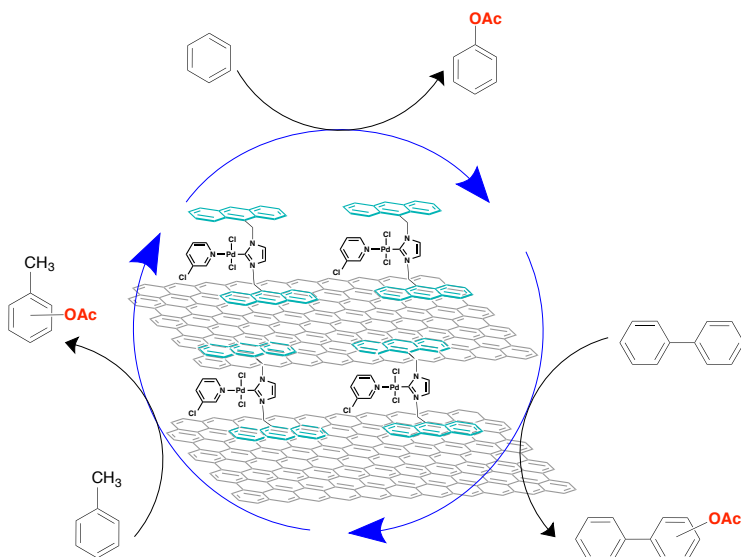
Scheme 1. π-Stacked *N*HC-Pd(II) complex catalyzes undirected C–H acetoxylation of arenes.

2

This modified complex was supported on reduced graphene oxide (rGO) and the so obtained system was applied in undirected C–H acetoxylation of arenes. The reactivity and regioselectivity of the heterogeneous system was evaluated and shows good activity for the formation of acetoxylated products in many examples.

Results and discussion
NHC–Pd^{II} complex synthesis

The synthesis of **1a** was reported previously.[27] The carbene transfer agent **1b** was prepared by the silver oxide route in moderate yield.[28, 29] The metalation step was confirmed by ^{1}H and ^{13}C NMR spectra, which showed a clear downfield shift of the carbene carbon around 183.1 ppm. Transmetallation of **1b** with PdCl$_2$(PhCN)$_2$ followed by chloropyridine addition gave **1c** in good yield (Scheme 2). The ^{13}C NMR spectrum of **1c** exhibited a signal at 147.4 ppm, which was assigned to the carbenic carbon (Pd-C$_{carbene}$).

π-Stacked catalyst synthesis and characterization

Complex **1c** was supported onto reduced graphene oxide (rGO) (see Scheme S1) by mixing the complex and rGO in dichloromethane in an ultrasound bath for 40 min and stirring the mixture for 1 day (Scheme 2). Notably, the colour of the solution turned from intense yellow to pale yellow, indicating that complex **1c** was retained on the rGO material. The resulting material containing the NHC–Pd^{II} complex π-stacked onto rGO (**1@rGO**), was separated by centrifugation and washed extensively with dichloromethane to remove unsupported **1c**.
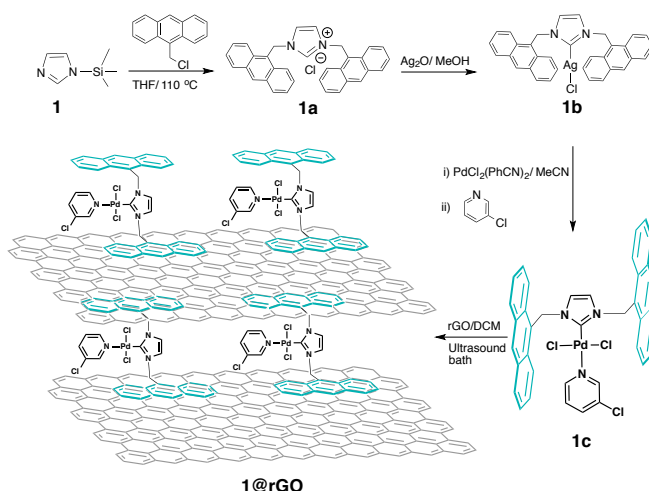
Scheme 2. Synthesis and heterogenization of double anthracene-tagged Pd(II) carbene complex

The ^{1}H NMR spectrum of the supernatant revealed the presence of **1c** in the solution; thus, all the complex had not been deposited onto rGO during the immobilization step. The palladium content of **1@rGO** was determined by an inductively coupled plasma-optical emission spectroscopy (ICP-OES) analysis. The results confirmed 2.5 wt % of Pd loaded on the rGO. Figure 1a shows high resolution transmission electron microscope (HRTEM) image of the native rGO support. The rGO sheet shows an intralayer distance around 3.8-4.3Å in areas where the sheets can be viewed edge-on.[30] Figure 1b shows a HRTEM image of the **1@rGO**. No indication of metallic Pd particles from the process of attaching the Pd-containing molecules could be found. X-ray energy-dispersive spectrometry (XEDS) data confirmed the presence of Pd and Cl at the **1@rGO** sheets, whereas these elements were absent in the native rGO support (Figure 1c).
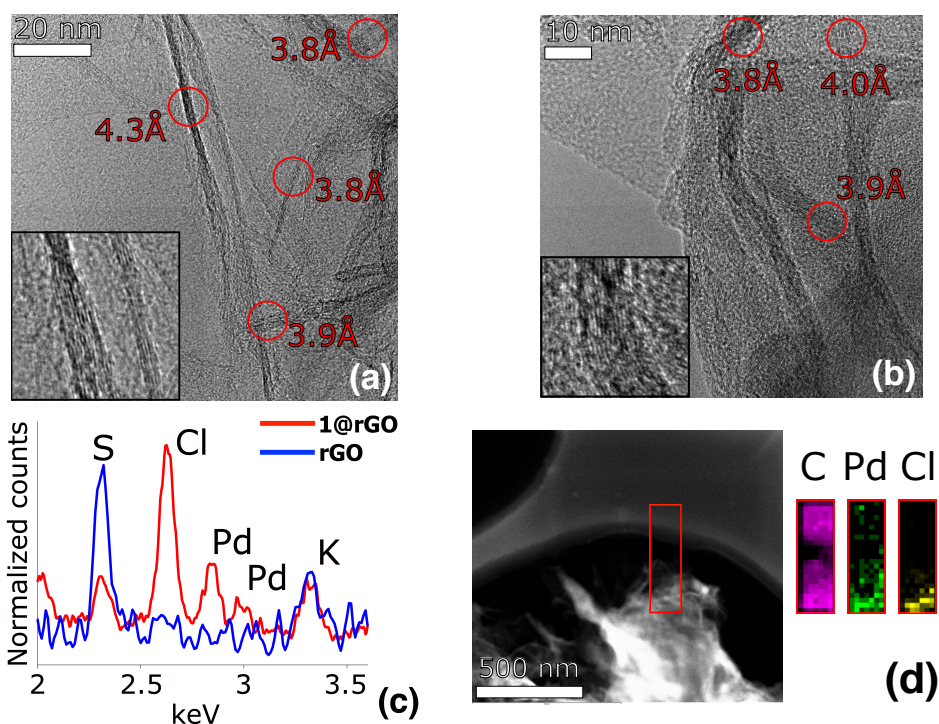
Figure 1. **(a)** and **(b)**, HRTEM images of rGO and **1@rGO** respectively, showing resolved individual graphene-like sheets with insets enhancing the lattice from which distances are measured. Some measurements are marked in both images. **(c)** EDX spectra, averaged for three sites of **1@rGO** (red line) and three sites of rGO (blue line). **(d)** High angle annular dark-field (HAADF) STEM image and XEDS-mapping of **1@rGO**. The red box in the STEM image marks the areas for which the elemental mapping was carried out. Note that there is no indication of Pd or Cl on the amorphous carbon film from the TEM support grid (upper part of the image).

the XEDS mapping (Figure 1d) of **1@rGO** shows a homogeneous dispersion of Pd and Cl at the graphene sheets.

X-ray photoelectron spectroscopy (XPS) analysis gives a direct evidence about the oxidation state of Pd of **1@rGO** as shown in Figures 2. The X-ray photoelectron (XP) spectra of complex **1c** and **1@rGO** show the Pd $3d_{5/2}$ and Pd $3d_{3/2}$ peaks at approximately 337.9 and 343.4 eV binding energy in the range of the expected energies for a Pd(II) species (Figure 2a).[20, 31] In addition, a peak at lower binding energy at around 337.6 eV is seen as the result of supporting **1c** on rGO. This shift to lower binding energy must be associated with a change in the Pd environment. The occurrence of this new peak, which is still within the Pd(II) region, in the XP spectrum of **1@rGO**, can probably be explained by the replacement of the chloropyridine ligand by a noncovalent π-interaction of the polycyclic aromatic system of rGO. The Cl $2p_{3/2}$ XP spectrum of **1c** exhibits a low-energy peak (ca. 197.9 eV) which is assigned to the palladium chlorine atom and a high-energy peak (ca. 198.7 eV) assigned to the chloropyridine chlorine (Figure 2b).[32] The ratio between the palladium and chloropyridine chlorine peaks is 2:1 as expected. Cl 2p spectrum of **1@rGO** showed significant broadening in the spectral features and shifts by 1.5 eV toward higher binding energies compared to the spectrum of complex **1c** (Figure 2b). Such a shift could be due to a transfer of chloropyridine from palladium to the rGO surface during the support reaction. The spectrum could also contain more components, and providing a more complicated scenario for the dissociated chloropyridine ligand (for more details see the Supporting Information Figure S1a). In order to investigate the fate of the chloropyridine and understand the change in Cl 2p binding energy, we performed an XPS analysis for only chloropyridine deposited onto rGO (**chloropyridine@rGO**) (see the Supporting Information for details). In the Cl $2p_{3/2}$ XP spectrum of **chloropyridine@rGO** only one peak at higher energy around 200.28 eV is found, matching the shifted peak in **1@rGO** (Figure 2b). In all, these results corroborate that there is no reduction of palladium during the formation of **1@rGO**, although the chloropyridine ligand is displaced by the π-interaction with the support. The N 1s spectra for **1c** is shown in Figure S1b (Supporting Information). The high energy peak (ca. 401.1 eV) is related to the imidazole nitrogen[25, 33] and the lower energy peak (ca. 400.4 eV) is assigned to the chloropyridine nitrogen; the ratio between the peaks is 2:1 as expected. Peak broadening towards lower and higher binding energies is observed in the N 1s spectra of **1@rGO**. This significant broadening can be assigned to the variation of the N chemical environment, as a consequence of the pyrazole formation at the edges of rGO during the synthesis of the rGO support[34] and the dissociation of chloropyridine, which opens up different interaction possibilities as shown in Scheme S1 in the Supporting Information. Thermogravimetric analysis (TGA) shows that **1@rGO** possesses a high thermal stability (see Figure S2 for details).
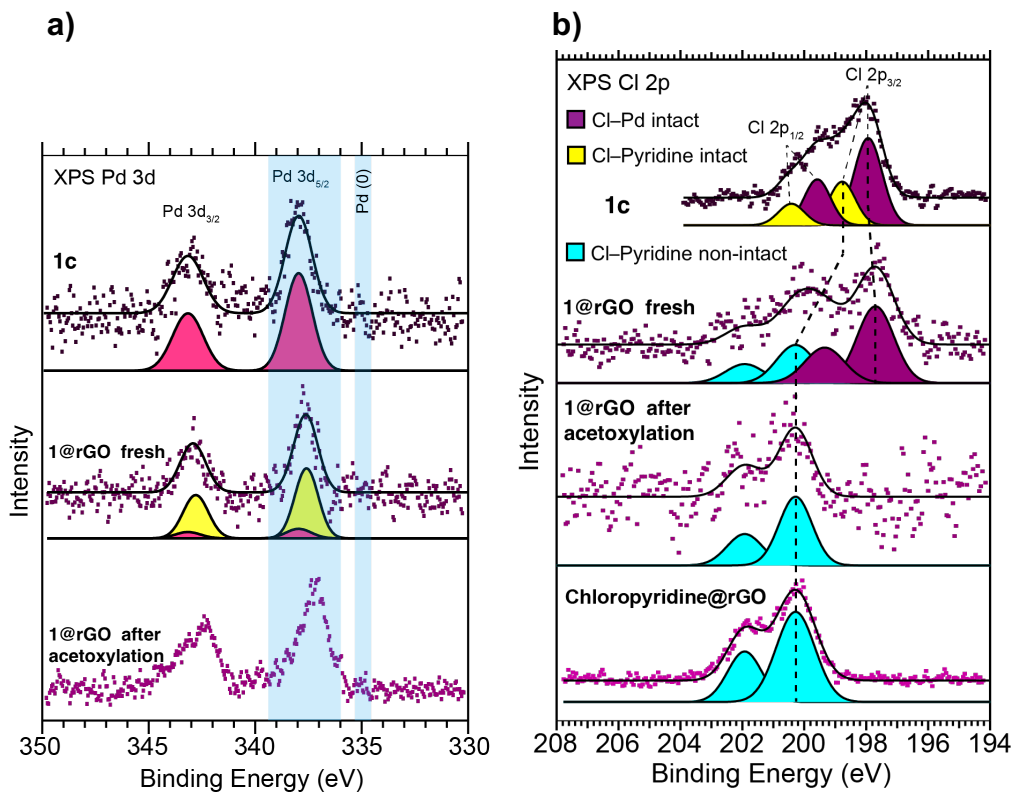
Figure 2. (a) and **(b)** Pd 3d and Cl 2p XP spectra of the indicated samples.

Activity in non-directed C–H acetoxylation

Benzene was chosen as a model substrate for non-directed acetoxylation and it was used in excess over the oxidant PhI(OAc)$_2$ (PIDA) (5:1). The catalyst (**1@rGO**) loading was 0.3 mol %, and, initially, different solvent systems were sceened as summarized in Table 1. The best combination was HFIP/Ac$_2$O giving over 50 turnovers but, gratifyingly, the inexpensive ^{G}AcOH/Ac$_2$O solvent system also worked we set out to optimize conditions for this.

Table 1. Screening of solvents in the **1@rGO** catalysed C–H acetoxylation of benzene

$$[1@rGO]^a$$
[mol. catalyst/ mol. oxidant]= 0.3%
1 equiv. [PhI(OAc)₂]
Solvent:Anhydride (9:1)
104°C, 24h

5 equiv. → Ph–OAc
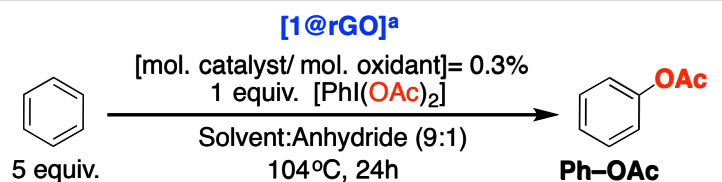
Entry	Solvent/Anhydride[b]	Yield[c] (%)	TON
1	CH₃CN/Ac₂O	Nd	-
2	AcOH/Ac₂O	5	16
3	AcOH/TFAA	11	35
4	HFIP/Ac₂O	16[d]	51
5	TFA/Ac₂O	7	22

[a]Pd loading is 2.5 wt%. [PIDA]= (0.05M). [b]Solvent/Anhydride= 9:1. [c]Yield and selectivity were determined by GC using a calibration curve based on decane as an internal standard. [d]Solvent/Anhydride= 5:1. TFAA= Trifluoroacetic anhydride, TFA= Trifluoroacetic acid, HFIP= Hexafluoroisopropanol.

The optimization of the concentration of the oxidant (PIDA) is shown in Figure 3a. The results show a significant increase in the yield up to 40% of Ph–OAc product upon increasing [PIDA] to 0.6 M. Using an excess of benzene also further increased the yield with the best result of 50% found at 30 eq. of benzene and [PIDA] = 1.0 M. Lower concentrations of PIDA (0.6 M) gave a slightly lower yield of 46% (Figure 3b). After catalysis, **1@rGO** was analyzed by XPS. The Pd $3d_{5/2}$ and Pd $3d_{3/2}$ peaks after acetoxylation reaction showed a broadening towards lower and higher binding energies compared to fresh **1@rGO** (Figure 2a). The identified broadening is probably related to an increased variation in the chemical environments of the Pd atoms after catalysis and to ligand exchange between chloride and acetoxy group, similarly to what was previously observed.[20] Undoubtedly, though, the XPS results show that the palladium remains in oxidation state (II) after the reaction.

7
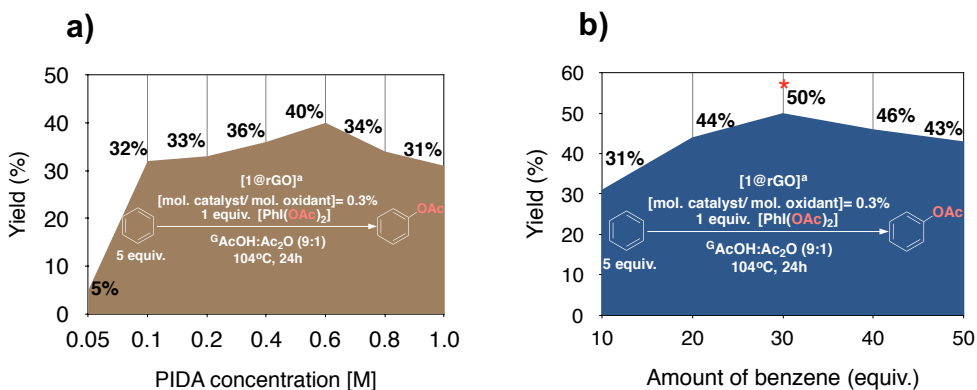
Figure 3. a) Optimization of PIDA concentration, **b)** optimization of amount of benzene using [PIDA]=1M.
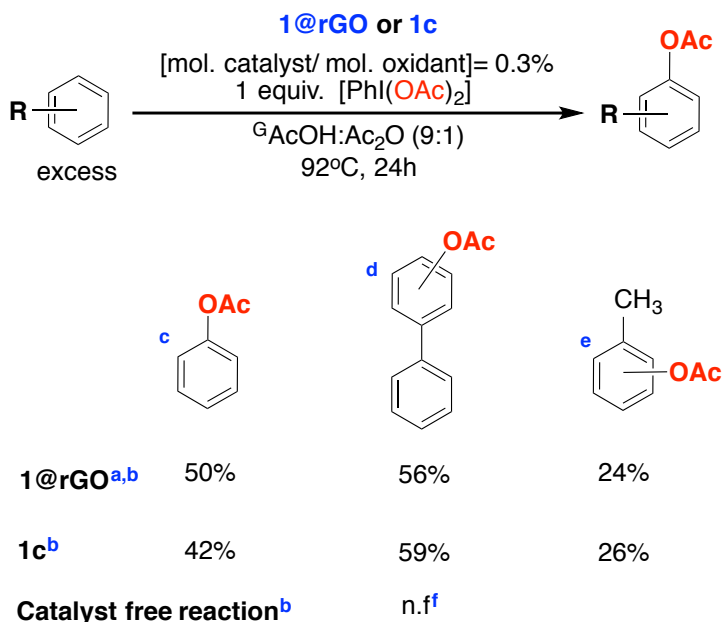
Figure 4. [a]Pd loading in the catalyst is 2.5 wt%. [PIDA]= 1 M. [b]Yields were determined by GC using a calibration curve based on decane as an internal standard. [c]30 equiv. of benzene was used. [d]2.5 equiv. of biphenyl was used and [PIDA]= 0.6 M. [e]5 equiv. of toluene was used. [f]No products were formed.

Oxidation of other arenes

The scope of C–H acetoxylation for other arenes using the reaction conditions as shown in Figure 4 was investigated. In the acetoxylation of benzene, **1@rGO** showed an increase in the yield of acetoxybenzene compared to homogeneous catalyst **1c** (Figure 3b and Figure 4). Furthermore, **1@rGO** and **1c** showed similar GC yields for acetoxylation of substrates biphenyl and toluene. Without catalyst, no formation of acetoxybiphenyl derivatives was observed according to GC.

Conclusions

A new heterogeneous catalytic system for undirected C–H oxidation reaction of arenes is described. It is based on depositing an NHC Pd system with anthracene side arms on a reduced graphene oxide surface. Characterization shows that the complex retains the oxidation state Pd(II) upon deposition and that the supporting pyridine ligand is displaced and deposited on the surface. The catalytic efficiency of the supported catalyst in acetoxylation of benzene is improved compared to the homogeneous analogue. Furthermore, the immobilized catalyst catalyzed undirected C–H acetoxylation of toluene as well as biphenyl with similar efficiency compared to the homogeneous analogue.

Experimental details

All manipulations were conducted under ambient conditions, unless noted. Solvents and chemicals were purchased from commercial suppliers and used as received. The imidazolium salt **1a** was prepared according to a previously reported procedure.[27] Graphene oxide was prepared from graphite powder (natural, universal grade, 200 mesh, 99.9995%) by Hummer's method.[35] The reduced graphene oxide was prepared by reduction of a suspension of exfoliated graphene oxide sheets in water with hydrazine hydrate.[36] NMR spectra were acquired on a Bruker Avance 400 FT-NMR spectrometer (^{1}H: 400.1 MHz) or a Varian Unity INOVA 500 spectrometer (^{1}H: 499.76 MHz). ^{1}H and ^{13}C NMR chemical shifts are reported in parts per million and referenced to the signals of deuterated solvents. Multiplicities are abbreviated as follows: (s) singlet, (d) doublet, (t) triplet, (q) quartet, (m) multiplet and (br) broad. Elemental analyses were performed by H. Kolbe Mikroanalytisches Laboratorium, Mülheim an der Ruhr, Germany.

1. Procedure for acetoxylation of benzene catalyzed by 1@rGO catalysts

The catalytic reactions were performed in a glass vial with a magnetic stir bar. The vial was loaded with benzene (0.60 g, 7.7 mmol, 30 equiv.), PhI(OAc)$_2$ (0.083 g, 0.25 mmol, 1 equiv.), catalyst (0.3 mol% with respect to the oxidant), glacial acetic acid (230 μl), and acetic anhydride (25.7 μl) and sealed tightly by using a screw cap. The mixture was heated to 92 °C using a heating block. At the end of the reaction the vessel was cooled to room temperature, and the catalyst was separated by centrifugation. The mixture was diluted with Et$_2$O (5 ml), shaken for 2 min, and extracted with a saturated aqueous solution of K$_2$CO$_3$ (9M in water, 3×2ml). The organic layer was then separated and the solvent was removed by evaporation. CH$_2$Cl$_2$ (1.2 ml) and decane (20 μl, as an internal standard for quantitative GC analysis) were added to the resulting solids and analyzed by GC.

2. Synthesis of 1c

1,3-bis(Anthracen-9-ylmethyl)-imidazol-2-ylidene silver chloride (I) **1b**
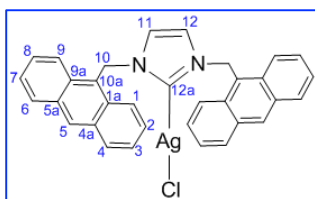
Silver (I) oxide (0.10 g, 0.43 mmol) was added to a 70 ml dry CH$_3$OH solution of **1a** (0.37 g, 0.76 mmol) and the reaction vessel was covered by aluminium foil and stirred at ambient temperature for 24 h. The suspension was filtered through celite and the solvent was removed in vacuum. The solids dissolved in CH$_2$Cl$_2$ and upon addition of n-pentane, a yellowish solid product **1b** was formed immediately, which was filtered on a frit and dried under vacuum in 44% yield (0.20 g).

Characterization of complex **1b***:*

1b: ^{1}H NMR (400 MHz, CDCl$_3$): δ 8.56 (s, 2H), 8.24 (dd, J = 8.9, 1.0 Hz, 4H), 8.05 (dd, J = 8.5, 1.4 Hz, 4H), 7.66 (ddd, J = 8.9, 6.6, 1.3 Hz, 4H), 7.52 (ddd, J = 8.5, 6.6, 1.0 Hz, 4H), 6.3 (s, 4H), 6.2 (s, 2H). ^{13}C NMR (400 MHz, CDCl$_3$) δ 183.06, 136.86, 131.42, 130.76, 129.48, 129.24, 127.39, 125.33, 124.64, 122.95, 118.95, 43.05.

Dichlorido(3-chloropyridine-N)[1,3-bis(anthracen-9-ylmethyl)imidazol-2-ylidene] palladium(II) **1c**
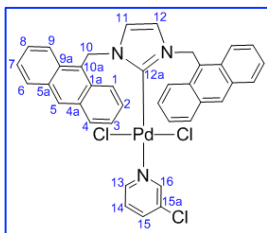
Pd(PhCN)$_2$Cl$_2$ (0.11 g, 0.3 mmol) was added to a solution of **1b** (0.18 g, 0.3 mmol) in 100 ml of CH$_3$CN and the reaction mixture was stirred at room temperature for 24 h. (0.15 g, 1.3 mmol) of 3-chloropyridine was added to the suspension, then filtered through Celite after 3 h. The solvent was removed in vacuum and a yellow solid of **1c** was precipitated by addition of pentane, isolated by filtration and washed with pentane in 47% yield (0.18 g).

Characterization of complex **1c***:*

1c: ^{1}H NMR (400 MHz, CDCl$_3$): δ 9.33 (d, *J*=2.3 Hz, 1H, H16), 9.23 (dd, *J*=5.5, 1.3 Hz, 1H, H13), 8.53 (d, *J*=10.0 Hz, 6H, H1, H5 and H9), 8.04 (d, *J*=8.5 Hz, 4H, H4 and H6), 7.86 (ddd, *J*=8.2, 2.2 and 1.3 Hz, 1H, H15), 7.64-7.47 (m, 8H, H2, H3, H7 and H8), 7.44 (dd, *J*=7.8 and 5.5 Hz, 1H, H14), 6.86 (s, 4H, H10), 5.92 (s, 2H, H11 and H12). ^{13}C NMR (400 MHz, CD$_3$CN): δ 150.6 (C16), 149.5 (C13), 147.3 (C12a), 138.3 (C15), 132.9 (C10a), 131.5 (C4a), 131.4 (C5a), 129.8 (C1a and C9a), 129.2 (C4 and C6), 127.6 (C1 and C9), 125.5 (C2, C3, C7 and C8), 125.1 (C15a), 124.2 (C5), 124.1 (C14), 120.5 (C11 and C12), 47.7 (C10). Anal. Calcd for C$_{38}$H$_{28}$Cl$_3$N$_3$Pd: C, 61.73; H, 3.82; N, 5.68. Found: C, 60.78; H, 4.15; N, 5.33.

3.   Supporting procedure and characterization of 1@rGO catalyst

0.02 g of rGO were suspended in 7 ml dry CH$_2$Cl$_2$ and sonicated for 45 min. 0.01 g of complex **1c** in 5ml dry CH$_2$Cl$_2$ were added to the sonicated rGO and stirred vigorously for two days at room temperature. The supported catalyst was separated by centrifugation, washed extensively with CH$_2$Cl$_2$, and dried under vacuum.
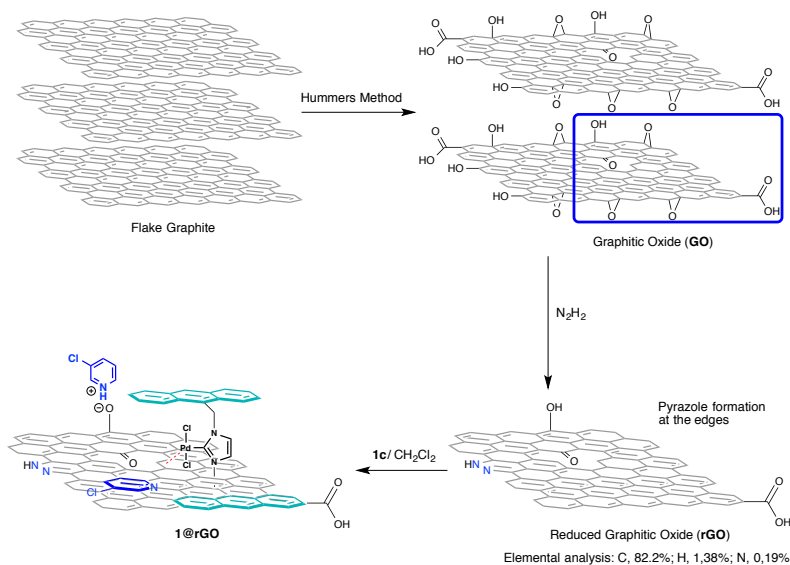
Scheme S1. Synthesis of rGO and the proposed scenario of chloropyridine decomposition after the immobilzation step of **1c**.

High-resolution transmission electron microscopy (HRTEM). The samples were imaged using a JEOL 3000F transmission electron microscope (field emission gun, operated at 300 kV using both conventional TEM and scanning TEM), with a point resolution of 0.17 nm in conventional TEM mode. Sample preparation was performed by dipping a copper TEM-grid covered by a lacy carbon film into a dispersion of the rGO or **1@rGO** in ethanol. The microscope was equipped with an energy-dispersive X-ray spectrometer (XEDS) system from Oxford Instrument with a silicon drift detector (SDD) for compositional analysis. High resolution TEM (HRTEM) images were scrutinized for Pd particles and investigated by Fourier analysis.

X-ray photoelectron spectroscopy (XPS). The measurements were carried out at the XPS end station of the HIPPIE beamline of the MAX IV Laboratory in Lund, Sweden. The analysis chamber is equipped with a SCIENTA HiPP-3 hemispherical electron energy analyser and a separate preparation chamber, which is equipped with surface analysis and preparation tools. The presented data were collected using a SCIENTA SAX100 Al K$_\alpha$ X-ray anode combined with a VG SCIENTA XM780 monochromator (photon energy 1486.7 eV). The anode was operated at 10 kV electron acceleration voltage and 25 mA emission current. The experiment was performed at a pressure lower than 10^{-9} mbar. Single crystal

samples were dissolved and polymer samples were dispersed in dichloromethane and then the samples were dropped onto the highly oriented pyrolytic graphite HOPG surface. All spectra were energy-calibrated with respect to the C 1s core level of graphite of HOPG at 284.42 eV.[37] No signs of sample charging were detected: all lines could be reproduced reliably at the same energy. In particular, the C 1s line was always found at the same binding energy. Background removal was done by using a Shirley or low-degree polynomial background in the case of the Pd 3d spectra and a Shirley background in the case of the Cl 2p spectra. From the N 1s spectra a polynomial background was removed. Curve fitting of the Cl 2p and N 1s spectra was carried out using the Igor Pro software package of Wavemetrics, Inc. using symmetric Voigt lineshapes. The spin-orbit split components in the Cl 2p spectra were restrained to have a 1:2 area ratio between the Cl $2p_{1/2}$ and Cl $2p_{3/2}$ peaks.

Preparation of Chloropyridine@rGO

0.02 g of rGO were suspended in 7 ml dry CH_2Cl_2 and sonicated for 45 min. 3-chloropyridine (3.7 mg, 0.033 mmol) was added to the sonicated rGO and stirred vigorously for two days at room temperature. The solids were separated by centrifugation, washed extensively with CH_2Cl_2, and dried under vacuum.

Inductively coupled plasma-optical emission spectroscope (ICP-OES).
Pd loadings were measured by a PerkinElmer Optima 8300. Samples (20 mg) were treated with a muffle stove at 1000 °C for 4 h. After cooling to room temperature, 3 ml of aqua regia was added and stirred for 30 min at 100 °C. The resulting solution was filtrated and the filtrate was diluted to 50 ml with distilled water.

Thermogravimetric analysis (TGA).
The thermal stability of the samples under study was investigated by using a Q500 analyser (TA Instruments). The first heating scan was from 25-500 °C under N_2 and the second heating scan was from 500-600 °C under air, the heating rates were 10 °C/min.

Gas chromatography analysis (GC).
The analyses were done using an Hewlett-Packard 5890 II instrument with a flame ionization detector (FID) and a capillary column (CP-Sil 19CB 14% cyanopropyl-phenyl/86% dimethylpolysiloxane, 0.2 μm, 0.2 mm, 25 m) with decane as an internal standard. The retention times of different compounds in the gas chromatogram were identified using commercially available and synthesized pure compounds.
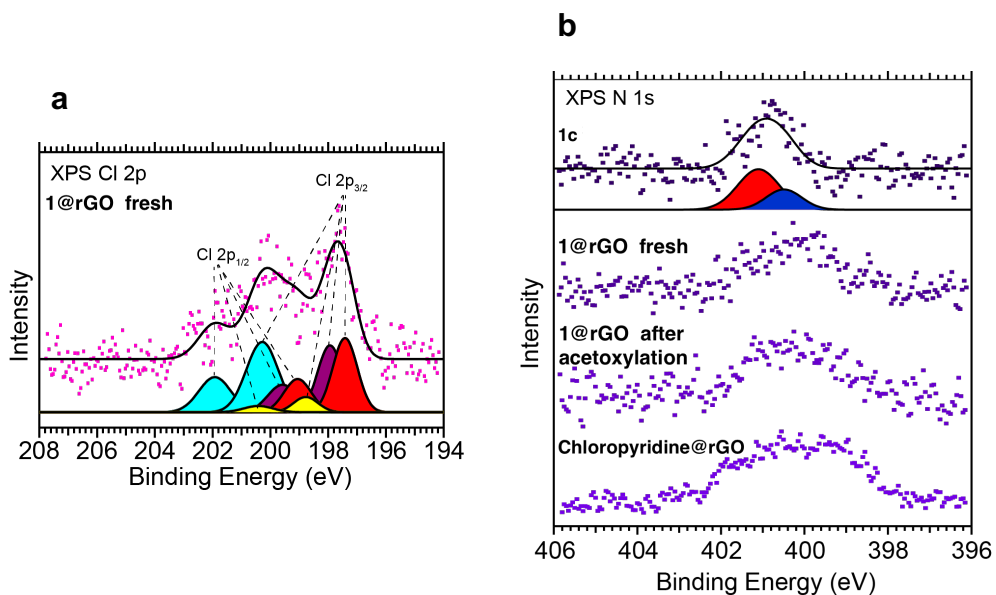
Figure S1. a) Cl 2p XP spectra of fresh **1@rGO**, showing the proposed fitting for extra components. **b)** N 1s XP spectra of complex **1c**, fresh **1@rGO, 1@rGO** after acetoxylation reaction, and chloropyridine deposited on rGO.
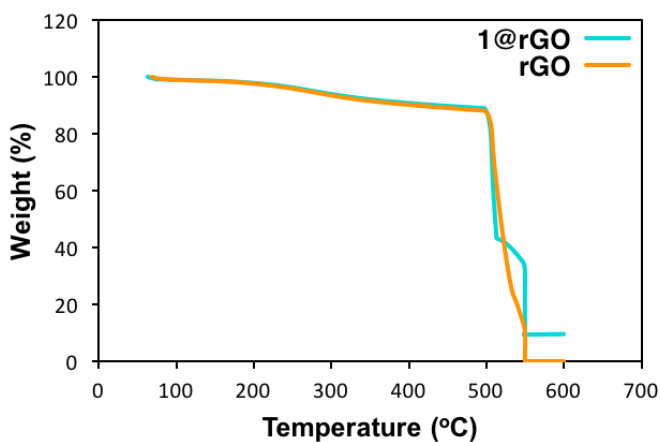
Figure S2. TGA curves of rGO and **1@rGO**. The heating rate was 10 °C min^{-1} under N$_2$ over a temperature range 25-500 °C and under air over a temperature range 500-600 °C.

14

References

1. S. Hubner, J. G. de Vries and V. Farina, *Adv. Synth. Catal.*, 2016, **358**, 3-25.
2. J. H. P. Tyman, *Synthetic and natural phenols*, Elsevier, Amsterdam The Netherlands ; New York, 1996.
3. L. Eberson and L. Jönsson, *J. Chem. Soc. Chem. Comm.*, 1974.
4. L. M. Stock, K. Tse, L. J. Vorvick and S. A. Walstrum, *J. Org. Chem.*, 1981, **46**, 1757-1759.
5. T. Yoneyama and R. H. Crabtree, *J. Mol. Catal. A-Chem.*, 1996, **108**, 35-40.
6. M. H. Emmert, A. K. Cook, Y. J. Xie and M. Sanford, *Angew. Chem. Int. Edit.*, 2011, **50**, 9409-9412.
7. B. V. Popp and S. S. Stahl, *Chem. Eur. J.*, 2009, **15**, 2915-2922.
8. C. Valderas, K. Naksomboon and M. A. Fernandez-Ibanez, *ChemCatChem*, 2016, **8**, 3213-3217.
9. D. Wang, A. B. Weinstein, P. B. White and S. S. Stahl, *Chem. Rev.*, 2017, ASAP.
10. G. A. Price, A. Hassan, N. Chandrasoma, A. R. Bogdan, S. W. Djuric and M. G. Organ, *Angew. Chem. Int. Ed. Engl.*, 2017, 56,13347-13350.
11. X. M. Zeng, T. X. Zhang, Y. C. Qin, Z. J. Wei and M. M. Luo, *Dalton Trans.*, 2009, 8341-8348.
12. G. Li, H. Q. Yang, W. Li and G. L. Zhang, *Green Chem.*, 2011, **13**, 2939-2947.
13. D. B. Bagal, R. A. Watile, M. V. Khedkar, K. P. Dhake and B. M. Bhanage, *Catal. Sci. Technol.*, 2012, **2**, 354-358.
14. G. Borja, A. Monge-Marcet, R. Pleixats, T. Parella, X. Cattoen and M. W. C. Man, *Eur. J. Org. Chem.*, 2012, 3625-3635.
15. V. Sans, F. Gelat, M. I. Burguete, E. Garcia-Verdugo and S. V. Luis, *Macromol. Symp.*, 2012, **317**, 259-266.
16. K. V. Bukhryakov, C. Mugemana, K. B. Vu and V. O. Rodionov, *Org. Lett.*, 2015, **17**, 4826-4829.
17. S. N. Jadhav, A. S. Kumbhar, S. S. Mali, C. K. Hong and R. S. Salunkhe, *New J. Chem.*, 2015, **39**, 2333-2341.
18. A. Martinez, J. L. Krinsky, I. Penafiel, S. Castillon, K. Loponov, A. Lapkin, C. Godard and C. Claver, *Catal. Sci. Technol.*, 2015, **5**, 310-319.
19. C. A. Wang, Y. W. Li, X. M. Hou, Y. F. Han, K. Nie and J. P. Zhang, *ChemistrySelect*, 2016, **1**, 1371-1376.
20. M. H. Majeed, P. Shayesteh, L. R. Wallenberg, A. R. Persson, N. Johansson, L. Ye, J. Schnadt and O. F. Wendt, *Chem. Eur. J.*, 2017, **23**, 8457-8465.
21. R. Zhong, A. C. Lindhorst, F. J. Groche and F. E. Kuhn, *Chem. Rev.*, 2017, **117**, 1970-2058.
22. M. H. Majeed, P. Shayesteh, P. Tunå, A. R. Persson, R. Gritcenko, L. R. Wallenberg, C. Hulteberg, L. Ye, J. Schnadt, and O. F. Wendt, Unpublished manuscript.

23. A. M. Mähärrämov, K. T. Mahmudov, M. N. Kopylovich and A. J. L. Pombeiro, *Non-covalent interactions in the synthesis and design of new compounds*, John Wiley & Sons, Hoboken, New Jersey, 2016.
24. S. Sabater, J. A. Mata and E. Peris, *ACS Catal.*, 2014, **4**, 2038-2047.
25. S. Sabater, J. A. Mata and E. Peris, *Organometallics*, 2015, **34**, 1186-1190.
26. D. Ventura-Espinosa, A. Carretero-Cerdan, M. Baya, H. Garcia and J. A. Mata, *Chem. Eur. J.*, 2017, **23**, 10815-10821.
27. C. L. Fu, L. J. Meng, Q. H. Lu, Z. F. Fei and P. J. Dyson, *Adv. Funct. Mater.*, 2008, **18**, 857-864.
28. M. Viji, A. K. Nair, P. C. Nandajan and D. Ramaiah, *RSC Adv.*, 2014, **4**, 47982-47986.
29. A. Citta, E. Schuh, F. Mohr, A. Folda, M. L. Massimino, A. Bindoli, A. Casini and M. P. Rigobello, *Metallomics*, 2013, **5**, 1006-1015.
30. F. Ossler, J. B. Wagner, S. E. Canton and L. R. Wallenberg, *Carbon*, 2010, **48**, 4203-4206.
31. S. K. Movahed, R. Esmatpoursalmani and A. Bazgir, *RSC Adv.*, 2014, **4**, 14586-14591.
32. Senhkova, O.; Bolbat, E.; Ericson, F.; Shayesteh, P.; Chaudhary, S.; Johansson, N.; Head, A. R.; Persson, P.; Wendt, O. F.; Schnadt, J. Unpublished Manuscript.
33. S. Men, D. S. Mitchell, K. R. Lovelock and P. Licence, *ChemPhysChem*, 2015, **16**, 2211-2218.
34. S. Park, Y. C. Hu, J. O. Hwang, E. S. Lee, L. B. Casabianca, W. W. Cai, J. R. Potts, H. W. Ha, S. S. Chen, J. Oh, S. O. Kim, Y. H. Kim, Y. Ishii and R. S. Ruoff, *Nat. Commun.*, 2012, **3**.
35. W. S. Hummers and R. E. Offeman, *J. Am. Chem. Soc.*, 1958, **80**, 1339-1339.
36. S. Stankovich, D. A. Dikin, R. D. Piner, K. A. Kohlhaas, A. Kleinhammes, Y. Jia, Y. Wu, S. T. Nguyen and R. S. Ruoff, *Carbon*, 2007, **45**, 1558-1565.
37. T. Balasubramanian, J. N. Andersen and L. Wallden, *Phys. Rev. B*, 2001, **64**.

Paper V

Reduced graphene oxide supported Pd(II) carbene complex: activity and selectivity in directed C–H halogenation of arenes

Maitham H. Majeed,[a] Dino Redzic,[a] Payam Shayesteh,[b] Axel R. Persson,[a,c] L. Reine Wallenberg,[a,c] Joachim Schnadt,[b] and Ola F. Wendt*[a]

[a]Centre for Analysis and Synthesis, Department of Chemistry, Lund University, Box 124, SE-221 00 Lund, Sweden

[b]Division of Synchrotron Radiation Physics, Department of Physics, Lund University, Box 118, SE-221 00 Lund, Sweden

[c]National Center for High Resolution Electron Microscopy and NanoLund, Lund University, Box 124, SE-221 00 Lund, Sweden

Abstract

A new catalytic system based on π-π stacking of an N-heterocyclic carbene (NHC) palladium complex on reduced graphene oxide (rGO) was synthesized and characterized. The system exhibited excellent regioselectivities in ligand directed C–H activation/halogenation reactions with different heterocyclic organic substrates. The catalyst was successfully re-used up to five runs with operational simplicity and ease of recovery. Hot filtration test confirmed the heterogeneous character of the catalytically active solids.

Introduction

Using transition metal catalysis to functionalize unreactive C–H bonds into C–halogen bonds is an intense area of research as it could facilitate the production of bulk chemicals and minimize the chemical waste by shortening the reaction pathways in a large number of transformations. The halogenation of heterocyclic compounds can yield various pharmaceuticals that are important and irreplaceable components in everyday life (Fig. 1). The presence of halogen atoms in the structures has a direct impact on the activity, solubility and pharmacokinetics of the drug.[1-5]
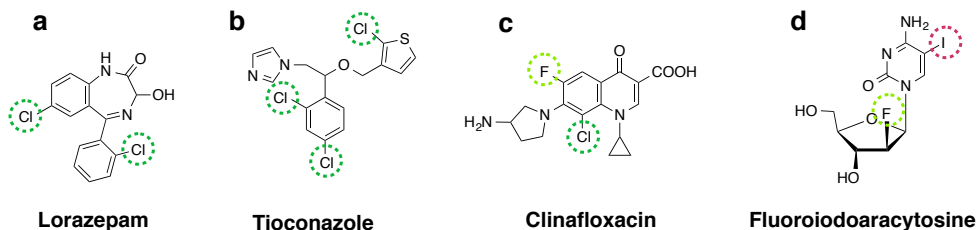
Figure 1. Examples of chemical structures of drugs containing halogenated heterocycles: **a)** a psychoactive drug, **b)** an antifungal agent, **c)** an antibiotic and d) an antiviral agent.[4]

The selective directed C–H bond halogenation of arenes (functionalization of C–H bond with the assistance of chelation) is an important methodology and has profound applications in organic synthesis.[6-11] Thus, in the current work we investigate ligand-directed C–H halogenation using an N-heterocyclic carbene Pd^{II} (NHC-Pd^{II}) complex supported on reduced graphene oxide by noncovalent interactions (π-π stacking) with the aim of showing their efficiency and regioselectivity in a number of heterogeneously catalyzed reactions. The catalyst shows a superior regioselectivity compared to the homogeneous analogue in C–H iodination and bromination of phenylpyridine. Moreover, the π-stacked catalyst can easily be separated, recovered and recycled up to five times with 100% selectivity of the mono-halogenated product.

Results and discussion

Synthesis and characterization

Complex **1** was synthesized according to a previously reported method.[12] The metallated complex **1** showed a downfield shift of the carbene carbon around 180 ppm, according to ^{1}H and ^{13}C NMR spectra. Addition of $PdCl_2(PhCN)_2$ to **1** in the transmetallation step, followed by chloropyridine addition gave **2** in good yield (Scheme 1). The ^{13}C NMR spectrum of **2** exhibited a signal at 147.56 ppm, which is assigned to the carbenic carbon (Pd-$C_{carbene}$).
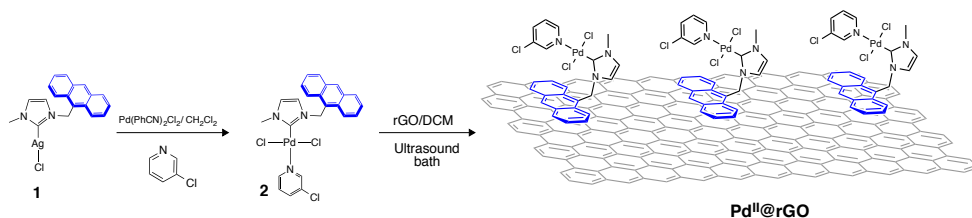
Scheme 1. Synthesis and heterogenization of an anthracene-tagged Pd(II) carbene complex.
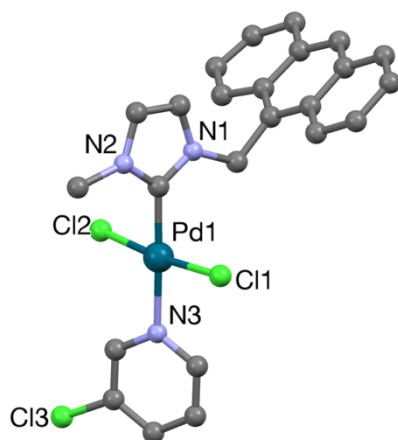
Figure 2. Molecular structure of **2** with thermal ellipsoids displayed at 50% probability. Hydrogen atoms have been omitted for clarity. Selected bond lengths (Å) and bond angles (°) with estimated standard deviations of **2** crystal: Pd1—C 1.956(2), Pd1—N3 2.141(2), Cl1—Pd1—Cl2 174.01 (11).

The structure of complex **2** was confirmed by X-ray diffraction (XRD) and the molecular structure with selected bond distances and angles is shown in Fig. 2. Subsequently, freshly sonicated reduced graphene oxide (rGO) flakes were stirred vigorously for two days with **2** in dry dichloromethane (Scheme 1). At the end of the supporting procedure, the palladium complex π-stacked on rGO (**Pd^{II}@rGO**) was separated by centrifugation and washed extensively with dichloromethane to remove any unsupported complex **2**.
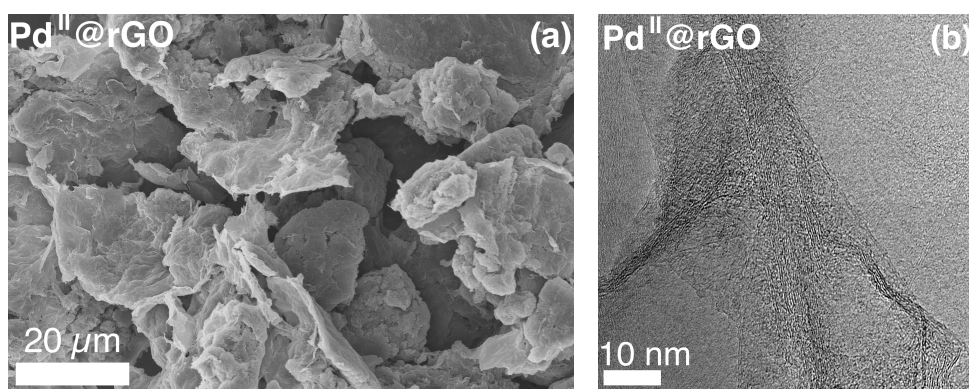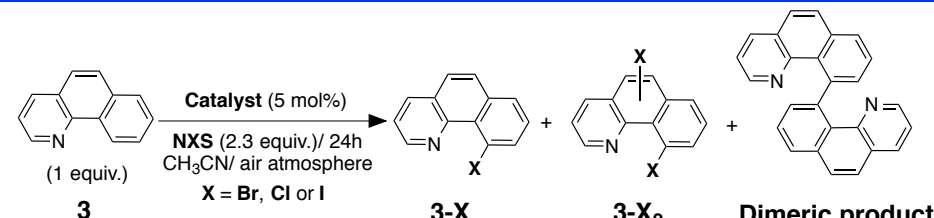
Figure 3. (a) and **(b)** SEM and STEM images of **Pd^{II}@rGO** catalyst.

A scanning electron microscopy (SEM) image revealed crumpled features in the support layers in the structure of **Pd^{II}@rGO** (Fig. 3a). High resolution transmission electron microscope (HRTEM) images and Fast fourier transform (FFT) analysis did not detect any presence of metallic palladium in **Pd^{II}@rGO** after the immobilization step (Fig. 3b). The density and dispersity of elements Pd, Cl, N and C in **Pd^{II}@rGO** were evaluated by X-ray energy-dispersive spectroscopy (XEDS) and EDX mapping. Pd, Cl and N are found to be homogeneously dispersed on the surface of the graphene sheets in **Pd^{II}@rGO**, while the high density of C element is expected and inevitable in the immobilized solids (Fig. 4a and 4b). However, as can be also seen in Fig. 4b, the native rGO support is free of Pd, Cl and N. Inductively coupled plasma-optical emission spectroscopy (ICP-OES) analysis confirmed that the loading of palladium in **Pd^{II}@rGO** is 2.0 w%. The **Pd^{II}@rGO** possesses a high thermal stability according to thermogravimetric analysis (TGA) (see Figure S1 for details).
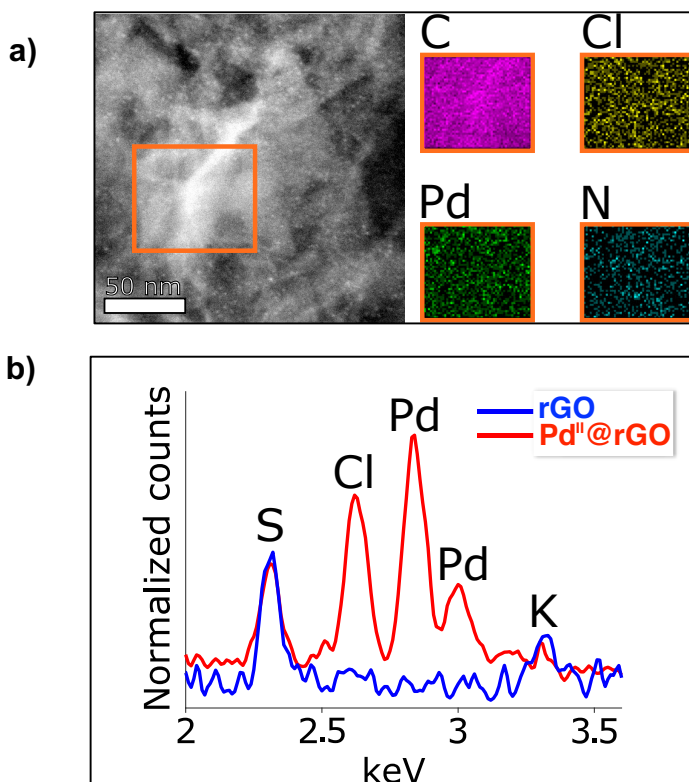
Figure 4. (a) STEM image and dark-field STEM of **Pd^{II}@rGO**, the red box in the STEM image marks the areas for which the elemental mapping was carried out. **(d)** EDX spectra of **Pd^{II}@rGO** (red line) and rGO (blue line).

Table 1. C–H halogenation of benzo[*h*]quinoline using Pd(II) based catalysts.

Entry	Catalyst	Temp. °C	X	3-X (%)[a]	3-X$_2$ (%)[a]	D.P. (%)[a]
1	Pd^{II}@rGO	60	Br	5.6	n.f	n.f
2	Pd^{II}@rGO	100	Br	16.2[c]	n.f	n.f
3	Pd^{II}@rGO [b]	100	Br	9	n.f	n.f
4	Pd^{II}@rGO	120	Br	9.4	traces	n.f
5	None	100	Br	n.f	n.f	n.f
6	2	100	Br	13.3	traces	n.f
7	Pd^{II}@rGO	100	Cl	27	12	n.f
8	Pd^{II}@rGO	100	I	n.f	n.f	n.f
9	Pd^{II}@rGO [b]	100	I	n.f	n.f	n.f

[a] Yield and selectivity were determined by GC using a calibration curve based on decane as an internal standard. D.P.= dimeric product, n.f.= not formed. [b] Solvent is ^{G}AcOH. [c] Traces of mono-chlorinated adduct was detected in GC-MS and analyzed by ^{1}HNMR.

Directed C–H halogenation of benzo[*h*]quinoline

Initially, we screened the directed C–H bromination of benzo[*h*]quinoline **3** at different temperatures using N-bromosuccinimide as an oxidant and **Pd^{II}@rGO** as a catalyst under the reaction conditions as summarized in Table 1. A significant improvement in the yield of **3-Br** up to 16.2 % was found when the temperature was increased from 60 to 100 °C (Table 1, Entries 1 and 2). No di-substituted or dimeric products (due to homo coupling) were observed, but traces of the mono-chlorinated adduct was detected by GC-MS analysis, probably originating from the chlorides on the palladium in **2**. Increasing the temperature further up to 120 °C lead to a decrease in the yield of **3-Br** to 9.4% and formation of the di-substituted product **3-Br$_2$** in trace amounts. This is probably due to un-catalyzed bromination taking place at this temperature (Table 1, Entry 4). Switching to ^{G}AcOH as a solvent afforded only 9% yield of **3-Br** (Table1, Entry 3); in the absence of catalyst there was no conversion at 100 °C (Table1, Entry 5). For comparison, **3-Br** was obtained in a lower yield of 13 % upon using complex **2** as a homogenous catalyst, in addition to formation of **3-Br$_2$** in trace amounts (Table 1, Entry 6). Furthermore, mono-chlorinated and di-chlorinated products were formed in 27% and 12% yield, respectively using NCS as an oxidant and **Pd^{II}@rGO** as a catalyst. There is no formation of iodo-substituted products using

5

different solvents (Table 1, Entries 8 and 9), which could be related to the high planarity of benzo[*h*]quinoline substrate and the size of the iodine.

Time profile and hot filtration test

The time profile study was done according to the reaction conditions shown in Fig. 5. No induction period was observed and the catalysis almost stopped after 12 hours. Furthermore, a hot filtration experiment was performed, where the solid catalyst was filtered off after 20 minutes of reaction and the filtrate was evaluated after 18 h. From this it is clear that the reaction did not proceed in the absence of the solid catalysts, corroborating its heterogeneous character (Fig. 5).
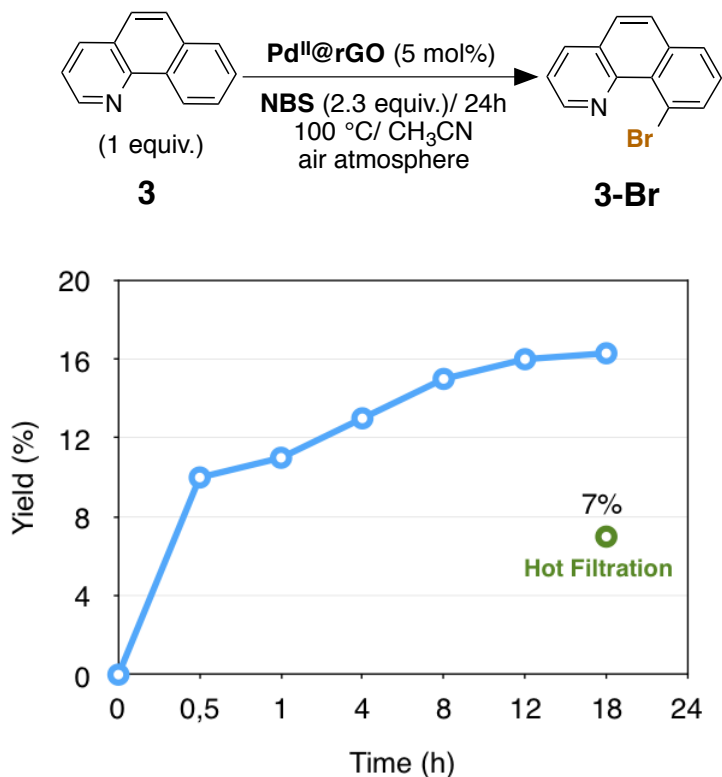
Figure 5. Time profile and hot filtration test of the indicated catalysis reaction.

Bromination and iodination of phenylpyridine

Generally, phenylpyridine **4** was smoothly transformed into the corresponding brominated and iodinated products at mild reaction conditions as shown in Fig. 6. Notably, **Pd^{II}@rGO** showed a high regioselectivity compared to the homogeneous analogue, affording only mono-brominated **4-Br** and mono-iodinated **4-I** products in moderate to good yields (30 and 52% respectively) as shown in Fig. 6a and 6b.
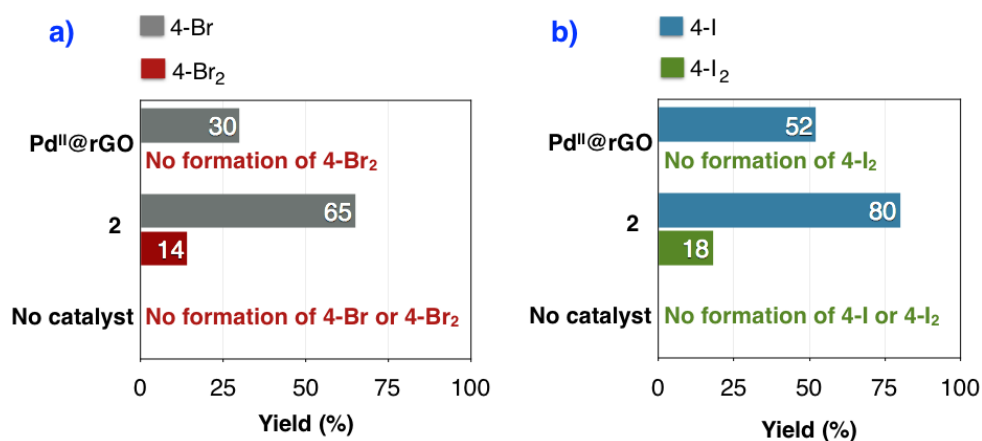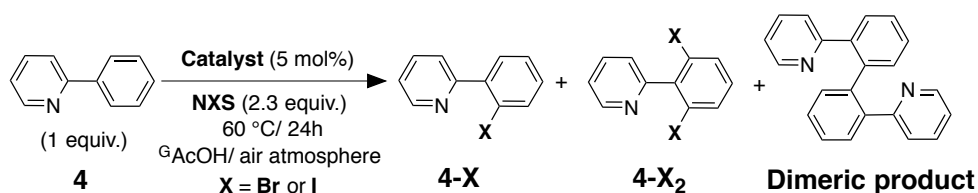
Figure 6. Heterogeneous, homogenous and uncatalyzed reaction yields in bromination and iodination of **4**. Yields and selectivity were determined by GC using a calibration curve based on decane as an internal standard.

It is worth noting that although **2** was less selective for bromination and iodination of phenylpyridine it gave higher yields of mono-halogenated products of the indicated catalysis reactions. There was no dimeric product in either reactions and, without catalyst, there is no conversion (<1%) and one can rule out any non-catalytic parallel reactions such as electrophilic aromatic substitution reactions.

Recyclability of Pd^{II}@rGO

With these results in hand, we set out to test the reusability of **Pd^{II}@rGO** in the iodination of phenylpyridine. The results shown in Fig. 7 indicate that although there is some loss of activity after the first run, the following four runs show no apparent loss of activity within the experimental fluctuation.
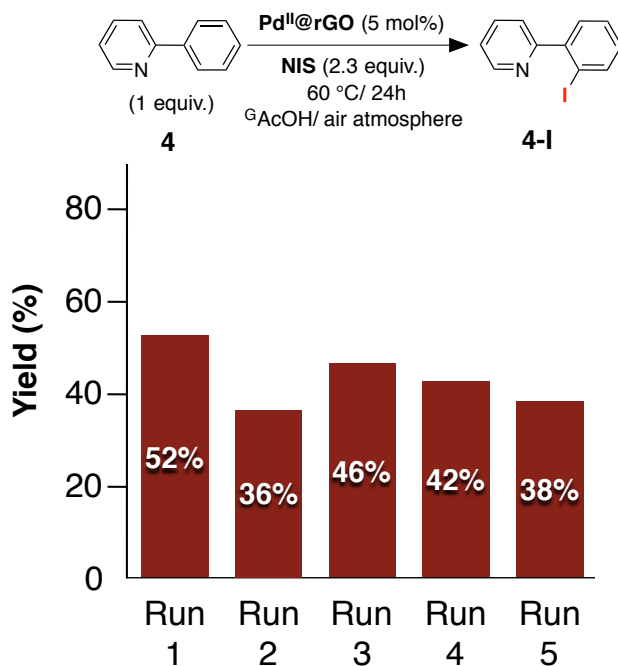
Figure 7. Recyclability test of **Pd^{II}@rGO** catalyzed iodination reaction of phenylpyridine. Yields were determined by GC using a calibration curve based on decane as an internal standard.

XPS study before and after catalysis

To evaluate the oxidation state of the Pd in our heterogeneous catalyst system, it was analyzed using X-ray photoelectron spectroscopy (XPS) before and after catalysis. The XP spectra of **2** and **Pd^{II}@rGO** (Fig. 8) show the Pd $3d_{5/2}$ and Pd $3d_{3/2}$ peaks at approximately 337.8 and 343.2 eV binding energy binding energy (BE) respectively, which is within the range of the BE of a Pd(II) species (Fig. 8a). Due to the π-stacking and the subsequent change in the Pd environment, we observed significate changes associated with the XP spectra of **Pd^{II}@rGO** (Fig. 8a and 8b). Firstly, a peak at lower binding energy of around 337.6 eV appeared in the Pd $3d_{5/2}$ spectrum and secondly the Cl 2p peaks shows broadening in the

spectral features of **Pd^{II}@rGO** and a new peak shifted by 1.5 eV toward higher binding energies compared to the spectrum of **2** (Figure 8b). This could be interpreted as a dissociation of the chloropyridine ligand onto the rGO surface during the supporting reaction, which has previously been observed with a similar type of catalyst.[13] This was confirmed through an XPS analysis of supported neat chloropyridine on rGO; the Cl 2p spectrum of this is in agreement with the new peak in **Pd^{II}@rGO** (Figure 8b). Furthermore, the intensities of the Cl 2p peaks associated with the Pd–Cl species were substantially decreased after chlorination, bromination and iodination catalytic reactions (Figure 8b). Indeed, these results point to a substitution of chloride on palladium by other ligands which could be bromide, iodide or acetate. This is in line with GC-MS and ^{1}H NMR analyses, where traces of mono-chlorinated adduct were detected during the bromination reaction of benzo[*h*]quinoline using **Pd^{II}@rGO** (see Table 1).
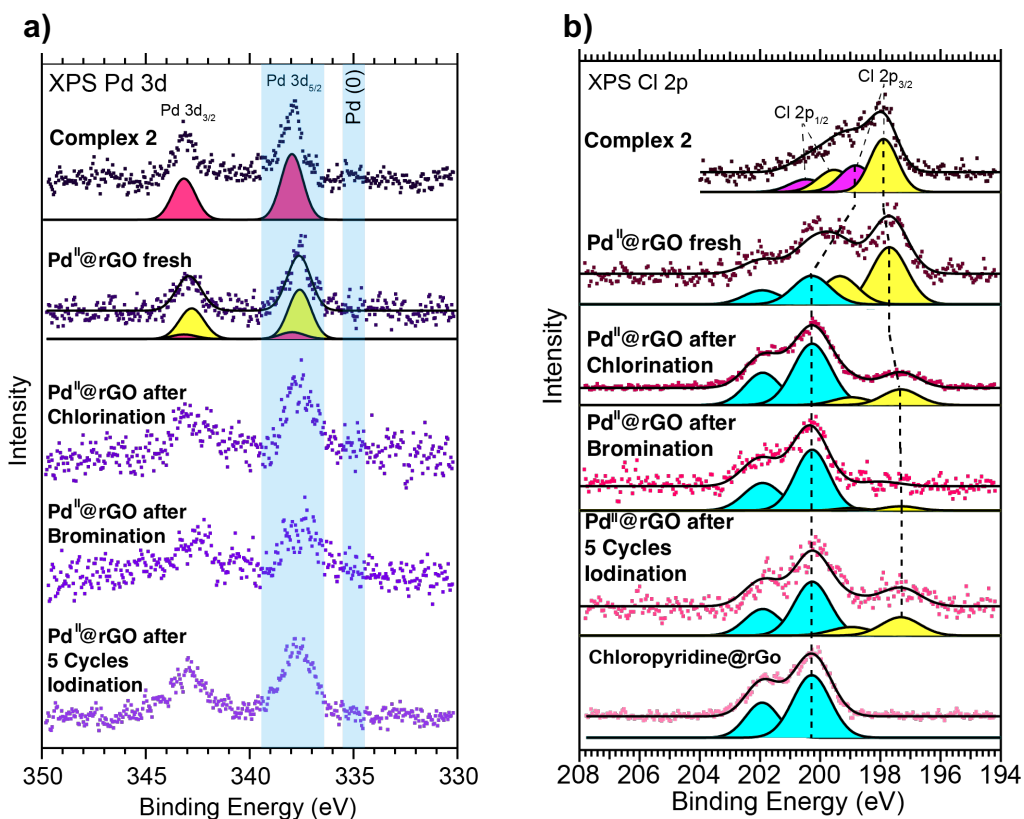
Figure 8. **(a)** and **(b)** Pd 3d and Cl 2p XP spectra of the indicated samples.

Thus, we conclude that during the reductive elimination step the palladium intermediate can eliminate Cl– benzo[*h*]quinoline and in general the chlorides on palladium tend to be lost during catalysis. Importantly, the supported material **Pd^{II}@rGO** contains no Pd in the metallic state, and it retains the Pd(II) oxidation state even after five catalysis cycles. The N 1s spectrum of **2** shows a higher energy peak (ca. 401.2 eV) related to the imidazole nitrogen and a lower energy peak (ca. 400.5 eV) associated with the chloropyridine nitrogen,[13] and the ratio between the peaks is 2:1 as expected (Fig. S2 in the Supporting Information). Peak broadening towards lower and higher binding energies is observed in the N 1s spectra of **Pd^{II}@rGO** both before and after catalysis, indicating a higher dispersity in the N chemical environment.

Conclusions

We describe a new heterogeneous catalytic system based on supporting a palladium NHC complex with one anthracene arm on reduced graphene oxide through π-π stacking. This material catalyzes the directed C–H halogenation of (hetero)arenes with fair-good yields and excellent regioselectivity. HRTEM, XEDS, EDX mapping, and XPS analysis results confirmed the that catalyst maintains its molecular Pd(II) state in the supported material and that it is homogeneously dispersed on the surface. The recyclability of this supported system was shown for iodination of phenylpyridine and this also shows that the material maintains the Pd (II) oxidation state after five runs with no reduction to Pd nanoparticles. There is, however, a slow substitution of chlorides on the palladium during catalysis.

Experimental data

General. All manipulations were conducted under ambient conditions, unless noted. Solvents and chemicals were purchased from commercial suppliers and used as received. Complex **1** was prepared according to a previously reported procedure.[14] Graphene oxide and the reduced graphene oxide were prepared by reported methods.[15,16] NMR spectra were acquired on a Bruker Avance 400 FT-NMR spectrometer (^{1}H: 400.1 MHz) or a Varian Unity INOVA 500 spectrometer (^{1}H: 499.76 MHz). ^{1}H and ^{13}C NMR chemical shifts are reported in parts per million and referenced to the signals of deuterated solvents. Multiplicities are abbreviated as follows: (s) singlet, (d) doublet, (t) triplet, (q) quartet, (m) multiplet and (br) broad. Elemental analyses were performed by H. Kolbe Mikroanalytisches Laboratorium, Mülheim an der Ruhr, Germany.

High-resolution transmission electron microscopy (HRTEM). The samples were imaged using a JEOL 3000F transmission electron microscope (field emission

gun, operated at 300 kV using both conventional TEM and scanning TEM), with a point resolution of 0.17 nm in conventional TEM mode. Sample preparation was performed by dipping a copper TEM-grid covered by a lacy carbon film into a dispersion of the rGO or **Pd^{II}@rGO** in ethanol. The microscope was used with an energy-dispersive X-ray spectroscopy (XEDS) system from Oxford Instrument with a silicon drift detector (SDD) for compositional analysis. Additionally, high resolution TEM (HRTEM) in combination with Fast Fourier transform analysis were used for detection of lattice fringes in the search for the existence of metallic Pd in the sample.

Inductively coupled plasma-optical emission spectroscopy (ICP-OES). Pd loadings were measured by a PerkinElmer Optima 8300. Samples (20 mg) were treated with a muffle stove at 1000 °C for 4 h. After cooling to room temperature, 3 ml of aqua regia was added and stirred for 30 min at 100 °C. The resulting solution was filtrated and the filtrate was diluted to 50 ml with de-ionized water.

Thermogravimetric analysis (TGA). The thermal stability of the samples under study was investigated using a Q500 analyser (TA Instruments). The first heating scan was from 25-500 °C under N_2 and the second heating scan was from 500-600 °C under air; the heating rates were 10 °C/min.

Gas chromatography analysis (GC). The analyses were done using a Hewlett-Packard 5890 II instrument with a flame ionization detector (FID) and a capillary column (CP-Sil 19CB 14% cyanopropyl-phenyl/86% dimethylpolysiloxane, 0.2 μm, 0.2 mm, 25 m) with decane as an internal standard. The retention times of different compounds in the gas chromatogram were identified using commercially available and synthesized pure compounds according to previously reported methods.[17]

Scanning electron microscopy (SEM). The characterization was carried out using a SEM LEO 1560 (Zeiss, Oberkochen, Germany) operated at 10 kV. To avoid charging the samples were coated with a 10 nm Pt coating prior to SEM imaging.

X-ray photoelectron spectroscopy (XPS). The measurements were carried out at the XPS end station of the HIPPIE beamline of the MAX IV Laboratory in Lund, Sweden. The station houses an analysis chamber equipped with a Scienta Omicron HiPP-3 hemispherical electron energy analyser and a separate preparation chamber equipped with surface analysis and preparation tools. The XPS data were collected using a Scienta Omicron SAX100 Al K$_\alpha$ X-ray anode combined with a VG SCIENTA XM 780 monochromator (photon energy 1486.7 eV). The anode was operated at 10 kV electron acceleration voltage and 25 mA emission current. The experiment was performed at a pressure lower than 10^{-9} mbar. Single crystal samples were dissolved and graphene samples were dispersed in dichloromethane and then the samples were dropped onto the highly oriented pyrolytic graphite

HOPG surface. All spectra were energy calibrated with respect to the C 1s core level of graphite of HOPG at 284.42 eV.[18] No signs of sample charging were detected: all lines could be reproduced reliably at the same energy. In particular, the C 1s line was always found at the same binding energy. Background removal was done by using a Shirley or low-degree polynomial background in the case of the Pd 3d spectra and a Shirley background in the case of the Cl 2p spectra. In the case of the N 1s spectra a polynomial background removal was applied. Curve fitting of the Cl 2p and N 1s spectra was carried out using the Igor Pro software package of Wavemetrics, Inc. using symmetric Voigt lineshapes. The spin-orbit split components in the Cl 2p spectra were restrained to have a 1:2 area ratio between the Cl $2p_{1/2}$ and Cl $2p_{3/2}$ peaks.

Synthesis of complex 2. Complex **1** (0.55 g, 1.3 mmol), 50 ml of dry CH_2Cl_2 and $Pd(PhCN)_2Cl_2$ (0.50 g, 1.3 mmol) were charged in a 50 ml Schlenk flask. The reaction was stirred for 24 h and (0.66 g, 5.8 mmol) of 3-chloropyridine was added to the cloudy solution; after 3h the mixture was filtered through Celite. The yellow solid product **2** was precipitated by addition of pentane, filtered on a frit and dried under vacuum giving 0.67 g (91% yield).
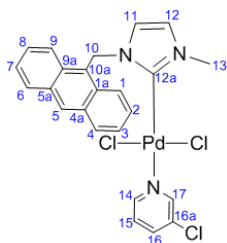
Characterization of 2. ^{1}H NMR (400 MHz, CD$_3$CN): δ 9.19 (d, *J*= 2.3 Hz, 1H, H17), 9.09 (dd, *J*= 5.5, 1.3 Hz, 1H, H14), 8.59 (s, 1H, H5), 8.46 (d, *J*= 8.8 Hz, 2H, H4 and H6), 8.07 (d, *J*= 8.4 Hz, 2H, H1 and H9), 7.82 (ddd, *J*= 8.2, 2.3, 1.3 Hz, 1H, H16), 7.64-7.47 (m, 4H, H2, H3, H7 and H8), 7.38 (ddd, *J*= 8.2, 5.5, 0.5 Hz, 1H, H15), 6.76 (s, 2H, H10), 6.76 (s, 1H, H12), 6.12 (s, 1H, H11), 4.20 (s, 3H, H13). ^{13}C NMR (400 MHz, CD$_3$CN): δ 150.5 (C17), 149.4 (C14), 147.5 (C12a), 138.3 (C16), 132.9 (C10a), 131.5 (C4a), 131.4 (C5a), 129.8 (C1a and C9a), 129.3 (C4 and C6), 127.7 (C1 and C9), 125.6 (C2, C3, C7 and C8), 125.0 (C16a), 124.1 (C5), 124.0 (C15), 122.7 (C12), 121.0 (C11), 47.4 (C10), 38.2 (C13). Anal. Calcd for $C_{42}H_{40}Cl_4N_4Pd_2$: C, 51.18; H, 3.58; N, 7.46. Found: C, 50.81; H, 3.97; N, 7.26.

Bromination of 3 catalyzed by Pd^{II}@rGO. 1 equivalent (19.2 mg, 0.1 mmol) of benzo[*h*]quinoline **3**, 2.3 equivalents (43.9 mg, 2.4 mmol) of N-bromosuccinimide (NBS) and 5 mol% (29.1 mg) **Pd^{II}@rGO** were stirred at 100°C in a Teflon-cap screw vial with approximately 1 ml CH$_3$CN. The reaction proceeded for 24 hours. At the end of the reaction, the reaction mixture was diluted with CH$_2$Cl$_2$ and then centrifuged for 15 minutes. The catalyst was shaken with CH$_2$Cl$_2$ (3 ml x 5), centrifuged, and the solvents collected and evaporated. To refresh the catalyst, **Pd^{II}@rGO** was washed with 3-chloropyridine, centrifuged and dried overnight. A final wash and centrifugation was carried out to wash away unbonded 3-chloropyridine. The evaporated mother layers from catalysis were either subjected to a preparative TLC for analysis or injected into the GC in the cases where calibration curves were available. All products were analyzed by GC-MS and NMR spectroscopy.
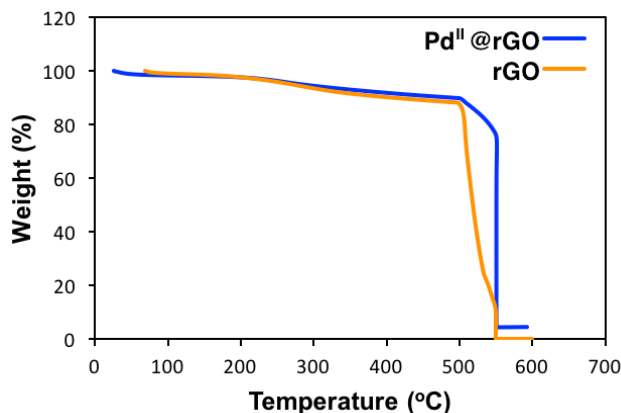
Figure S1. TGA curves of rGO and **Pd^{II}@rGO**.
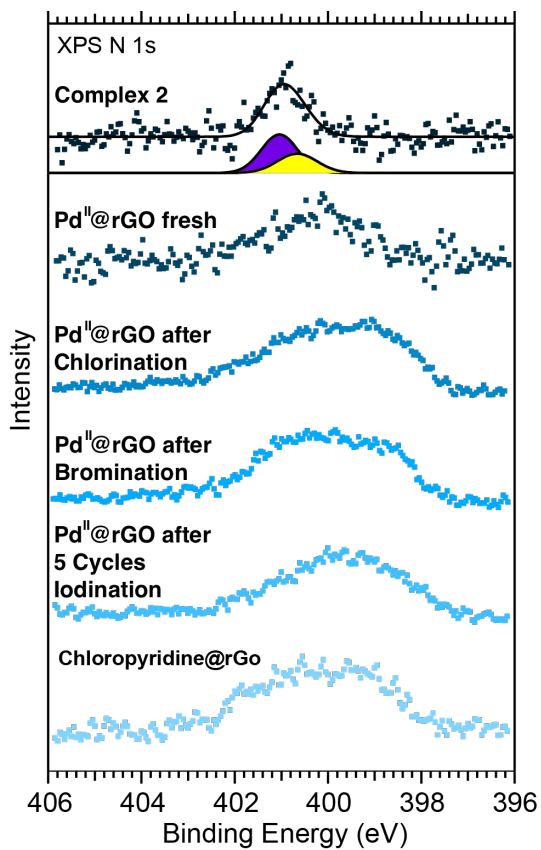
Figure S2. N 1s XP spectra of the indicated samples.

References

1. Ford, M. C.; Ho, P. S. *J. Med. Chem.* **2016,** *59* (5), 1655.
2. Ho, P. S. *Top Curr. Chem.* **2015,** *358*, 241.
3. Lim, S. J.; Fox, P. *Sci. Total. Environ.* **2014,** *470*, 348.
4. Iskra, J.; Decker, A., Halogenated heterocycles synthesis, application and environment. In *Topics in Heterocyclic Chemistry,* Springer, Berlin ; New York, **2012**.
5. Taylor, A. P.; Robinson, R. P.; Fobian, Y. M.; Blakemore, D. C.; Jones, L. H.; Fadeyi, O. *Org. Biomol. Chem.* **2016,** *14* (28), 6611.
6. Whitfield, S. R.; Sanford, M. S. *J. Am. Chem. Soc.* **2007,** *129* (49), 15142.
7. Racowski, J. M.; Sanford, M. S. *Top. Organometal. Chem.* **2011,** *35*, 61.
8. Moghaddam, F. M.; Tavakoli, G.; Saeednia, B.; Langer, P.; Jafari, B. *J. Org. Chem.* **2016,** *81* (9), 3868.
9. Ma, X. T.; Tian, S. K. *Adv. Synth. Catal.* **2013,** *355* (2-3), 337.
10. Kalyani, D.; Sanford, M. S. *Top. Organometal. Chem.* **2007,** *24*, 85.
11. Kalyani, D.; Dick, A. R.; Anani, W. Q.; Sanford, M. S. *Tetrahedron* **2006,** *62* (49), 11483.
12. Citta, A.; Schuh, E.; Mohr, F.; Folda, A.; Massimino, M. L.; Bindoli, A.; Casini, A.; Rigobello, M. P. *Metallomics* **2013,** *5* (8), 1006.
13. Senhkova, O.; Bolbat, E.; Ericson, F.; Shayesteh, P.; Chaudhary, S.; Johansson, N.; Head, A. R.; Persson, P.; Wendt, O. F.; Schnadt, J. Unpublished Manuscript.
14. Citta, A.; Schuh, E.; Mohr, F.; Folda, A.; Massimino, M. L.; Bindoli, A.; Casini, A.; Rigobello, M. P. *Metallomics* **2013,** 5, 8, 1006.
15. Hummers, W. S.; Offeman, R. E., Preparation of Graphitic Oxide. *J Am Chem Soc* **1958,** *80* (6), 1339.
16. Stankovich, S.; Dikin, D. A.; Piner, R. D.; Kohlhaas, K. A.; Kleinhammes, A.; Jia, Y.; Wu, Y.; Nguyen, S. T.; Ruoff, R. S., Synthesis of graphene-based nanosheets via chemical reduction of exfoliated graphite oxide. *Carbon* **2007,** *45* (7), 1558-1565.
17. Weimar, M.; Correa da Costa, R.; Lee, F.; Fuchter, M. J. *Org. Lett.* **2013,** 15, 7.
18. Balasubramanian, T.; Andersen, J. N.; Wallden, L. *Phys. Rev. B* **2001,** *64*, 20.

Paper VI

Operando X-ray absorption spectroscopy investigation of the active species in Pd(II)@rGO catalysed C–H oxygenation reactions

Ning Yuan,[a,b,c],† Maitham H. Majeed,[d],† Éva Bajnóczi,[c] Niclas Heidenreich,[e] Norbert Stock,[e] Ingmar Persson,[c] Ola F. Wendt,[d] Xiaodong Zou[a,b]*.

[a]Berzelii Center EXSELENT on Porous Materials, Stockholm University, SE-106 91 Stockholm, Sweden

[b]Department of Materials and Environmental Chemistry, Stockholm University, SE-106 91 Stockholm, Sweden

[c]Department of Molecular Sciences, Swedish University of Agricultural Sciences, SE-75007 Uppsala, Sweden

[d]Center for Analysis and Synthesis, Department of Chemistry, Lund University, Box 124, SE-221 00 Lund, Sweden

[e]Institute für Anorganische Chemie, Christian-Albrechts-Universität zu Kiel, DE-24118 Kiel, Germany

†These authors contributed equally to this work.

Abstract

The mechanism of undirected C–H oxygenation reaction catalysed by a Pd(II)–NHC π-stacked onto reduced graphene oxide was successfully investigated using *in situ* X-ray absorption spectroscopy (XAS) study. The supported complex is activated in the initial step of the reaction by changing its coordination environment around the Pd centre, while the oxidation state of Pd(II) is retained. Over the reaction, the active species is partially reduced to Pd(0) forming small nanoclusters.

Introduction

The formation of carbon–oxygen (C–O) bonds from C–H bonds could enable the green synthesis of pharmaceuticals and other important compounds. Such transformations are usually catalysed by transition metals (TMs) and in general very attractive strategies for organic synthesis. Most examples include homogeneous catalysts, but heterogenized transition metal catalysts are in demand, not only because these supported systems are recyclable and easy to separate from the reaction mixture, but also for their potential to introduce novel

chemical reactivity.[1-3] Recently, reduced graphene oxide (rGO) was successfully applied as a supporting material for different types of transition metal *N*-heterocyclic carbene TM–NHC complexes and applied for many transformations.[4-8] This includes examples of C–H oxygenation and, although mechanistic information for Pd(II)–NHC catalysed undirected C–H oxygenation under homogeneous reaction conditions is available,[9] the mechanism of such reactions catalysed by heterogeneous Pd(II)–NHC catalysts remains unclear. Specifically, there are no in-depth studies yet reporting an insight into the catalytically active species that is present during the reaction in rGO supported TM–NHC complexes. Therefore, here we present results from an X-ray absorption spectroscopy (XAS) study that sheds some light on the above mentioned issue. XAS, as an element selective method, is a powerful tool to investigate the oxidation state of a specific element and its local structure even in a multi-element compound. Different sample states (solid, liquid or gas) can be measured by XAS even with concentrations of investigated elements in the low millimolar range. These advantages make XAS a suitable technique to study catalysts where the major focus is on the structure of catalytically active centres, such as the structure of palladium complexes imbedded in metal organic frameworks.[10-11] The preparation of a catalyst can also be investigated by measuring the catalyst at different synthetic stages in an *ex situ* manner.[12] With reasonable time resolution of XAS measurements and proper reactors that can be adapted to the beamlines, *in situ* XAS measurement has provided opportunities to follow the structural changes of the catalytic center during various reactions in both gas-solid[13] and liquid-solid[14] systems. Together with other techniques, the active species of a catalyst during the reaction and its recyclability can be understood, which can pave the way to develop catalysts with better performance and longer lifetime. Recently, Wendt and co-workers focused on developing and applying supported heterogeneous Pd(II)–NHC catalysts in undirected C–H oxygenation of benzene.[2] Although, these systems afforded good yields of the acetoxylated product up to 50%, the reaction pathway and the nature of the catalytically active center are still not fully understood. Here we report on a mechanistic investigation of C–H acetoxylation of benzene catalysed by a Pd–NHC supported on rGO.

Experimental section

Reactor for in situ XAS measurement

A custom-made reactor (Figure 1) developed at Christian-Albrechts University (Kiel, Germany) in cooperation with the beamline staff at the P08 beamline, PETRA III, DESY (Hamburg, Germany) was used to perform the reactions and collect in situ XAS data.[15] Basically, the reactor consists of an aluminum casing that holds Duran© glass vials with a maximum volume of 6 ml.
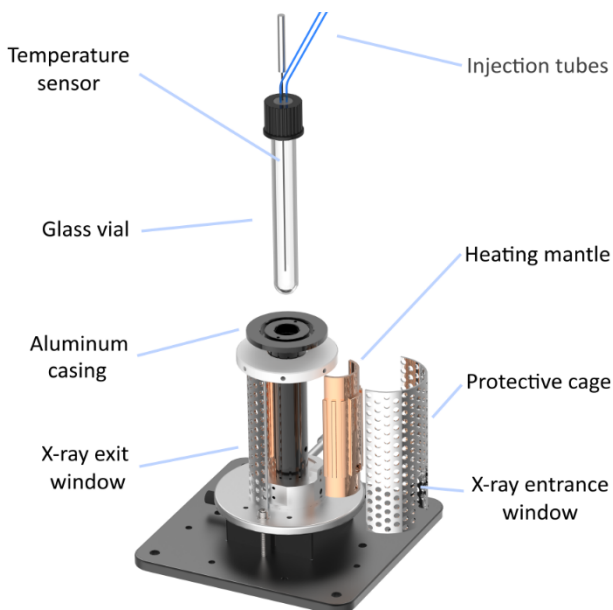
Figure 1. The reactor that was used to collect in situ XAS data.

The inner diameter of the vials is 10 mm and the thickness of the glass wall is 1.0 mm. It includes an in-built miniaturized stirring plate and temperature and the addition of reagents can be controlled remotely. The whole reactor was aligned on the beamline in transmission geometry.

XAS experiments

In situ XAS measurements were performed at the beamline P64 at DESY (PetraIII), Hamburg, Germany. Pd K-edge (24.35 keV)[16] radiation was used with an energy range from 24.15 to 25.00 keV in a continuous scanning mode. All XAS data collection was in transmission mode and the acquisition of each XAS scan was set at 5 min with considerations of both time resolution and data quality. The XAS data were either treated as individual scans or an average of several scans with identical features to improve the data quality. A palladium foil reference was always measured simultaneously and its first inflection point of the absorption edge was defined as Pd K-edge position. The data treatment was performed with the EXAFSPAK package including pre-edge subtraction, spline removal, normalization and Fourier transformation.[17] The experimental k^3-weighted EXAFS oscillations were analyzed by non-linear least-squares fits of the data to the EXAFS equation, refining the model parameters, number of backscattering atoms (N), mean interatomic distances (R), Debye-Waller factor coefficients (σ^2) and

3

threshold energy (E_o). FEFF7 was used to calculate the theoretical phases and amplitudes.[18] It should be noticed that the distances read in Fourier transformed EXAFS spectra were without phase correction and true distance values were determined from EXAFS refinements. The standard deviations reported for the refined parameters were obtained from k^3 weighted least-squares refinements of the EXAFS function $\chi(k)$, and without including systematic errors. For a well-defined interaction, the accuracy of the distances given for an individual complex is between ±0.005 and ±0.02 Å.

Catalytic reactions for in situ XAS measurement

Benzene (1.75 g, 22.44 mmol, 21.77 equiv.), PhI(OAc)$_2$ (0.33 g, 1.03 mmol, 1 equiv.), **1@rGO** (0.10 g, 9 mol% with respect to the oxidant), glacial acetic acid (1.50 ml), and acetic anhydride (0.17 ml) were transferred into the reaction vessel which was sealed in the preparation room and transported immediately to the hutch for measurements. The reaction mixture was stirred at 90 °C during the *in situ* XAS measurements.

Results and discussion

Preparation of 1@rGO

Complex **1** was synthesized according to a previously reported procedure.[19] Complex **1** was supported onto rGO according to an adaptation of the procedure by Peris and co-workers,[6] as summarized in Scheme 1. XAS data of complex **1** and **1@rGO** were collected in powder form using regular sample holders. Figure 2a shows the X-ray absorption near edge spectra (XANES) spectra of these two materials together with Pd foil. Both complex **1** and **1@rGO** have an edge position at ca. 24354 eV which is 4 eV higher than the Pd foil reference. This confirms that the Pd has an oxidation state of +II in both catalysts.[20] The XANES features of **1@rGO** are a little bit smeared out compared to the unsupported complex, indicating a slight but noticeable local structure difference between complex **1** and **1@rGO**.
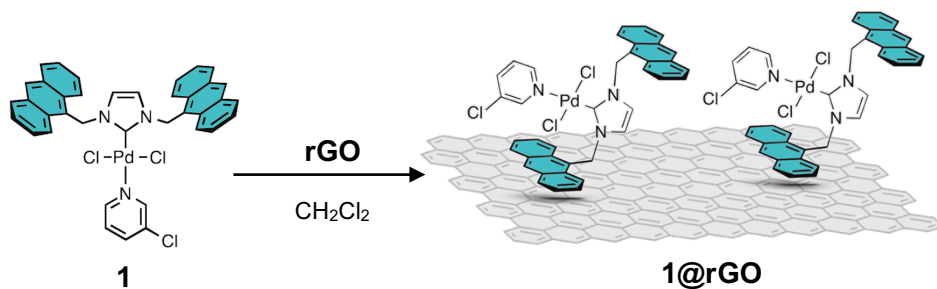
Scheme 1. Immobilization of complex **1** on rGO results **1@rGO** catalyst.

However, their Fourier transformed EXAFS spectra (Figure 2b) are almost identical confirming the same coordination environment around the Pd atoms. The results of EXAFS refinements (k: 2-11.5 Å^{-1}) agree well with the crystal structure of complex **1**. The main peaks at ca. 1.5 Å without phase correction correspond to Pd-N/C bonds. The bond distances were determined to be 1.97 Å for complex **1** and 1.95 Å for **1@rGO** with a coordination number of two for both of them. Debye-Waller factor coefficients of Pd- N/C single scattering are relatively high which proves that the ligands bound to Pd at this distance are different. The main peaks at ca. 1.8 Å correspond to Pd–Cl bonds. The bond distances in both materials were determined to be 2.30 Å with a coordination number of two and a small bond distance distribution. By combining XANES and EXAFS it can be concluded that during the loading of complex **1** onto rGO, the complex remained intact, but the geometry of the ligands around Pd slightly changed according to the XANES spectra.
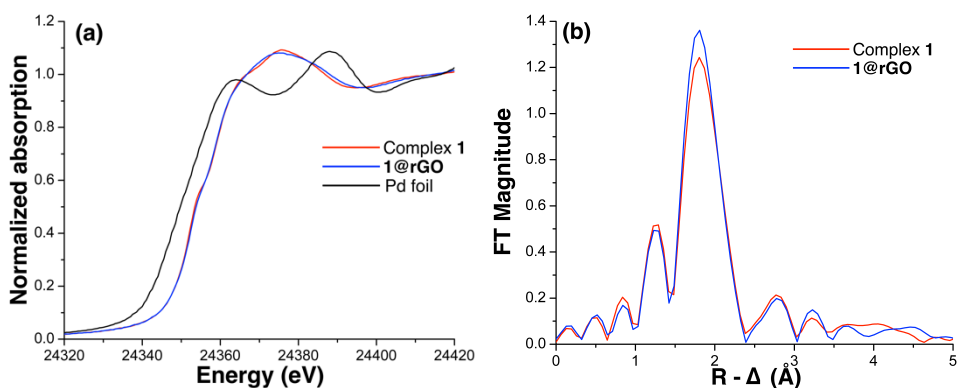
Figure 2. **(a)** XANES spectra and **(b)** Fourier transformed EXAFS spectra without phase correction of complex **1** and **1@rGO**.

Activation of 1@rGO

The activation mechanism for **1@rGO** in the acetoxylation reaction of benzene was investigated. The XAS data acquisition was conducted at room temperature for 15 min and for 5 minutes at 90 °C in the *in situ* reactor. However, the XAS data quality of the individual *in situ* scans were fairly poor (most probably due to the low concentration of Pd in the reaction mixture) at this initial stage, therefore it was not possible to analyze them in detail. Therefore, the catalyst, after the altogether 20 min measurement, was centrifuged and the catalyst suspension was transported to a regular solid sample holder for measurement. With this procedure

XAS data with acceptable quality were obtained and are presented in Figure 3. Significant changes were observed in both XANES spectra (Figure 3a) and Fourier transformed EXAFS spectra indicating a structure evolution from fresh **1@rGO** catalyst to its active phase in the reaction mixture. The Pd remains in the oxidation state +II even in the active phase. The change in the XANES spectra could indicate a partial loss of chloride. In Figure 3 the EXAFS range for both materials are from 2 to 9 Å^{-1} for better comparison (a.k.a. the resolutions of the peaks are the same). Under this resolution, the main peaks consist of signals from both Pd–N/C and Pd–Cl bonds. It is noted that the main peak shifts leftwards from fresh **1@rGO** to its active state, probably due to a partial loss of Cl. A model of Pd–N/C/O with a coordination number of three together with one Pd–Cl was used to perform EXAFS refinement and the quality is acceptable (Supporting Information, Figure S1). In this case, one Cl was replaced by an acetoxy group.
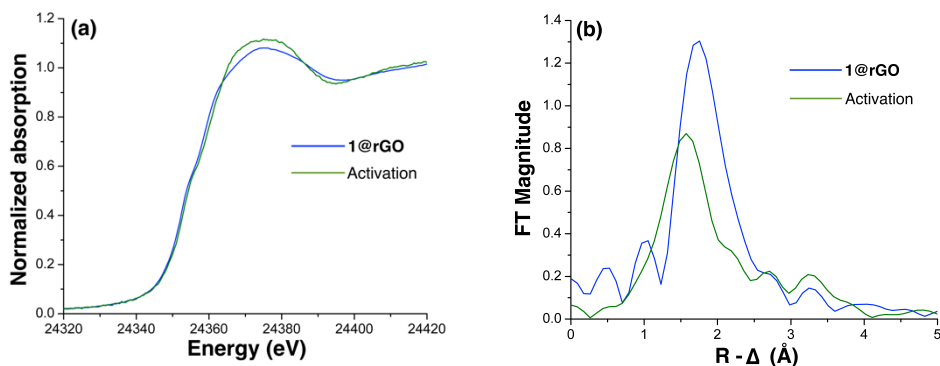
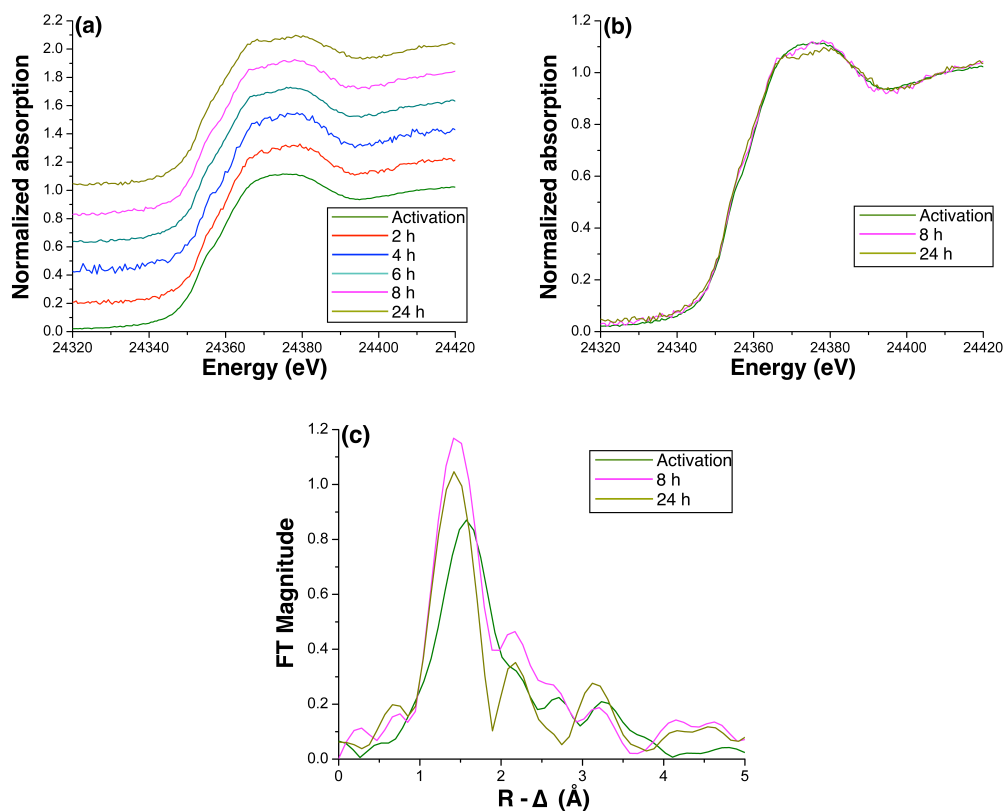
Figure 3. (a) XANES spectra and **(b)** Fourier transformed EXAFS spectra without phase correction of **1@rGO** and its active phase in the reaction mixture.

In situ XAS studies of the C–H activation reaction

In situ XAS measurements were performed during the C–H activation reaction catalyzed by the activated **1@rGO** to follow the possible changes of the active species at different stages of the reaction. Figure 4a shows selected XANES spectra of the measurement. The spectra at 2 and 4 hours are from two individual scans during the *in situ* measurement with slightly lower data quality.

Figure 4. **(a)** Selected *in situ* XANES spectra that cover the whole experiment of heterogeneous catalytic reaction. **(b)** Selected *in situ* XANES spectra with focus on the scans with feature development. **(c)** Selected Fourier transformed EXAFS spectra without phase correction focusing on the scans with structural evolution.

Their XANES spectra, however, were almost identical confirming that the active species remained unchanged during this timeframe. There is a slight shift towards higher energies in edge position (ca. 1 eV) but it is still close to that expected for Pd(II). This suggests that Pd(II) is the resting state of the catalyst in the catalytic cycle, i.e. the state in which most of the Pd atoms are at a specific time. However, the slightly higher edge position might indicate that a small part of the Pd atoms have higher oxidation states (+III or +IV). This information supports the proposed Pd(II–IV–II) reaction mechanism.[9] Due to the relatively long reaction time, the vial in which the reactions proceeded was moved from the beam after 4 h but the heating and stirring was continued under the same conditions and further data was collected at 6, 8 and 24 hours after the reaction started. In order to observe the

minor but important changes that took place, XANES spectra of the activated catalyst and of the system after 8 and 24 hours were selected and plotted in Figure 4b. Clear changes of the XANES features can be recognized. From the XANES spectrum of the activated catalyst to the one 8 hours into the catalytic reaction, the small bump at 24355 eV shifted upwards at 8 hours and at 24 hours this feature disappeared. Meanwhile, the XANES wave after the absorption edge started to flatten and then split into two smaller waves which is a typical XANES feature of metallic Pd. The edge position slightly shifted to lower energy also indicating a small degree of reduction. Fourier transformed EXAFS spectra in Figure 4c were used to determine the coordination environments of Pd atoms in the activated catalyst and catalysts at 8 hours and 24 hours. The positions of the main peak had a significant shift to shorter distance suggesting further loss of Cl ligands and it was confirmed by refinement showing no Pd–Cl signals in the spectra at 8 and 24 hours. In addition, a peak at ca. 2.2 Å without phase correction became significant which is best refined as a Pd–Pd bond. The Pd–Pd bond distance and coordination number of distances of the 8 h sample was 2.67 Å and 1.5 respectively. For the 24 h sample, Pd–Pd bond distance remained similar while the coordination number of distances increased to 3. This means that a small amount of the Pd complexes were reduced to metallic Pd nanoclusters. The average size of Pd nanoclusters was smaller than 1 nm due to the low average coordination number of Pd-Pd bond and relatively short bond distance compared with bulk Pd metal and Pd nanoparticles in other materials.[21,22] The fraction of metallic Pd nanoclusters increased from 8 h to 24 h.

Conclusions

An *in situ* XAS study was successfully performed to investigate the reaction mechanism of a newly developed supported catalyst, **1@rGO,** for the C–H oxygenation of benzene. The Pd in **1@rGO** was confirmed to have the same ligands as in complex **1** but with different geometry. The catalyst went through an activation process in the beginning of the reaction by changing the coordination environment of Pd atoms while keeping the oxidation state unchanged. There is an indication that a small fraction of the Pd atoms have a higher oxidation state at this point. One of the Cl ligands was probably replaced by an acetoxy group at this stage. This new phase was the active species for the reaction and it was stable up to 6 hours under the measurements condition. Then the active species slowly underwent a transformation into small Pd nanoclusters while losing the last Cl ligand. The catalyst in the end of the reaction consists of a minor fraction of metallic Pd nanoclusters and a major fraction of Pd(II) complexes species.

References

1.	Hu, M. L.; Safarifard, V.; Doustkhah, E.; Rostamnia, S.; Morsali, A.; Nouruzi, N.; Beheshti, S.; Akhbari, K. *Micropor. Mesopor. Mat.* **2018**, *256*, 111.

2.	Majeed, M. H.; Shayesteh, P.; Wallenberg, L. R.; Persson, A. R.; Johansson, N.; Ye, L.; Schnadt, J.; Wendt, O. F. *Chem. Eur. J.* **2017**, *23*, 8457.

3.	Perez-Mayoral, E.; Calvino-Casilda, V.; Soriano, E. *Catal. Sci. Technol.* **2016,** *6*, 1265.

4.	Gonell, S.; Peris, E. *ACS Catal.* **2014**, *4*, 2811.

5.	Ruiz-Botella, S.; Peris, E. *Organometallics* **2014**, *33*, 5509.

6.	Sabater, S.; Mata, J. A.; Peris, E. *ACS Catal.* **2014**, *4*, 2038.

7.	Sabater, S.; Mata, J. A.; Peris, E. *Organometallics* **2015**, *34*, 1186.

8.	Ventura-Espinosa, D.; Carretero-Cerdan, A.; Baya, M.; Garcia, H.; Mata, J. A. *Chem. Eur. J.* **2017**, *23*, 10815.

9.	Tato, F.; Garcia-Dominguez, A.; Cardenas, D. J. *Organometallics* **2013**, *32*, 7487.

10.	Pascanu, V.; Gomez, A. B.; Ayats, C.; Platero-Prats, A. E.; Carson, F.; Su, J.; Yao, Q. X.; Pericas, M. A.; Zou, X. D.; Martin-Matute, B. *ACS Catal.* **2015**, *5*, 472.

11.	Bloch, E. D.; Britt, D.; Lee, C.; Doonan, C. J.; Uribe-Romo, F. J.; Furukawa, H.; Long, J. R.; Yaghi, O. M. *J. Am. Chem. Soc.* **2010**, *132*, 14382.

12.	Bruneau, A.; Gustafson, K. P. J.; Yuan, N.; Tai, C. W.; Persson, I.; Zou, X.; Backvall, J. E. *Chem. Eur. J.* **2017,** *23*, 12886.

13.	a) Jung, U.; Elsen, A.; Li, Y.; Smith, J. G.; Small, M. W.; Stach E. A.; Frenkel, A. I.; Nuzzo, R. G. *ACS Catal.* **2015**, *5,* 1539; b) Smit, E. De; Cinquini, F.; Beale, A. M.; Safonova, O. V; Beek, W. Van; Sautet, P.; Weckhuysen, B. M.; Supe, N.; Horowitz, R. J.; Cedex, F.-G. *J. Am. Chem. Soc.* **2010**, *132*, 14928; c) Rønning, M.; Tsakoumis, N. E.; Voronov, A.; Johnsen, R. E.; Norby, P.; Van Beek, W.; Borg, Ø; Rytter, E.; Holmen, A. *Catal. Today* **2010**, *155*, 289; d) van Beek, W.; Safonova, O. V.; Wiker, G.; Emerich, H. *Phase Transitions* **2011**, *84*, 726–732; e) Grunwaldt, J.-D.; Clausen, B. S. *Topics Catal.* **2002**, *18*, 37; f) Matam, S. K.; Aguirre, M. H.; Weidenkaff, A.; Ferri, D. *J. Phys. Chem. C* **2010**, *114*, 9439; g) Reina, T. R.; Xu, W.; Ivanova, S.; Centeno, M. Á.; Hanson, J.; Rodriguez, J. A.; Odriozola, J. A. *Catal. Today* **2013**, *205*, 41; h) Cassinelli, W. H.; Martins, L.; Passos, A. R.; Pulcinelli, S. H.; Santilli, C. V.; Rochet, A.; Briois, V. *Catal. Today* **2014**, *229*, 114; i) Braglia, L.; Borfecchia, E.; Martini, A.; Bugaev, A. L.; Soldatov, A. V; Øien-Ødegaard, S.; Bleken, B. T. L.; Olsbye, U.; Lillerud, K. P.; Lomachenko, K. A.; Agostini, G.; Manzoli, M.; Lamberti, C. *Phys. Chem. Chem. Phys.* 2017; j) Andersen, C. W.;

Borfecchia, E.; Bremholm, M.; Jørgensen, M. R. V.; Vennestrøm, P. N. R.; Lamberti, C.; Lundegaard, L. F.; Iversen, B. B. *Angew. Chemie Int. Ed.* **2017**, *56*, 10367; k) Barzan, C.; Piovano, A.; Braglia, L.; Martino, G. A.; Lamberti, C.; Bordiga, S.; Groppo, E. *J. Am. Chem. Soc.* **2017**; l) Øien, S.; Agostini, G.; Svelle, S.; Borfecchia, E.; Lomachenko, K. A.; Mino, L.; Gallo, E.; Bordiga, S.; Olsbye, U.; Lillerud, K. P.; Lamberti, C. *Chem. Mater.* **2015**, *27*, 1042; m) Zhou, Y.; Doronkin, D. E.; Chen, M.; Wei, S.; Grunwaldt, J.-D. *ACS Catal.* **2016**, *6*, 7799; n) Stötzel, J.; Frahm, R.; Kimmerle, B.; Nachtegaal, M.; Grunwaldt, J.-D. *J. Phys. Chem. C* **2012**, *116*, 599; o) Doronkin, D. E.; Casapu, M.; Günter, T.; Müller, O.; Frahm, R.; Grunwaldt, J.-D. *J. Phys. Chem. C* **2014**, *118*, 10204.

14.   a) Gorlin, Y.; Lassalle-Kaiser, B.; Benck, J. D.; Gul, S.; Webb, S. M.; Yachandra, V. K.; Yano, J.; Jaramillo, T. F. *J. Am. Chem. Soc.* **2013**, *135*, 8525; b) Newton, M. A.; Brazier, J. B.; Barreiro, E. M.; Parry, S.; Emmerich, H.; Adrio, L. A.; Mulligan, C. J.; Hellgardt, K.; Hii, K. K. *Green Chem.* **2016**, *18*, 406.

15.   Heidenreich, N.; Rütt, U.; Köppen, M.; Inge, A. K.; Beier, S.; Dippel, A.-C.; Suren, R.; Stock, N. *Rev. Sci. Instrum.* **2017**, *88*, 104102.

16.   Thompson, A.; Attwood, D.; Gullikson, E.; Howells, M.; Kim, K.-J.; Kirz, J.; Kortright, J.; Lindau, I.; Liu, Y.; Pianetta, P.; Robinson, A.; Scofield, J.; Underwood, J.; Williams, G.; Winick, H. *X-ray data booklet*, Lawrence Berkeley National Laboratory, Berkeley, 3rd Ed., **2009**.

17.   George, G. N.; Pickering, I. J. EXAFSPAK – A Suite of Computer Programs for Analysis of X-ray Absorption Spectra, SSRL, Stanford, CA. **1993**.

18.   Zabinsky, S. I.; Rehr, J. J.; Ankudinov, A.; Albers, R. C.; Eller, M. J. *Phys. Rev. B* **1995**, *52*, 2995.

19.   Unpublished Manuscript.

20.   Jalilehvand, F. *Structural of Hydrated Ions and Cyano Complexes by X-Ray Absorption Spectroscopy*, Royal Institute of Technology, Stockholm, **2000**, electronic version.

21.   a) Krüger, S.; Vent, S.; Nörtemann, F.; Staufer, M.; Rösch, N. *J. Chem. Phys.* **2001**, *115*, 2082; b) Qi, W.; Huang, B.; Wang, M. *Nanoscale Res. Lett.* **2009**, *4*, 269.

22.   a) Reimann, S.; Stötzel, J.; Frahm, R.; Kleist, W.; Grunwaldt, J. D.; Baiker, A. *J. Am. Chem. Soc.* **2011**, *133*, 3921; b) Grunwaldt, J.-D.; Caravati, M.; Baiker, A. *J. Phys. Chem. B* **2006**, *110*, 9916; c) Pikna, L.; Milkovič, O.; Saksl, K.; Heželová, M.; Smrčová, M.; Puliš, P.; Michalik, S.; Gamcová, J. *J. Solid State Chem.* **2014**, *212*, 197; d) Agostini, G.; Lamberti, C.; Pellegrini, R.; Leofanti, G.; Giannici, F.; Longo, A.; Groppo, E. *ACS Catal.* **2014**, *4*, 187; e) Shimizu, K.; Kubo, T.; Satsuma, A.; Kamachi, T.;

Yoshizawa, K. *ACS Catal*. **2012**, *2*, 2467; f) Ellis, P. J.; Fairlamb, I. J. S.; Hackett, S. F. J.; Wilson, K.; Lee, A. F. *Angew. Chem.*, *Int. Ed.* **2010**, *49*, 1820.

Supporting Information:

a

b

c
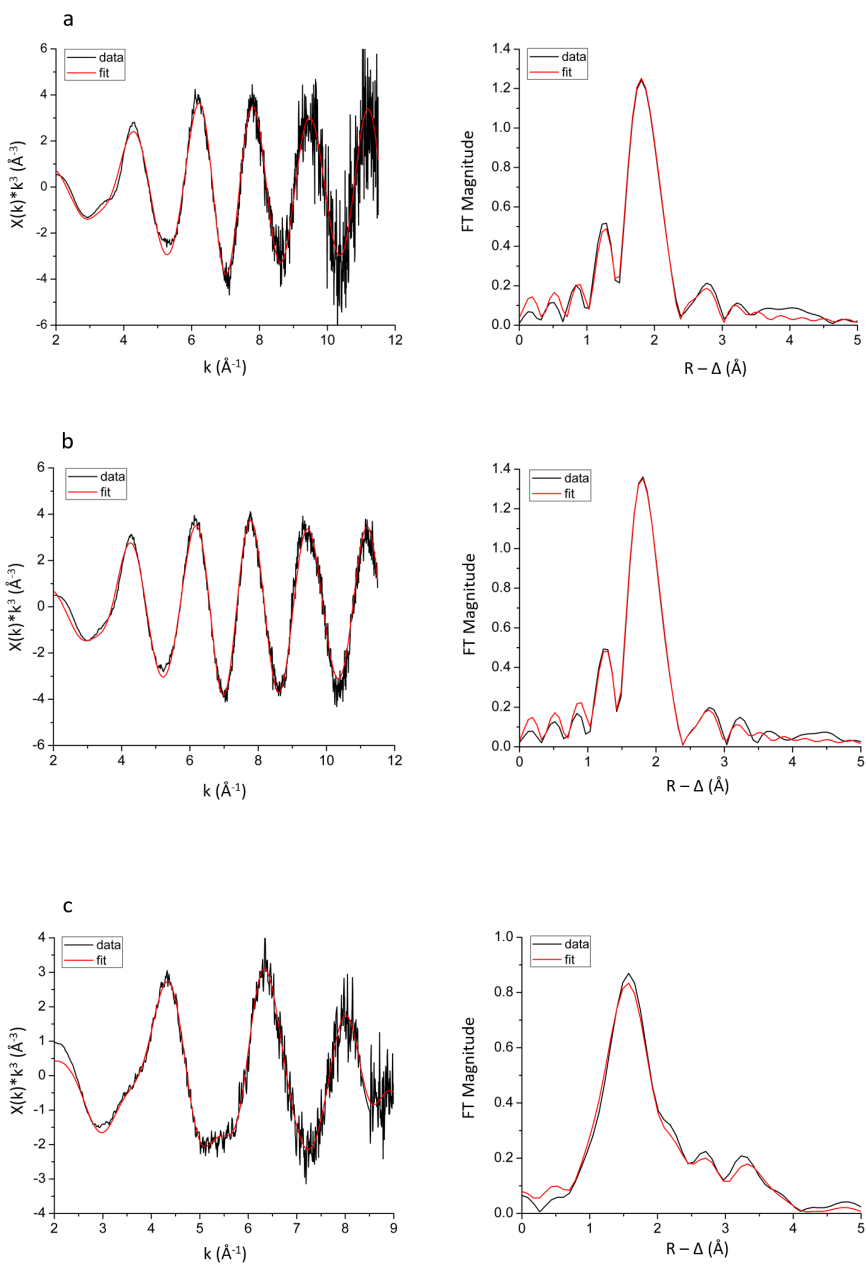
Figure S1. Fit of the Pd K-edge EXAFS spectra (left) and the Fourier transforms (right) of **(a)** complex 1, **(b) 1@rGO** fresh, **(c)** activated **1@rGO**, **(d) 1@rGO** at 8 h and **(e) 1@rGO** at 24 h of the operando XAS measurement.

d

e
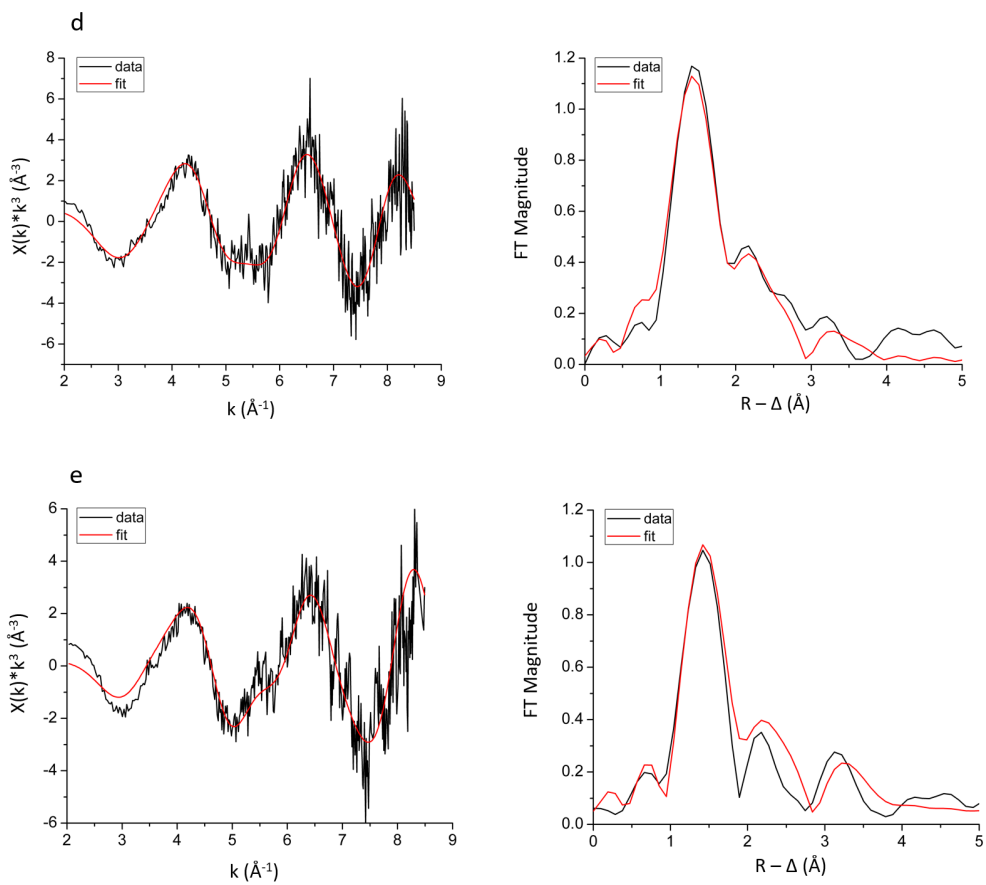
Figure S1. Continued.

13

Table 1. Refined distances (d/Å), mean number of distances (N) and Debye-Waller factor coefficients (σ^2) from EXAFS refinements in Figure S1.

Catalyst	d(Pd-N/C/O) (Å)[a]	CN[b]	σ^2	d(Pd-Cl) (Å)[a]	CN[b]	σ^2	d(Pd-Pd) (Å)[a]	CN[b]	σ^2
Complex 1	1.97(1)	2.0	0.010(1)	2.296(4)	2.0	0.0018(4)	-	-	-
1@rGO fresh	1.951(4)	2.0	0,0112(5)	2.296(1)	2.0	0.0022(1)	-	-	-
Activated **1@rGO**	1.998(8)	3.0	0.0093(8)	2.259(7)	1.0	0.0034(8)	-	-	-
1@rGO at 8 h	2.014(8)	3.5	0.004(1)	-	-	-	2.67(1)	1.5	0.008(1)
1@rGO at 24 h	2.037(7)	3.0	0.0048(7)	-	-	-	2.62(1)	3.0	0.0124(7)

[a] The standard deviations in parentheses were obtained from k^3-weighted least square refinements of the EXAFS function $\chi(k)$ and do not include systematic errors of the measurement. [b] The coordination numbers are average values and the estimated error of the coordination is *ca*. 25% of the given value when refined. Underscored parameters have been optimized and fixed in the refinements.